INTEGRATED ISOTOPE-GEOCHEMICAL INVESTIGATION IN THE SELECTED GEOTHERMAL AREAS OF INDIA

By

Sitangshu Chatterjee

Enrollment Number: CHEM01201504010

Bhabha Atomic Research Centre

A thesis submitted to the

Board of Studies in Chemical Science

In partial fulfilment of requirements

For the Degree of

DOCTOR OF PHILOSOPHY

of

HOMI BHABHA NATIONAL INSTITUTE

January 2021

Homi Bhabha National Institute

Recommendations of the Viva Voce Committee

As members of the Viva Voce Committee, we certify that we have read the dissertation prepared by **Mr. Sitangshu Chatterjee** entitled **"Integrated Isotope-Geochemical Investigation in the Selected Geothermal Areas of India"** and recommend that it may be accepted as fulfilling the thesis requirement for the award of Degree of Doctor of Philosophy.

Chairman – Dr. B. S. Tomar		**Date:** 2/7/2021
Guide / Convener – Dr. Ashutosh Dash		**Date:** 2/7/2021
Examiner – Dr. Abhijit Mukherjee		**Date:** 4 June 2021
Member 1- Dr. H.J. Pant		**Date:** 2/7/2021
Member 2- Dr. Ratikant Mishra		**Date:** 2/7/2021
Member 3- Dr. Smruti Dash		**Date:** 02/07/2021
Technical Adviser (TA)- Dr. U. K. Sinha		**Date:** 02/07/2021

Final approval and acceptance of this thesis is contingent upon the candidate's submission of the final copies of the thesis to HBNI.

I/We hereby certify that I/we have read this thesis prepared under my/our direction and recommend that it may be accepted as fulfilling the thesis requirement.

Date: 02/07/2021

Place: MUMBAI

(Signature)
Guide

STATEMENT BY AUTHOR

This dissertation entitled **"Integrated Isotope-geochemical Investigation in the Selected Geothermal Areas of India"** has been submitted in partial fulfillment of requirements for an advanced degree at Homi Bhabha National Institute (HBNI) and is deposited in the Library to be made available to borrowers under rules of the HBNI.

Brief quotations from this dissertation are allowable without special permission, provided that accurate acknowledgement of source is made. Requests for permission for extended quotation from or reproduction of this manuscript in whole or in part may be granted by the Competent Authority of HBNI when in his or her judgment the proposed use of the material is in the interests of scholarship. In all other instances, however, permission must be obtained from the author.

Sitangshu Chatterjee.

(Sitangshu Chatterjee)

DECLARATION

I, hereby declare that the investigation presented in the thesis entitled **"Integrated Isotope-geochemical Investigation in the Selected Geothermal Areas of India"** has been carried out by me. The work is original and has not been submitted earlier as a whole or in part for a degree / diploma at this or any other Institution / University.

Sitangshu Chatterjee.

(Sitangshu Chatterjee)

LIST OF PUBLICATIONS

Journals

1. Understanding water circulation with tritium tracer in the Tural-Rajwadi geothermal area, India. **Sitangshu Chatterjee**, M. A. Gusyev, U.K. Sinha, H.V. Mohokar, Ashutosh Dash. **Applied Geochemistry**, 2019, 109: 104373.

2. Multicomponent versus Classical Geothermometry: Applicability of Both Geothermometers in a Medium-Enthalpy Geothermal System in India. **Sitangshu Chatterjee**, U.K. Sinha, B.P. Biswal, A. Jaryal, S. Patbhaje, Ashutosh Dash. **Aquatic Geochemistry**, 2019, 25, 91–108. DOI: 10.1007/s10498-019-09355-w.

3. An Integrated Isotope-Geochemical Approach to Characterize a Medium Enthalpy Geothermal System in India. **Sitangshu Chatterjee**, Uday K. Sinha, B.P.Biswal, A. Jaryal, P.K.Jain, S. Patbhaje, Ashutosh Dash. **Aquatic Geochemistry**, 2019, 25, 63–89. DOI: 10.1007/s10498-019-09352-z.

4. Application of lumped parameter model to estimate mean transit time (MTT) of the thermal water using environmental tracer (^{3}H): Insight from Uttarakhand geothermal area (India). **Sitangshu Chatterjee**, U.K. Sinha, Md. Arzoo Ansari, H.V. Mohokar, Ashutosh Dash. **Applied Geochemistry**, 2018, 94, 1–10, DOI 10.1016/j.apgeochem.2018.04.013.

5. Isotope-geochemical characterization and geothermometrical modelling of Uttarakhand geothermal field, India. **Sitangshu Chatterjee**, U.K. Sinha, A.S. Deodhar, Md. Arzoo Ansari, Nathu Singh, A. Srivastava, R.K Aggarwal, Ashutosh Dash. **Environmental Earth Science**, 2017, 76: 638. DOI 10.1007/s12665-017-6973-2.

6. A multi-isotope approach (O, H, C, S, B and Sr) to understand the source of water and solutes in some the thermal springs from West Coast geothermal area, India. **Sitangshu Chatterjee**, Md. Arzoo Ansari, A.S. Deodhar, U.K. Sinha, Ashutosh

Dash. **Arabian Journal of Geosciences**, 2017, 10: 242, 1-11. DOI 10.1007/s12517-017-3022-0.

7. Characterization of subsurface processes and estimation of reservoir temperature in Tural and Rajwadi geothermal fields, Maharashtra, India. **Sitangshu Chatterjee**, Suman Sharma, Md. Arzoo Ansari, Archana S. Deodhar, Upananda Low, U.K. Sinha and Ashutosh Dash. **Geothermics**, 2016, 59, 77-89. DOI 10.1016/j.geothermics.2015.10.011.

Conferences/Symposia

1. Application of environmental isotopes (^{3}H & ^{14}C) in age dating of thermal water. **Sitangshu Chatterjee**, A. Jaryal, U.K. Sinha. 14th biennial DAE-BRNS symposium on Nuclear and Radiochemistry (**NUCAR-2019**), January 15-19, pp. 272.
2. Role of Isotope techniques in characterizing thermal fluid- insights from Godavari valley geothermal field, Telengana. **Sitangshu Chatterjee** and U.K. Sinha. Centre for water resources, JNTUH, Hyderabad. 5th National conference on "Water, Environment & Society (**NCWES-2018**), June 4 – 6, 2018, pp. 135-140.
3. Environmental isotope studies in geothermal fields of Uttarakhand, India. **Sitangshu Chatterjee**, U.K. Sinha, A.S. Deodhar, Ajay Jaryal and Ashutosh Dash. 13th biennial DAE-BRNS symposium on Nuclear and Radiochemistry (**NUCAR-2017**), February 6-10, pp. 333-335.
4. An application of isotope techniques in Manuguru geothermal field of Godavari valley, India. **Sitangshu Chatterjee**, A.S. Deodhar, Ajay Jaryal, U.K. Sinha, Ashutosh Dash, Bishnu Prasad Biswal. Proceedings of the international conference on Recent Advances in Analytical Sciences (**RAAS-2016**), 2016, April 7-9, pp. 90-92.

Sitangshu Chatterjee.

(Sitangshu Chatterjee)

Dedicated

To

My Family

ACKNOWLEDGEMENTS

First and foremost, I wish to express my sincere gratitude to my guide Prof. Ashutosh Dash for his whole hearted support, encouragement and guidance during the course of this work. I also wish to convey my deep regards to the esteemed members of my doctoral committee, Prof. B.S. Tomar, Dr. H. J. Pant, Dr. U. K. Sinha, Dr. Smruti Dash, Dr. Ratikant Mishra for their insightful comments and suggestions during the progress of this research work.

I express my profound sense of gratitude to Dr. U. K. Sinha, Head, Isotope Hydrology Section, for his constant encouragement and constructive comments. I must also mention the valuable support of my colleagues especially Dr. K. Tirumalesh, Mrs. Diksha Pant, Mr. AS Roy, Mr. Ajay Jaryal, Mr. H. V. Mohokar, Mr. S. N. Kamble for their unstinted help and cooperation. The support of Smt. Archana Deodhar, Dr. Noble Jacob, Mr. Arzoo Ansari, Mr. G.N. Mendhekar is also acknowledged.

I also thank Dr. P.K. Pujari, Group director, RC&IG for his constant support during my PhD tenure. I also extend my deepest regards to the officers of Geological Survey of India who were associated with the geothermal projects and helped me immensely during the field campaigns. My sincerest thanks go to the people of Analytical Chemistry Division (ACD), Fuel Chemistry Division (FCD), Radioanalytical Chemistry Division (RACD) for always being there whenever I sought their help.

Nothing can be accomplished without support from family. I am forever indebted to my parents from whom I learned a great deal of life. Their infallible love and support has always been my pillar of strength. I owe my special gratitude to my lovely wife Nabanita and my son Swarnava for making this journey smooth and beautiful. Last but not the least; I thank my younger brother Subrangshu for always bringing joy and happiness in my life.

Finally, I would like to thank the God, the Almighty for His blessings to face the complexities of life and complete this project successfully.

LIST OF SYMBOLS

Symbol	Definition of symbol
%	Percentage
σ	Sigma (measurement of standard deviation)
°C	Degree centigrade
µS/cm	microSiemens per Centimeter (conductivity unit)
‰	Per mil (parts per thousand)
A	Measured ^{14}C activity in pMc
A_O	Initial ^{14}C activity in pMc
GWh	Gigawatt hours
K	Thermodynamic Equilibrium Constant
mS/cm	milliSiemens per Centimeter (conductivity unit)
mW/m^2	milliWatt per square metre
n	Number of samples
η	Effective porosity of the rocks
Q	Ion Activity Product (Reaction Quotient)
Q_w	Cumulative flow rate of the thermal springs in Litre/sec
R_{sample}	Isotopic ratio ($^{18}O/^{16}O$ or $^{2}H/^{1}H$ etc.) of the sample
$R_{standard}$	Isotopic ratio ($^{18}O/^{16}O$ or $^{2}H/^{1}H$ etc.) of the standard
$T_{adiabatic}$	Estimated outlet temperature of the thermal spring (°C)
T_{gw}	Tritium concentration of the ground water
TJ/year	TeraJoule per year
$T_{m,\ old}$	MTT of the old thermal water in years

$T_{m,\ true}$	MTT of the mixed thermal water in years
$T_{m,\ young}$	MTT of the young water component in years
$T_{shallow}$	Temperature of the non-thermal groundwater (°C)
T_{sp}	Tritium concentration of the mixed spring
$T_{thermal}$	Calculated reservoir temperature (°C)
V_{res}	Volume of the reservoir
V_w	Volume of the reservoir water in km^3
x	Fraction of cold water
α	Fractionation factor
δ	Delta (per mil)
µL	microLitre

LIST OF ABBRIVIATIONS

Abbreviation	Full form
μM	Micromolar
BDL	Below Detection Limit
BFL	Best Fit Line
BMM	Binary Mixing Model
BP	Before Present
CAIS	Common Analyte Internal Standardisation
cfact	Concentration/dilution Factor
CF-IRMS	Continuous Flow Isotope Ratio Mass Spectrometer
CGWB	Central Ground Water Board
DIC	Dissolved Inorganic Carbon
DM	Dispersion Model
DO	Dissolved Oxygen
EA	Elementar Analyser
EC	Electrical Conductivity
EGB	Eastern Ghats Belt
EGS	Enhanced Geothermal System
EL	Evaporation Line
EMM	Exponential Mixing Model
EPM	Exponential Piston-Flow Model
GMWL	Global Meteoric Water Line
GNIP	Global Network of Isotopes in Precipitation

GPS	Global Positioning System
GSI	Geological survey of India
HCA	Hierarchical Cluster Analysis
HDPE	High Density Polyethylene
HDR	Hot Dry Rock
HGB	Himalayan Geothermal Belt
ICP-MS	Inductively Coupled Plasma Mass Spectrometer
ICP-oa-TOFMS	Inductively Coupled Plasma Orthogonal Acceleration Time Of Flight Mass Spectrometer
ICP-OES	Inductively Coupled Plasma Optical Emission Spectrometry
IR	Infrared
IRMS	Isotope Ratio Mass Spectrometer
ITSZ	Indus Tsangpo Suture Zone
LDPE	Low Density Polyethylene
LMWL	Local Meteroic Water Line
LPM	Lumped Parameter Model
MBT	Main Boundary Thrust
MCT	Main Central Thrust
MTT	Mean Transit Time
NIST	National Institute of Standards and Technology
PC	Principal Component
PCA	Principal Component Analysis
PEM	Partial Exponential Model
PFM	Piston-Flow Model
pMc	Percent Modern Carbon

PMT	Photo Multiplier Tube
RMED	Median of Absolute Values of Saturation Indices
RMSE	Root Mean Square Error
RSD	Relative Standard Deviation
SCCL	Singareni Collieries Company Limited
SCR	Sample Channel Ratio
SDEV	Standard Deviation
SI	Saturation Index
SLAP	Standard Light Antarctic Precipitation
SONATA	Son - Narmada – Tapi Lineament
SQP	Spectral Quench Parameter
SRM	Standard Reference Material
stwf	Steam Weight Fraction Factor
TCD	Thermal Conductivity Detector
TDS	Total Dissolved Solid
TTD	Transit Time Distribution Functions
TU	Tritium Unit
UNDP	United Nations Development Programme
VCDT	Vienna-Canyon Diablo Troilite
VPDB	Vienna Pee Dee Belemnite
VSMOW	Vienna Standard Mean Ocean Water
WHO	World Health Organization

CONTENTS

LIST OF FIGURES

LIST OF TABLES

CHAPTER 6

Summary and scope of the future study

6.1 Summary

The integrated isotope geochemical assessment of the three geothermal areas in India having entirely different geological settings provides very unique information regarding their origin, geochemical evolution, source of the solutes, mixing phenomenon, residence time and subsurface reservoir temperature. The comparative analysis of all the three geothermal areas has been given in table 6.1. The major salient features of this study are:

(1) All the thermal springs found in the Tural-Rajwadi (Deccan Trap region), Godavari Valley (Sedimentary formation) and Uttarakhand region (Himalayan belt) are meteoric in origin. Based on the isotopic evidence the probability of magmatic water is found to be negligible even in the Uttarakhand geothermal region which is a part of tectonically active Himalayan geothermal system.

(2) Tural-Rajwadi geothermal area located near the sea shows comparatively enriched stable isotopic value than the Godavari valley geothermal area which is situated deep inside the island (continental effect).

(3) Among all the three geothermal areas, Uttarakhand geothermal area shows most depleted stable isotopic values due to its high altitude. Stable isotopic variation among the various thermal springs in the Uttarakhand region is ascribed due to their different recharge altitude. Badrinath thermal water (BTHS-1) has the most depleted isotopic signature due to its highest altitude of recharge.

(4) Oxygen-18 isotopic shift is observed only in the Tural-Rajwadi geothermal area probably due to the significant rock-water interaction at elevated temperature over longer duration. (5) Geochemically thermal waters in the Tural-Rajwadi region are more mature (Na-Cl type) compared to the thermal waters in Godvari valley and Uttarkkand region (bicarbonate type).

(6) Geochemical evolution of the thermal waters in these three areas is identified using various graphical plots and statistical techniques.

(7) Application of the lumped parameter models (LPM) along with the tritium time series data in precipitation are found to be very useful in constraining the mean transit time (MTT) of the thermal water. In Tural-Rajwadi geothermal area, this method especially helps to estimate the MTT of the younger fraction present in the mixed thermal water.

(8) Tritium dating also allows in quantifying the extent of mixing of the thermal water with the non-thermal water. The highest extent of mixing is observed in the Tapoban thermal spring (THS-1) of Uttarakhand geothermal area.

(9) Carbon-14 dating technique helps to estimate the transit time of the very old thermal water present in the Tural-Rajwadi and the Godavari valley geothermal area.

(10) Among the three geothermal areas investigated in this study, the thermal waters from the Uttarakhand geothermal area have the least transit time (range varies from 40 to 112 years) i.e. they represent the most younger geothermal system. On the other hand, the geothermal systems from the peninsular India i.e. Tural-Rajwadi (rang varies from 6000 to 15000 years) and Godavari valley (range varies from 9900 to 18600 years) contains much more old thermal waters.

(11) Chemical geothermometers, mixing models as well as multicomponent geothermometry technique have been simultaneously applied to better constrain the reservoir temperature. Among the various chemical geothermometers, only the quartz geothermometer provides somewhat reliable estimation of reservoir temperature in all the three geothermal areas. Cation geothermometer, namely Na-K geothermometer is applicable only in the Tural-Rajwadi geothermal area due to the probable attainment of the respective mineral equilibrium. However

integrated multicomponent solute geothermometry technique carried out by the GeoT computer code is found to be most effective technique in estimating the reservoir temperature of these medium enthalpy geothermal fields. The subsurface reservoir temperature is found to be highest in the Tural-Rajwadi geothermal area (160° ± 10 °C) whereas the estimated reservoir temperature in Uttarakhand and Godavari valley geothermal area is found to be similar (~130 ± 10 °C).

Table 6.1 *Comparative analysis of three geothermal areas*

	Tural - Rajwadi, Maharashtra	**Godavari valley, Telengana**	**Chamoli, Uttarakhand**
Formation	**Granitic**	**Sedimentary**	**Quartzite**
Surface Temperature	**54-61 °C**	**50-75 °C**	**56-92 °C**
Reservoir Temperature	**~160 °C**	**~ 130 ± 10 °C**	**~130 ± 5 °C**
Geochemical nature	**Na-Cl type**	**Na-HCO_3 type**	**Ca–Mg-HCO_3 type**
Origin	**Meteoric**	**Meteoric**	**Meteoric**
Stable isotope	**$\delta^{18}O$: -1 to -2‰ $\delta^{2}H$: -7to -10 ‰**	**$\delta^{18}O$: -2 to -3‰ $\delta^{2}H$: -13 to -18 ‰**	**$\delta^{18}O$: -9 to -11 ‰ $\delta^{2}H$: -61 to -86 ‰**
Tritium	**0.8 to 1.2 TU**	**0.6 to 1.4 TU**	**3.6 to 7.5 TU**
Transit time	**~ 13500 years BP**	**~ 11400 year to 18600 year BP**	**40-110 year BP**

(12) Although the estimated reservoir temperature of the Uttarakhand and Godavari valley geothermal area is found to be similar, the surface discharge temperatures of the thermal springs are found to be highest in the Uttarakhand region which can be ascribed to the rapid circulation (less transit time) of the thermal waters through faults and fractures resulting less amount of conductive heat loss. On the other hand the conductive heat loss is found to be highest in the Tural-Rajwadi geothermal area.

6.2 Future scope of the study

The future scope of this work involves the periodic analysis of the both stable and radioactive isotopes which is very essential to know the long term variation in their concentrations. The quantification of the rock-water interaction needs to be carried out in the Tural-Rajwadi geothermal area to find out the possible correlation with the oxygen-18 shift observed in the thermal waters. In future, efforts would be made to explore the application of various isotope geothermometers (like sulphate-water geothermometer) which will further narrow down the uncertainties in the temperature estimation of the geothermal reservoir. Apart from these, the geophysical studies as well as shallow and deep drilling need to be performed to further explore the geothermal resources in these areas.

SYNOPSIS

The term ‘Geothermal’ is essentially composed of two Greek words - ‘geo’ means earth and ‘therme’ means heat. Thus geothermal energy is basically the thermal energy stored in the earth which can be exploited in many ways from generating the electricity to simple space heating purpose. Geothermal electricity provides an affordable and sustainable solution to reduce dependency on fossil fuels and several countries like USA, Philippines, Indonesia, New Zealand, Mexico, Iceland, Turkey, El Salvador, Costa Rica, Italy, Japan, Kenya etc. are tapping the geothermal resource to generate electricity. Currently the amount of geothermal electricity produced worldwide is 73,689 GWh [1]. Apart from generating electricity, geothermal energy is also used in various direct applications such as heat pumps, space heating, greenhouse heating, aquaculture pond heating, agricultural drying, industrial uses, bathing and swimming, snow melting etc. Till 2010, the total utilization of geothermal energy worldwide in various direct applications is estimated to be 4, 23,830 TJ/year [2]. The existence of the geothermal source is manifested by the presence of thermal waters, mud pots and/or fumaroles. Geothermal fields are found throughout the world having wide range of geological, hydrological and geophysical characteristics. India also has a vast resource of thermal manifestations. Till now around 400 thermal sprouts have been identified and they are grouped in seven geothermal provinces i.e. Himalaya, Sohana, SONATA (Son-Narmada-Tapti), Cambey, West Coast, Godavari and Mahanadi [3]. Although geological, hydrogeological and geophysical characterizations of various geothermal fields in India have started way back from 1970’s there is a lack of exhaustive isotopic investigation in most of the geothermal sites. Isotope technique has become an indispensible tool in characterizing the thermal fluids since the widespread use of mass spectrometer in 1960’s [4, 5, 6, 7, 8]. Application of isotopes (both stable and radiogenic) is found to be very useful in providing

vital information about the origin of thermal fluid, identifying possible recharge area, mixing between waters of different temperature and origins, source of the solutes dissolved in the thermal fluids, subsurface circulation time of the thermal waters and estimation of subsurface reservoir temperature. Among different stable isotopes, the variations in the $^{18}O/^{16}O$, $^{2}H/^{1}H$, $^{13}C/^{12}C$, $^{34}S/^{32}S$, $^{11}B/^{10}B$ and $^{87}Sr/^{86}Sr$ isotopic ratio have been widely used in accessing different hydrological characteristics of thermal fluids. $^{18}O/^{16}O$ and $^{2}H/^{1}H$ ratio are generally used to identify the source and origin of thermal water, evaluate the mixing phenomenon between the thermal and non-thermal water, indicate the vapor separation process and quantify the isotopic fractionation during boiling of thermal fluids (if boiling happens). ^{13}C of dissolved inorganic carbon (DIC) elucidates the source of DIC in the water. Similarly sulphur ($^{34}S/^{32}S$) and boron ($^{11}B/^{10}B$) isotopic ratio acts as a good tracer to find the source of dissolved sulfate and boron respectively in the thermal waters. Sr ($^{87}Sr/^{86}Sr$) isotopes act as a powerful tool to identify the rock-water interaction and puts better constraint about the type of the reservoir rocks. Among radioactive isotopes, tritium (^{3}H) is used mainly for dating of waters and to quantify the extent of mixing between thermal and non-thermal water. Carbon-14 is generally used for dating of very old thermal waters which contains negligible tritium concentrations. Thus simultaneous application of multiple isotopes is found to be extremely useful in characterizing various hydrological phenomenons such as mixing, boiling etc., that thermal waters undergo during its ascent towards the surface as well as deducing the source of the dissolved solutes in thermal waters.

Apart from isotopic analysis, chemical analysis of the thermal waters also plays a major role in the exploration and further planning to exploit the geothermal resources. The principal purpose of the geochemical analysis is to predict the subsurface reservoir temperature of the geothermal systems by using various chemical geothermometers. The basic principle of chemical geothermometers is that aqueous concentrations of certain

chemical components show temperature dependent equilibrium with the minerals in the aquifer rock. Two types of chemical geothermometers are commonly employed: silica geothermometer and cation geothermometer. Silica geothermometer is based on experimentally determined variations in the solubility of different silica species as a function of temperature and pressure. Quartz geothermometer and chalcedony geothermometer are the two main variants of the silica geothermometers. On the other hand the cation geothermometers are based on the partitioning of alkali ions between solid and liquid phases-

$$K^+ + Na\text{- feldspar} = Na^+ + K\text{-feldspar}$$

Cation geothermometer can be Na-K, Na-K-Ca, Na-K-Ca-Mg, Na-Li and K-Mg types. Different geothermometers are found to be valid in different temperature range and their equilibration rates also vary significantly. Good conformity in the temperature estimates obtained from various geothermometers points out to the probable range of subsurface reservoir temperature. Thus integrated isotope-geochemical characterization of geothermal resources is absolutely imperative in the exploration of geothermal resources as this information is very vital for deciding the future course of exploiting thermal fluids. In this thesis work, isotope-geochemical characterization has been carried out in three geothermal fields namely Tural-Rajwadi geothermal area of West Coast geothermal province, Manuguru geothermal area of Godavari valley geothermal province and Tapoban-Badrinath geothermal area of Himalayan geothermal province. Each geothermal area is located in entirely different geological settings. Achaean basement hoist the Tural-Rajwadi geothermal area, whereas Manuguru geothermal area is located in the sedimentary formation and central crystalline group of rocks forms the basement of Tapoban-Badrinath geothermal area. In-depth isotope-geochemical characterization of the thermal and non-thermal waters in these three promising geothermal areas has not been carried out before. The broad objectives of this research work is to understand the source of constituents in the thermal water and non-thermal water,

identify the hydro-geochemical processes that affects the composition of the thermal water, identification of source and origin of thermal waters, estimation of transit time of thermal waters and calculation of reservoir temperature using different chemical geothermometers, mixing models and geothermometrical modelling techniques. The thesis work has been structured into six chapters.

Chapter 1: Introduction

First chapter of the thesis gives brief description about different types of the geothermal systems, their mode of classification and utilities. An overview about the genesis of thermal waters, origin and source of dissolved solutes has been given. Although most of the thermal waters found across the globes represent recycled meteoric waters but some of them represent mixed water of various sources like sea water, river water, brines etc. Application of isotopes (both stable and radiogenic) is found to be very useful in providing information about the origin of thermal fluid, identifying possible recharge area, mixing between waters of different temperature and origins, degree of rock-water interaction, source of the solutes dissolved in the thermal fluids, subsurface circulation time of the thermal waters and estimation of subsurface reservoir temperature. Detailed description about the role of various isotopes as well as the role of chemical analysis in characterizing thermal fluids has also been elucidated. Finally overview about the different types of geothermal area and the subsequent work carried out in Indian sub-continent has also been discussed. Previous work carried out so far in the Tural-Rajwadi, Manuguru and Uttarakhand geothermal areas and the motivations for carrying out the present research work is described individually in chapter 3, chapter 4 and chapter 5 respectively.

Chapter 2: Sampling and analytical techniques

This chapter deals with the sampling and measurement protocol of various stable (^{18}O, ^{2}H, ^{13}C, ^{34}S, ^{11}B and ^{87}Sr) and radioisotopes (3H and 14C) employed in this current study.

Among these isotopes ^{18}O, ^{2}H, ^{13}C and ^{34}S were measured in isotope ratio mass spectrometer (IRMS) whereas ^{3}H and ^{14}C were measured in liquid scintillation counter (LSC). ^{11}B and ^{87}Sr isotopes were measured in inductively coupled plasma orthogonal acceleration time of flight mass spectrometer (ICP-oa-TOFMS). Apart from isotopes, measurement techniques of various major and trace elements dissolved in thermal waters are also discussed. Major cations (Na, K, Ca and Mg) and anions (Cl, SO_4) were generally measured using ion chromatography techniques whereas measurements of various trace elements like B, Sr, Li, Rb, Cs etc. were carried out using ICP-MS technique. Dissolved silica concentration was measured using ICP-OES technique whereas standard titrimetric method was used to determine carbonate and bicarbonate concentrations. Chemometric analysis such as hierarchical cluster analysis (HCA) and principal component analysis (PCA) was performed using the statistical software package XLSTAT. The geochemical program, PHREEQC, based on the thermodynamic database WATEQF was adopted to calculate the mineral saturation states of the relevant water samples [9]. Multicomponent geothermometry calculation for estimation of reservoir temperature was performed using a stand-alone computer program, GeoT (version 2.1) [10].

Chapter 3: Multi-isotope (O, H, C, B, S, Sr) and geochemical investigation in Tural-Rajwadi geothermal field, Maharashtra, India

This chapter describes the integrated isotope-geochemical characterization of Tural-Rajwadi geothermal field situated in the west coast geothermal province of India. The objectives of this study were to find out the origin of thermal waters, to estimate the residence time, to deduce the source of dissolved constituents and subsurface temperature estimation. The chapter is structured into various subsections such as background study, study area description, methodology, results and discussions. Geochemically thermal waters in Tural-

Rajwadi region were found to be of Na-Cl type i.e. old and matured water. From the $^{18}O/^{16}O$ and $^{2}H/^{1}H$ measurements, thermal waters in Tural-Rajwadi region were seen to be depleted compared to local precipitation indicating old recharge. ^{14}C dating of the thermal waters had shown that residence time of Tural thermal spring was 13500±1500 years BP (Before Present) whereas for Rajwadi spring it was 6900± 900 years BP. $\delta^{34}S$ analysis of dissolved sulphate confirmed the marine origin whereas $\delta^{13}C$ value of dissolved inorganic carbon indicated that DIC of the thermal springs was derived primarily from silicate weathering by CO_2 from the C_3 plants. The boron isotopic values ($\delta^{11}B$) were in good agreement with fluid signature derived from both sea water coupled with rock/water interaction. The $^{87}Sr/^{86}Sr$ ratios gave conclusive evidence that the thermal waters had circulated deep down to the basement and these basement rocks (archean granite) were the predominant source of dissolved strontium in the thermal waters. The average subsurface temperature in this geothermal area was estimated to be $160^0 \pm 10^0$C.

Chapter 4: Isotope-geochemical characterization of Godavari valley geothermal field of Telengana

This chapter is devoted to the isotope geochemical study carried out in Godavari valley geothermal field situated in the Manuguru area of Telangana, India. The Godavari valley geothermal field, a NNW-SSE trending graben on a precambrian platform, is filled with Gondwana sedimentary formations and contains several thermal discharges having surface temperature ranging from 37 to 81 ^{O}C. Geochemically the thermal waters were found to be Na-HCO_3 type whereas water type of non-thermal water samples varies from mixed cation (Ca, Na)-HCO_3-Cl type to mixed cation (Ca, Na, Mg)-Cl type. Among various geochemical processes, silicate weathering and ion-exchange mechanisms were found to be the major controlling factors of the solute chemistry in the study area. The carbon isotope composition of DIC ($\delta^{13}C$) also confirms the silicate weathering mechanism with soil CO_2 coming from

C3 type of plants. Calculations of mineral saturation indices carried out by the PHREEQC geochemical code indicated that thermal waters were supersaturated with respect to calcite, dolomite, aragonite, chalcedony, quartz but undersaturated with respect to gypsum. The stable isotopic signature (δ^2H, $\delta^{18}O$) of the thermal springs revealed their meteoric origin. Lower tritium concentration of the thermal springs indicated long residence times (>50 years) of the recharging waters. From the radiocarbon dating (^{14}C), the approximate residence time of the thermal waters was estimated to be 9952 yr to 18663 yr BP (before present). In this current study, subsurface temperature of Godavari valley geothermal area which falls under the category of medium enthalpy geothermal system was estimated by applying chemical geothemometers, multicomponent geothermometry and mixing models. The estimated subsurface temperature range obtained from applying the quartz geothermometers varied from 72 to 120^{O}C whereas abnormally high subsurface temperature (175-1103^{O}C) obtained from different Na-K geothermometers. To overcome this problem and to better constrain the reservoir temperature, multicomponent solute geothermometry modelling was carried out by applying the GeoT computer code. In this modelling technique, thermal water in Godavari valley geothermal field was found to attain simultaneous equilibrium with respect to minerals like quartz, chalcedony, crystobalite, magnesite, calcite etc. in the temperature range of 130±10^{0}C, which was the most probable subsurface temperature of the geothermal reservoir. The statistical approach of 'best clustering minerals' used in this model helped to overcome the problems encountered in cation or single component geothermometers applied in the medium enthalpy geothermal systems and estimated the reservoir temperature more accurately.

Chapter 5: Isotopic and geochemical fingerprinting of thermal waters in Chamoli district of Uttarakhand, India.

This chapter is mainly focused on the isotopic as well as geochemical investigation of thermal and non-thermal waters found in the Chamoli district of Uttarakhand, India. Thermal manifestations in Uttarakhand state were mainly centered around the Badrinath and Tapoban area, Chamoli district at an elevation of 1700-3200 m above mean sea level. Geothermal activity in this area was manifested by the cluster of several thermal springs (46-92^{0}C). The thermal waters were mainly Ca-Mg-HCO_3 type with moderate silica and TDS concentrations. Stable isotopes ($\delta^{18}O$, δ^2H) data confirmed the meteoric origin of the thermal waters with no oxygen-18 shift. Lumped parameter models (LPM) were used in this study to calculate the mean residence time of the thermal fluids using tritium concentrations in both precipitation and thermal water. The estimated mean transit time of the Tapoban thermal water is found to be between 40 to 44 years whereas for Badrinath thermal water it ranges from 102 to 112 years. Among the different classical geothermometers, none of the cationic geothermometer was found to be useful to estimate subsurface reservoir temperature as all the thermal waters fall in the 'immature region' of the Na-K-Mg ternary diagram. Quartz geothermometry provided a wide range (96-140^{0}C) of base temperature. Reservoir temperature was estimated using multicomponent solute geothermometry by applying GeoT computer code. GeoT modelling results suggested that thermal waters had attained simultaneous equilibrium with respect to minerals like calcite, quartz, chalcedony, brucite, tridymite, crystobalite, talc etc. in the temperature range of 130 ± 5^{0}C which could be taken as the most probable subsurface temperature of the geothermal reservoir.

Chapter 6: Summary and Scope of future study

This chapter summarizes the results of the studies carried out as a part of this thesis. The important outcomes of the study are following:

(i) The present work conclusively proves the meteoric origin of the thermal springs in all the three study area. No component of magmatic water is found even in the Uttarakhand geothermal field which is a part of tectonically active Himalyan geothermal province.

(ii) Stable isotopic variation in Himalayan thermal springs is due to their different recharge altitude. Thermal springs having higher the recharge showed depleted isotopic composition.

(iii) Simultaneous use of tritium and C-14 helped to deduce the transit time very effectively. Among all the three geothermal areas, thermal springs in the Uttarakhand geothermal area showed least transit time i.e. they represent most younger geothermal systems.

(iv) Among all the chemical geothermometers, quartz geothermometer provides somewhat reliable base temperature. However, multicomponent geothermometry (GeoT) modelling was found to most effective in constraining the subsurface reservoir temperature of these medium enthalpy geothermal systems

The future study involves periodic analysis of stable isotopes which is very essential to know the long term variation in the isotopic characteristics of the thermal springs. Moreover extent of rock-water interaction needs to be quantified in the future to find the correlation with isotopic shift found in the Tural-Rajwadi geothermal system. In future efforts will be made to explore the application of different isotope geothermometry which will further narrow down the uncertainties in the temperature estimation of subsurface geothermal reservoir.

References

[1] "Geothermal power generation in the world 2010–2014 update report", R. Bertani, *Geothermics*, **2016**, *60***,** 31-43.

[2] "Direct utilization of geothermal energy 2010 worldwide review", J. W. Lund, D. H.Freeston, T. L. Boyd, *Geothermics*, **2011**, *40(3)***,** 159-180.

[3] "Potential Geothermal Energy Resources of India: A Review", H. K. Singh, D. Chandrasekharam, G. Trupti, P. Mohite, B. Singh, C. Varun, S. K. Sinha, *Curr Sustainable Renewable Energy Rep,* **2016**, *3*, 80–91.

[4] "Environmental isotopes in geothermal studies", C. Panichi, R. Gonfiantini, *Geothermics*, **1977**, *6(3-4)***,** 143-161.

[5] "Isotopic evidence on environments of geothermal systems", A. H. Truesdell, J. R. Hulston, *Handbook of Environmental Isotope Geochemistry; Volume 1, The Terrestrial Environment* (P. Fritz, J.-Ch. Fontes, Eds) Elsevier, Amsterdam , **1980**, 179-226.

[6] "Geochemistry and dynamics of the Yellowstone National Park hydrothermal system", R. O. Fournier, *Ann. Rev. Earth Planet. Sci. Lett.,* **1989**, *17*, 13-53.

[7] "Isotopic composition of water and steam discharges", W. F. Giggenbach, *in Application of Geochemistry in Geothermal Reservoirs Development (D'Amore F., Coordinator), UNITAR/UNDP*, **1992**, 253-273.

[8] "Stable isotope geochemistry and origin of water in sedimentary basins", Y. K. Kharaka, J. J. Thordsen, *Isotope Signatures and Sedimentary Records (N. Clauer, S.Chaudhuri, Eds) Springer-Verlag*, *Berlin*, **1992**, 411-466.

[9] "User's guide to PHREEQC (version 2) - a computer program for speciation, batch-reaction, one-dimensional transport, and inverse geochemical calculations", D. L. Parkhurst, C. A. J. Appelo, *U.S. Geological Survey Water-Resources Investigations Report*, 99–4259, **1999**.

[10] "Integrated multicomponent solute geothermometry", N. Spycher, L. Peiffer, E. Sonnenthal, G. Saldi, M. H. Reed, B. M. Kennedy, *Geothermics*, **2014**, *51*, 113–123.

CHAPTER 1

Introduction

1.1 Background

The term ‘Geothermal’ is essentially composed of two Greek words- ‘geo’ means earth and ‘therme’ means heat. Thus geothermal energy is basically the thermal energy stored in the earth which can be exploited in many ways from generating the electricity to simple space heating purpose. Geothermal electricity provides an affordable and sustainable solution to reduce dependency on the fossil fuels and several countries like USA, Philippines, Indonesia, New Zealand, Mexico, Iceland, Turkey, El Salvador, Costa Rica, Italy, Japan, Kenya etc. are tapping the geothermal resource to generate the electricity. Currently the amount of geothermal electricity produced worldwide is 73,689 GWh (Bertani, 2016). Apart from generating the electricity, geothermal energy is also used in various direct applications such as heat pumps, space heating, greenhouse heating, aquaculture pond heating, agricultural drying, industrial uses, bathing and swimming, snow melting etc. Till 2010, the total utilisation of geothermal energy worldwide in various direct applications is estimated to be 4, 23, 830 TJ/year (Lund et al., 2011). The existence of the geothermal source is manifested by the presence of thermal waters, mud pots and/or fumaroles. Geothermal fields are found throughout the world having wide range of geological, hydrological and geophysical characteristics.

1.1.1 Classification

The classification of the geothermal fields can be made based on the various parameters:

1.1.1.1 Reservoir temperature

The reservoir temperature (or enthalpy) is one of the most important parameters in classifying the geothermal sources. The temperature used in the classification purpose is mostly the average reservoir temperature which can be measured in the exploration wells or estimated from the different geothermometers or by some other means (Hochstein, 1990). However

there is no universal agreement regarding the range of temperature values. According to Benderitter and Cormy (1990), if the temperature of the reservoir is less than 100 °C, it is known as **low temperature** or **low enthalpy** geothermal system. In **medium enthalpy** (or **temperature**) geothermal system, the reservoir temperature falls between 100 to 200 °C whereas in **high temperature** (or **enthalpy**) geothermal system the reservoir temperature exceeds 200 °C. Low temperature geothermal systems are typically suitable for direct applications (i.e. space heating, agricultural drying etc.) while the high temperature geothermal systems can be utilised for electricity generation. Electricity can also be generated from the medium enthalpy geothermal sources by using the binary cycle.

1.1.1.2 Fluid type

Based on the composition of reservoir fluids, geothermal fields can further be classified as **liquid dominated** or **vapour dominated**. The liquid dominated geothermal areas are commonly observed whereas the occurrence of vapour dominated geothermal systems are very rare. Some of the best known vapour dominated geothermal areas are Larderello, Italy and The Geysers, USA. Apart from these types, there are also **two-phase** geothermal reservoirs where steam and water exist in different proportions

1.1.1.3 Heat Source

Geothermal systems can also be divided as **volcanogenic** and **non-volcanogenic** based on the nature of heat source. **Volcanogenic** geothermal systems are in one way or another associated with volcanic activity and the heat source is found to be magma or hot intrusion. Volcanogenic geothermal areas invariably belong to the high temperature systems. Most of them are found to be near plate boundaries while some of them can be found in the continental rift zones and hotspot environments. In **non-volcanogenic** geothermal systems the water gets heated up due to the deep circulation through faults and fractures. Non-

volcanogenic geothermal fields can be either high temperature or low temperature systems depending on the regional geothermal gradient, permeability (primary or secondary) of the rock and depth of the circulation.

Apart from the above mentioned classifications, there exits some other parameters to distinguish different geothermal systems such as dynamic (convective), static (conductive), low relief, high relief, geo-pressured and hot dry rock (HDR) system.

1.2 Genesis of thermal water

The origin of thermal water can be manifold in nature. Thermal water may be simply the meteoric water which has gained temperature due to the downward travel of several kilometres through the faults and fractures or it may represent the formation/connate water buried in the host sediments. The other sources of thermal fluids can be the evolved oceanic water, magmatic water and/or juvenile water.

Before the advent of mass spectroscopic techniques, people believed that thermal waters were magmatic in origin i.e. magmas were the source of heat and dissolved solutes in the thermal fluids (White, 1957). This long standing debate on the origin of the thermal water had largely been settled due to the pioneering work carried out by Craig and his colleagues (Craig et al., 1956; Craig, 1963) on the isotopic contents of the thermal waters. They showed that the thermal water contained deuterium signature similar to that of the local precipitation thereby conclusively establishing the meteoric origin of the thermal waters. Although majority of the thermal waters across the globe are meteoric in origin but thermal waters from many geothermal areas are also found to be originated due to the differential extent of mixing between various sources. Thermal waters along the convergent plate boundaries around the Pacific 'Ring of Fire' are found to be the mixture of 'andestic' water and local groundwater in varying proportions (Giggenbach, 1992). This 'andesitic' water is basically the recycled

seawater which has entered in to the subduction system either in the form of pore water or as the water of hydration in the clay minerals. In Las Tres Vírgenes (LTV) geothermal area of NW-Mexico, the thermal fluid is found to be the mixture of Late Pleistocene-Early Holocene meteoric water (58 to 75%) and fossil seawater (25 to 42%) whereas the thermal water from nearby Cerro Prieto (CP) geothermal field is nothing but the infiltrated Colorado River water (Birkle et al., 2016). The origin of Salton Sea geothermal brine having hyper saline compositions (TDS varies from 14.7 to 26.5 wt. %) is ascribed to the hydrothermal metamorphism and the dissolution of halite and calcium sulphate from the deeply buried lacustrine evaporites (McKibben et al., 1988). Likewise the thermal water from the Cumali Seferihisar and Bodrum Karaada geothermal systems of Western Turkey is found to be deeply circulated sea water (Vengosh et al., 2002). The formation of geothermal brine in the Upper Rhine Graben is explained as the mixing between primary brine formed by evaporation of seawater (probably until the stage of halite precipitation) with the dilute meteoric water having contributions from halite dissolution in the Triassic period (Sanjuan et al., 2016). Juvenile water can be another source of thermal waters (White, 1986). Juvenile water is classified as the water that has never appeared at the Earth's surface or circulated in the atmosphere. Most of the information about the D/H ratio of juvenile water comes from the study of oceanic basalts (Craig and Lupton, 1976). Since hydrogen escapes rapidly from the earth's atmosphere compared to deuterium so oceans should be enriched in deuterium relative to the juvenile water from the mantle (Craig and Lupton, 1976). However the obtained δD values (-80 ± 5 ‰) from the MORBs, Hawaiian submarine and subaerial tholeiites and alkali basalts are poorly constrained (Kyser and O'Neil, 1984). However the existence of juvenile ^{3}He and CO_2 clearly suggests the existence of juvenile water but its presence in the thermal water has not been identified conclusively till date (Ármannsson and Fridriksson, 2009).

Likewise there are other geothermal systems which do not exhibit simple meteoric origin and multi-isotope tracing along with geochemical characterisation is essential to idemtify the genesis of such mixed thermal waters. A conceptual diagram showing the various sources of thermal waters is shown in the Fig. 1.1

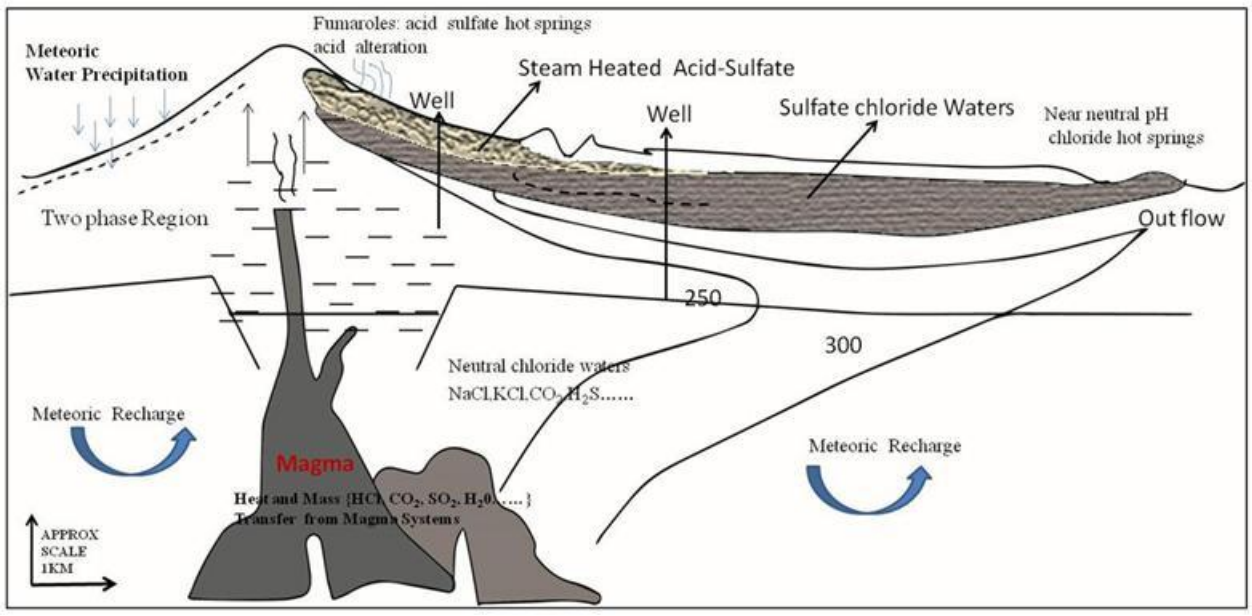

Fig. 1.1 *Conceptual diagram showing the various sources of thermal waters in a liquid dominated geothermal system* (modified after Nicholson, 1993)

1.3 Origin and classification of solutes

Chemical composition of the thermal water is generally seen to be characteristically different from that of the local non-thermal groundwater system which had prompted earlier researchers to presume magma as the only source of dissolved solutes in the thermal water. However this assumption was proved to be wrong when Craig (1963) demonstrated that the thermal waters were generally meteoric in origin and could not be magmatic. Later Ellis & Mahon (1964, 1967) and Mahon (1967), through their classic rock-water experimental studies showed that all the dissolved solutes in the thermal water can be derived from the progressive rock-water reaction between the interacting groundwater and host mineral suites. Similarly

Bischoff et al. (1981) showed that the chemical compositions of seawater influenced geothermal systems found in the Iceland area, could be reproduced by carrying experiment with seawater and basalt. All these studies essentially point out the rock-water interaction as the major source of most of the dissolved constituents however mixing with the formation water and/or seawater or magmatic water can significantly alter the final composition of the thermal waters. Chloride, boron, sulphur, fluoride, carbon, hydrogen along with many other elements generally exists in magmas as fugitive components which leave the magma during the process of degassing and eventually comes in the solution. In Wairakei geothermal area, New Zealand, it is found that both rock leaching and the magna degassing are the main controlling factors of the observed chloride output from the system (White, 1970). Likewise in the Krafla geothermal system of Iceland, contribution from the fugitive components of magmatic source becomes evident from the elevated concentration of the CO_2 emission from the discharging well and fumaroles just few months after the volcanic eruption (Armannsson et al., 1982).

Apart from the contribution from different sources, there exist two other important yet competing processes that make the relative proportion of the dissolved constituents in the thermal waters quite different than that of the interacting rocks. The first process is the dissolution of the primary rock minerals while the other one is the precipitation of the secondary minerals. Dissolution of the primary rock minerals increases the concentration of the solutes whereas the precipitation of secondary minerals tends to remove them from the solution. The interplay of both these processes ultimately determines the overall concentration of the solutes.

The dissolved constituents in the thermal waters can be broadly classified in to two categories: as **conservative** and **reactive** constituents. **Conservative** constituents are also known as non-reactive, incompatible or inert species. They generally serve as ideal tracers

because once added in the liquid phase, they remain unchanged thereby providing information about their own origin as well as source of the parent liquids (allowing their origin to be traced back to their source components). Cl, B, Li, Rb, Cs, N_2, He, Ar etc.are some of the dissolved constituents which are widely considered as **conservative** tracers in the thermal waters. However conservative behaviour of these elements varies greatly depending upon the geological setting of the thermal area. In Geyser geothermal area of Iceland, lithium does not act as conservative element due to its uptake in the secondary minerals (Arnorsson, 2000). Similarly in New Zealand geothermal system, rubidium (Rb) is found to be incorporated in illite at high temperature (> 300 °C) whereas caesium (Cs) gets incorporated in secondary zeolites at comparatively lower temperature (< 250 °C) thereby losing their conservative behaviour (Goguel, 1983). On the other hand, reactive constituents often termed as geoindicators, tend to equilibrate with the rock mineralogy and get dissolved or precipitated depending upon the change of the state of the geothermal system (i.e. temperature, pressure etc.). Na, K, Ca, Mg, SiO_2 etc. are some of the most important **reactive** components present in the thermal waters. Temperature and the mineral composition of the rock are the two important factors that effectively control the solubility of these reactive components. For example, the solubility of the dissolved silica concentration in the thermal water is controlled both by the nature of silicate minerals (i.e. quartz or chalcedony or amorphous silica) present in the host rock and the prevailing reservoir temperature of the geothermal system. Thermal waters in the Iceland region are found to be equilibrated with chalcedony at temperature below 180 °C whereas equilibrium with the quartz controls the silica concentration at temperature above 180 °C (Arnorsson, 1975). Similarly Na/K ratio has largely been governed by the exchange reaction between alkali feldspar and the Na and K concentrations present in the aqueous solution. Pure albite, k-feldspar, low albite, microcline etc. are some of the variants of alkali feldspar which are assumed to control the Na/K ratio in

geothermal system hoisted in volcanic rocks having composition ranging from basaltic to silicic in nature whereas the same Na/K ratio in the geothermal systems associated with the sedimentary rocks is governed by the exchange reaction with clays rather the alkali feldspar (Arnorsson, 2000). In addition to the above mentioned classifications, the dissolved solutes can be distinguished based on their mobility. Mobility refers to the ratio of the respective constituents present in the fluid as well as in the rocks. The fully mobile component mostly occupies the fluid phase relative to the rock. In most of the cases, conservative constituents (i.e. Cl, B etc) are found to be highly mobile.

1.4 Role of isotopes in characterizing thermal waters

Isotope technique has become an indispensible tool in characterising the thermal fluids with the rapid use of mass spectrometer since 1960's (Panichi and Gonfiantini, 1977; Truesdell and Hulston, 1980; Fournier, 1989a; Giggenbach, 1992; Kharaka and Thordsen, 1992). Application of isotopes (both stable and radiogenic) is found to be very useful in providing information about the origin of thermal fluid, identifying possible recharge area, mixing between waters having different temperature and origins, degree of rock-water interaction, source of the solutes dissolved in the thermal fluids, subsurface circulation time of the thermal waters and estimation of reservoir temperature**.** Among different stable isotopes, the variations in the $^{18}O/^{16}O$, $^{2}H/^{1}H$, $^{13}C/^{12}C$, $^{34}S/^{32}S$, $^{11}B/^{10}B$ and $^{87}Sr/^{86}Sr$ isotopic ratio have been widely used in accessing different hydrological characteristics of thermal fluids. On the other hand, radioactive environmental isotopes like tritium (^{3}H) and ^{14}C have been used mainly for estimating the residence time of the thermal waters.

1.4.1 Role of $^{18}O/^{16}O$ and $^{2}H/^{1}H$

The deuterium and oxygen-18 values of the natural waters originating from the atmospheric precipitation (not undergoing evaporation) generally follow the linear correlation:

$$\delta^2H = 8* \delta^{18}O + 10 \quad 1.1$$

The line defined by the above equation is termed as "Global Meteoric Water Line (GMWL)" (Craig, 1961) and serves as a reference line to understand many physicochemical processes (i.e. evaporation, condensation, rock-water exchange etc.). For example, Water samples that undergo evaporation fall away from the GMWL and generally have slope in the range 4 to 6. Delta ("δ") denotes the difference in isotopic ratio (R) of sample with respect to the reference standard. Due to the small value of δ, it is generally multiplied with 1000 and is reported as per mil deviation:

$$\delta = \{(R_{sample} - R_{standard})/R_{standard}\} * 1000 \quad 1.2$$

where R_{sample} = isotopic ratio ($^{18}O/^{16}O$ or $^{2}H/^{1}H$) of the sample and $R_{standard}$ = isotopic ratio $^{18}O/^{16}O$ or $^{2}H/^{1}H$) of the standard. VSMOW (Vienna Standard Mean Ocean Water) is the internationally accepted reference for measuring ^{18}O and ^{2}H in water.

The isotopic ratio of $^{18}O/^{16}O$ and $^{2}H/^{1}H$ in thermal waters are mainly used to identify the origin of the thermal water, evaluate the mixing phenomenon between thermal and non-thermal water, quantify the isotopic fractionation during stages of steam separation and estimate the reservoir temperature using isotope geothermometer.

1.4.1.1 Origin of thermal water

Prior to the development of nuclear analytical techniques, it was assumed that thermal waters were juvenile or magma derived fluids (White, 1957). But later Craig (Craig et al., 1956; Craig, 1963) showed that the thermal water had similar δ^2H signature as that of the local meteoric water. This observation essentially established that the thermal waters are nothing but the meteoric water which has gained heat during their deep subsurface circulation through faults and fractures. Although the thermal waters had same δ^2H value as that of the local

precipitation yet they exhibited positive parallel shift in $\delta^{18}O$ values as shown in the fig. 1.1. The reason for this "oxygen-18 shift" is due to the isotopic exchange that takes place between the ^{18}O atoms of the water molecule with that of the silicate or carbonate minerals present in the aquifers. The extent of this "oxygen-18 shift" is in turn depends on the various factors such as temperature of the reservoir, initial difference in isotopic ratio between rock and water, rock-water ratio, rate of circulation, porosity and residence time of the thermal water.

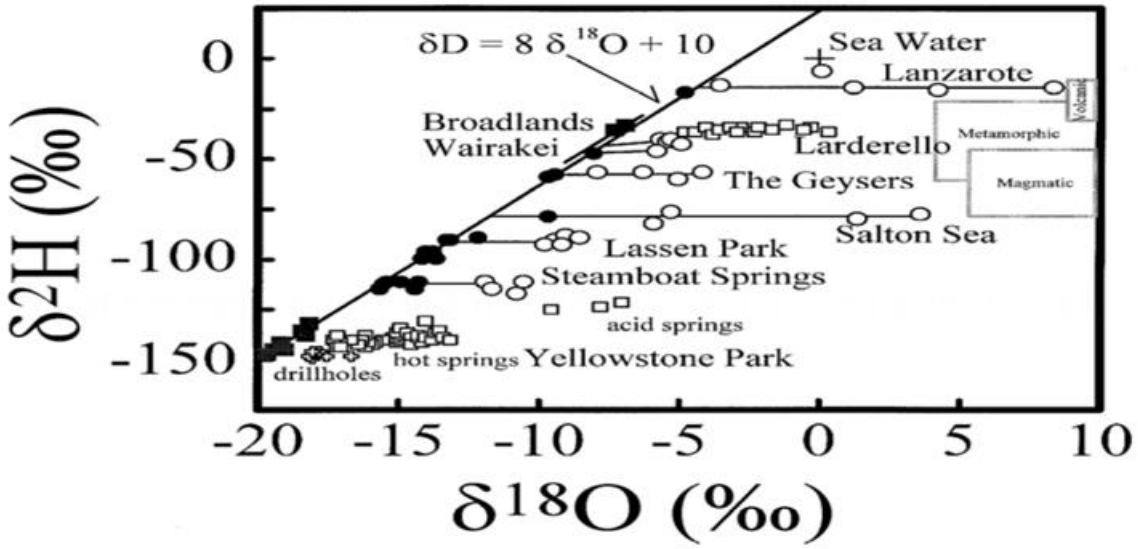

Fig. 1.2 *Oxygen-18 and deuterium compositions of hot springs (open square symbols), drillholes (plus symbol), thermal wells (open circle symbols) and local meteoric waters (filled circle and filled square symbols)* (Kharaka and Mariner, 2005)

The $\delta^{18}O$ values of the silicate and carbonate rocks are found to be considerably higher than the meteoric waters. Silicate minerals generally have $\delta^{18}O$ values in the range of ~ +8 to +12‰ VSMOW whereas carbonate minerals are more enriched in $\delta^{18}O$ having values ~ +29‰ VSMOW (Clark and Fritz, 1997). So thermal waters circulating through the carbonate aquifers are expected to have higher oxygen-18 shift compared to the silicate dominated aquifers. For example, Lanzarote and Salton Sea geothermal system, hoisted in carbonate dominated aquifer system shows highest O-18 shift compared to the other geothermal systems as shown in Fig. 1.1. On the other hand, if the geothermal system is old and/or has

high water to rock ratio, then the amount of fresh rock surface available for isotopic exchange would be very small resulting diminished oxygen-18 shift (i.e. Wairakei geothermal system with $\delta^{18}O$ shift ~ 1‰). Deuterium value of the thermal water practically remains unchanged during this rock-water isotopic exchange as most of the rocks (silicate or carbonate) contain < 1% hydrogen by mass (Kharaka & Mariner, 2005). However, in some geothermal systems concomitant change in the deuterium value has been observed along with the change in the oxygen-18 values. Few geothermal systems hoisted in the sedimentary formation or having rocks higher in clay minerals are found to undergo significant deuterium shifts (Kharaka and Thordsen, 1992; Kharaka et al., 2002). Moreover geothermal systems associated with andesitic magmatism situated in the Pacific "Ring of Fire" show enriched $\delta^{2}H$ and $\delta^{18}O$ compared to the local precipitation. This enrichment happens due to the differential extent of mixing of "andesitic water" with local precipitation (Giggenbach, 1992). Similar type of enrichment in $\delta^{2}H$ and $\delta^{18}O$ values of thermal water compared to the local meteoric water is generally found in high temperature geothermal systems where boiling and steam loss phenomenon take place (Truesdell et al., 1977). Not only that, if geothermal system gets recharged from high altitude area compared to the local precipitation or it contains "ice age" component of water (i.e. recharge took place in last glaciation age i.e. more than the 10,000 years old) then those thermal water are found to exhibit depleted deuterium content compared to the local precipitation (Arnason, 1977a; Chatterjee et al., 2017a, Chatterjee et al. 2017b). All the above examples clearly demonstrate that the variation in the deuterium isotopic signature of the thermal water depends on many factors apart from the deuterium contents of interacting rocks.

1.4.1.2 Mixing phenomenon

Deuterium and oxygen-18 act as a powerful tracer to identify the mixing phenomenon between the thermal and non-thermal water. Linear relationship between $\delta^{2}H$ and chloride is

considered as the best evidence for mixing phenomenon as both the tracers act conservatively in most of the geothermal systems. During the ascent towards the surface if the parent thermal water gets mixed with the dilute groundwater then a wide range of compositions are observed in the surrounding sprouts depending upon the extent of mixing. Such type of mixing is observed in the Long Valley, California where thermal water from a geothermal well exhibits linear relationship between δ^2H and chloride due to the mixing process (Mariner and Wiley, 1976). Similar type of linear relationship between $\delta^{18}O$ and chloride is also observed provided the oxygen-18 composition of the thermal water does not change significantly due to rock-water interaction.

1.4.1.3 Quantification of the isotopic fractionation during steam separation

In high temperature geothermal systems, thermal waters generally undergo subsurface boiling and steam separation process in varying proportions resulting significant fractionation in the isotopic composition. Steam separation processes can be classified as 'single-stage' or 'continuous' steam separation processes. In 'single-stage' steam separation process the steam and the boiling water remain in contact with each other until they get discharged at the surface whereas in 'continuous' steam separation process steam is getting continuously removed as and when formed from the residual fluid. The extent of isotopic fractionation is found to be highest in the single stage process than in the continuous stage steam separation (Truesdell et al., 1977). Deuterium and oxygen-18 isotopes are proved to be very useful in quantifying this fractionation process and identification of nature of steam separation process. The equilibrium concentration of oxygen and deuterium in the steam and water fraction depends upon the temperature. The oxygen-18 isotopes are found to be concentrated in the liquid phase below the critical point (374 °C) of the water and the rate of fractionation increases with decreasing temperature (Truesdell et al., 1977). On the other hand, below 221 °C, deuterium isotope gets concentrated in the liquid phase with deceasing temperature

whereas from 221 °C up to the critical point of the water, deuterium gets enriched in the vapour phase (Truesdell et al., 1977). The role of deuterium and oxygen-18 isotopes in delineating the single stage or multistage steam separation processes has been exemplified in the classic study carried out by Truesdell et al. (1977) in the Norris Geyser Basin of Yellowstone National Park, USA. In the Norris Geyser Basin, boiling (single stage and continuous) of the parent geothermal fluid coupled with the non-equilibrium evaporation and the mixing with the dilute groundwater have produced thermal spring waters having chloride in the range from near zero to almost 800 mg/L and deuterium value ranges from - 120‰ to -146‰ (Kharaka & Mariner, 2005). Giggenbach (1978) also conducted similar type of study in the Waikite and EL Tatio geothermal fields.

1.4.1.4 Isotope geothermometer

Fractionation of isotopes of a particular element between compounds is a temperature dependent phenomenon and therefore can potentially be used as a geothermometer. For lighter elements such as hydrogen, carbon, oxygen, sulphur etc. this fractionation is quite significant. However before application of any isotopic exchange reaction as a potential geothermometer equation, certain conditions should be fulfilled (Nicholson, 1993):

a. For exchange to take place, isotopes of that particular element must be present in two different components
b. The components should be in isotopic equilibrium
c. The rate of isotopic exchange should be fast enough to attain equilibrium compared to the residence time of the fluid
d. The degree of fractionation should preferably be detectable and vary consistently with temperature.

The general expression of isotopic fractionation between two species, A and B, is given below:

$$1000 \ln \alpha = \delta_A - \delta_B \quad (1.3)$$

where δ_A and δ_B denote the isotopic ratio in species A and B respectively α is the fractionation factor.

1.4.1.4.1 sulphate-water oxygen isotope geothermometer

The fractionation of oxygen-18 between dissolved sulphate (and bisulphate) and liquid water led to the development of sulphate-water oxygen isotope geothermometer. The equilibrium reaction is given by:

$$S^{16}O_4 + H_2{}^{18}O = S^{18}O^{16}O_3 + H_2{}^{16}O \quad (1.4)$$

This geothermometer is based on the experimentally determined fractionation factors for the sulfate-water system given by Lloyd (1968) and later by Mizutani and Rafter (1969). According to Llyod (1968), the equilibrium fractionation equation between the dissolved sulphate and water is:

$$1000 \ln \alpha_{(SO4\text{-}H2O)} = 2.88 \times 10^6/T^2 - 4.1 \quad (1.5)$$

The above equation is later modified by Mizutani and Rafter (1969):

$$1000 \ln \alpha_{(SO4\text{-}H2O)} = 3.251 \times 10^6/T^2 - 5.6 \quad (1.6)$$

The isotopic exchange rate of oxygen-18 in this pair is found to be dependent on both pH and temperature (Llyod, 1968). However for nearly neutral-chloride type of water, variation of pH does not significantly alter the equilibrium position (Mackenzie and Truesdell, 1977). The main drawback of employing this geothermometer is the addition of extraneous sulphate to the parent thermal water from various sources like oxidation of hydrogen sulphide to

sulphate, dissolution of evaporite minerals, sea water mixing etc. which may modify the isotopic composition of the dissolved sulphate thereby masking the isotopic composition of deep geothermal fluid (Sakai, 1977).

Likewise oxygen-18, fractionation of deuterium is mainly used in two isotope geothermometers: water-hydrogen gas isotope geothermometer and methane-hydrogen gas isotope geothermometer

1.4.1.4.2 Water-hydrogen gas isotope geothermometer

This geothermometer is based on the fractionation of the deuterium between the hydrogen gas and water. The equilibrium reaction is given by:

$$H_2O_{(l)} + HD_{(aq)} = HDO_{(l)} + H_{2(aq)} \quad 1.7$$

and the fractionation equation is given by (Arnorsson, 2000):

$$1000\ln \alpha_{(HD\text{-}H2O)} = 396.8 \times 10^3/T + 25.196 \times 10^6/T^2 - 284 \quad 1.8$$

The above equation is valid in the temperature range 100-400 °C for equilibrium between H_2 and steam. This isotope geothermometer was extensively and successfully used to determine the subsurface temperature in most of the Icelandic geothermal systems (Arnason, 1977b).

1.4.1.4.3 Methane-hydrogen gas isotope geothermometer

This geothermometer is based on the fractionation of deuterium between methane and hydrogen gas and is governed by the following equilibrium reaction:

$$CH_4 + HD = CH_3D + H_2 \quad 1.9$$

The temperature equation for the above geothermometer after incorporating the fractionation factor as calculated by Bottinga (1969) is given by:

$$1000\ln \alpha_{(HD\text{-}CH4)} = 288.9 \times 10^3/T + 31.86 \times 10^6/T^2 - 238.28 \quad 1.10$$

Application of the above equation to estimate the subsurface temperature of geothermal systems in Yellowstone National Park, USA and Broadlands, NZ yields significant deviation from the measured drillhole temperature (Gunter and Musgrave, 1971; Lyon, 1974). Subsequent revision of the fractionation factors leads another altogether different equation (Panichi and Gonfiantini, 1977):

$$1000\ln \alpha_{(HD\text{-}CH4)} = 181.27 \times 10^6/T^2 - 8.95 \times 10^{12}/T^4 - 90.9 \text{ (valid at } t > 200\ ^\circ C) \quad 1.11$$

This modified equation provides somewhat better agreement with the measured drillhole temperature.

1.4.2 Role of $^{13}C/^{12}C$

$^{13}C/^{12}C$ is very useful in deducing the source and evolution of the dissolved carbon in thermal fluids (both liquid and gas) because of the large variations observed in various carbon reservoirs. The most depleted carbon isotopic signature ($\delta^{13}C$) is found in the biogenic methane (up to - 80‰) whereas most enriched value is seen in the chondrite carbonate (up to + 60‰) (Fig. 1.2). $\delta^{13}C$ measurement of the dissolved inorganic carbon (DIC) in the thermal waters helps to ascertain the predominant nature of the weathering mechanism (silicate or carbonate weathering) and the source of soil CO_2 (C_3 or C_4 type of plants) (Chatterjee et al., 2017a, 2019a) whereas $\delta^{13}C$ of the associated gas phase reflects many potential sources (e.g. mantle-derived, thermal breakdown (i.e. decarbonation) of carbonate sediments, methanogenesis, oxidation of organic matter etc.) that generate the CO_2 (Ballentine et al., 1991; Lollar and Ballentine, 2009). Carbon-13 analysis of most of the gases emanating from the various geothermal fields (Ngawha, Broadlands and Tikitere**)** of New Zealand reveals their magmatic origin (Llyon and Hulston, 1984). Only Wairakei geothermal field of New Zealand shows somewhat enriched ^{13}C values in the collected CO_2 gases which happens due

to the mixing between magmatic CO_2 and the CO_2 generated from the decomposition of the crustal (greywacke) carbonate (Llyon and Hulston, 1984). ^{13}C isotopic composition of CO_2 in Icelandic gases also suggests that CO_2 is mostly magmatic in origin (Sano et al., 1985). Similar to the stable isotopic composition of the CO_2, $\delta^{13}C$ analysis of the methane gas also helps to identify the processes (i.e. thermogenic decomposition of the organic matter or microbial activity) contributing to the hydrocarbon production (Fiebag et al., 2015). $\delta^{13}C$ values of the methane gas samples collected from the Taupo Volcanic Zone (TVZ) of the New Zealand suggests high temperature decomposition of the kerogen (organic matter in the sedimentary rocks) as the main governing process (Hulston, 2004) whereas $\delta^{13}C$ of CH_4 in Icelandic geothermal gases reveals the reaction between graphite and water in magma as the predominant process (Sano et al., 1985). Similarly ^{13}C isotopic analysis of CO_2 gases in the vapour dominated Larderello geothermal field of Italy, points out to the crustal origin whereas carbon isotopes of methane indicates a complex thermogenic origin (Gherardi et al., 2005). In Larderello geothermal field of Italy, the CO_2 derived from the Paleozoic metamorphic rocks of the deeper reservoir ($\delta^{13}C < -4‰$) is found to be depleted in ^{13}C with respect to the CO_2 generated from the dolostones, anhydrites and Mesozoic carbonates which forms the upper reservoir ($\delta^{13}C$ generally $> -4‰$) (Gherardi et al., 2005).

Apart from deducing the origin of the gases, ^{13}C isotopic fractionation between CO_2 and CH_4 constitutes an important isotope geothermometer to estimate the subsurface reservoir temperature. The relevant equilibrium reaction is given below:

$$^{13}CH_4 + {}^{12}CO_2 = {}^{12}CH_4 + {}^{13}CO_2 \qquad 1.12$$

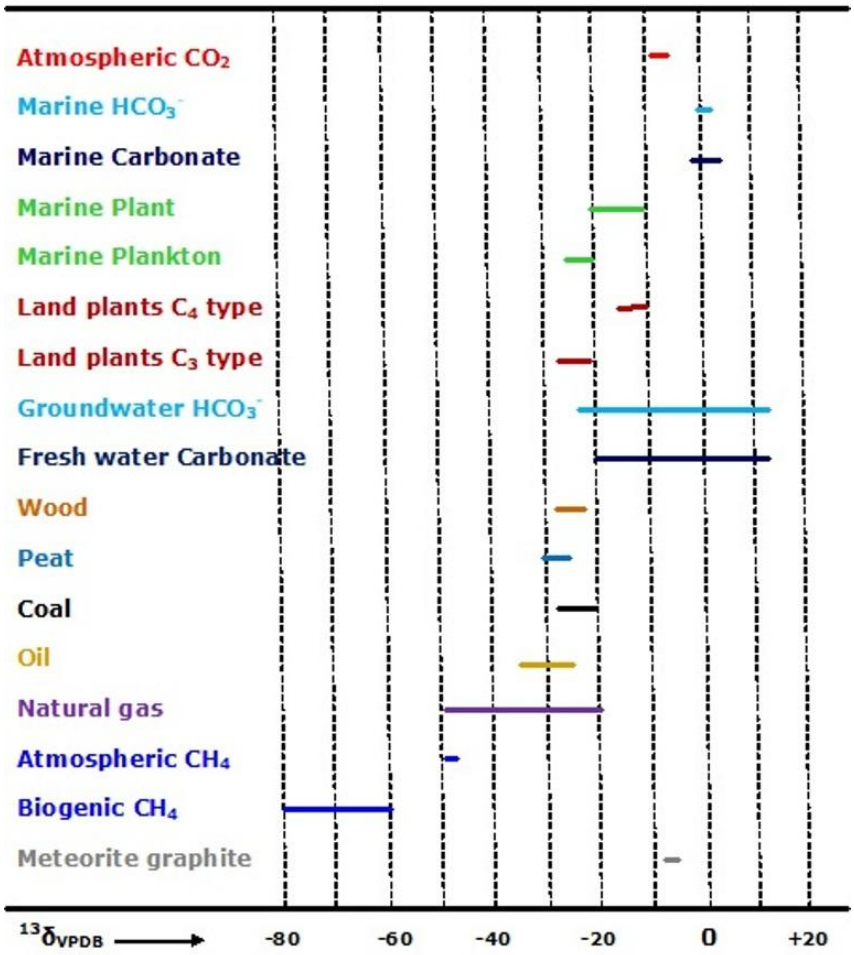

Fig. 1.3 *Range of $\delta^{13}C$ values in natural reservoirs* (modified after Clark and Fritz, 1997)

Initially this isotope geothermometer, based on the fractionation factors calculated by Urey (1947) and Craig (1953) gave reasonable estimate of subsurface temperature at the Wairaki geothermal field, New Zealand (Hulston and McCabe, 1962). Later the revised fractionation factors developed by the Bottinga (1969) and Richet et al. (1977) yielded significantly higher estimation of the reservoir temperature in several geothermal areas (Lyon, 1974; Panichi and Gonfiantini, 1977). Recently, based on the experimental calibration results of the CH_4 - CO_2 isotopic exchange reaction (Horita, 2001), a new temperature equation has been derived by Hulston (2004):

$$T\ (°C) = -91.5 + 11200/\ (10^3 \ln \alpha_{(CO2\text{-}CH4)} + 3.6) \qquad 1.13$$

which calculates the reservoir temperature more accurately in the Larderello geothermal field of Italy (Gherardi et al., 2005).

1.4.3 Role of $^{34}S/^{32}S$

Sulphur isotope ($^{34}S/^{32}S$) acts as a useful indicator to trace the origin of the dissolved sulphate in the thermal waters. The most common sources of dissolved sulphate are (Fig.1.3):

a. dissolution of sulphate containing minerals (i.e. anhydrite, gypsum etc.) which generally has enriched isotopic signature ($\delta^{34}S$) ranging from +10 to +30‰ versus VCDT (Vienna-Canyon Diablo Troilite) (Claypool et al., 1980).
b. input of marine sulphate which has nearly constant value of +20‰ versus VCDT (Longinelli and Craig, 1967).
c. contribution from sedimentary sulphide which has a wide range of largely negative $\delta^{34}S$ value, averaging mostly around ~ -12‰ versus VCDT (Bottrell and Newton, 2006; Dotsika et al., 2010).
d. anthropogenic source of sulphate having $\delta^{34}S$ value ranging from +4‰ to +6‰ versus VCDT (Karim and Veizer, 2000; Sack and Sharma, 2014).

In case of acidic thermal fluids, oxidation of the H_2S gas at the surface, hydrolysis of the magmatic SO_2 gas and hydrolysis of the native sulphur at the shallow depth are found to be main sources of dissolved sulphate. The sulphur isotopes are effectively used to differentiate among the various sources of dissolved sulphate in the acidic thermal waters found in Indonesia and Philipines geothermal areas (Abidin et al., 2005; Bayon and Ferrer, 2005).

The fractionation of sulphur isotopes between SO_4 and H_2S species also constitutes an isotope geothermometer and the corresponding equilibrium reaction is given below:

$$^{32}SO_4 + H_2{}^{34}S = {}^{34}SO_4 + H_2{}^{32}S \qquad 1.14$$

This above isotopic exchange is highly dependent on the pH, temperature and total sulphur content of the thermal fluids. Isotopic equilibrium is found to establish rapidly in acidic thermal water, whereas in alkaline or neutral conditions it may take around thousand years (Robinson, 1973; Truesdell and Hulston, 1980; Hulston, 1983). Due to non-attainment of the necessary equilibrium, this geothermometer often yields very high subsurface temperature as a result its application is rather limited (Hulston, 1983; Abidin et al., 2005).

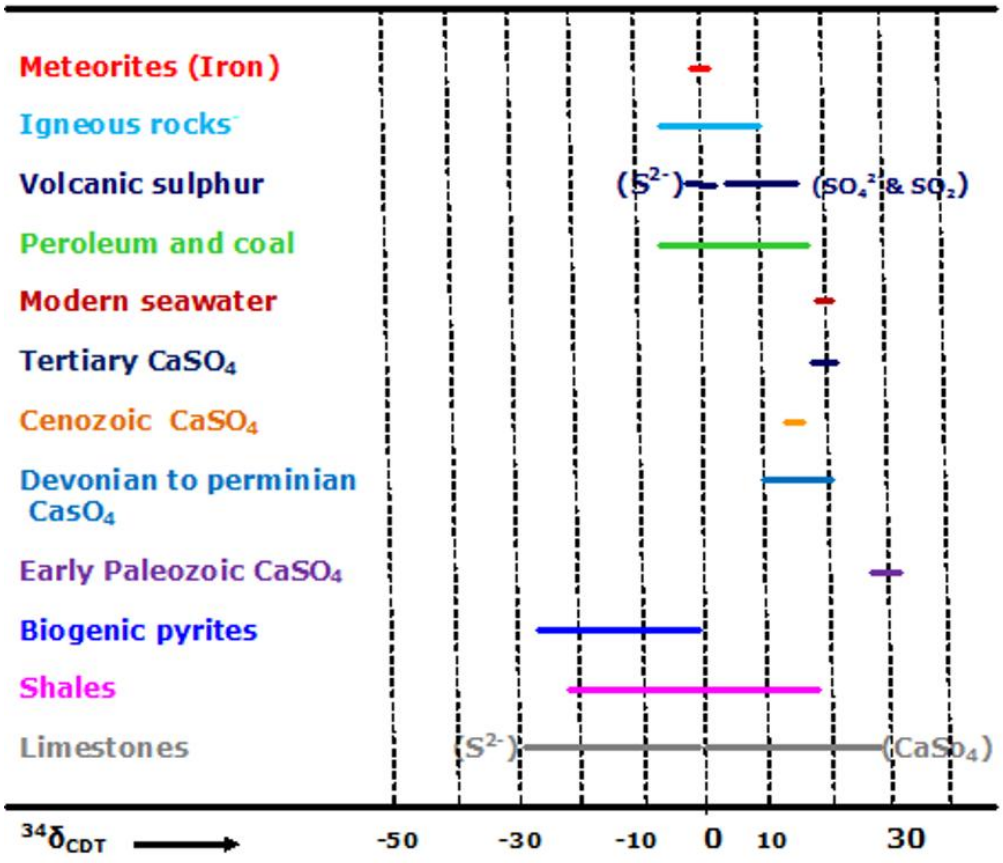

Fig. 1.4 *Range of $\delta^{34}S$ values among different species* (modified from Krouse, 1989)

1.4.4 Role of $^{11}B/^{10}B$

Boron contains two stable isotopes, ^{10}B and ^{11}B, and undergo large isotopic fractionation (as high as 27–30‰) depending upon the pH-dependent equilibrium between two trigonal species: un-dissociated boric acid $\{B(OH)_3\}$ and the tetrahedral anion, $B(OH)_4^-$. In nature, the variation of $\delta^{11}B$ ranges from -70‰ to +75‰ (Xiao et al., 2013). Some of the major sources

of dissolved boron are: granites, fresh as well as altered oceanic basalts, marine clay minerals, metamorphic rocks, sea water, non marine inputs etc. Each of these sources has distinct isotopic composition of boron (Fig. 1.4). This large isotopic variation among different natural reservoirs of boron has made it an excellent tracer to indentify the origin of dissolved boron, extent of rock-water interaction, mixing among the various sources (Dotsika et al., 2010). $\delta^{11}B$ values of thermal waters from the Central Macedonia, Greece clearly establish the non-

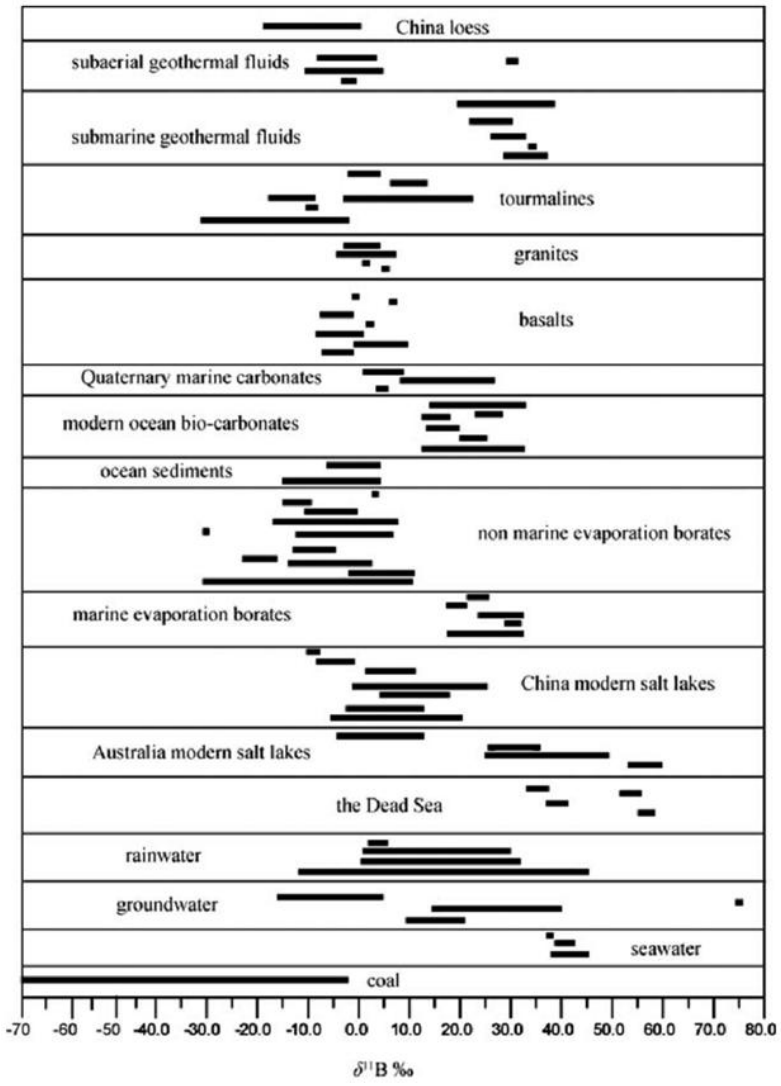

Fig. 1.5 *Range of $\delta^{11}B$ values in various reservoirs* (Xiao et al., 2013)

marine origin and deep seated circulation through the igneous rocks (Dotsika et al., 2010). Similarly using the boron isotopic value, Vengosh et al. (2002) is able to identify the origin of

Tuzla brine geothermal water in Western Turkey region. However routine use of boron isotopes is rather limited in the geothermal studies.

1.4.5 Role of $^{87}Sr/^{86}Sr$

The variation in the strontium isotopic ratio ($^{87}Sr/^{86}Sr$) among the different natural reservoirs makes it another useful geochemical tracer to understand the extent of rock-water interaction and puts better constraint about the type of reservoir rocks. Strontium isotopic ratio has also been used to calculate the rock-water ratio and identification of mixing among various Sr-bearing sources (Elderfield and Greaves, 1981; Negrel et al., 1988). Silicate and carbonate rocks, rainwater, seawater, karstic water, anthropogenic sources etc. are some of the main reservoirs of strontium which have distinct isotopic composition (Fig. 1.5) (Dotsika et al., 2010).

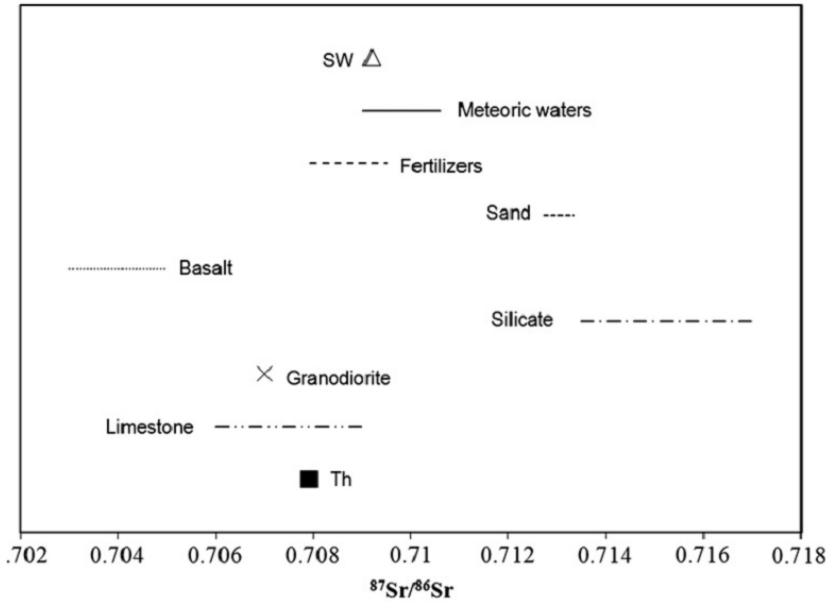

Fig. 1.6 *Range of $^{87}Sr/^{86}Sr$ ratios in various reservoirs* (Dotsika et al., 2010)

Strontium isotope geochemistry of the Icelandic geothermal systems reveals that geothermal sea water has lower $^{87}Sr/^{86}Sr$ ratio compared to the modern day sea water which has been attributed to the rock leaching followed by the partial removal into the alteration minerals

such as epidote and chlorite. The extent of rock- water equilibrium and the rock-water ratio is also computed in the Icelandic geothermal systems based on the strontium isotopic analysis (Elderfield and Greaves, 1981). Strontium isotopic ratio in the thermal waters from the Central Macedonia, Greece clearly suggests the deep seated karstic aquifers are the predominant source of dissolved strontium budget whereas shallow limestone aquifer has negligible contribution (Dotsika et al., 2010).

1.4.6 Role of ^{3}H and ^{14}C

Tritium (^{3}H) and the carbon-14 are the two most important radioactive environmental isotopes which have found some applications in the geothermal studies. These two isotopes are mainly used for age dating of the thermal waters. Tritium, a constituent of water molecule (in the form of ^{3}HHO), having half-life of 12.32 years acts as a direct tracer to understand the water movement and its transit time. Although tritium has been extensively used to estimate the transit time of non-thermal groundwater (Morgenstern et al., 2010; Cartwright and Morgenstern, 2016, 2018; Gusyev et al., 2016 and the references cited therein), its application to the geothermal systems is rather limited (Pearson and Truesdell, 1978; Shevenell and Goff, 1995; Gardner et al., 2011; Apollaro et al., 2015, 2016). Most of the thermal waters around the globe contain negligible tritium concentration due to the long subsurface residence time of the thermal waters (>50 years). However for mixed thermal water (i.e. when thermal water gets mixed with non-thermal groundwater during its ascent towards the surface), the transit time can be estimated using both tritium and appropriate modeling techniques (Chatterjee et al., 2018, 2019b).

Carbon-14 (half life of 5730 years) on the other hand can be used mainly for the dating of very old thermal waters. But in many high temperature volcanic regions, addition of ^{14}C-free metamorphic CO_2 has made the application of ^{14}C dating technique impracticable (Panichi

and Gonfiantini, 1977). Similarly in carbonate aquifers, the dilution of initial carbon-14 due to addition of the ^{14}C-free carbonate from the source rocks makes this dating technique more complicated. However in silicate dominated geothermal systems (absence of dilution by ^{14}C-free carbonate), carbon-14 dating technique can be used with some confidence to estimate the transit time of very old thermal waters (Chatterjee et al., 2019a).

Thus from the above discussion, it is clearly evident that application of multi isotope tracing is absolutely essential to characterize the thermal waters from a particular geothermal field.

1.5 Role of chemical analysis in geothermal exploration

Chemical analysis of the thermal waters performed during the various stages of exploration, development and utilization of geothermal resources is particularly useful as it provides a whole gamut of information at a relatively low cost. During the exploration phase, geochemical data is mainly used to evaluate the origin of thermal waters, determine the compositional characteristics of thermal waters, geochemical evolution during the flow path, estimate the subsurface reservoir temperature based on the chemical geothermometry. In the subsequent drilling and exploitation stage, the chemical analysis of the discharged fluids is generally used to calculate the steam to water ratios in the prevailing aquifers (if boiling happens), provide information about the quality of the thermal fluids along with its probable environmental impact to the surrounding potable water bodies, identify any significant changes in the water chemistry during the long term testing of the well discharges as well as the scaling and corrosion tendencies of the ejecting thermal fluids. The main chemical components that are usually analysed in most of the geothermal fields are pH, total dissolved solids (TDS), electrical conductivity (EC), dissolved oxygen, alkalinity, silica, cations (sodium, potassium, calcium, magnesium, iron, aluminium etc.), anions (chloride, sulphate, fluoride), trace elements (lithium, boron, strontium, rubidium etc.). In few geothermal areas

(mostly high temperature gas dominated), some major gaseous components such as CO_2, H_2S, N_2, CH_4, H_2, NH_3 etc. are also collected and analysed simultaneously. The concentration of the dissolved constituents in the thermal water is primarily controlled by the two competing reactions: dissolution of the primary rock minerals and subsequent precipitation (secondary minerals) from the solution during the ascent of thermal fluids towards the surface. Recharging water (mostly meteoric water) having low dissolved solids (TDS) generally remain undersaturated in comparison to the primary rock forming minerals. So as the rock-water interaction progresses, the dissolved solid content of the recharging water gradually increases and approaches saturation (equilibrium) with respect to the rock-forming minerals. This attainment of fluid-mineral equilibrium forms the basis of chemical geothermometers which are widely used to estimate the subsurface temperature of the geothermal reservoirs. However this assumption of attainment of equilibrium is not a universal phenomenon and is highly dependent on several factors such as: local mineralogy, subsurface temperature, residence time of the fluids, rock-water ratio. Chemical geothermometers, based on the chemical parameters of the thermal waters, are unarguably the most important geochemical tool to estimate the subsurface temperature without performing deep drilling. Chemical geothermometers can be classified in to two categories such as solute geothermometers and gas or steam geothermometers.

1.5.1 Solute geothermometers

Since 1960s, several solute geothermometers such as silica (Fournier, 1977), Na-K (Fournier, 1979a, Arnorsson, 1983, Giggenbach, 1988), Na-K-Ca (Fournier and Truesdell, 1973), K-Mg geothermometer (Giggenbach, 1988) have been developed and widely used worldwide to predict the subsurface temperature of the geothermal reservoirs. The rate of reaction of all these geothermometers is different and each of them is valid in a particular temperature range. Moreover applicability of a particular geothermometer in a specified geothermal area is

highly dependent on the aquifer mineralogy. So it is very unlikely that in a particular geological formation all of these geothermometers simultaneously will yield same temperature estimation of the geothermal reservoir.

1.5.1.1 Silica geothermometer

Dissolved silica concentration in the thermal waters is mostly controlled by the solubility of the quartz minerals except in the geothermal systems hoisted in young basaltic formation having temperatures below ~180 °C, in which the silica concentration is found to be controlled by the solubility of chalcedony, a metastable silica polymorph (Arnorsson, 1975; Arnorsson et al., 1982). Based on the extensive experimental data on the solubility of the quartz from low temperature and pressure to high temperature, several quartz geothermometric equations have been developed (Fournier, 1977; Fournier and Potter, 1982a; 1982b). However the most commonly used equation is:

$$T\,(°C) = 1309 / (5.19 - \log SiO_2) - 273.15 \qquad \text{Fournier (1977)} \qquad 1.15$$

where silica concentration is expressed in mg/L unit. The above equation is applicable to the thermal water which gets cooled solely by the conduction mechanism. However for vigorously boiling springs and well discharges when there is a substantial loss of steam due to the boiling (resulting increase in the silica concentrations), the following quartz geothermometric equation is applicable:

$$T\,(°C) = 1522 / (5.75 - \log SiO_2) - 273.15 \qquad \text{Fournier (1977)} \qquad 1.16$$

Chalcedony, another polymorph of silica, is found to control the solubility of dissolved silica in the thermal waters of Iceland when reservoir temperature is below ~180 °C (Arnorsson, 1975) and the governing equation is:

$$T\,(°C) = 1112 / (4.91 - \log SiO_2) - 273.15 \qquad \text{Arnorsson (1983)} \qquad 1.17$$

However if the reservoir temperature calculated by the chalcedeony geothermometer falls below 100 °C then the amorphous silica controls the dissolved silica concentration (Karingithi, 2009). The corresponding equation is given below:

$$T\ (°C) = 731 / (4.52 - \log SiO_2) - 273.15 \qquad \text{Fournier (1977)} \qquad 1.18$$

In low pH thermal water (i.e. CO_2 rich water), amorphous silica mainly controls the dissolved silica concentration as the solubility of quartz and chalcedony cannot cope with the rate of dissolution of the silicate minerals in such systems.

As the silica geothermometer is dependent on the absolute concentration rather than the ratio of the concentrations, so it gets easily affected by the various processes such as boiling and the mixing with the non-thermal water etc. Due to the boiling and steam separation, the residual fluid becomes concentrated in the dissolved silica resulting overestimation of the reservoir temperature. Similarly when thermal water gets mixed with the cold water, the estimated reservoir temperature often gives underestimated values.

1.5.1.2 Na-K geothermometer

Na-K geothermometer is based on the temperature dependent ion-exchange reaction given below:

$$NaAlSi_3O_8 + K^- = KAlSi_3O_8 + Na^+ \qquad 1.19$$

Early observation of low Na/K ratio associated with the high temperature major upflow regions in the Wairakei geothermal field of New Zealand, led to the development of Na-K geothermometers (Ellis and Wilson, 1960) and subsequently many experimentally calibrated Na-K geothermometry equations have been derived by several researchers (Fournier, 1979a; Arnorsson, 1983; Giggenbach, 1988; Tonani, 1980; Nieva and Nieva, 1987). The Na/K geothermometer based on the exchange reaction between low albite and microcline is found

to be suitable in the Icelandic geothermal systems which are hoisted in the volcanic rocks having composition ranging from basaltic to silicic in nature (Arnorsson and Stefansson, 1999). This Na-K geothermometer works well when reservoir temperature lies in the range of 180-350 °C and gives anomalous results at low temperature notably less than 120 °C (Ellis, 1979). Contrary to the silica geothermometer, as Na-K geothermometer is based on the concentration ratio so it gets less affected by dilution or boiling phenomenon. However in case of ammonia rich this Na-K geothermometer is found to give erroneous estimate of reservoir temperature (Fournier, 1989b).

1.5.1.3 Na-K-Ca geothermometer

Na-K-Ca geothermometer, developed by Fournier and Truesdell (1973) is found to be successful in estimating reservoir temperature of thermal waters having high calcium concentration provided calcite does not get precipitated out from the solution. The main advantage of this empirically calibrated geothermometer is that unlike silica or Na-K geothermometers, it provides somewhat reliable estimate of subsurface temperature for low temperature, non-equilibrated geothermal systems. Two major factors which affect this geothermometer are the partial pressure of the CO_2 (P_{CO2}) and the high amount of dissolved magnesium (> 1mg/kg) concentration (Fournier and Potter, 1979). Despite having several drawbacks (Arnorsson et al., 1983; Benjamin et al., 1983), Na-K-Ca geothermometer has proved to be an effective tool in geothermal exploration technique (Nicholson, 1993).

1.5.1.4 K-Mg geothermometer

The K-Mg geothermometer, developed by Giggenbach (1988), is based on the equilibrium constant calculated for the following reaction:

$$2.8\ \text{K-feldspar} + 1.6\ \text{Water} + Mg^{2+} = 0.8\text{K-mica} + 0.2\text{chlorite} + 5.4\text{quartz} + 2K^{+} \qquad 1.20$$

and the corresponding temperature equation is given as:

$$T\ (°C) = 4410 / [(14.00 - \log (K^2/Mg)] - 273.15 \quad 1.21$$

This geothermometer is generally used in low to medium enthalpy geothermal systems where Na-K and Na-K-Ca geothermometers are not applicable due to non-attainment of equilibrium with respect to alkali feldspars.

1.5.1.5 Na-K-Mg geothermometer

Na-K-Mg geothermometer is basically the combination of both Na-K and K-Mg geothermometers. Combining both the Na-K and K-Mg ratios, Giggenbach (1988) first used this geothermometer in the form of a ternary diagram to estimate the reservoir temperature as well as to classify the thermal waters as 'fully equilibrated', 'partially equilibrated' and 'immature' waters based on the extent of equilibrium that waters have attained with the host rocks. This diagram provides an easy eye ball classification to determine whether application of cation geothermometer (specifically Na-K geothermometer) is suitable for reservoir temperature estimation. Thermal water falling in the 'immature' region is not at all suitable whether the water samples falling in the fully equilibrated region are found to be most suitable for application of cation geothermometers. The main drawback of this geothermometer lies in the fact that the K/Mg ratio changes very rapidly during cooling of the ascending geothermal water in the upflow zone compared to the Na/K ratio. As a result Na-K and K-Mg geothermometer estimate very different reservoir temperature (K-Mg geothermometer generally gives lower temperature compared to the Na-K geothermometer) of the thermal waters which have undergone significant interaction in the upflow zone.

Apart from the above mentioned ones, there are several other geothermometers like Li-Mg (Kharaka and Mariner, 1989), Na-Li (Kharaka et al., 1982; Fouillac and Michard, 1981), Na-Ca (Tonani, 1980), K-Ca (Tonani, 1980) but their applicability is found to be very limited.

1.5.2 Gas or steam geothermometers

Gas or steam geothermometers, mainly applicable in the volcanic and vapour dominated geothermal fields, are normally classified based on the gas-gas and/or mineral-gas equilibrium reaction. The development and the application of these gas geothermometers are pioneered by several researchers (Giggenbach, 1980; D'Amore and Panichi, 1980; Arnorsson and Gunnlaugsson, 1985; D'Amore, 1992; Giggenbach, 1991). Some of the widely used gas geothermometers are:

1.5.2.1 Fischer-Tropsch Geothermometer (FT)

This geothermometer is based on the thermal breakdown of methane:

$$CH_4 + 2H_2O = CO_2 + 4H_2 \qquad 1.22$$

and the corresponding temperature dependence equation is:

$$\log (P_{CO2}) + 4\log (P_{H2}) - \log (P_{CH4}) - 2\log (P_{H2O}) = 10.76 - 9323/T \text{ (where T is in °K)} \qquad 1.23$$

This geothermometer is perhaps the most widely used one due to the non-dependency of the mineral buffers and redox state of the system (Nehring and D'Amore, 1984; Arnorsson and Gunnlaugsson, 1985; Giggenbach, 1987). However the application of this geothermometer in several geothermal fields has given both underestimation as well as the overestimation of the reservoir temperature (Arnorsson and Gunnlaugsson, 1985).

1.5.2.2 CO_2-H_2S-H_2-CH_4 geothermometer

This empirical geothermometer is based on the analysed concentrations (in vol %) of CO_2, H_2S, H_2, CH_4 gases and the corresponding temperature equation is (D'Amore and Panichi, 1980):

$$T\,(°K) = 24775/\ \{2\log (CH_4/CO_2) - 6\log (H_2/CO_2) - 3\log (H_2S/CO_2) + 7\log (P_{CO2}) + 36.05\} \qquad 1.24$$

The main drawback of this geothermometer is that the partial pressure of CO_2 is arbitrarily fixed based on the relative concentration of the CO_2 present in the total gas mixture resulting mismatch in the calculated temperature in several geothermal systems (Arnorsson & Gunnlaugsson, 1985; Giggenbach, 1993; Pang and Reed, 1998).

1.5.2.3 CO_2 - geothermometer

This empirical geothermometer, developed by Arnorsson and Gunnlaugsson (1985) basically relates the amount of CO_2 with the subsurface temperature and the corresponding equation is given as:

$$\log CO_2 = 37.43 + 73192/T - 11829 \times 10^3/T^2 + 0.18923T - 86.187 \times \log T \quad 1.25$$

where T is in °K and CO_2 in moles per kg of steam. This geothermometer has been applied to both fumaroles and well discharges having temperature greater than 100 °C. The upper temperature limit of this geothermometer is governed by the stability of the calcite (calcite should not precipitate out) in the geothermal system.

1.5.2.4 CO_2-H_2 geothermometer

This geothermometer, based on the oxidation of elemental carbon, was first proposed by Nehring and D'Amore (1984) considering the following reaction:

$$2H_2O + C = 2\ H_2 + CO_2 \quad 1.26$$

The temperature estimated by this gas geothermometer matches comparatively well with temperature calculated by applying other chemical geothermometers (Na-K-Ca) in Cerro Prieto geothermal field, Mexico. However this geothermometer has not been used widely due to the absence of graphite (coal) in most of the geothermal systems.

1.5.2.5 CO - geothermometer

The reaction governing the CO geothermometer is as follows:

$$CO_2 + H_2 = CO + H_2O \quad 1.27$$

Several geothermometry equations have been developed by D'Amore et al. (1987) and Giggenbach (1987) based on the above equation. The reservoir temperature estimated by this geothermometer gives good conformity in Larderello steam samples, Italy (D'Amore et al., 1987). Giggenbach (1987) used this geothermometer in the White Island fumaroles, New Zealand. Later Chinodini and Cioni (1989) have proposed CO-geothermometer based on the new reaction:

$$CH_4 + 3CO_2 = 4CO + 2H_2O \quad 1.28$$

The other geothermometers are: Hydrogen Sulfide (H_2S) geothermometer (Arnorsson and Gunnlaugsson, 1985), Hydrogen Sulfide – Hydrogen (HSH) geothermometer (Giggenbach, 1980; Giggenbach, 1987), Nitrogen-Ammonia-Hydrogen (NAH) geothermometer (Giggenbach, 1980; Nehring and D'Amore, 1984).

1.5.2.6 CO_2/Ar – H_2/Ar geothermometer

This geothermometer is based on the gas ratio grids to overcome the difficulty associated in maintaining the constant gas/steam ratio in the samples collected from the surface. The gases that are least soluble in the water are preferably chosen to construct the ratio grids so that effects of near surface condensation, partial boiling and two-phase reservoir conditions should be minimized (Giggenbach & Goguel, 1989). Argon on the other hand is generally used as a proxy of the partial pressure of water vapor (P_{H2O}) as argon concentration in the thermal water is assumed to be same as that of the air saturated water. In the CO_2/Ar – H_2/Ar geothermometer, hydrogen and carbon dioxide geothermometers have been combined to

construct the gas ratio grids. The main drawback of this geothermometer is the possibility of air contamination in the argon concentration. The other problem is that in some geothermal systems the argon concentration deviate significantly compared to the air saturated water (Norman and Moore, 1999; Mazor and Truesdell, 1984). Despite all these uncertainties, this geothermometer is found to be quite versatile and provide reasonable estimation of reservoir temperature (Powell, 2000).

The other gas ratio geothermometers for example CO/CO_2 - CH_4/CO_2 (Giggenbach and Goguel, 1989), CO/CO_2 - H_2/Ar (Giggenbach & Glover, 1992) and H_2/Ar - CH_4/CO_2 (Giggenbach, 1993) have also been used in some of the other geothermal fields with varying degree of success. For low to medium enthalpy geothermal fields the application of these gas geothermometers are rather limited.

Basically the main purpose of applying the different geothermometers (solute as well as gas) is to predict the subsurface temperature as accurately as possible. However careful selection of the best suitable geothermometer should always be made based on the available information about the local geology, types of interacting rocks and their mineral assemblages. Good conformity among several geothermometers provides confidence in the estimated reservoir temperature.

1.6 Geothermal scenario in India

India is endowed with enormous thermal water manifestations (nearly 400 thermal springs) which are broadly distributed in seven geothermal provinces (Fig. 1.6) based on their geotectonic settings (Singh et al., 2016):

1.6.1 Himalayan geothermal province

1.6.2 West coast geothermal province

1.6.3 SONATA (Son-Narmada- Tapi) geothermal province

1.6.4 Cambay geothermal province

1.6.5 Godavari valley geothermal province

1.6.6 Mahanadi geothermal province

1.6.7 Sohana geothermal province

Earlier Krishnaswamy and Shanker (1982) had categorized twelve geothermal provinces such as:

1. Himalayan geothermal province
2. Naga-Lusai geothermal province
3. Andaman-Nicobar island geothermal province
4. Sohana geothermal province
5. Cambay geothermal province
6. West coast geothermal province
7. SONATA (Son-Narmada- Tapi) geothermal province
8. Mahanadi geothermal province
9. Godavari geothermal province
10. Damodar valley geothermal province
11. East Indian geothermal province
12. South Indian geothermal province

The main geological criteria used in classifying different geothermal provinces are (GSI, 2002):

a. Presence in orogenic region associated with Cenozoic folding
b. Occurrence in structural depression/graben (non-orogenic) which have undergone upliftment in late Tertiary and Quaternary period
c. Presence of deep fault zones having recent seismicity

d. Associated with Tertiary or Quaternary volcanic activity

Among different geothermal provinces only Himalayan geothermal province, Naga-Lusai geothermal province and Andaman-Nicobar island geothermal province fall in the orogenic belt whereas rest of the geothermal provinces fall in the non-orogenic region. The documentation work on various thermal springs spread across India started way back in 1862 when Schlagintweit (1862) attempted to enlist the explored thermal springs which was compiled later by Oldham (1882). Further preliminary study was carried out by several workers namely Ghosh (1954), Deb and Mukherjee (1969) and Krishnaswamy (1965). Their work focused mainly on the distribution pattern, recording of the surface temperature, medicinal qualities of the thermal springs. From 1970's after the recommendation of the Hot spring committee of Govt. of India, Geological survey of India (GSI) in collaboration with UNDP started systematic geological, hydrogeological and geochemical mapping of the thermal springs (GSI, 1987; GSI, 1991; GSI, 2002). For systematic survey, highest priority was accorded to Himalayan geothermal province, West coast geothermal province followed by Cambay, SONATA and Godavari valley geothermal area.

1.6.1 Himalayan geothermal province

Himalayan geothermal province falls in the orognic belt and has the highest potential to generate geothermal electricity. Some of the promising geothermal fields of Himalayan geothermal province are: Puga and Chumathang (Indus valley, Ladakh), Panamik (Nubra valley, Ladakh), Parbati and Beas valley (Himachal Pradesh), Tapoban and Badrinath area (Uttarakhand). Puga geothermal area is considered to have the highest capability for producing geothermal electricity in the Indian sub-continent. As a result, this area has been subjected to detailed geological mapping (Craig et al., 2013), isotopic analysis (Thussu, 2002; Tiwari et al., 2016), geochemical characterization (Saxena and D'Amore, 1984), resistivity

survey (Singh et al., 1983) and magnetotelluric studies (Harinarayana et al., 2004, 2006; Azeez and Harinarayana, 2007). Recently Jha and Puppala (2018) have developed a

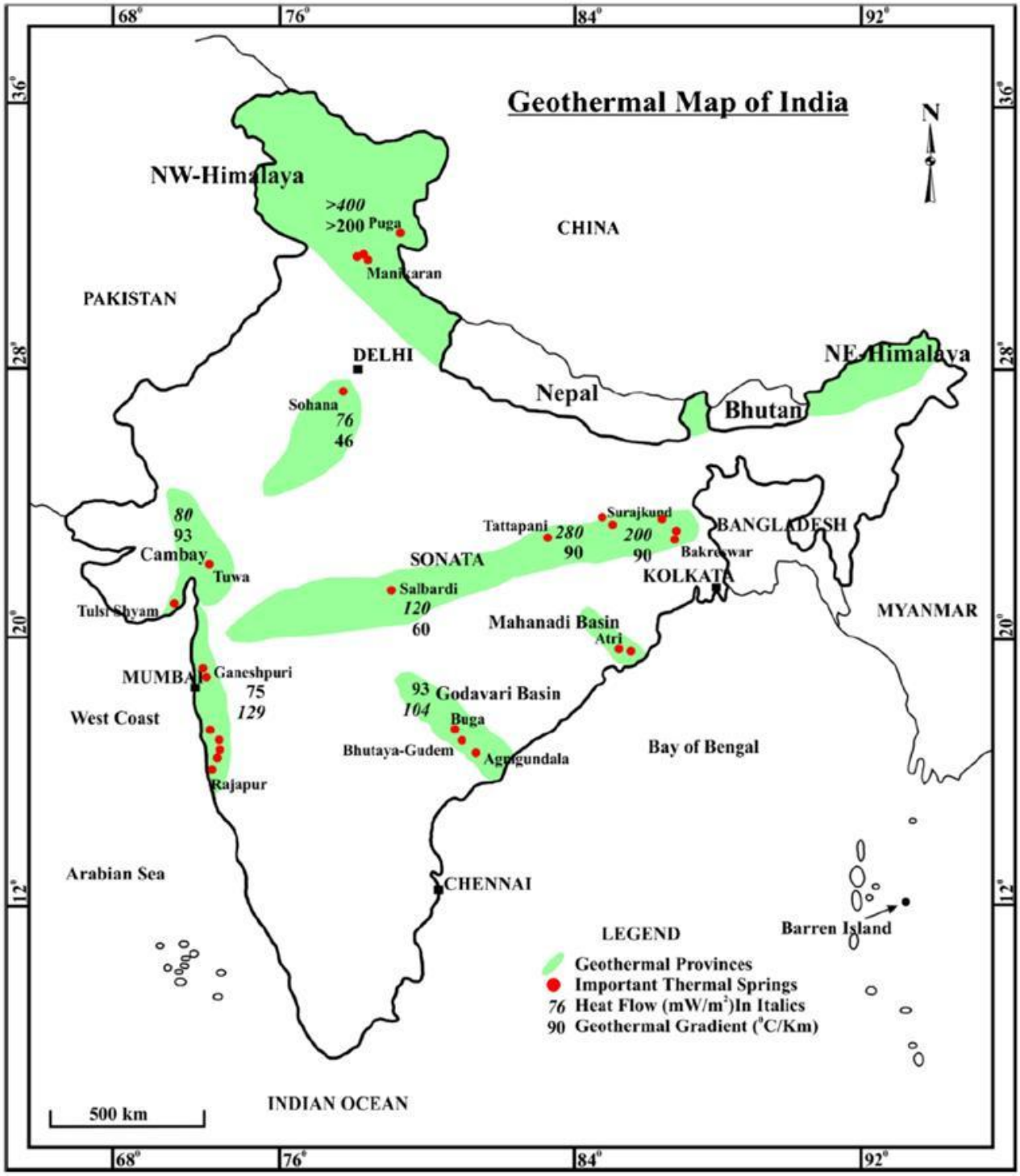

Fig. 1.7 *Major geothermal provinces in India* (Singh et al., 2016)

conceptual model to map the spatial variation of thermo-hydro-geological properties of the Puga reservoir. Reservoir temperature in Puga region estimated by chemical geothermometry is found to be ~ 250 °C (Saxena and D'Amore, 1984) while the thermal studies predict reservoir temperature of more than 220 °C at a depth of about 2.5 km (Craig et al., 2013). The primary heat source of Puga geothermal region is thought to be young granitic intrusions and shallow crustal melting processes (Gupta et al., 1983; Chandrasekharam, 2001). Stable isotopic signature suggests the meteoric origin of the thermal waters and negligible tritium concentration indicates long subsurface circulation of Puga thermal waters (Craig et al., 2013). Several studies have pointed out that it is possible to harness 5000 MWh of geothermal energy from Puga valley and it is expected to sustain a 20 MWe power plant (Craig et al., 2013). Extensive isotope and geochemical characterization studies have also been conducted on the thermal springs present in the Beas and Parbati valley of north-west Himalaya, India (Husain et al., 2020). Resistivity survey and shallow temperature measurements in this geothermal area were carried out by Kumar et al. (1982). Isotopic analysis ($\delta^{18}O$ and $\delta^{2}H$) suggests meteoric water precipitating at the higher altitude as the recharge source of Parbati valley geothermal springs (Giggenbach et al., 1983). Mixing models as well as sulphate-water oxygen isotope geothermometer predict 120–140 °C as the probable sub-surface reservoir temperature which can increase up to 160 °C at greater depths (Giggenbach et al., 1983). Salinity in few thermal discharges is explained as the mixing between saline and fresh water components (Chandrasekharam et al., 2005). Geochemical evolution of these thermal springs is elaborated by several researchers (Gupta, 1996; Cinti et al., 2009; Husain et al., 2020). Stable isotope data of few thermal springs from the Uttarakhand geothermal area indicates their meteoric origin (Sharma et al., 1996a). Tritium concentration of the thermal springs shows the presence of significant modern water component (i.e. age < 50 years) (Sharma et al., 1996a). Recently Tiwari et al. (2016, 2020)

has tried to quantify the biogenic carbon dioxide flux degassing from the Himalayan geothermal areas.

1.6.2 West coast geothermal province

Apart from Himalayan geothermal province, several researchers have also studied the geological, geochemical and tectonic aspects of the thermal springs from peninsular India. West coast geothermal province has attracted a deal of attention due to the presence of nearly sixty thermal manifestations spread across eighteen localities (Dowgiallo, 1977; Muthuraman and Mathur, 1981; Pitale et al., 1987; Muthuraman, 1987; Minissale et al., 2000; Reddy et al., 2013, Chandrasekhar et al., 2018). The West coast geothermal province falls under the Deccan trap terrain of India which was formed due to solidification of molten lava around 65 million year ago (Courtillot et al., 1999). Although most of the thermal springs circulate through Deccan basalt, some of thermal springs show evidence of circulating through the underlain basement rocks i.e. Achaean granite (Singh et al., 2016; Chandrasekhar et al., 2018). Isotopic analysis ($\delta^{18}O$ and $\delta^{2}H$) of few thermal waters (namely Sativali, Haloli, Pasupada, Akloli, Koknere) of this geothermal area reveals their meteoric origin (Minissale et al., 2000). Based on the cation and gas geothemometry the subsurface temperature in this region is estimated to vary from 120 to 150 °C (Singh et al., 2016). The analysis of the gas samples shows the presence of relatively high quantity of helium which indicates the presence of very old and deeply circulated geothermal system prevalent in this West coast area (Minissale et al., 2000).

1.6.3 SONATA geothermal province

SONATA geothermal province is another promising geothermal area due to the presence of several high temperature thermal springs along this rift system. The prominent thermal springs are: Tattapani (Chhattisgarh), Bakreswar and Tantloi (West Bengal) and Surajkund

(Jharkhand). The origin of the SONATA rift system is attributed to the interaction between two protocontinents during the development of the Indian plate (Naqvi et al., 1978). The Tattapani geothermal area, situated at the eastern flank of the SONATA rift system, comprises several thermal water manifestations having temperature ranging from 50 to 98 °C. The ENE-WSW Tattapani fault and NE-SW cross faults are found to control the geothermal activity in this area. Geochemical characteristics of the thermal springs in Tattapani geothermal area have been investigated by several researchers (Chandrasekharam and Antu, 1995; Sharma et al., 1996b). The reservoir temperature estimated by the chemical geothermometry varies from 205 to 217 °C (Chandrasekharam and Antu, 1995). The meteoric origin of these thermal springs is revealed by the stable isotope ($\delta^{18}O$ and $\delta^{2}H$) analysis (Sharma et al., 1996b). Tritium analysis of some of the thermal and non-thermal water indicates some extent of mixing in the upflow zone and the residence time of the thermal waters is estimated to be around 30-40 years (Sharma et al., 1996b). Beside that the presence of granitic intrusive at shallow depth below the Gondwana sedimentary formation makes Tattapani as well as the whole SONATA geothermal province to be one of the best sites for establishing enhanced geothermal system in India (Singh et al., 2016).

Bakreswar and Tantloi geothermal area situated in the extreme eastern part of the SONATA rift zone is characterized by the presence of a cluster of thermal water springs with surface temperature varying from 45 to 71 °C. The chemical analysis of the thermal springs in this region does not exhibit any significant spatial and temporal variation in composition during the last several decades (Chowdhury et al., 1964; Deb and Mukherjee, 1969; Mukhopadhyay, 1996). Stable isotope data clearly suggests the meteoric origin of thermal waters whereas negligible tritium concentration of thermal springs indicates long subsurface circulation time (Majumdar et al., 2005). Dissolution of the fluorite mineral is thought to be responsible for higher concentration of dissolved fluoride in the thermal water (Majumdar et al., 2009).

Chemical geothermometers suggest 100 ± 5 °C as the most probable reservoir temperature in the Bakreswar and Tantloi geothermal area. High helium content, low Kr/Xe ratio and very low $\delta^{15}N$ value are some of the additional important characteristics of this geothermal area (Majumdar et al., 2009).

Surajkund geothermal area, located in the Jharkhand state and a part of SONATA rift system has same geological settings as that of the Bakreswar and Tantloi geothermal area. Surface temperature of the thermal springs in this area ranges from 40 to 89 °C. Geochemical analysis coupled with multivariate statistical analysis (PCA and correlation analysis) and isotopic characterization has recently been carried out by Singh et al. (2020). Application of quartz and cation geothermometer has provided a wide range (116 to 188 °C) of subsurface reservoir temperature in this region.

1.6.4 Cambay geothermal province

Cambay basin also hoists several thermal springs spread over both Gujarat and Rajasthan state of India. Cambay basin, a rift basin formed during the Late Cretaceous period, is bound on the east as well as on the west direction by two deep seated N-S oriented faults (Singh et al., 2016). Surface emergence temperature of the thermal springs in the Gujarat region varies from 40 to 93 °C whereas in Rajasthan area surface temperature ranges from 35 to 47 °C. The extensive chemical and isotope studies carried out in the Cambay basin reveal that although these deep seated thermal waters are predominantly meteoric in origin but there may be some mixing with fresh or connate sea water which might have been percolated though the various faults bordering the Cambay basin (Minissale et al., 2003). Chemical geothermometers estimate ~150 °C as the maximum subsurface temperature in this region. The isotopic analysis of the associated helium gas shows predominantly crustal $^{3}He/^{4}He$ values thus negating any contribution from mantle helium (Minissale et al., 2003).

1.6.5 Godavari valley geothermal province

Godavari valley geothermal province, a NNW-SSE oriented graben structure hoists several thermal discharges with surface temperature ranging from 36 to 80 °C. This area falls within zone II (100 - 180 mW/m^2) region on the heat flow map of India having thermal gradient of 60 °C/km (Ravi Shanker, 1988). Geochemical analysis of some of the thermal springs in this region was reported earlier by Saxena and Gupta (1985) and later by Chandrasekharam et al. (1996). Saxena and Gupta (1985) estimated the subsurface reservoir temperature in the range of 100 to 150 °C whereas temperature estimated by Chandrasekharam et al. (1996) varied from 173 to 215 °C.

1.6.6 Mahanadi geothermal province

Mahanadi geothermal province falls in the tectonically stable non-orogenic Eastern Ghats Belt (EGB) in the Indian shield. The Eastern Ghat Belt (EGB) trending NE-SW along the coastal side of peninsular India, has formed as a result of a Neoproterozoic collisional event between east Antarctica and the Indian cratons, resulting the creation of a number of shear zones and faults (Dasgupta et al., 2013; Dasgupta and Sengupta, 2003). Thermal springs of this region are mostly confined in the Attri, Tarabalo, Athmalik and Taptapani region of Odisha state having surface temperature ranging from 42 to 59 °C. The ^{2}H and ^{18}O measurements of few thermal springs in this region show the meteoric origin of these thermal springs (Navada et al., 1995). Zimik et al. (2017) has showed that there is no appreciable temporal variation in the water chemistry of the thermal springs. In a recent study, Keesari et al. (2020) has estimated the C-14 ages of three thermal manifestations and their age ranges from 4964 to 17,714 years. Mahala et al. (2012) has estimated the subsurface reservoir temperature using only Na-K and Na-K-Ca geothermometry and the estimated temperature varies from 92 to 277 °C. On the other hand, the estimated reservoir temperature by using chalcedony and K-Mg geothermometers ranges from 94 to 107 °C (Navada et al., 1995). This

geothermal province is considered to be one of the potential sites for developing both wet and enhanced geothermal system (EGS) geothermal projects in the future (Chandrasekharam and Chandrasekhar, 2010).

1.6.7 Sohana geothermal province

Sohana geothermal province located at the Haryana state is the least explored geothermal area in terms of geochemical and isotopic analysis. Thermal activity in this region is confined within a tectonic depression formed due to down-faulting of a central block belonging to Delhi mobile belt (Singh at al., 2016). The maximum base temperature is reported to be around 100 °C (Pandy and Negi, 1995).

1.7 Scope and objectives of the present study

Integrated isotope and geochemical characterization of the thermal waters are extremely valuable in providing information about the origin of thermal fluid, identifying possible recharge area and mixing between waters of different temperature and origins, deciphering geochemical evolution and source of the solutes dissolved in the thermal fluids, estimating the transit time and subsurface reservoir temperature. Although geological, hydrogeological, geophysical mapping of the geothermal resources in India have been extensively carried out, isotope based investigations are rather limited barring some selected areas like Puga and Chumathang (Indus valley, Ladakh), Panamik (Nubra valley, Ladakh), Parbati and Beas valley (Himachal Pradesh), Gujarat-Rajasthan (Cambay basin), Tattapani (Chhattisgarh), Bakreswar and Tantloi (West Bengal) and Surajkund (Jharkhand) geothermal areas. Till now, no isotopic characterisation is done in the remaining promising geothermal areas like Tural-Rajwadi (West Coast area), Manuguru (Godavari valley area) and Tapoban-Badrinath (Uttarakhand area). Geologically, each of this geothermal area is unique and there are many unanswered questions regarding the origin, source, subsurface temperature and residence time

of the thermal waters found in these regions. For example, in Tural-Rajwadi geothermal area, there is no consensus in the estimation of subsurface reservoir temperature and the reported temperature vaied from 61 to 282 °C (Pitale et al., 1987; Muthuraman, 1987; Sarolkar, 2005) which is not practically possible. There is also ambiguity in establishing sea water component in the thermal waters of Tural-Rjwadi geothermal area. Few reachers (Muthuraman, 1987; Chandrasekharam et al., 1989) proposed the mixing of sea water with that of the meteoric water followed by the extensive rock-water interaction as the main governing geochemical process in this region which was later ruled out by Absar et al. (1996) and Reddy et al. (2013) due to the lack of any relationship between $\delta^{18}O$ and Cl of thermal discharges. The mixing phenonomenon between thermal and non-thermal water is also not established conclusively. Pitale et al. (1987) and Sarolkar (2005) suggested the mixing of surrounding ground water with thermal water in the Tural-Rajwadi region which was later ruled out by Reddy et al. (2013) due to the lack of long term variation in the chemical constituents. Moreover there is no information about the transit time of the thermal water which is absolutely essential to determine the sustanibility of the geothermal system. Similarly no isotopic study has been carried out in the Godavari valley geothermal area to ascertain the source and origin of thermal waters. Earlier estimation of subsurface reservoir temperature in the Godavari valley geothermal area varied from 100 to 215 °C (Saxena and Gupta, 1985, Chandrasekharam et al., 1996). Detailed study about the geochemical evolution as well as the estimation of residence time of the thermal waters is conspicuously absent in this promising geothermal area. Likewise in Utttarakhand geothermal area, there is lack of integrated isotope-geochemical study to find the source, origin, reservoir temperature and residence time of the thermal fluids. The present thesis is devoted to fill these data gaps using multi isotopes and geochemical techniques.

Geothermal systems in Indian subcontinent are mostly liquid dominated and are associated either with deep seated rift systems or with continental collision zones. The general hypothesis regarding the origin and evolution of thermal fluids in the dynamic liquid dominated geothermal systems can be summarized as follows. Based on the isotopic evidence, it is established that the thermal waters are largely meteoric in origin. These meteoric waters penetrate the earth's crust through fault and fractures and travel up to several kilometres beneath the surface. During descend, these meteoric waters get heated, react with host rock and finally rise to the surface by convection. Meteoric water, being low in dissolved solids, remains under saturated with respect to most of the primary minerals. So when this rainwater enters into the soil and bedrock, it starts to dissolve the rock minerals and gradually approaches the saturation (equilibrium) with respect to the rock minerals. This attainment of the equilibrium forms the basis of the development of several chemical geothermometers. The principal purpose of the chemical geothermometers is to determine the subsurface temperature of the geothermal reservoir based on the chemical analysis of the thermal springs or the fumaroles. The concept of equilibrium between certain aqueous solutes and the aquifer minerals is always assumed before applying any chemical geothermometers which is not necessarily true in all the cases. Therefore interpretation the results of the geothermometers requires utmost caution. Similarly the transit time estimation of geothermal systems by using ^{14}C or ^{3}H sometimes become difficult due to the fact that the contamination from various sources of carbon (i.e. metamorphic carbon, magmatic carbon etc.) except from the rock dissolution can make ^{14}C dating technique ineffective. On the other hand tritium has too short half life to determine residence time of very old geothermal systems. However in case of relatively young geothermal system, tritium can provide useful information about the transit time of the thermal waters.

In this present study, the broad objectives of the in-depth isotope-geochemical assessment of three promising geothermal areas (Tural-Rajwadi geothermal area of West coast geothermal province, Godavari valley geothermal area and Tapoban-Badrinath geothermal area) are to understand the origin of the thermal waters, estimation of the residence time, calculation of subsurface reservoir temperature, identification of the source of dissolved constituents and understanding the geochemical evolution. The isotopic ratio of $^{18}O/^{16}O$ and $^{2}H/^{1}H$ in thermal waters are mainly used to identify the origin (meteoric or magmatic or oceanic) of the thermal water, evaluate the mixing phenomenon between thermal and non-thermal water and to estimate the recharge altitude. $\delta^{13}C$ measurement of the dissolved inorganic carbon (DIC) in the thermal waters is carried out to ascertain the predominant nature of the weathering mechanism (silicate or carbonate weathering) and the source of soil CO_2 (C_3 or C_4 type of plants). In Tural-Rajwadi geothermal area, $\delta^{34}S$ of the dissolved sulphate is measured mainly to distinguish the source of dissolved sulphate in thermal waters. The predominant sources of dissolved sulphate can be: marine sulphate, dissolution of the sulphate bearing minerals (i.e. anhydrite, gypsum etc.), oxidation of sedimentary sulphide and anthropogenic sulphate. The involvement of sea water can be proved unequivocally based on the $\delta^{34}S$ value of the dissolved sulphate. Similarly $\delta^{11}B$ values of the dissolved boron can act as an excellent tracer to identify the source of dissolved boron in thermal waters. The main sources of dissolved boron are igneous rocks, metamorphic rocks, altered oceanic basalts and/or marine water. The measurement of $^{87}Sr/^{86}Sr$ ratio of dissolved strontium is carried out to understand whether the thermal water in Tural-Rajwadi region has percolated deep down to the Achaean granitic basement or is circulating within the Deccan flood basalts. Apart from the above mentioned stable isotopes, environmental radioactive isotopes mainly tritium and carbon-14 have also been used to calculate the transit time of the thermal waters. Tritium is used for dating of the relatively younger thermal water found in Uttarakhand geothermal area whereas carbon-14 is

used to calculate the residence time of the very old thermal water of Tural-Rajwadi and Godavari Valley geothermal area. Chemical geothermometers, mixing model and multicomponent geothermometry techniques have been employed to better constrain the subsurface reservoir temperature. In this study efforts have also been made to understand the probable role of geological settings on the variations in the chemical and isotopic content of the thermal springs.

CHAPTER 2

Sampling and analytical techniques

One important prerequisite to get any substantial information from a hydrological study is the proper sample collection from the field and the subsequent measurement performed in the laboratory. Proper sampling and field measurements of both physicochemical and isotopic parameters are critical to ensure high quality analysis and reliable interpretation of data. The aim of this chapter is to give a broad insight about the various techniques used for measuring stable isotopes, radioactive isotopes as well as chemical parameters used in this study.

2.1 Sampling Protocol

2.1.1 Location of sampling point (coordinates)

The location of sampling points was recorded as accurately as possible by using the global positioning system (GPS). The coordinates, i.e. latitude, longitude as well as the altitude and the nearby landmarks were also recorded along with the date and time of sampling.

2.1.2 Measurement of physico-chemical parameters

Several physico-chemical parameters like conductivity, TDS, temperature, pH, dissolved oxygen and alkalinity were measured onsite using multiparameter meter (HI 9828).

2.1.2.1 Conductivity

The conductivity meter of the multiparameter meter (HI 9828) was generally calibrated before the use in the field. Normally, two-point calibration was done by choosing one low EC standard (84 µS/cm) and other high EC standard (1.413 mS/cm). The electrode was rinsed with distilled or well water before every measurement. To measure sample's conductivity, the conductivity meter was dipped into a beaker containing sample solution. Once the reading stabilized, the temperature, conductivity and total dissolved solids (TDS) of the water sample was recorded.

2.1.2.2 pH

The pH meter of the multiparameter meter (HI 9828) was also calibrated before the use in the field by following the manufacturer's instructions. Three standard solutions or pH buffers were generally used for this calibration. After the calibration, the electrode was dipped into the sample to get the reading. While measuring the pH, the electrode was not stirred to prevent the change in sample pH through degassing of carbon dioxide. After the measurement, the electrode was cleaned and stored by dipping in to the storage solution.

2.1.2.3 Dissolved oxygen (DO)

Dissolved oxygen values of the water samples were measured by a DO probe attached to multiparameter meter (HI 9828). The calibration of the DO meter was carried out before the field sampling by using both the standard solutions and distilled water. The dissolved oxygen value of the sample is then recorded and is usually expressed in milligrams per litre or parts per million (ppm).

2.1.2.4 Alkalinity

Alkalinity was usually measured through chemical titration using commercially available field kits. The supplied vial in the kit was filled up to the mark with the water sample. A drop or two of phenolphthalein solution was added in to the water sample. After addition of phenolphthalein solution the colourless sample became pink in colour. It was then titrated with the acid supplied in the kit. The beaker was shaken after addition of one drop of the acid and the colour change was noted. The procedure was repeated until the solution became colourless. The amount of acid used to reach this point was recorded. Next, a drop or two of total alkalinity indicator solution was added to the sample. It was then titrated further to the end point as indicated in the kit. In this case the colour changed from green to brown. Once again the amount of acid used was recorded and the alkalinity value was calculated in mg/L HCO_3.

2.1.3 Collection of samples for chemical analysis

Filtration of samples in the field was required for laboratory measurement of cations and anions. For the measurement of major cations and trace elements, the filtered water sample (about 125 mL) was acidified using a few drops of ultrapure concentrated nitric acid. The lid was then tightly closed and the bottle was properly shaken. For anions, no acidification was needed. The sample bottles were then labelled carefully with the relevant information about the sample.

2.1.4 Stable isotope sampling (^{2}H & ^{18}O)

For oxygen-18 and deuterium measurements, a 50 mL double capped polyethylene bottle was filled directly from the source in such a way so that there was no air bubble trapped inside the bottle. No filtration or addition of chemical was required. The bottle was then clearly labelled with all relevant details. During sampling, storage and transportation to the laboratory special care was taken to avoid the evaporation of the sample.

2.1.5 Tritium sampling

For tritium sampling, unfiltered and unacidified water sample was collected in a 500 mL polyethylene bottle. The sample bottles were then labelled properly and carefully with labels/waterproof markers.

2.1.6 ^{14}C and ^{13}C sampling

For carbon-14 analysis by liquid scintillation technique, minimum 2.5 g of carbon was required. This amount of carbon was obtained by precipitating all dissolved inorganic carbon from a 40–60 L sample volume, depending upon the alkalinity of the water. Therefore, sample processing in the field was essential to avoid shipment of large volumes of water to the laboratory. In this method, all inorganic carbonate species are precipitated from the water at high pH and the wet precipitate was shipped to the laboratory. The field apparatus consists of a 60 L specially fabricated plastic container. A wide mouthed plastic bottle of 1 L capacity

was screwed at the bottom of the container. The amount of water to be processed was calculated using the alkalinity measurement from the field. Generally, a minimum amount of 50 L was processed. About 50 mL of carbonate-free concentrated sodium hydroxide was added to raise the pH of the sample to about 11. The pH of the sample was tested by using pH paper. Carbonate-free sodium hydroxide solution was prepared in the laboratory just prior to the sampling campaign. After adding sodium hydroxide, exposure to the atmosphere was minimized to reduce the contamination by atmospheric carbon dioxide by closing the lid. The sample was stirred using the stirrer. About 5 g of ferrous ammonium sulphate was then added into the sample to facilitate the coagulation of the carbonate precipitate. About 350 ml of saturated barium chloride ($BaCl_2$) solution (1/3 of the supplied 1 L bottle) was then added to precipitate the barium carbonate. After that, 50 ml of praestol (polyacrylamide) solution (acts as a settler) was added and mixed thoroughly. After 30 minutes, the whole solution was checked for complete precipitation. For that, a small amount of $BaCl_2$ solution (~25 ml) was added without any stirring. The sign of any cloudiness indicated incomplete precipitation and in that case more $BaCl_2$ was added to ensure complete precipitation. Generally, after 30 minutes to one hour all the precipitate settled down into 1-L bottle attached at the lower end of the precipitation tank. The one litre bottle was removed and capped tightly. Another one litre bottle was screwed at the lower end of the precipitation tank if more precipitate remained. Two to three bottles were required depending upon the quantity of precipitate. The sample was then labelled with date, sample number, well number, details of location etc. To avoid shipment of large number of bottles, different precipitate fractions of the same sample were mixed into one bottle by removing the clear supernatant liquid.

About 10 mg of this precipitate was dried and stored separately for cabon-13 isotope measurement.

2.1.7 ^{34}S sampling

For $\delta^{34}S$ measurement, water samples were collected in one litre high density polyethylene (HDPE) bottle for the precipitation of $BaSO_4$. In this method, water was acidified (pH = 2 to 3) by adding ultrapure concentrated HCl (Hydrochloric Acid) with continuous stirring to remove the dissolved carbonate and bi-carbonate from the water. After that barium chloride solution was directly added to the sample until complete precipitation of barium sulphate. The precipitated barium sulphate was then dried and stored for further analysis in mass spectrometer.

2.1.8 Boron isotope sampling

Samples for measuring boron concentration as well as its isotopic composition ($^{11}B/^{10}B$) were collected in the acid cleaned low density polyethylene (LDPE) bottles (30mL). The unacidified samples were filtered through 0.45 μm filters prior to the collection in the LDPE bottles.

2.1.9 Strontium isotope sampling

For $^{87}Sr/^{86}Sr$ isotope measurement, water samples were collected in acid cleaned low density polyethylene (LDPE) bottles (30mL). Ten drops of concentrated ultrapure nitric acid (~3% total acid) was added to the plastic bottles. One acid cleaned LDPE bottle was filled with Milli-Q water to generate analytical 'blanks' (Chesson et al., 2012).

2.2 Measurement techniques of isotopes

Stable isotope ratio like $^{2}H/^{1}H$, $^{18}O/^{16}O$, $^{13}C/^{12}C$, $^{34}S/^{32}S$, $^{11}B/^{10}B$ and $^{87}Sr/^{86}Sr$ were measured in mass spectrometer whereas radioactive isotopes like ^{3}H and ^{14}C were measured by using liquid scintillation counter.

2.2.1 Basic principles of mass spectrometer

Mass spectrometry is a powerful analytical technique generally used to identify unknown compounds within a sample, quantify known materials and to elucidate the structure and chemical properties of various molecules. The basic process involves the conversion of the sample into gaseous ions which are then characterized on the basis of their mass to charge ratios (m/z) and relative abundances. A typical mass spectrometer is composed of four major components: ionisation source, separation system, detector and data system. Various types of mass spectrometers having different source, separation system and detection techniques are available depending on their use. A gas source mass spectrometer typically consists of a source, flight tube and collector. To analyse a gaseous sample, firstly the gas molecules become ionised by the ionisation source and then the newly formed positive ions get accelrated by the positive potential of the ionisation chamber. The ions then enters the flight tube through a source slit. The flight tube forms the arc of a circle that passes between the poles of the magnet. As the ions travel down the tube, they are separated into beams of different radii corresponding to different masses. In the collector, ions of the selected mass units are transmitted through the resolving slit and get detected by the Faraday cup. The ion current from the cup is proportional to the number of incident ions and therefore to the partial pressure of the equivalent isotopic molecular species in the sample gas. Multiple Faraday cups are often used to obtain simultaneous detection of different isotopes. Schematic diagram of a typical IRMS is shown in Fig. 2.1.

2.2.1.1 Measurement protocol of stable isotopes

2.2.1.2 Measurement of $\delta^{18}O$ in water samples

The water equilibrium method is an indirect way of analysing small amount of aqueous sample for measuring $^{18}O/^{16}O$ ratio. The analysis is not carried out directly on the sample but

on the equilibration gas that is introduced into the headspace of the sample vessel along with the flow of helium. To get the oxygen isotopic composition, water sample under a fixed temperature is equilibrated with carbon dioxide gas and change in the isotopic composition of the CO_2 is measured. The isotopic exchange reaction can be expressed as:

$$C\,^{16}O\,^{16}O + H_2\,^{18}O \leftrightarrow C\,^{16}O\,^{18}O + H_2\,^{16}O \qquad 2.1$$

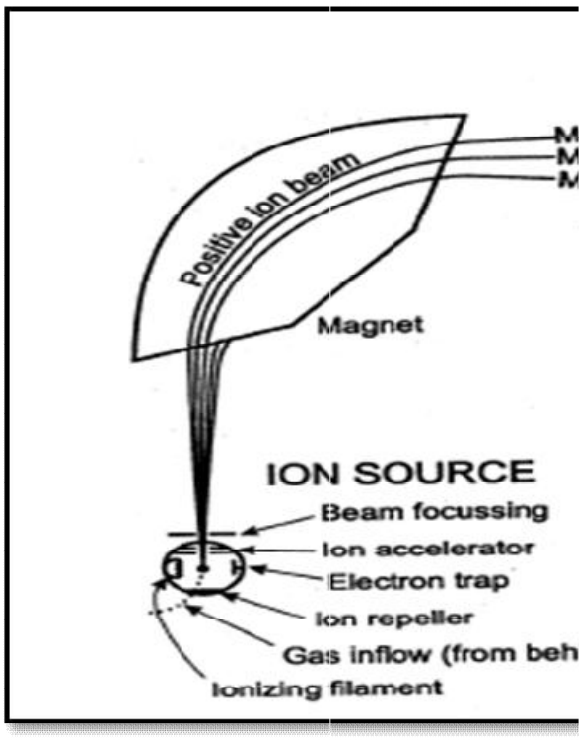

Fig 2.1 *Schematic of an isotope ratio mass spectrometer measuring CO_2*

The equilibration time is strongly dependent on temperature and the rate of equilibration approximately doubles for every 8 °C rise in temperature. Presence of excess dissolved salts generally reduces the equilibration rate and that should be compensated by increasing the equilibration time.

In the present study, continuous flow (CF) isotope ratio mass spectrometer (IsoPrime 100) attached to a Multiflow unit was used to measure the $^{18}O/^{16}O$ ratio. Multiflow unit is basically an automated sample injection system for the measurement of both δD and $\delta^{18}O$ in aqueous samples. Multiflow unit allowed automated sample equilibration and analysis up to sixty

sample vials in every batch. For $\delta^{18}O$ analysis 200µl of aqueous sample was equilibrated with the equilibrating gas having composition of 5% CO_2 in helium at two bar pressure. Flushing time of the each vial was set at five minute. Equilibration temperature was maintained at 30 °C for duration of 6 hours. After the equilibration process, the headspace gas was sampled with the needle and passed to the Isoprime mass spectrometer for isotopic analysis. The results were reported in δ-notation and expressed in units of parts per thousand (denoted as ‰). The δ value is defined as a relative difference in the isotopic ratio between sample and standard solution. The δ notation is represented as:

$$(\delta\ ‰) = \{(R_{sample} / R_{standard}) - 1\} * 1000 \qquad 2.2$$

where R_{sample} represents the isotope ratio of a sample ($^2H/^1H$, $^{13}C/^{12}C$, $^{18}O/^{16}O$ etc.) and $R_{standard}$ the corresponding ratio in a standard. The standards used for the $\delta^{18}O$ measurement were VSMOW (Vienna Standard Mean Ocean Water) and SLAP (Standard Light Antarctic Precipitation). The precision of measurement for $\delta^{18}O$ was ± 0.1 ‰ (2σ).

2.2.1.3 Measurement of δ^2H in water samples

In this study $^2H/^1H$ ratio was measured by pyrolysis method. In this method, pyrolysis of liquid water was carried out by reduction of water to CO and H_2 at 1450 °C in a glassy carbon furnace. In this technique, 0.5 µl water samples were injected in a glassy carbon tube and the sample was pyrolyzed at 1450 °C. After passing through an absorption tube (to absorb H_2S traces and moisture), the carrier gas helium carried the hydrogen and CO into the thermal conductivity detector (TCD) and afterward to the IRMS. The hydrogen did not get adsorb in the adsorption column and directly reached to the IRMS. After the deuterium analysis had been completed the gas path was switched over and the gases from the pyrolysis tube were flushed into the open and the CO was desorbed from the column after flushing with pure helium. In case of ^2H measurement also the results were reported in δ-notation and expressed

in units of parts per thousand (denoted as ‰). The measured values were then normalized on VSMOW/SLAP scale. The precision of measurement for δ^2H was ± 0.5 ‰ (2σ).

2.2.1.4 Measurement of $\delta^{13}C$ in water samples

For $\delta^{13}C$ measurement, the dried barium carbonate which was precipitated during the sampling program was combusted in Elementar Analyser (EA) attached to the continuous flow isotope ratio mass spectrometer (CF-IRMS). The measurement procedure involved weighing of the solid sample (0.3 gram) into a small tin capsule which was combustd at 1150 °C in a combustion tube. Constant flow of helium carried these combustion products over an oxidation catalyst. The oxidation products were then passed through a reduction reactor. Copper granules within the reduction reactor reduced the nitrogen oxides to N_2, SO_3 to SO_2 which got adsorbed into the temperature dependent desorption columns. Unadsorbed CO_2 gas directly went to the IRMS where carbon isotope ratio $^{13}C/^{12}C$ was measured against a pulse of reference gas of known composition. Each sample gas was then desorbed separately by controlling the temperature of the desorption column(s). Carbon isotope ($\delta^{13}C$) values were also reported in permil (‰) notation with respect to VPDB (Vienna Pee Dee Belemnite). The precision of measurement was ± 0.30‰ (2σ precision).

2.2.1.5 Measurement of $\delta^{34}S$ in water samples

For $\delta^{34}S$ measurement, the dried barium sulphate precipitate which was collected in the field was weighed (~0.3g) and sealed in a tin capsule for combustion in to the elementar analyser (EA) coupled with IRMS. The constant flow of helium carried the combustion products through the oxidation catalyst. The oxidation products later got reduced in the reduction reactor. Copper granules within the reduction reactor reduced nitrogen oxides to N_2, SO_3 to SO_2 which adsorbed into temperature dependent desorption columns. Pure CO_2 gas did not get adsorbed and directly went to the IRMS. After that with sequential increase in temperature of the desorption column, N_2 and lastly SO_2 gas got liberated. Pure SO_2 gas went

to the IRMS where sulphur isotope ratio $^{34}S/^{32}S$ was measured against a pulse of reference gas of known composition. Sulphur isotope ($\delta^{34}S$) values were also reported in permil (‰) notation with respect to VCDT (Vienna-Canyon Diablo Troilite). The precision of measurement was ±0.2‰ for $\delta^{34}S$ (2σ precision).

2.2.1.6 Measurement of $\delta^{11}B$ in water samples

Boron isotopic compositions were determined using inductively coupled plasma orthogonal acceleration time of flight mass spectrometer (ICP-oa-TOFMS). The detailed methodology of measuring isotopic ratio of boron has been described elsewhere (Saha et al., 2015). Mainly non-acidified samples were used for boron isotopic determination. In this method, 10 mL of the aqueous sample was nearly evaporated to 0.5 mL which was then added drop wise to 1 g of U_3O_8 (free from boron) kept under the IR lamp. The pyrohydrolysis of the dried sample and the subsequent mass spectrometric analysis were then carried out (Saha et al., 2015). Common analyte internal standardisation (CAIS) method was adopted to correct the mass bias effect and short-term fluctuations (Saha et al., 2015). The $^{11}B/^{10}B$ ratio of ten replicate analysis of NIST SRM 951 (boric acid, Standard Reference Material) obtained after the correction using the CAIS equation was found to be 4.0435 ± 0.0182 (2σ, extended uncertainty). The long-term (over a period of 5 h) external reproducibility based on the replicate analysis was around ±0.45%.

2.2.1.7 Measurement of $^{87}Sr/^{86}Sr$ in water samples

Before measuring the $^{87}Sr/^{86}Sr$ ratio of water sample, the chemical purification of Sr was performed using an ion-exchange column (Sr-Spec) according to the method described by Pin and Bassin (1992). Chemical purification was done to minimise the matrix effect in the strontium isotope ratio measurement. After chemical separation, strontium isotopic ratio was measured using ICP-oa-TOFMS. The reproducibility of the measurements was verified by repeated analysis of NIST SRM 987, strontium carbonate (Standard Reference Material) and

the mean value was obtained as 0.7190 ± 0.0010 (1σ, n = 10). The result showed that the mass bias on $^{87}Sr/^{86}Sr$ was typically around 1.2%. The long-term stability on $^{87}Sr/^{86}Sr$ ratio was monitored by replicate analysis over a period of 5 hours and was found to deviate only by ±0.4% relative standard deviation (RSD). This demonstrated that the long-term fluctuation on this ratio was negligible. Henceforth, this mass bias factor was applied to correct the measured Sr isotope ratio of the samples (external calibration).

2.2.2 Basic principles of liquid scintillation spectrometry

The two environmental radioactive isotopes which have widespread application in geothermal studies are tritium (half-life 12.43 y) and carbon-14 (half-life 5730 y). Liquid scintillation spectrometry is the most sensitive and widely used technique for the detection and quantification of environmental tritium and carbon-14. In the scintillation process, a part or whole of the kinetic energy of an ionizing particle (e.g. β-particle emanating from tritium and carbon-14) gets converted into the generation of a number of photons as the particle is progressively slowed down and/or stopped in the scintillation material. This process is called luminescence. When the scintillation material is an organic solvent containing small amount of special organic compounds (solutes), it is referred to as liquid scintillation solution or cocktail. In liquid scintillation solution the counting efficiency is found to be high even for low energy charged particles (about 67% for ^{3}H and 98% for ^{14}C) because the decaying nucleus and scintillation solution remain in intimate contact. A liquid Scintillation solution consists of three basic parts: The solvent(s), the solute(s) and the sample. In low level counting it is advantageous if the sample itself acts as solvent. The beta decay electrons produce exited solvent molecules. The excitation energy migrates from one solvent molecule to other until it is transferred to a solute molecule. The excitation energy ultimately gets released as photon. This energy transfer processes are quantitative and the number of emitted photons is proportional to the energy of the ionizing solvent. The solute is chosen in sucha a

way that its fluorescence yield should be high and the photon emissions can be efficiently converted into detectible light components by commercially available photo multiplier tube (PMT). When the photons are detected by a PMT, a voltage pulse proportional to the number of detected photons is produced as its output. If decay product is energetic enough to produce several photons, there is high probability that each of the PMT will detect enough photons to produce a simultaneous voltage pulse. Whenever the output pulses from each PMT occur within a very small interval (< 25 nanoseconds) they are considered to be coincident. The total response for the decay product is obtained by summing the outputs of both PMTs for each coincident event. This technique commonly called as pulse summation not only increases the signal to noise ratio but also improves the resolution (Horrocks, 1974). The scintillation photon yield can be reduced by several different quenching processes (Gibson, 1980). Elimination of variable quench will enhance the counting accuracy. Several different methods are available to monitor the level of quench in each sample. Some of these methods are internal standardization, sample channel ratio (SCR), external standard count rate, external standard channel ratio and methods based on the analysis of spectral shapes such as H-number and spectral end point spectral quench parameter SQP(I) (Quantulus 1220 counter). Modern liquid scintillation counters use dedicated microprocessor computers and provide automated quench correction methods based on any of the above techniques. In this study, Quantulus 1220 Liquid Scintillation Counter (Perkin Elmer, USA) was used for the measurement of tritium and carbon-14 concentration.

2.2.2.1 Measurement of ^{3}H in water samples

Tritium exist in water molecule majorly in the form of HTO however the natural concentration of tritium is extremely low i.e. $^{3}H/^{1}H = 10^{-18}$. As a result some degree of electrolytic enrichment is carried out to obtain the measurable concentration. To perform this electrolytic enrichment, 250 g of the distilled water sample comprising 0.5g of sodium

peroxide was put into the electrolytic cell having perforated mild steel as cathode and stainless steel as anode. The reactions of electrolytic enrichment process are given as:

Anode (+): $2OH^- \rightarrow H_2O + 1/2\ O_2 + 2e^-$ 2.4

Cathode (-): $2H^+ + 2e^- \rightarrow H_2$ 2.5

As the electrolysis process progressed, the volume of the solution gradually reduced resulting the increase in the alkalinity. This extra alkali was neutralized by adding lead chloride (~2g). Otherwise it would cause quenching of the scintillator mixture. The governing equation is:

$2NaOH + PbCl_2 \rightarrow 2NaCl + Pb(OH)_2$ 2.6

Later 14 ml of Scintillator was added to the 8g of the enriched sample in high-density polythene scintillation vials and was counted in Quantallus 1220 liquid scintillation counter. The sample was counted for 500 minute each (50 min each sample for 10 cycles). After counting, the cpm (count per minute) values were obtained by selecting the channel that has the best figure of merits (square of efficiency /background). For quality assurance of the lab generated data in every batch spiked samples and distilled water samples were added to keep the check on the consistency of measurement. The tritium values are normally reported in terms of tritium Units (TU) where 1 TU is equal to 0.118 Bq/Kg or 3.19 pCi/Kg.

2.2.2.1 Measurement of ^{14}C in water samples

In the field, the dissolved inorganic carbon (DIC) was precipitated as barium carbonate which was brought back in the laboratory. In the laboratory, carbon was released from precipitates in the form of carbon dioxide by reacting it with phosphoric acid in a closed vacuum line. The evolved carbon dioxide was passed through the moisture trap which was dipped in the mixture of acetone and liquid nitrogen (temperature ~ -70˚C). This step helped to remove the moisture from the system as it acted as a quencher of scintillation. The evolved carbon dioxide was stored in the cylinder for 15-30 days to allow the decay of radon gas trapped along in the process. After that the carbon-dioxide was passed through a U-shaped pressure

equalizer column having sinter disc and a mixture of carbosorb (11.5ml) i.e. 2-methoxyethylamine and permafluor (11ml) i.e. mixture of toluene, PPO and BIS-MSB (scintillator). The disc facilitated the gas to bubble through the system which enhanced the interaction time. For quality assured results, the standard (SRM 4990C - Oxalic acid) for carbon-14 and background sample were prepared similarly. Samples, standard and background samples were then transferred into 22 mL teflon vials and counted in a low level Quantulus 1220 liquid scintillation counter for 20 cycles of 50 min. each (1000 minutes counting). After counting, the cpm values were obtained by selecting the channel that has the best figure of merits (square of efficiency /background).

2.3 Measurement techniques for chemical species

Chemical analysis of major ions (cations and anions) was mostly carried out by ion chromatography technique. Dionex ion chromatograph (DX-500) was used to measure major cations (Na^+, K^+, Ca^{2+} and Mg^{2+}) and anions (Cl^- and SO_4^{2-}). In ion chromatography technique, the ions get separated based on their retention time in the stationary phase (ion exchange column). The retention time is governed by the extent of interaction of that ion with the material of ion exchange column. The ions get eluted when suitable mobile phase (buffer solution) is passed through the column. In the present study CS-12A column coupled with CG-12A guard column was used to measure the cations whereas AS-11 column coupled with AG-11 guard column was used to separate the anions. The cation exchange column was made up with copolymer of divinylbenzene and ethylbenzene functionalized with carboxylic acid group whereas anion exchange column was comprised of copolymer of divinylbenzene and ethylbenzene functionalized with ammonium group. For cation separation, 21 mN H_2SO_4 solution was used as the mobile phase in isocratic mode whereas for anion separation NaOH solution (5-35 mN) was used as mobile phase in gradient mode. Calibration and quantification was done using the Peaknet software. The RSD (Relative Standard Deviation)

of the analysis was typically <3% for major ions. Dissolved silica concentration was measured by inductively coupled plasma optical emission spectrometry (ICP-OES) (Model: ACTIVA, M/S HORIBA Scientific). For measurement in ICP-OES method the nearly evaporated sample solution was converted into aerosol droplets by nebuliser. The aerosol droplets were then introduced in argon plasma chamber operating at 6000K temperature. At such high temperature the silica atoms got excited, ionized and atomized. The electronically excited silica atoms while returning to the ground states emitted photons which were measured by the photo multiplier tube (PMT) as a detectable signal. This signal intensity was proportional to the concentration of the silica in the water sample. Standard NIST solution was used to calibrate the instrument.

The trace elements mainly lithium, rubidium, boron, strontium, caesium was measured using ICP-MS (Model: OptiMass 8000R, M/S GBC Scientific Equipment Ltd., Australia). The sample introduction technique was similar to the ICP-OES. The ICP-MS allowed determination of elements with atomic mass ranging from 5 to 225. RSD (Relative Standard Deviation) of the trace element analysis was typically within ~6%.

2.4 Statistical analysis

Hierarchical cluster analysis (HCA) and principal component analysis (PCA), the two major multivariate statistical analysis techniques, were used in the present study. The multivariate techniques were used to reduce the dimensionality of the input data set so that the underlying information can be revealed with fewer numbers of variables. In HCA, dendogram basically represents the different clusters of samples based on their similarities or dissimilarities. Samples of a same cluster have similar properties than those in the other clusters. PCA on the other hand uses a mathematical dimension reduction procedure to reduce the original dimensions into smaller set of principal components (PC). The first PC generally contains the largest variation of the dataset followed by PC2, PC3 and so on. In this current study,

chemometric analysis such as hierarchical cluster analysis (HCA) and principal component analysis (PCA) were performed using the statistical software package XLSTAT.

2.5 Mineral saturation study

Mineral saturation study is very useful to ascertain the types of the minerals controlling the concentration of the dissolved solutes. In the present study the geochemical program, PHREEQC, based on the thermodynamic database WATEQF was adopted to calculate the mineral saturation states of the relevant water samples.

PHREEQC uses ion-association and Debye Hückel expressions to account for the non-ideality of aqueous solutions. This type of aqueous model is adequate at low ionic strength but may break down at higher ionic strengths (in the range of seawater and above). The activity coefficients of the major cations ions are found to fit mostly from chloride salts so the model may do reasonably well for major ions in chloride dominated waters. However, all of the ion pairs and complexes use the Davies equation for activity coefficients, which is purely speculation. So any calculation that involves large amounts of complexion at high ionic strength (>0.5 molal) is questionable. For high ionic strength waters, the specific interaction approach to thermodynamic properties of aqueous solutions should be used (PHRQPITZ reaction model should be used then).

The other limitation of the aqueous model is lack of internal consistency in the data present in the database. Most of the log K's and enthalpies of reaction have been taken from various literature sources. No systematic attempt has been made to determine the aqueous model that was used to develop the log K's or whether the aqueous model defined by the current database file is consistent with the original experimental data. The database files provided with the program thus should be considered to be preliminary

2.6 Multicomponent geothermometrical modeling

The multicomponent geothermometry is based on the computation of the saturation indices (log (Q/K)) of potential reservoir minerals over a range of temperatures and then estimating the reservoir temperature by the clustering of the saturation indices close to zero (Reed and Spycher, 1984; Pang and Reed, 1998; Spycher et al., 2014). This multicomponent approach present advantages over the "classical" geothermometry methods (i.e. silica and cation geothermometry) as it depends on the complete analysis of the fluids and has solid thermodynamic basis rather than depending on the solubility of few minerals or semi-empirical correlations and thus can be applied to any geothermal systems. In this modelling technique, prior to the calculation of the saturation indices, the composition of the deep fluid can be reconstructed by applying corrections for dilution or mixing phenomenon. The effect of degassing during the assent of thermal fluids to the surface can also be corrected by numerically adding gases to the analysed fluid composition. In this study a stand-alone computer program (GeoT) was used to perform the multicomponent geothermometry calculation. The program was basically a homogenous geochemical speciation algorithm which solved the mass balance/mass action equation using Newton-Raphson iterative method (Xu et al., 2016). The detailed procedure of this method is described elsewhere by Spycher et al. (2014). For calculation of saturation indices log (Q/K)) of the selected minerals, both the ion activity product (Q) and the thermodynamic equilibrium constants were computed. The thermodynamic database SOLTHERM.H06 was used in this program to compute both the ion activity product (Q) and the thermodynamic equilibrium constant (K). GeoT also computed different statistical parameters i.e. median (RMED), standard deviation (SDEV), mean (MEAN) and root mean square error (RMSE) of saturation indices as well as the temperatures at which these statistical parameters attained the minimum value (T_{RMED}, T_{MEAN}, T_{SDEV} and T_{RMSE}). For a perfectly clustered system T_{RMED}, T_{MEAN}, T_{SDEV} and T_{RMSE} should be identical

and the corresponding temperature gave the estimation of the reservoir temperature. However this method also has certain limitations which are described below:

1. Estimation of reservoir temperature by this method requires complete chemical analysis of fluids as well as exhaustive mineralogical data. The accessibility of this mineralogical data is not always possible due to the difficulty in deep drilling in the geothermal systems thereby limiting the application of GeoT.

2. Thermal water while coming towards the surface can undergo steam loss or can get mixed with non-thermal water. The convergence of the saturation indices of the minerals at a particular temperature is found to be highly dependent on the steam loss, dilution or concentration (by some factor), and/or mixing with other waters. All these factors should be taken in to account and 'reconstruction' of the deep fluid should be carried out in that case to have the proper estimation of reservoir temperature.

3. Unknown concentrations of one or more specific elements in the deep fluid need be computed by assuming that the concentration of each element is constrained by thermodynamic equilibrium between that element and a respective mineral. For example, the unknown concentration of aluminium ion can be ascertained by using the "Fix-Al" method developed by Pang and Reed (1998).

4. Moreover as GeoT method is based on the thermodynamic equilibrium computations, the sensitivity of the method depends upon the choice of the thermodynamic database. Deviations up to 20˚C in estimated temperatures have been observed depending upon the choice of database, mostly because of differences in the solubility constants (and composition) of certain minerals and also due to the differences in aqueous species dissociation constants (as, for example, with aluminium species) (Spycher et al., 2014).

2.7 Lumped parameter modelling (LPM)

In hydrologic systems, the lumped parameter models are generally used to estimate the mean transit time of the system in conjunction with a conservative tracer. In tritium dating, mean transit times (MTTs) are estimated using the convolution integral (Maloszewski and Zuber, 1982) with selected lumped parameter models:

$$C_{out}(t) = \int_0^{\infty} C_{in}(t-\tau)g(\tau)\exp[-\lambda\tau]d\tau \qquad 2.7$$

where C_{out} (t) is the output concentration of the tracer at time t, C_{in} (t-τ) is the input concentration of the tracer at the lag time t-τ, g(τ) is the response function or transit time distribution function (TTD) of the groundwater at the sampling point and λ is the tritium radioactive decay estimated from tritium half-life of 12.32 years. The most commonly used transit time distribution functions (TTD) of the LPM are: piston-flow model (PFM), exponential mixing model (EMM), exponential piston-flow model (EPM), and dispersion model (DM).

The piston-flow model (PFM) assumes a tracer travels from the inlet position (recharge area) to the outlet position (a well or spring) without hydrodynamic dispersion or mixing. In this model the TTD is given by:

$$g(\tau) = \delta(\tau-\tau_m) \qquad \delta = \text{Dirac delta function} \qquad 2.8$$

$$\text{and } C_{out}(t) = C_{in}(t-\tau_m)\exp(-\lambda\tau_m) \text{ for } t = \tau_m;\ 0 \text{ for } t \neq \tau_m \qquad 2.9$$

The exponential mixing model (EMM) is generally applicable to the homogeneous, unconfined aquifers of constant thickness receiving uniform recharge. This situation leads to the vertical stratification of groundwater age, which increases logarithmically from zero at the water table to ages that approach infinity at the base of the aquifer (Vogel, 1967; Appelo and Postma, 1996). The TTD for EMM is as follows:

$$g(\tau) = (1/\tau_m) \exp(-\tau/\tau_m) \quad 2.10$$

In this model, water parcels with different transit times combine in the outflow to approximate the exponential TTD. It is mathematically equivalent to the well-mixed model.

The exponential-piston flow model (EPM) is basically a combination of EMM and PFM which has two unknown parameters (Maloszewski and Zuber, 1982). The TTD is given by:

$$g(\tau) = 0 \quad \text{for } \tau < \tau_m (1\text{-}f) \quad 2.11$$

$$g(\tau) = (1/f\tau_m) \exp(-\tau/f\tau_m + 1/f - 1) \text{ for } \tau \geq \tau_m (1\text{-}f) \quad 2.12$$

where f is the ratio of the exponential volume to the total volume. The EPM also can be used to describe piston-flow transport within the unsaturated zone followed by exponential mixing.

The dispersion model is based on a solution of one dimensional advection dispersion equation for a semi-infinite medium with an instantaneous injection and detection of the tracer in the fluid flux (Kreft and Zuber, 1978; Maloszewski and Zuber, 1982) having a TTD of:

$$g(\tau) = 1/\tau \ \{4\pi (P_D) \tau/\tau_m\}^{1/2} exp\ [-\{(1-\tau/\tau_m)^2\}/4(P_D) \tau/\tau_m] \quad 2.13$$

where P_D is known as the dispersion parameter. In practice, the dispersion parameter describes the relative width and height of the age distribution and is mainly a measure of the relative importance of dispersion (mixing) to advection (Zuber and Maloszewski, 2001).

In this current study, TracerLPM (version 1) was used to evaluate the MTT of the thermal water from environmental tracer data (^3H) using lumped parameter models. TracerLPM is an interactive Excel® (2007 or later) workbook program that allows a comprehensive interpretive approach consisting of hydrogeological conceptualization, visual examination of data and models, and also best-fit parameter estimation (Jurgens et al. 2012). The TracerLPM workbook contains mainly four LPMs i.e. piston-flow model (PFM), exponential mixing

model (EMM), exponential piston-flow model (EPM), and dispersion model (DM). There is another partial exponential model (PEM) which is a special case of EPM depending upon the aquifer configuration.

TracerLPM can simulate outlet concentrations for tracers in groundwater with a wide range of ages (less than1 year to more than 10,000 years). The general procedure for determining the LPM and mean age of a sample is to select a model based on the conceptualization of the physical system and vary the mean age and any additional model parameters until the model output concentration matches the measured concentrations. The best-fit models are evaluated by calculating the total difference between the modelled and observed tracer concentrations. The total difference is measured either by the relative error or relative squared error. In general, the relative error is a more restrictive and accurate measure of the difference between modelled and observed tracer values than the relative squared difference. However this approach contains several assumptions such as:

1. First and foremost, it is impossible to describe a large hydrologic system by a particular model. There would be a mixture of various flow systems depending upon the field scale heterogeneity. Input of tracer concentrations is also highly variable both spatially and temporally.

2. Each of the models (PFM, EMM, EPM, DM etc) has their own limitations. PFM is the most simplified among all these where constant input of tracer is assumed which is also not true always. For example, it is well known that under moderate climatic conditions the recharge of aquifers takes place mainly in winter and early spring. Consequently, while establishing the tritium input function, the summer infiltration is completely neglected. However, if the stable isotopic composition of groundwater reflects that of the average precipitation there is no reason to reject the influence of summer tritium input. This is

because even if no net recharge takes place in summer months, the water which reaches the water table in winter months is usually a mixture of both winter and summer water.

3. Judicious use of the model is also essential for actual interpretation of age. For example, the lack of tritium generally means that water recharged in the hydrogen-bomb era is absent (i.e., after 1952). However, for highly dispersive systems (e.g. those described by the exponential model or the dispersive model with a large value of the dispersion parameter), water having measurable tritium can have an age of 100 years, or more.

4. Seasonal variations of the tritium concentration in precipitation can cause serious difficulties in calculating the input function. The account this, the best method would be to estimate the mean tritium concentration for each year weighted by the net infiltration rates. However this requires monthly tritium records in precipitation as well as precipitation amount (corrected for the evapotranspiration phenomenon) which is not easily available in every place.

5. If the conservative radioactive tracer spends significant amount of time in a stagnant phase then the age of tracer and age of the water is not equivalent.

6. Transit time estimation by using tritium requires long term records of tritium in the precipitation occurring in the study area which is not available in most of the time. In that case the correlation method is applied to fill the missing tritium data from a nearby IAEA station which introduces some uncertainty in the age estimation.

7. Uncertainty in the tritium amount present in rainfall as well as the tritium measurement error affect the overall uncertainty in the age estimation.

Inspite of all these limitations, this LPM technique provides very useful informations regarding the MTT of the hydrologic systems.

CHAPTER 3

Multi-isotope (O, H, C, B, S, Sr) and geochemical investigation in Tural-Rajwadi geothermal field, Maharashtra, India

3.1 Background

Tural-Rajwadi geothermal area, near the Tural and Rajwadi villages of Chiplun taluka in Ratnagiri District of Maharashtra, is situated in the western part of the volcanic Deccan trap region of India. This Deccan trap region, popularly known as the West Coast geothermal belt is one of the promising geothermal fields in India due to the ubiquitous presence of sixty hot springs spread over eighteen localities. Geothermal activity in this area is manifested by the cluster of seven thermal springs having surface temperature ranging from 50 to 62 °C. High heat flow values (96.5 mW/m^2) and steep geothermal gradient (59 °C/km) encountered in the shallow depth range (5-100m) are the important characteristics of the Tural-Rajwadi geothermal field (GSI, 1987). Following the recommendations of the Hot spring committee constituted by the Govt. of India, Geological Survey of India (GSI) under the UNDP assistance carried out intensive geochemical, geological and hydrogeological studies in this area to evaluate the potential of the geothermal reservoirs (GSI, 1987; GSI, 1991). Analysis of the gaseous emanation from the Tural region revealed the presence of large quantities of helium (3.2%) along with the N_2 (78.4%), CO_2 (16.8%), O_2 (0.07%), Ar (1.34%), CH_4 (1.05%), NH_3 (0.011%) and H_2 (0.0061%) (GSI, 1987). Although several researchers (Pitale et al., 1987; Muthuraman, 1987; Sarolkar, 2005) had previously tried to estimate the subsurface reservoir temperature based on the different chemical geothermometers, there exists some glaring discrepancies in their results. Pitale et al. (1987) reported reservoir temperature as low as 95 °C estimated from Na-K geothermometer whereas Na-K-Ca geothermometer gave the subsurface temperature ranging from 78 to 125 °C. Later, the reservoir temperature (68 to 74 °C) calculated by Muthuraman (1987) using Na-K-Ca geothermometry was found to be slightly higher than surface discharge temperature (61 °C). On the other hand using Na-K gethermometer, Sarolkar (2005) estimated 170 °C as reservoir temperature in Tural region whereas in Rajwadi region the reservoir temperature varied from

113 °C to 282 °C. Similar anomaly in the estimation of reservoir temperature was observed even if quartz geothermometer was applied. Quartz geothermometer (conductive cooling) gave temperature range 146 to 149 °C (Pitale et al., 1987) but using the same geothermometer, Sarolkar (2005) estimated 64 to 127 °C as most probable reservoir temperature. Basically there is no consensus regarding the estimation of reservoir temperature. There is also ambiguity in establishing mixing phenomenon between thermal water with non-thermal water. Pitale et al. (1987) and Sarolkar (2005) suggested the mixing of surrounding ground water with thermal water in this region which was later ruled out by Reddy et al. (2013) due to the lack of long term variation in the chemical constituents. Similarly there is no unequivocal evidence about the presence of sea water component in the thermal waters. Dowgiallo (1977) as well as Gonfiantini (1977) ascribed the dissolution of paleomarine evaporates as the major source of dissolved salt content in these thermal waters. According to Muthuraman and Mathur (1981), although there was evidence of sea water ingression in this study area but the thermal waters had undergone extensive re-equilibration and rock-water interaction resulting the loss of magnesium, potassium, sodium from the sea water and proportionate gain in the calcium concentration. Experimental rock-water study carried out by Muthuraman (1987) and later by Chandrasekharam et al. (1989) indicated that the thermal water in this region might have originated through interaction of sea water and meteoric water with that of the host rock basalt at some elevated temperature. But it remained uncertain whether this sea water is of modern origin or some connate water of marine origin caught up within the basaltic flows during the evolution of Deccan Traps (Chandrasekharam et al., 1989). This proposed hypothesis of mixing of sea water with that of the meteoric water was later ruled out by Absar et al. (1996) due to the complete lack of any relationship between $\delta^{18}O$ and Cl of thermal discharges which was also supported by Reddy et al (2013). Moreover there is no mean transit time (MTT) estimation of the thermal waters in the Tural-

Rajwadi area although historical tritium concentrations of these thermal waters are available (Giggenbach, 1977). Keeping in view of the above scenarios, a comprehensive investigation using multi-isotope (H, O, ^{3}H, C, S, B and Sr) tracing and geochemical characterisation of the thermal waters from Tural-Rajwadi geothermal field has been carried out. Tritium tracer based MTT of the thermal waters in the Tural-Rajwadi region is also calculated using the both short term tritium measurements of the local precipitation, historical tritium measurements of the thermal waters as well as the recent tritium measurements of the thermal waters. Subsurface reservoir temperature has been computed using both chemical geothermometers and mixing models.

3.2 Study area

The present study area, a part of Deccan trap terrain of India, is situated at the 17.28 degrees north near the Tural and Rajwadi villages of Ratnagiri district, Maharashtra. Thermal manifestations in this region are controlled by the fracture zones trending in N20°W-S20°E. The area is mostly covered by the lineaments in NNE-SSW direction although some lineaments in NNW-SSE direction can also be seen (Sarolkar, 2005). This area is covered by the thick pile of the basaltic lava flows which are 'aa' type (GSI, 1987). Eruption of these lava flows took place at the end of the Cretaceous period about 65 million years ago (Courtillot et al., 1999). Intertrappean sedimentary beds separate each successive lava flows which are comprised of mainly olivine, pyroxene and plagioclase phenocrysts (Sen, 1986). Fine to medium grained, dense, greyish coloured, moderately porphyritic basalts are generally observed in the trap flow surrounding the hot springs (GSI, 1987). The main three water bearing formations in the study area are: Deccan trap formation (age varies from Upper Cretaceous to Lower Eocene), laterite (Pleistocene age) and alluvial deposits (Recent to Sub-Recent). Primary porosity is found to be absent in the basalts due to lack of interconnections and secondary porosity whereas secondary porosity due to the presence of cracks, fissures

and cooling joints acts as a good conduit for circulation of ground water. Dug well samples in the study area generally tap the shallow unconfined aquifer in which the water table lies within 10 m bgl (below ground level) in the pre-monsoon time and during post-monsoon time water table lies within 5 metre bgl. In case of confined aquifer the depth of the water table lies within 10 metre bgl during post-monsoon time whereas in pre-monsoon time water table goes down and falls within 10-20 metre bgl.

Tural-Rajwadi geothermal area has a tropical monsoon climate with high level of humidity. This area mostly receives rainfall from southwest monsoon and the average annual rainfall is around 3906 mm. Almost 85% of the annual rainfall is received during the monsoon months i.e. from June to September. The monsoon normally withdraws by the end of September or early October and the post-monsoon season has generally no rainfall. The winter season usually lasts for three months from December to February whereas March, April and May months constitute the summer season.

3.3. Sampling details

Water samples from thermal springs, dug wells and bore wells were collected from the study area during the month of April, 2013. Sampling locations are shown in Fig. 3.1. Four thermal springs (THS-1, THS-2, THS-3 and THS-4), one dug well (shallow ground water) (TDW-1) and two bore wells (deep ground water) (TBW-1 and TBW-2) samples were collected from Tural region whereas samples from three thermal springs (RHS-1, RHS-2 and RHS-3) and one dug well (RDW-1) were collected from Rajwadi region. Few rain water samples were also collected in the month of July, 2013. Measurements of different physicochemical parameters (pH, electrical conductivity, temperature, total dissolved solids and dissolved oxygen) were carried out in the field itself by using multiparameter meter (HI 9828). Samples

were collected for measuring major cations (Na, K, Ca, Mg), anions (Cl, SO_4, HCO_3), trace

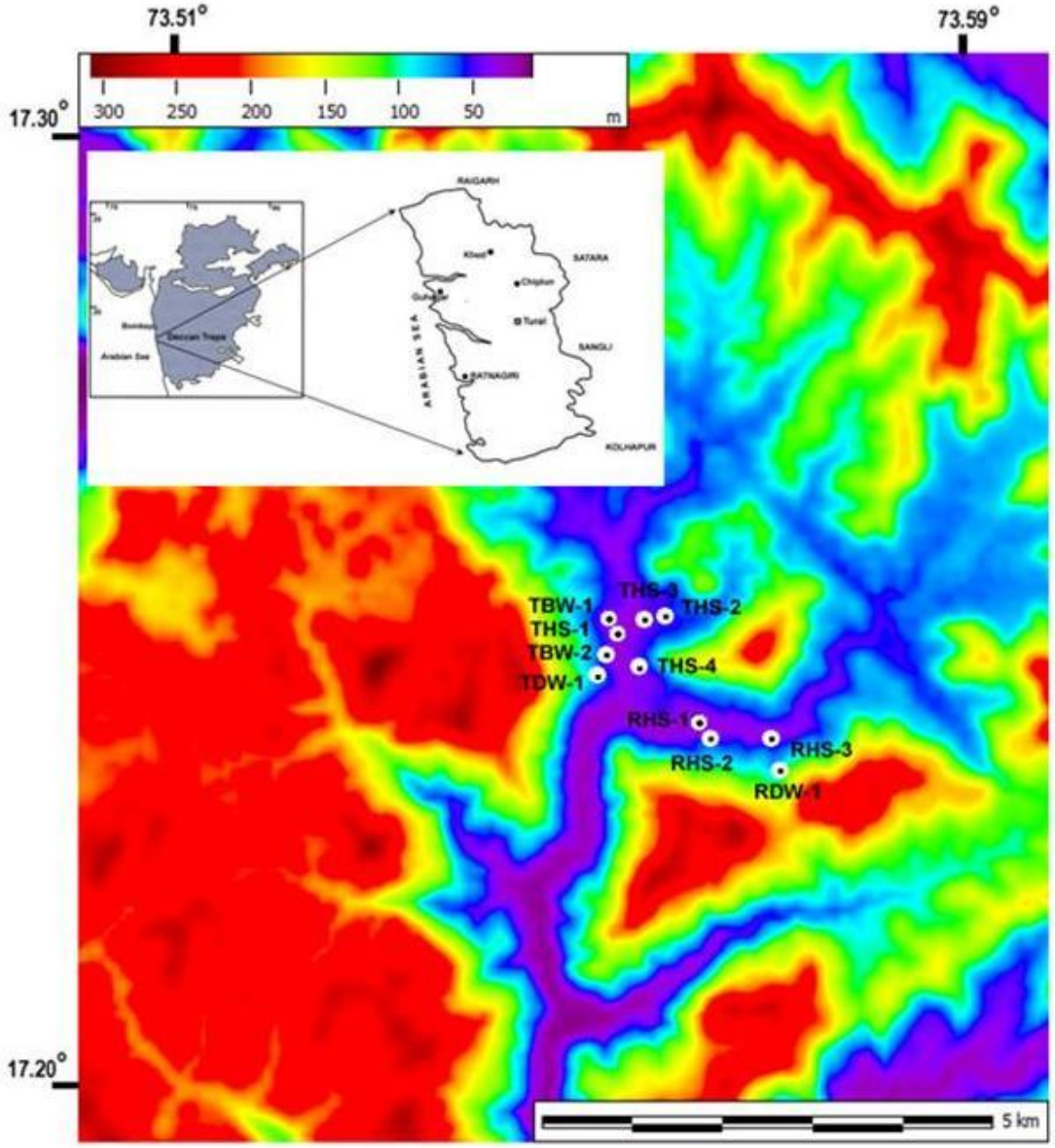

Fig. 3.1 *Location of Tural-Rajwadi geothermal field along with the sampling points*

elements (B, Li, Sr, Cs and Rb), dissolved silica and various isotopes (^{2}H, ^{18}O, ^{3}H, ^{13}C, ^{34}S, ^{11}B and $^{87}Sr/^{86}Sr$). Two main thermal springs (THS-1 and RHS-1) and two dug wells (TDW-1 and RDW-1) were again sampled for tritium (^{3}H) analysis in January, 2017.

3.4 Results and discussion

3.4.1 Hydrochemistry

Chemical parameters of thermal waters and non-thermal groundwater collected from the Tural-Rajwadi geothermal field are given in the Table 3.1. Thermal water samples are found to be slightly more alkaline (pH= 7.38-8.21) along with higher electrical conductivity (EC) (1289 to 1680 µS/cm) and total dissolved solids (TDS) (903 to 1167 ppm) compared to the non-thermal groundwaters. In thermal waters, sodium is found to be the dominant cation (210 to 250 ppm) followed by Ca (36.3 to 41.3 ppm), K (6 to 9 ppm) and Mg (0.45 to 1.2 ppm). Among the anions, chloride is found to be major ion (318.6 to 375.8 ppm) followed by sulphate (87.5 to 112.5 ppm) and bicarbonate (13 to 25 ppm) ions. Dissolved Silica concentrations (93 to 109 ppm) in the thermal water are found to considerably higher than the non-thermal groundwater samples (30 to 55 ppm). Groundwaters in the present study area are slightly acidic to nearly neutral (pH= 6.38 to 7.05) having low TDS (145 to 623 ppm) and low EC (207 to 890 µS/cm). The concentration of dissolved ions in the deep bore well samples is found to be higher than the shallow dug well samples due to the higher degree of dissolution of the aquifer minerals at the greater depth. The chemical compositions of the thermal waters, deep bore well and dug well samples are plotted in a trilinear piper plot (Fig. 3.2). In the piper plot it is seen that all the thermal waters of the Tural-Rajwadi area fall in the same region and have similar geochemical nature i.e. Na-Cl type. This water type (Na-Cl type) basically indicates that the thermal waters are old and mature in nature. One bore well sample (TBW-1) has different water type i.e. Na-Ca-Mg-Cl type whereas the other bore well sample (TBW-2) has similar water type (Na-Cl type) as that of the thermal waters. The similar chemical characteristics of the TBW-2 with that of the thermal manifestations essentially points out to the some extent of interconnection between the two systems. Dug well samples (TDW-1 and RDW-1) are found to be Ca-HCO_3 type indicating immature water type.

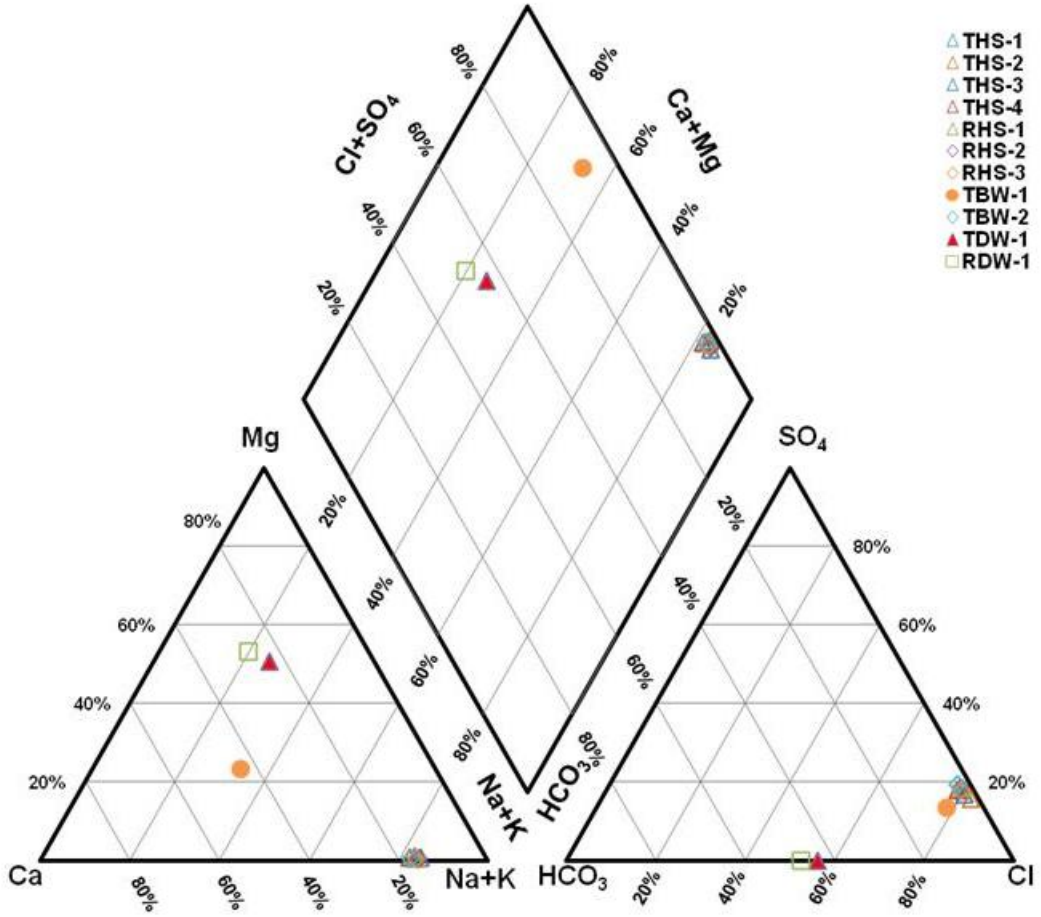

Fig. 3.2 *Piper diagram of groundwater samples in study area*

3.4.2 Subsurface processes

Thermal water during its ascent towards the surface can undergo variety of subsurface processes such as mixing with non-thermal water, conductive cooling, adiabatic boiling etc. which make the thermal water distinct in composition compared to the recharging water. The evidence of some of the processes is discussed in the subsequent sections.

3.4.2.1 Mixing with non-thermal water

Linear relationship between δ^2H and chloride provides the best evidence of mixing between thermal water and non-thermal water. In many occasions the linear relationship between

Table 3.1 *Chemical parameters of thermal and non-thermal water samples*

Sample ID	Temp (^{0}C)	Discharge rate (l/sec)	DO (mg/L)	pH	EC (µs/cm)	TDS (mg/L)	SiO_2 ppm	Na ppm	K ppm	Ca (ppm)	Mg (ppm)	Cl (ppm)	SO_4 (ppm)	HCO_3 (ppm)	B (ppm)	Li (ppm)	Cs (ppb)	Sr (ppb)
THS-1	61.5	6.2	7.17	7.38	1680	1167	109	235	8.0	41	1.0	358	110	19	0.23	0.11	40	820
THS-2	54	0.3	3.98	7.68	1574	1101	94	215	6.0	36	1.2	339	87	13	0.22	0.12	38	750
THS-3	58	0.3	2.50	7.74	1628	1094	110	250	9.0	40	1.2	375	105	22	0.24	0.13	36	705
THS-4	52	0.38	2.84	8.09	1289	903	95	210	7.1	39	1.1	318	98	25	0.23	0.09	32	675
RHS-1	50	4.45	5.34	8.21	1484	1039	99	235	7.0	40	0.4	351	110	18	0.25	0.11	28	600
RHS-2	58	4.45	1.27	8.0	1507	1054	97	240	7.3	39	0.5	355	112	19	0.27	0.12	30	680
RHS-3	54	0.1	1.50	7.94	1491	1050	93	230	6.4	40	0.6	342	105	20	0.24	0.1	20	350
TBW-1	35	-	6.80	7.05	890	623	55	55.0	0.6	64	20.0	204	47	36	bdl	bdl	bdl	bdl
TBW-2	46	-	2.62	7.80	1447	1015	108	235	6.2	43	0.5	349	117	22	bdl	bdl	bdl	bdl
TDW-1	28	-	4.02	6.50	439	307	39	25	0.4	nd	26	93	nd	125	bdl	bdl	bdl	bdl
RDW-1	28.2	-	7.10	6.38	207	145	30.0	21	0.3	nd	30	90	nd	140	bdl	bdl	bdl	bdl

Note: "bdl" = below detection limit, "-''means not measured

tritium-chloride, tritium-temperature, chloride-silica, chloride-sulphate etc. can also substantiate this mixing phenomenon (Arnorsson, 1985; Ahmad et al., 2002).

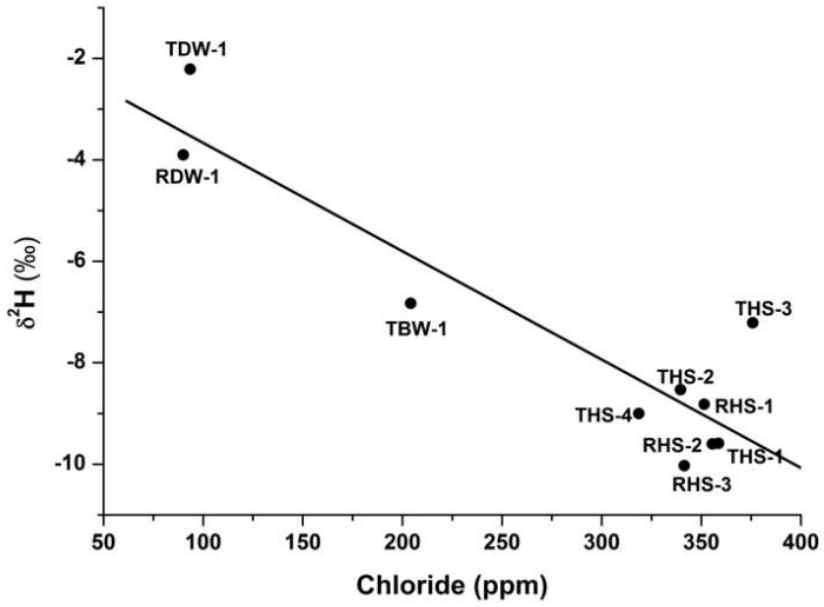

Fig. 3.3 *Relationship between chloride and δ^2H*

In the present study area it is seen that deuterium is negatively correlated with chloride concentration (Fig. 3.3). This negative correlation happens due to the mixing of thermal water having low deuterium and high chloride concentration with shallow groundwater having high deuterium and low chloride concentration. As water and steam are the only reservoirs of deuterium in geothermal systems so deuterium concentration is found to be very sensitive to boiling phenomenon (Truesdell et al., 1977). In the Fig. 3.3, THS-3 sample shows enriched deuterium value probably due to some extent of boiling. Like deuterium, $\delta^{18}O$ is also found to be negatively correlated with chloride for Tural and Rajwadi thermal waters (Fig. 3.4). This basically indicates that the thermal water is getting mixed with non-thermal shallow groundwater having enriched ^{18}O values and depleted chloride concentrations.

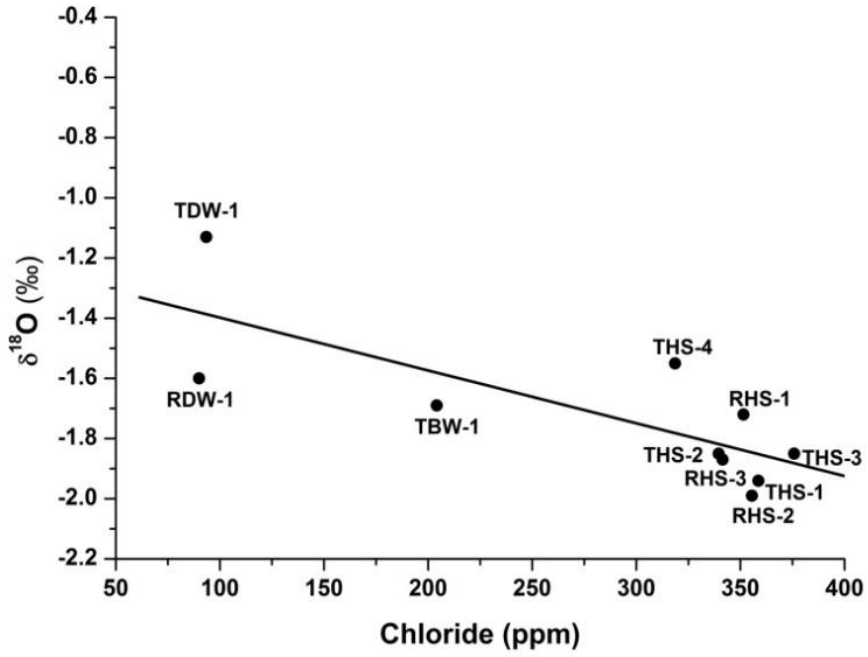

Fig. 3.4 *Relationship between chloride and $\delta^{18}O$*

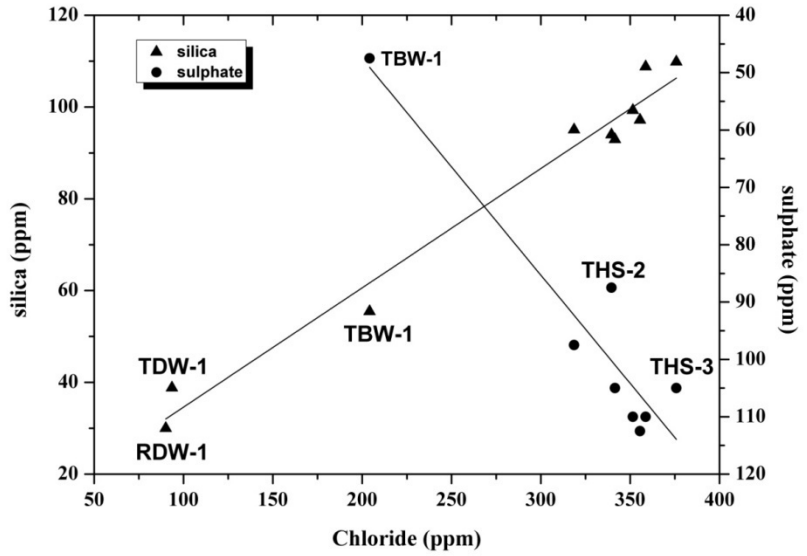

Fig. 3.5 *Plot between silica and sulphate with chloride*

The mixing phenomenon is further substantiated from the linear relationship between silica and sulphate with chloride concentrations (Fig. 3.5). This also points out to the fact that no

further dissolution or precipitation of silica has happened due to the dilution process (Arnorsson, 1985). Tritium is also found to be negatively correlated with chloride concentration (Fig. 3.6). This type of negative correlation takes place when high temperature thermal water having high concentration of chloride and low tritium content mixes with low temperature groundwater containing low chloride and high tritium values (Navada et al., 1995).

3.4.2.2 Quantification of mixing

The extent of mixing between the thermal and non-thermal waters in the Tural-Rajwadi geothermal area is quantified based on the tritium concentrations of both thermal and local groundwaters. Young water fractions present in the mixed thermal water can be approximately calculated based on the following equation (Sammel and Craig, 1981):

$$x = (T_{sp}/T_{gw}) \times 100 \qquad 3.1$$

where x represents the percentage of the young water fraction, T_{sp} represents the tritium concentration of the mixed spring and T_{gw} is the average tritium concentration in the local ground water samples. Assuming the tritium value of 3.17 TU obtained in the shallow dug well sample (TDW-1) as the representative value of T_{gw} in Tural region, the young water fraction is estimated to be about 32% for THS-1, 34% for THS-2, 27% for THS-3, 36% for THS-4 respectively. Similarly in the Rajwadi region, the tritium value of 3.08 TU found in the shallow dug well sample (RDW-1) is taken as T_{gw} and coldwater fraction is estimated to be about 28% for RHS-1 and 40% for RHS-2. So in the Tural-Rajwadi geothermal area, the deep seated thermal water samples are getting mixed with shallow cold groundwater samples in different proportion during its ascent towards the surface.

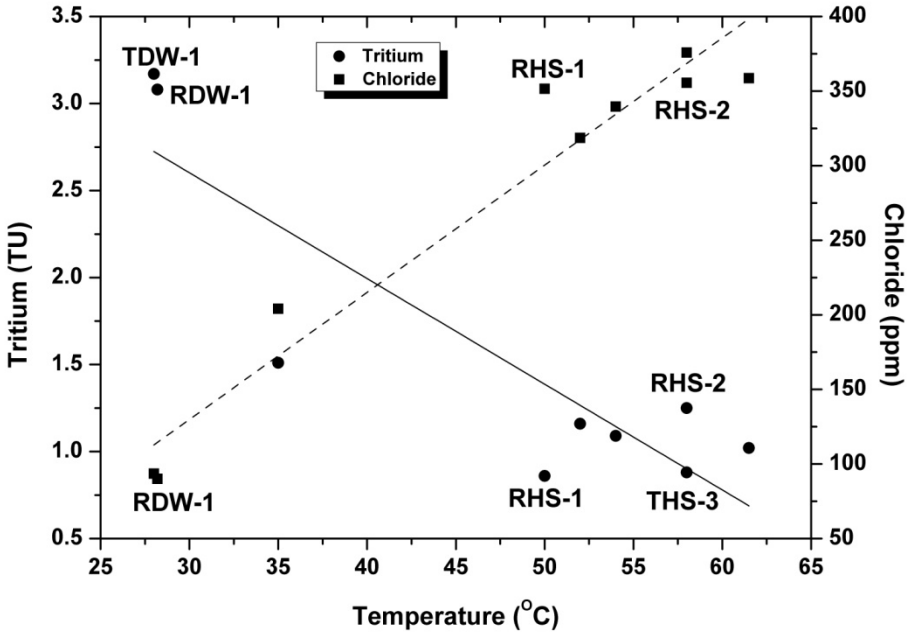

Fig. 3.6 *Plot between chloride and tritium with temperature*

3.4.2.3 Extent of conductive cooling

Thermal waters can undergo variety of cooling mechanisms such as dilution, conductive heat loss, adiabatic cooling before emerging out in the surface. In the present study area although thermal water undergo varying degree of dilution with non-thermal water, it cannot be the ultimate reason for cooling especially when the chemical composition of all the thermal manifestations are almost alike (Fournier, 1977). Graphical plot between the silica concentration and the surface temperature of the thermal springs is generally used to substantiate the conductive cooling phenomenon (Majumdar et al., 2009). Thermal waters from Tural-Rajwadi geothermal area are found to be supersaturated with respect to quartz at their surface discharge temperature as they fall between the solubility curves of quartz and amorphous silica (Fig 3.7). Despite the variation in their surface emergence temperature, the thermal springs show approximately horizontal alignment which indicates the existence of strong conductive cooling during the ascent of the thermal waters with no concomitant loss of

silica in its flow path. The absence of the silica precipitation is further corroborated by the linear relationship between silica and chloride (Fig. 3.5).

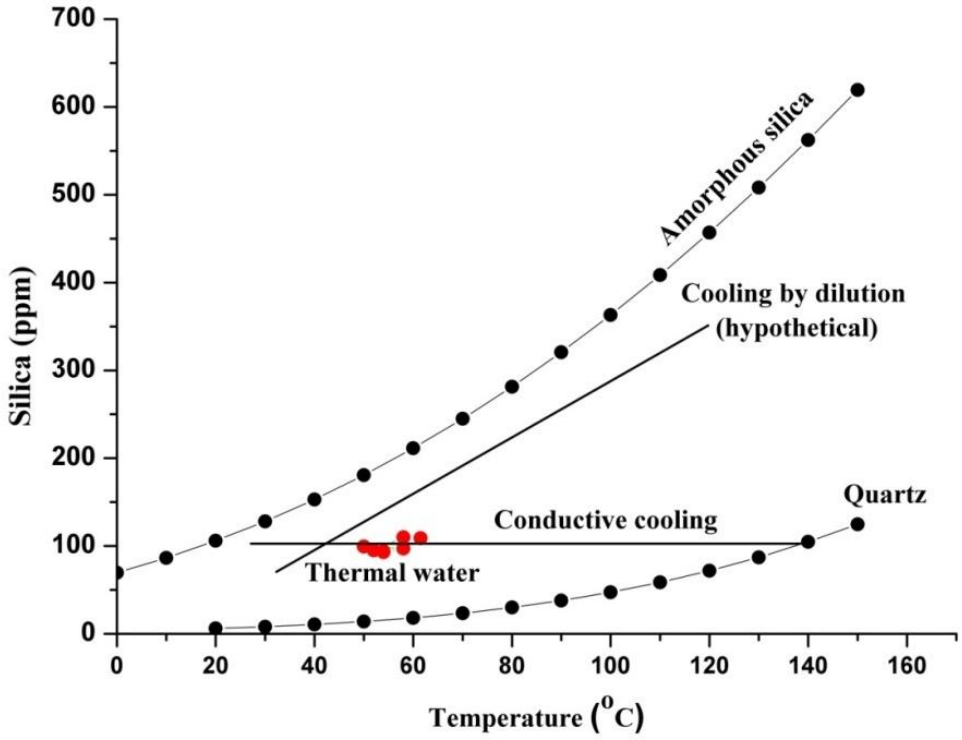

Fig 3.7 *Evidence of conductive cooling*

The quantification of the conductive cooling can also be made based on the premise that during mixing with the shallow ground water, no exo and/or endothermic reactions should take place i.e. mixing should be adiabatic in nature (Levet et al., 2006). Based on the above assumption, Levet et al. (2006) has proposed the following equation:

$$T_{adiabatic} = (1\text{-}x)\ T_{thermal} + x.T_{shallow} \qquad 3.2$$

where $T_{adiabatic}$ is the estimated outlet temperature of the spring, $T_{thermal}$ denotes the calculated reservoir temperature, $T_{shallow}$ represents the temperature of the shallow non-thermal groundwater and x represents the fraction of cold water component in thermal water. The

extent of conductive cooling is given by the difference between $T_{adiabatic}$ and T_{spring} (spring outlet temperature). The fraction of cold water component (x) values calculated previously using tritium concentrations of thermal and non-thermal waters (section 3.4.2.2), are used in this equation. Temperature of the shallow non-thermal groundwater ($T_{shallow}$) and reservoir temperature ($T_{thermal}$) is taken as 30 °C and 160 °C (calculated in the section 3.4.6) respectively. The extent of conductive cooling is shown in table 3.2. From the table 3.2, it is observed that thermal waters have undergone significant extent of conductive cooling (maximum up to 67 °C) before discharging out in the surface.

3.4.3 Isotope analysis

Stable isotopic ratios like $^{18}O/^{16}O$, $^{2}H/^{1}H$, $^{13}C/^{12}C$, $^{11}B/^{10}B$, $^{87}Sr/^{86}Sr$ along with the environmental radioactive isotopes like ^{3}H and ^{14}C provide very pertinent information regarding the origin of thermal water, source of dissolved solutes, mixing between various components, rock-water interaction and transit time estimation. The analyzed values of different isotopes are given in table 3.2.

3.4.3.1 ^{18}O and ^{2}H

The $\delta^{18}O$ and $\delta^{2}H$ values of the thermal and non-thermal water samples collected from the study area are shown in fig. 3.8 along with the GMWL (Global Meteoric Water Line) and LMWL (Local Meteroic Water Line). The LMWL is established based on the isotopic composition of the rain water samples collected from the study area and the corresponding equation is:

$$\delta^{2}H = 6.95 \pm 0.4\ \delta^{18}O + 6.97 \pm 0.7\ (r^2 = 0.97) \qquad 3.3$$

The above equation is almost identical to the LMWL equation [$\{\delta^{2}H = 7.4 \pm 0.5\ \delta^{18}O + 7.6(\pm 0.9)\}$ ($r^2 = 0.86$)] of Mumbai area established earlier by Despandhe et al. (2003). In Tural-Rajwadi geothermal area, $\delta^{18}O$ values of the thermal waters range from -1.55‰ to -

1.85‰ and δ^2H values vary from -7.21‰ to -10.03‰. These stable isotope data confirms the absence of any magmatic component which has very characteristic $\delta^{18}O$ values ranging from +6 to +9 ‰ and δ^2H values varying from -40 to -80 ‰ (Giggenbach, 1992). δ^2H - $\delta^{18}O$ plot (Fig. 3.8) reveals that thermal water samples show parallel ^{18}O-shift from the LMWL line. This type of ^{18}O-shift happens when the ^{18}O of the recharging meteoric water gets exchanged with rock minerals at high temperature resulting the enrichment of ^{18}O content in the thermal water. The extent of this ^{18}O shift is dependent on the various parameters such as: the rock mineralogy (igneous or carbonate), interaction time of the fluid, the reservoir temperature, the available surface area of the rock; rock-water ratio, permeability and porosity etc. (Nicholson, 1993). Greater extent of ^{18}O shift is generally seen in the carbonate aquifer (with original $\delta^{18}O$ values from +20 to +30‰) whereas ^{18}O shift is found to be not so prominent in the basaltic terrain due to the low oxygen-18 content of the basaltic rocks (initial $\delta^{18}O \approx +8‰$) (Truesdell and Hulston, 1980). Similarly if the geothermal system is old and has high water to rock ratio then host rock attains equilibrium with respect to oxygen exchange resulting small oxygen-18 shift in the thermal water. The present study area falls in the basaltic terrain and the highest ^{18}O shift is observed in THS-4 sample (~ 0.76‰) followed by RHS-1 sample (~ 0.56‰). This amount of oxygen-18 shift observed in the present study area is probably due to the longer residence time of the thermal water (13500 ± 1500 years for Tural and 6900 ± 900 years for Rajwadi thermal water) with reservoir rocks at elevated temperature (> 150 °C). The δ^2H - $\delta^{18}O$ plot (Fig. 3.8) also reveals that the thermal water samples have depleted isotopic values compared to the modern day precipitation. This essentially points out that the thermal water contains very old component of recharging water than that of the present day precipitation (Arnorsson, 2000). In fact by using tritium and C-14 data (section 3.4.4), it has been estimated that mean transit time (MTT) of the old thermal water of THS-1 and RHS-1 springs is approximately 13500 ± 1500 years and 6900 ± 900 years, respectively. On the other

hand shallow groundwater samples (TDW-1 and RDW-1) fall very close to the LMWL line indicating modern day recharge.

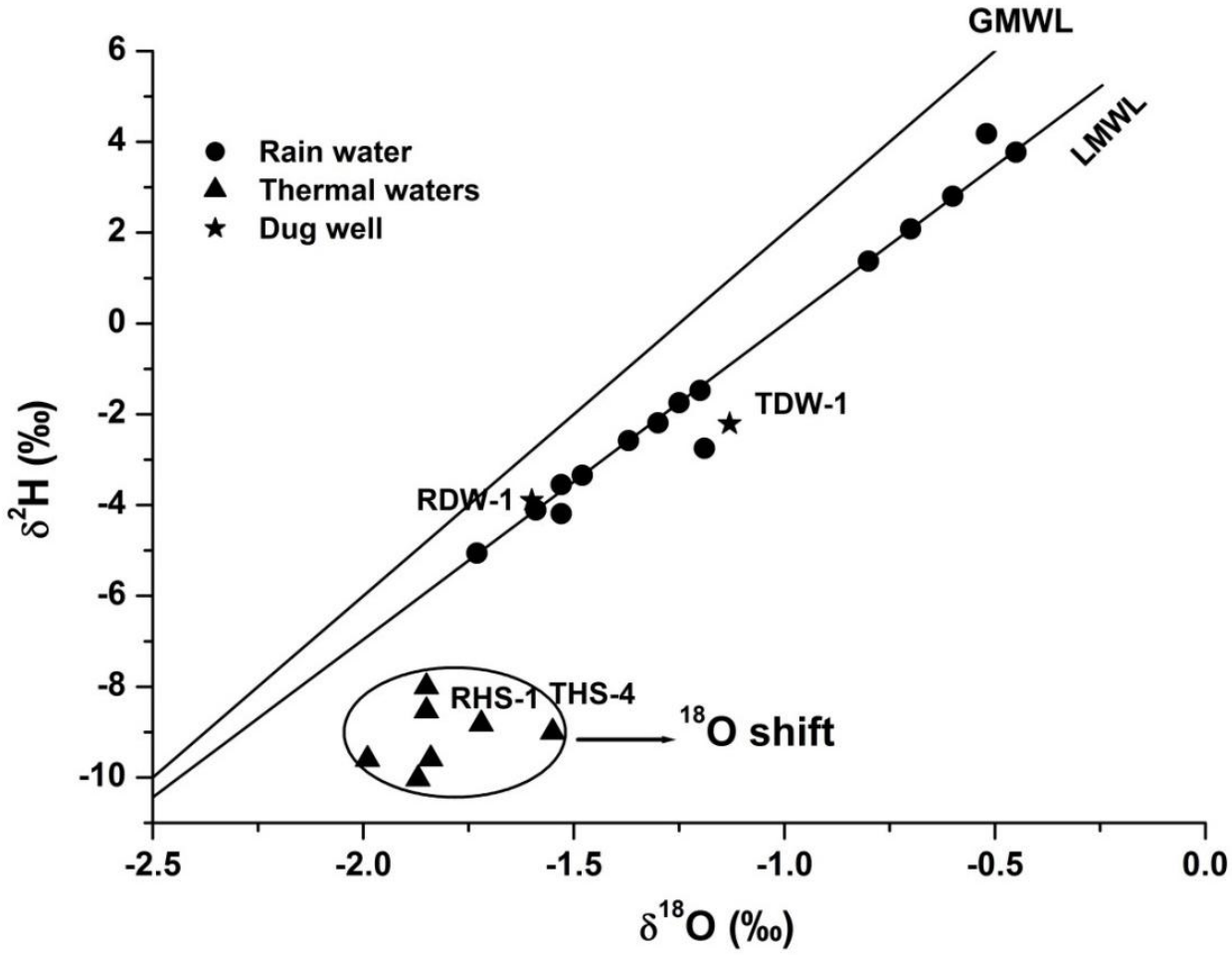

Fig. 3.8 *δ^2H- $\delta^{18}O$ plot of thermal, non-thermal and rain water samples*

3.4.3.2 $\delta^{13}C$ of dissolved inorganic carbon

$\delta^{13}C$ values of DIC (dissolved inorganic carbon) in the thermal water helps to identify the type of the weathering mechanism (silicate or carbonate weathering) as well as the source of soil CO_2 (C_3 or C_4 type of plants). The atmosphere which is the smallest global reservoir of carbon has average $\delta^{13}C$ value close to -8.1‰ (Das et al., 2005). On the other hand, plant carbon has depleted ^{13}C content than the atmospheric CO_2. The fractionation, which

Table 3.2 *Isotopic values and extent of conductive cooling*

Sample ID	$\delta^{18}O$ (‰)	$\delta^{2}H$ (‰)	$\delta^{11}B$ (‰)	$\delta^{13}C$ (‰)	$\delta^{34}S$ (‰)	$^{87}Sr/^{86}Sr$	^{3}H (TU)	Fraction of cold water component (x) (%)	T_{spring} (°C)	$T_{adiabatic}$ (°C)	Extent of conductive cooling ($T_{adiabatic}$ - T_{spring}) (°C)
THS-1	-1.84	-9.59	38.66	-19.74	20.43	0.7260	1.02	32	61.5	118	57
THS-2	-1.85	-8.53	38.66	-20.04	19.87	0.7233	1.09	34	54	115	61
THS-3	-1.85	-7.21	40.00	-19.85	20.25	0.7244	0.88	27	58	125	67
THS-4	-1.55	-9.00	34.50	-20.10	19.8	0.7220	1.16	36	52	113	61
RHS-1	-1.72	-8.82	35.57	-19.62	19.60	0.7512	0.86	28	50	95	45
RHS-2	-1.99	-9.60	37.64	-19.87	20.12	0.7298	1.25	40	58	108	50
RHS-3	-1.87	-10.03	41.01	-	-	0.7419	-	-	54	-	-
TDW-1	-1.13	-2.21	-	-	-	-	3.17	-	35	-	-
RDW-1	-1.6	-3.9	-	-	-	-	3.08	-	46	-	-

Note: "-'' *means not measured*

occurs during CO_2 uptake in the process of photosynthesis, depends on the type of plant and the climatic and ecological conditions. Thus the soil CO_2 generated from the root respiration of the C_3 type of plant has average $\delta^{13}C$ value close to -26‰ whereas for C_4 type of plants average $\delta^{13}C$ value of the soil CO_2 is found to be -12‰ (Clark and Fritz, 1997). Similarly weathering of silicates and/or carbonates requires the conversion of soil CO_2. In case of the silicate weathering if the soil CO_2 comes from the C_3 type of plants then the average $\delta^{13}C$ value is found to be around ~ -19.1‰ whereas with CO_2 derived from the C_4 type of vegetation, the $\delta^{13}C$ has the average value around ~ -5.1‰ (Das et al., 2005). On the otherhand in carbonate weathering, with soil CO_2 coming from the C_3 and C_4 type of vegetations, the $\delta^{13}C$ has average values of ~ -9.6‰ and ~ -2.6‰ respectively (Das et al., 2005). In the present study area, the thermal waters have average $\delta^{13}C$ value around ~ -19.8‰ which clearly shows that the DIC of the thermal springs is mainly controlled by the silica weathering with soil CO_2 derived from the C_3 type of vegetation.

3.4.3.3 $\delta^{34}S$ of SO_4

$\delta^{34}S$ of the dissolved sulphate acts as a very good indicator to trace the source of dissolved sulphate in the thermal water. In the Tural-Rajwadi geothermal area, the $\delta^{34}S$ of dissolved sulphate in the thermal waters ranges from +19.6 to +20.43‰ with respect to Vienna-Canyon Diablo Troilite (VCDT) thus putting the origin of sulphate squarely as marine origin.

3.4.3.4 $\delta^{11}B$ of dissolved boron

Large isotopic variation among the different reservoirs of boron has made it an excellent tracer to identify the source of dissolved boron in the water. The typical value of boron isotopes in different reservoirs are as follows:

1. $\delta^{11}B$ value varies from -5 to +5‰ in granites and fresh oceanic basalts (Spivack et al., 1987)

2. altered oceanic basalts and volcanic gases have $\delta^{11}B$ value varying from 0 to 9 ‰ and 1.5‰ to 6.5‰ respectively (Kanzaki et al., 1979)
3. $\delta^{11}B$ value of sea water is found to be constant at 39.5 ‰ (Spivack and Edmond, 1987)
4. igneous rocks and metamorphic rocks show $\delta^{11}B$ value ranging from -17‰ to -2‰ and -34‰ to 22‰ respectively (Marschall and Jiang 2011; Pennisi et al., 2006)
5. marine boron show $\delta^{11}B$ value varying from -12 to 58‰ whereas for non-marine boron $\delta^{11}B$ value ranges from -32‰ to 26‰ (Vengosh et al., 1994; Xiao et al., 2013)

In the present study area, the $\delta^{11}B$ value of the thermal waters ranges from +34.5 to +41‰ with an average of ~ +38‰ thus clearly pointing to the marine input. The potential sources of this marine input can be either from modern seawater, dissolution of marine evaporites and/or fossil sea water (Vengosh et al., 2002). From stable isotopes, tritium and ^{14}C values (discussed in section 3.4.4); it is evident that thermal waters of Tural-Rajwadi geothermal area do not contain significant modern component. Moreover thermal waters from the present study area have Na/Cl molar ratio close to 0.88 (Gurav et al., 2015) whereas dissolution of marine evaporites has characteristic Na/Cl molar ratio equal to 1. So from the above discussion it is clear that fossil seawater entrapped in the intertrappean beds is responsible for this marine signature. The thermal water showing $\delta^{11}B$ values less than modern day seawater ($\delta^{11}B$ = 39.5‰) is probably due to the rock-water interaction with the paleo-seawater. The basement rock hoisting the Tural-Rajwadi geothermal system is Achaean granites which has average $\delta^{11}B$ value close to zero. So thermal water showing comparatively low $\delta^{11}B$ values than the present day seawater ($\delta^{11}B$= 39.5‰) can be explained as a modification of high $\delta^{11}B$ value of fossil seawater due to extensive rock-water interaction at high temperatures.

3.4.3.5 $^{87}Sr/^{86}Sr$ ratio of dissolved strontium

Strontium isotopic ratio acts as a useful geochemical tracer to constrain the different types of reservoir rocks undergoing interaction with the thermal waters. Several researchers have also used the strontium isotopic ratio to calculate the rock-water ratio as well as quantify the extent of mixing between various strontium bearing reservoirs (Elderfield and Greaves, 1981, Negrel et al., 2001). Each natural reservoir of strontium such as silicate and carbonate rocks, rainwater, seawater, basalt, granite etc. has distinct isotopic composition (Dotsika et al., 2010). Based on the $^{87}Sr/^{86}Sr$ isotopic abundances, Deccan flood basalts have been classified in to eleven formations such as Jawhar, Igatpuri, Neral, Thakurvadi, Bhimashankar, Khandala, Poladpur, Ambenali, Mahabaleshwar, Panhala and Bushe formation. In these entire basaltic formations strontium isotopic ratio ($^{87}Sr/^{86}Sr$) varies from 0.70433 to 0.71972 (Mahoney, 1988) whereas strontium isotopic ratio ($^{87}Sr/^{86}Sr$) of the xenoliths varies from 0.70935 (carbonate) to 0.78479 (granite mylonite) (Ray et al., 2008). The $^{87}Sr/^{86}Sr$ ratios of all the thermal water samples in the Tural-Rajwadi geothermal area are found to vary from 0.7220 to 0.7512 which are quite high compared to the basaltic formation but lies well within the range of granite mylonite formation. Thus strontium isotopic signature gives unequivocal evidence that the thermal waters in this region has percolated deep down to the basement and the Achaean granitic basement rather than the Deccan flood basalts is controlling the strontium isotopic composition. Similar inference is also obtained when lithium, rubidium and caesium concentrations of the thermal waters are plotted in a ternary diagram (Fig. 3.9). According to Giggenbach and Goguel (1989), lithium, rubidium and caesium act as less reactive and conservative tracers in geothermal system as they are rather insensitive to dilution or steam loss phenomenon. Due to large differences in the concentrations of lithium, rubidium and caesium, scaling factors have been applied in the ternary diagram (Fig. 3.9) to evenly spread the data points. From the fig. 3.9, it is observed that thermal water of Tural-

Rajwadi region fall near the compositional area of the granite rather than the basalt. This clearly suggests that the interaction with the granitic basement controls the concentration of these conservative tracers.

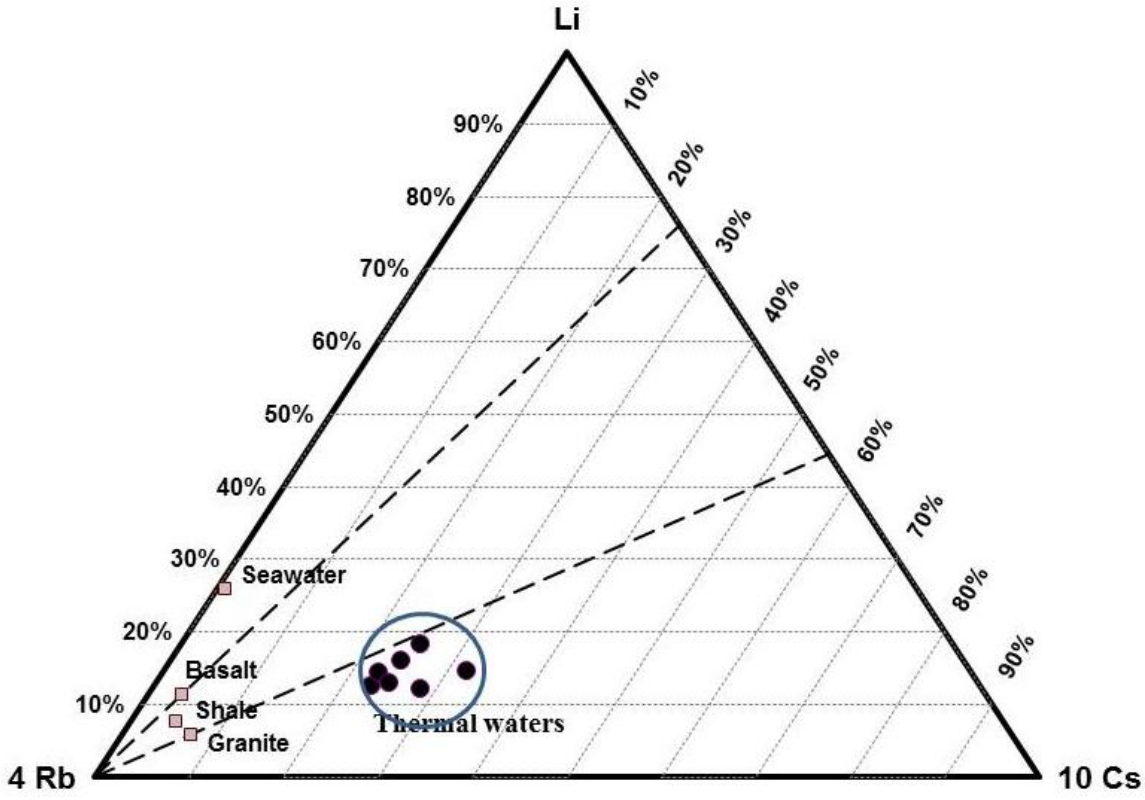

Fig. 3.9 *Li-Rb-Cs ternary diagram of the thermal waters*

3.4.4 Estimation of mean transit time (MTT)

Mean transit time (MTT) of the thermal waters in the Tural-Rajwadi geothermal area is estimated using the both historical and modern day tritium value of thermal waters in conjunction with the tritium values of the shallow dug wells, local precipitation water as well as available carbon-14 values of the thermal waters. Tritium concentrations of the two main thermal manifestations (THS-1 and RHS-1) of the study area are available for the year 1977, 2013 and 2017 respectively (Table 3.3).

Table 3.3 *Tritium concentrations in rainwater, thermal waters and dug well samples*

Sampling date	Rain gauge RG-1			Rain gauge RG-2			Spring THS-1		Spring RHS-1		Well TDW-1		Well RDW-1	
	Rain, mm	^{3}H, TU	±σ, TU	Rain, mm	^{3}H, TU	±σ, TU	^{3}H, TU	±σ, TU	^{3}H, TU	±σ, TU	^{3}H, TU	±σ, TU	^{3}H, TU	±σ, TU
4/1/2017	-	-	-	-	-	-	0.88	0.16	0.8	0.15	3.35	0.27	3.12	0.26
15/04/2013	-	-	-	-	-	-	1.02	0.17	0.86	0.16	3.17	0.3	3.08	0.29
15/07/1977	-	-	-	-	-	-	3.7	0.4	4.3	0.3	-	-	-	-
22/06/2010	263	4.56	0.34	263	4.54	0.34	-	-	-	-	-	-	-	-
7/7/2010	285	3.27	0.28	284	3.82	0.36	-	-	-	-	-	-	-	-
22/7/2010	129	3.34	0.36	129	3.28	0.29	-	-	-	-	-	-	-	-
6/8/2010	252	3.52	0.36	251	3.72	0.36	-	-	-	-	-	-	-	-
21/8/2010	120	2.97	0.37	118	3.19	0.28	-	-	-	-	-	-	-	-
5/9/2010	135	4.07	0.37	133	3.55	0.36	-	-	-	-	-	-	-	-
average	197	3.62	0.35	196	3.68	0.33	1.87	0.24	1.99	0.20	3.26	0.29	3.10	0.28
st. dev	77	0.59	0.03	77	0.49	0.04	1.59	0.14	2.00	0.08	0.13	0.02	0.03	0.02

Note: "-'' means not measured

In 2017, the measured tritium concentrations of THS-1 and RHS-1 samples are 0.88 ± 0.16 TU and 0.80 ± 0.15 TU respectively which are almost similar to the tritium values estimated in 2013. The present day tritium concentrations of THS-1 and RHS-1 are found to be about four times less compared to the tritium concentrations obtained in 1977 (Giggenbach, 1977). In 1977, the measured tritium values of THS-1 and RHS-1 were 3.7 ± 0.4 TU and 4.3 ± 0.3 TU respectively (Giggenbach, 1977). Moreover Reddy et al. (2013) has estimated the carbon-14 age of THS-1 and RHS-1 sample as 3080 ± 40 years BP (Before Present) 1720 ± 45 years BP. Considering the carbon-14 age as deduced by Reddy et al. (2013), the thermal waters in this region should contain tritium concentrations below the detection limit. However the presence of measurable amount of tritium in the thermal waters confirms that the thermal waters are essentially mixed water and the extent of dilution is found to be 32% for THS-1 and 28% for RHS-1 (section 3.4.4.3). The presence of young water fraction in the mixed thermal waters further suggests that the actual age of the deep thermal water should be higher than the age estimated by Reddy et al. (2013). Along with the thermal water samples, tritium measurements of two shallow dug well samples (TDW-1 and RDW-1) are also carried out during 2013 and 2017 field campaigns. During 2017, the tritium concentrations of TDW-1

and RDW-1 are found to be 3.35 ± 0.27 TU and 3.12 ± 0.26 TU respectively which are quite similar to the tritium values measured in 2013. The tritium concentrations of the shallow dug well samples are found to be similar to the average tritium values of local precipitation which was collected fortnightly from the month of June to September, 2010 which clearly establishes that the modern rainfall is the main source of recharge for the shallow unconfined aquifers. The tritium concentrations of the two rain gauges (RG-1 and RG-2) along with the tritium values of the nearby GNIP (Global Network of Isotopes in Precipitation) station are utilized to appropriately scale the long term tritium data of monthly precipitation available for the Tokyo area which essentially acts as an input function in the TracerLPM program. Using this input function, MTT of the young ground water is estimated using single LPM (Lumped Parameter Model) whereas MTT of the mixed thermal water is calculated by using the combination of two LPMs (binary mixing models) representing old thermal water and young groundwater.

3.4.4.1 Construction of tritium time series in precipitation

MTT estimation by using the LPM technique invariably requires long term continuous tritium measurements of precipitation which acts as the input function. In the present study area no continuous long term tritium data is available except during 2010 monsoon season. As a result continuous tritium time series data available for the Tokyo GNIP station are used after proper scaling for the latitude effect by following the methods of Gusyev et al. (2019). Two scaling factors representing the anthropogenic (1958-1977) and ambient levels of tritium (1978 onwards) are established in the present study area. The scaling factors are calculated from the regression lines drawn between the annual weighted tritium ratios of selected coastal GNIP stations and Tokyo area. The selected coastal GNIP stations are Mumbai {closest (~250 km away) from the study area} at 18.9° N, Kozhihode at 11.25° N, Bangkok (13.73° N), Jayapura (-2.53° N), Hong Kong (22.32° N), Kumamoto (32.49° N), Manila/Diliman

(14.64° N) and Yap (9.49° N). Fig. 3.10A shows the ratio of annual weighted tritium concentration in the precipitation of different coastal GNIP stations compared to the Tokyo area for the year 1961 to 2015. From the fig. 3.10A, it is observed that the lower altitudes have the smaller contribution of anthropogenic tritium in precipitation during the "bomb peak period" i.e. 1960-1970s compared with the Tokyo data. For example, GNIP Mumbai has the ratio between 0.24 and 0.59 during the 1961 to 1971 period. The same pattern is observed for the other coastal GNIP stations like Yap, Manila/Diliman and Jayapura. Using these weighted ratios along with the fitted regression line ($R^2 = 0.82$), the scaling factor of the latitude effect for the anthropogenic tritium levels turns out to be 0.35 (Fig. 3.10B). Another linear regression relationship ($R^2 = 0.82$) is established for the ambient tritium levels which has given scaling factor of 0.83 without taking into consideration of tritium measurements in local precipitation (Fig. 3.10B). However if we consider the tritium values of 2010 precipitation in the study area, the scaling factor for the ambient tritium levels of tritium turns out to be 1.78. So the tritium time series data of the Tokyo area is basically scaled with two scaling factors (0.35 for the 1958 to 1977 years and 1.78 for the subsequent years) to obtain the long term continuous tritium values in precipitation for the present study area (shown as a red dotted line in fig. 3.10D). Now this scaled tritium values in precipitation is further weighed with the monthly infiltration values to get the annual tritium concentration in recharge (shown as the solid black line in fig. 3.10D). Annual weighted infiltration values of tritium (C_{in}) are estimated from the following equation:

$$C_{in} = \sum_{i=1}^{12}\{(P_i - E_i)C_i\}/\sum_{i=1}^{12}(P_i - E_i) \qquad 3.4$$

where P_i, C_i and E_i denote the monthly precipitation, tritium concentration of i^{th} month and evaporation or evapotranspiration respectively. If monthly evaporation is found to be higher than the monthly precipitation value then no infiltration happens and the tritium concentration of precipitation corresponding to that month is excluded from the estimation of annual

weighted recharge. As the present study area lacks the continuous record of precipitation as well as of evaporation so monthly values of the Japanese 55-year Reanalysis (JRA-55) dataset (Fig. 3.10C) available from 1958 to 2017 (Harada et al., 2016) is used to estimate the annual weighted tritium concentration in recharge.

3.4.4.2 MTT estimation of the shallow dug wells

Exponential piston flow (EPM) model is used to estimate the MTT of the shallow dug well samples such as TDW-1 and RDW-1. Fig. 3.11A demonstrates the measured and simulated tritium concentrations of TDW-1 and RDW-1 samples whereas the estimated MTTs are shown in fig. 3.11B. TDW-1 and RDW-1 are denoted by square and cross symbols respectively. In Figure 3.11A, dashed lines demonstrate the simulated tritium concentrations of TDW- and RDW-1 using exponential piston model (EPM) with EPM ratio of 0.11, 2.33, 19 and estimated mean transit times (MTT) of 11-15, 8 and 9 years respectively. These simulated tritium concentrations lies within ±1σ analysis error of tritium measurements carried out in 2013 and 2017. The simulated tritium concentrations are found to be rather insensitive to the choice of EPM ratio and produce narrow range of estimated MTTs. From the figure 3.11B, it can be seen that MTTs of the TDW-1 and RDW-1 vary between 8 to 17 years and 7 to 24 years for the EPM ratio ranging between 0.01 and 19. The EPM ratio of 0.11(90% exponential) leads to the range of acceptable MTTs between 9 and 15 years and between 11 and 20 years for TDW-1 and RDW-1 respectively. Increasing piston flow contribution in the EPM ratio results in the narrower MTT range: 8-12 years for TDW-1 and 10-14 years for RDW-1 with 0.33 (75% exponential), 8-11 years for TDW-1 and 9-12 years for RWD-1 with 0.42 (70% exponential), 8-10 years for TDW-1 and 9-11 years for RDW-1 with 0.53 (65% exponential), 8-9 years for TDW-1 and 9-11 years for RDW-1 with 0.66 (60% exponential), and 8-9 years for TDW-1 and 8-11 years for RDW-1 with 0.81 (55% exponential).

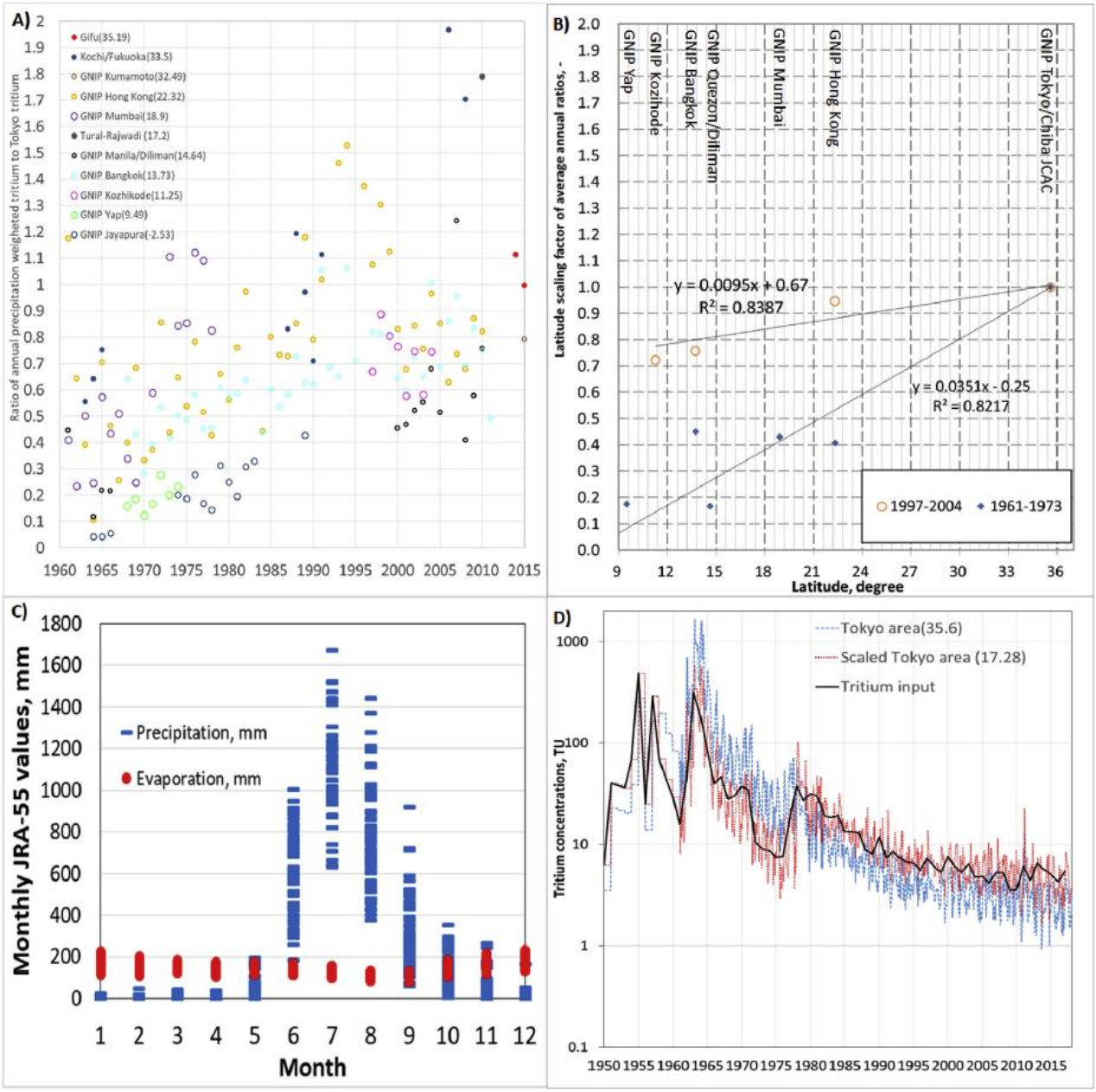

Fig. 3.10 *A) Ratio of annual weighted tritium concentrations is shown between selected coastal GNIP stations and Tokyo area from 1961 to 2015. B) Average of the estimated ratios is shown for the stations located between 9° and 36° N during 1961-1973 and 1997-2004. C) Monthly precipitation and evaporation values of the present study area extracted from the JRA-55 dataset. D) Scaled tritium time series data of the Tokyo area (red dotted line) along with the annual tritium concentration in recharge (solid black line).*

The EPM ratio of 1.85 (35% exponential) produces MTT of 8 year for both TDW-1 and RDW-1 samples. However in piston dominated flow, some of the MTTs are found to be non-

unique. RDW-1 sample show two non-unique MTTs such as 9-10 years or 37-41 years at EPM ratio of 5.67. Similarly when EPM ratio is 9, RDW-1 sample has same non-unique MTT of 9-10 years or 37 years. As the choice of such EPM ratio (largely piston flow) essentially indicates the piston flow travel of the infiltrated water thorough the unsaturated zone which is unlikely to occur in case of shallow groundwater samples so the older MTT solutions are discarded. Therefore, the representative MTTs of TDW-1 and RDW-1 samples are 12.5 ± 4.5 years and 15.5 ± 8.5 years respectively and the corresponding uncertainties in the estimation of MTT arising from the EPM ratio are also found to be low. The other main sources of uncertainties in the estimated MTT are uncertainties associated with the ^{3}H concentrations in the rainfall and the choice of scaling factors. Tritium measurements in the rainfall have about 15% error (± 1σ range) which is found to be considerably smaller than the scaling factor range used to scale the long term tritium records of Tokyo area. To access the effect of corresponding uncertainty, the tritium input concentrations are calculated by using the scaling factors such as 0.83 (50% of 1.78), 1.12 (35% of 1.78), 1.33 (25% of 1.78), 1.51 (15% of 1.78) and 1.69 (5% of 1.78), thus covering the entire range of scaling factors used for the ambient levels of tritium concentrations. With the decrease in the value of the scaling factor, the MTT is found to shift gradually from older to younger range. For example, the estimated MTTs of TDW-1 and RDW-1 become 9.0 ± 4.0 years and 12.5 ± 6.5 years when the scaling factor is changed to 1.68. Similarly with scaling factor of 1.51, the MTTs of TDW-1 and RDW-1 becomes 5.5 ± 1.5 years and 8.0 ± 3.0 years respectively. Furthermore upon using 1.33 as the scaling factor, the MTT of TDW-1 and RDW-1 turns out to be 3.5 ± 2.5 and 2.5 ± 1.5 years respectively. Interestingly the scaling factor of 0.83 produces unrealistically old MTTs for shallow groundwater systems which are not plausible. Thus uncertainty in the scaling factor is found to have less impact on the estimated MTT of the young groundwater systems compared to the uncertainty in the EPM ratio.

3.4.4.3 MTT estimation of thermal waters

MTT estimation of the thermal waters in the present study area is carried out by using binary mixing model (BMM) as these thermal waters essentially represent mixed water. The BMM is comprised of EPM for shallow groundwater and PFM for deep thermal water. Firstly the MTT of the young water fraction present in the thermal waters is estimated using the entire range of the EPM ratio varying between 0.01 to 19. The MTT range estimated for the young groundwater component in both THS-1 and RHS-1 are shown in fig. 3.11B. Tritium tracer MTTs of THS-1 and RHS-1 are represented by circle and dash symbols respectively. From the fig. 3.11B, it is observed that young groundwater component of THS-1 spring has few best-fit MTTs such as 16 years (EPM ratio = 19), 36 years (EPM ratio = 1.5), 38 ± 1 year (EPM ratio = 1.33) and 40 years (EPM ratio = 1). On the other hand, the MTT of the young water fraction in RHS-1 saample shows slightly wider variation such as 36 ± 4 years (EPM ratio = 0.01), 38.5 ± 3.5 years (EPM ratio = 0.05), 32–33 years (EPM ratio = 0.82), 34.5 ± 3.5 years (EPM ratio = 1), 36 years (EPM ratio = 1.22), 33–34 years (EPM ratio = 1.86) and 16 years (EPM ratio = 9). So the representative MTTs of the young groundwater fraction present in the THS-1 and RHS-1 are 28.0 ± 12.0 years and 29.5 ± 12.5 years respectively. The above well constrained MTTs are due to the availability of the three time tritium measurements of the thermal waters covering both the bomb peak and ambient levels of tritium as well as due to the small analytical error in the tritium measurements.

To estimate the MTT of the deep old thermal water, the carbon-14 ages {(in percent modern carbon (pMc)} of 2008 thermal water samples (THS-1 and RHS-1) collected by Reddy et al. (2013) is utilized. Reddy et al. (2013) only reports conventional carbon-14 ages with respect

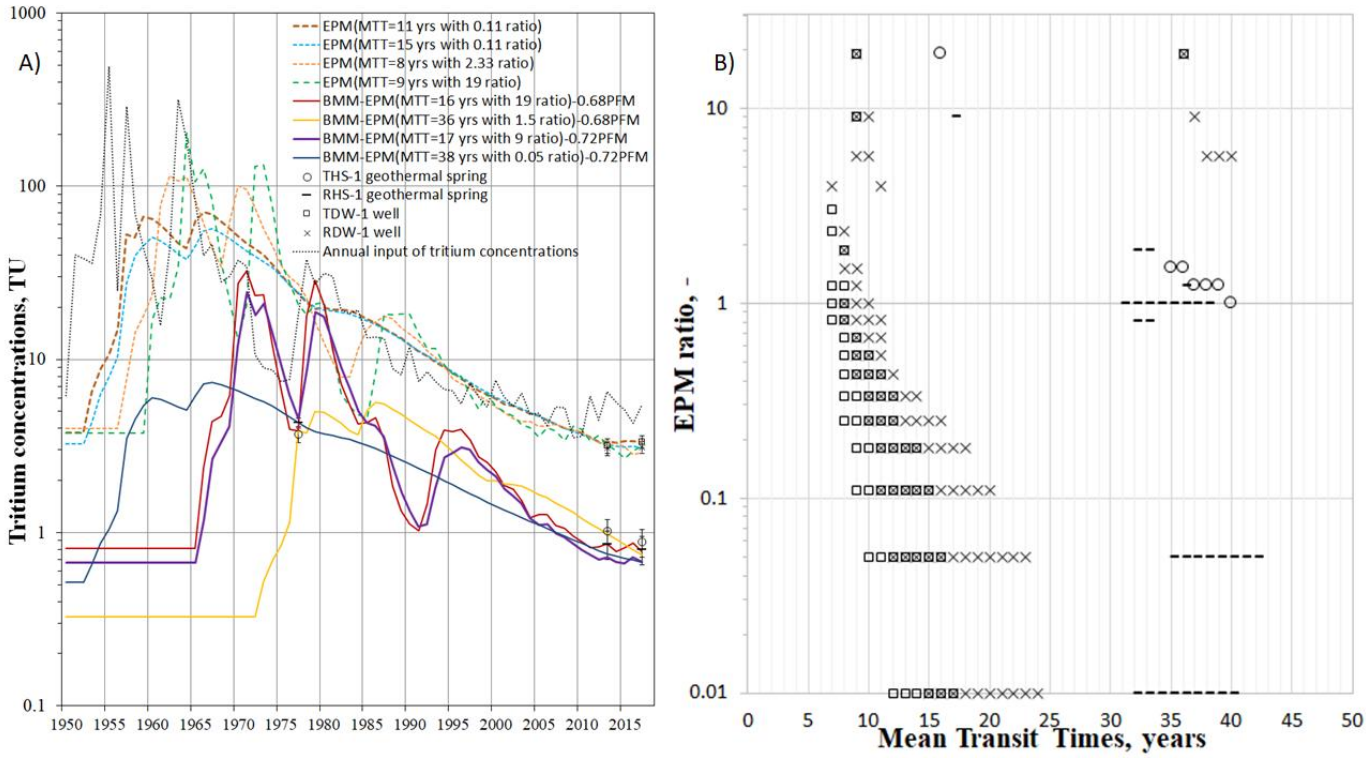

Fig 3.11 *A) Plot of measured as well as simulated (EPM and BMM) tritium concentration of dug wells (TDW-1 and RDW-1) and thermal waters (THS-1 and RHS-1). Dashed lines are used to demonstrate simulated tritium concentrations of shallow dug wells whereas solid lines are used for thermal waters. B) Estimated mean transit times (MTTs) of shallow dug wells and young water fraction present in the thermal waters using exponential piston model (EPM) ratio.*

to 1950 A.D. The estimated carbon-14 ages of THS-1 and RHS-1 are converted to the percent modern (pM) values (Stuiver and Polach, 1977) which are futher de-normalised by following the procedure as described by Mook and Van der Plicht (1999) using $\delta^{13}C$ values (-19.5‰) of thermal waters resulting 61.9 (± 0.31) pMc for THS-1 spring and 73.3 (± 0.41) pMc for RHS-1 spring. However these carbon-14 concentrations of the thermal waters are affected by the young water MTTs as some amount of modern carbon is present due to the mixing process. Thus using the carbon-14 concentrations of the 2008 samples along with the MTTs of the young water fractions (Fig. 3.11B), the MTTs of old thermal water (no mixing) of THS-1 and RHS-1 turns out to be 13500 ± 1500 years and 6900 ± 900 years respectively.

These calculated MTTs are found to be about five times older than the estimated MTTs reported by Reddy et al. (2013). Now the MTT of the mixed thermal water ($T_{m,\ true}$) is estimated by the BMM equation:

$$T_{m,\ true} = x\ T_{m,\ young} + (1- x)\ T_{m,\ old} \quad 3.5$$

$T_{m,\ young}$ and $T_{m,\ old}$ represent the MTTs of the young and the old component of the thermal waters whereas f denotes the extent of the young water fraction present in the mixed thermal water. For THS-1, using the values of $T_{m,\ young}$ as 28.0 ± 12.0 years, $T_{m,\ old}$ as 13500 ± 1500 years and 'x' as 0.32, the estimated MTT of mixed thermal water ($T_{m,\ true}$) turns out to be 9189 ± 1023 years. Similarly for RHS-1, estimated MTT of mixed thermal water ($T_{m,\ true}$) turns out to be 4701 ± 616 years using the values of $T_{m,\ young}$ as 29.5 ± 12.5years, $T_{m,\ old}$ as 6900 ± 900 years and 'x' as 0.28. These aggregated MTTs of the mixed thermal water are found to be two times older than the values given earlier by Reddy et al. (2013). These modified MTTs provide crucial information regarding the sustainability of the thermal waters as well as help to estimate the reservoir volume more accurately.

3.4.5 Estimation of the reservoir volume

The estimated MTT of the thermal water can further be utilised to calculate the volume of the reservoir water contributing to the natural discharge by applying the following equation at the steady state (Kazemi et al., 2006; Apollaro et al., 2015, 2016):

$$V_w = Q_w \times T_m \quad 3.6$$

where V_w, T_m and Q_w represent the volume of reservoir water contributing to the natural discharge, MTT of the thermal water and cumulative flow rate of the thermal springs respectively. Afterwards the reservoir volume can be approximated by dividing V_w with the effective porosity of the rocks (Apollaro et al., 2015, 2016):

$$V_{res} = V_w / \eta \quad 3.7$$

where V_{res} is the volume of the reservoir and η represents the effective porosity of the rocks hoisting the thermal system. In our present study area η generally varies between 0.01 and 0.03 for the Precambrian granite basement rock (Kushnir et al., 2018). In Tural area, the cumulative discharge of thermal sprouts is estimated to be 7.18 L/s. Incorporating the MTT value of 13500 ± 1500 years applicable for the old thermal water component in the Tural area, the volume of the old thermal water contributing to the natural discharge turns out to be 2.079 ± 0.231 km^3. Now varying the effective porosity values between 0.01 and 0.03 in equation 3.7, the estimated reservoir volume varies between 207.9 ± 23.1 km^3 and 69.3 ± 7.7 km^3 in the Tural area. Similarly in Rajwadi area, using the cumulative discharge of 8.9 L/s and MTT of 6900 ± 900 years leads to the thermal water volume of 1.394 ± 0.002 km^3 that is contributing to the natural discharge. Using the effective porosity values of 0.01 and 0.03 leads to the reservoir volume of old thermal water between 139.4 ± 0.2 km^3 and 46.5 ± 7.7 km^3, respectively. Thus the estimation of actual transit time and flow-rate measurements of the thermal springs actually helps to approximately calculate the volume of the geothermal reservoir and the volume of the reservoir water contributing to the natural discharge.

3.4.6 Estimation of reservoir temperature

3.4.6.1 Chemical geothermometers

Accurate estimation of the subsurface reservoir temperature of a geothermal system plays a very crucial role in the future planning and the further exploration of that particular geothermal area. The principal purpose of the geochemical analysis is to predict the reservoir temperature of the geothermal systems by using various chemical geothermometers. Since 1960's, numerous chemical geothermometers have been employed to predict the reservoir temperature of geothermal systems (Fournier and Truesdell, 1973; Truesdell and Fournier, 1977; Fournier, 1977; Fournier and Potter, 1979; Tonani, 1980; Fouillac and Michard, 1981; Arnorsson, 1983; Giggenbach, 1988). Chemical geothermometers are broadly classified in to

two categories such as silica geothermometer and cation geothermometer. Table 3.4 lists the estimated reservoir temperature in the Tural-Rajwadi geothermal area by applying various chemical geothermometers. Among various silica geothermometers, chalcedony and quartz geothermometer have been used in the present study area. Chalcedony geothermometer estimates reservoir temperature between 106 to 116 °C whereas quartz geothermometer (no steam loss) yielded reservoir temperature between 133 to 143 °C. Quartz geothermometer is more suitable in the present geological settings as quartz is found to control the dissolved silica concentration in the thermal waters of West Coast region (Saxena and Gupta, 1987). The suitability of applying cation geothermometers is verified using Na-K-Mg ternary diagram (Fig. 3.12) as proposed by Giggenbach (1988). The Na-K-Mg ternary diagram is generally used to classify thermal waters as fully equilibrated, partially equilibrated or immature with respect to source rock at given temperatures. From the fig. 3.12, it is observed that most of the thermal waters fall in the partial equilibrium region and the thermal water samples fall on the full equilibration line at 140-160 °C. The subsurface temperature obtained

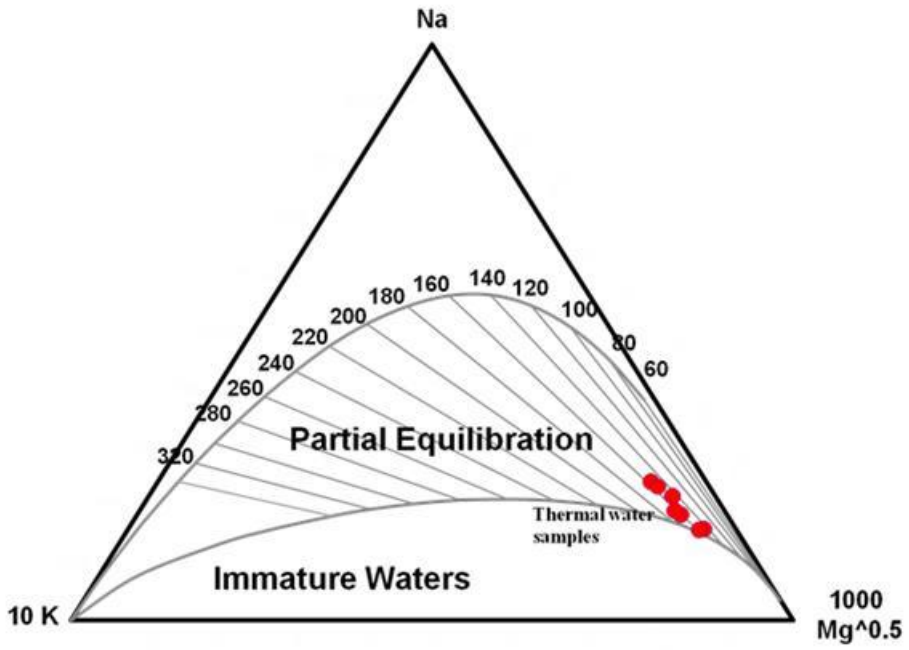

Fig. 3.12 *Na-K-Mg ternary diagram*

by applying quartz geothermometer (133-143 °C) is somewhat lower than the Na-K cation geothermometer (147-160 °C) because quartz geothermometer, being based on the absolute concentration of silica, gets more affected due to the dilution phenomenon compared to the Na-K geothermometer which is based on the ratio of Na and K concentrations. The estimated reservoir temperature (88 to 99 °C) provided by K-Mg geothermometer (Giggenbach, 1988) is too low to be considered in this study area. This happens because of the mixing with Mg rich young groundwater in the upflow region. Similarly the base temperature (77 to 91 °C) computed by the Na-K-Ca geothermometer is also unreliable due to the presence of high concentration of calcium coming from the relic sea water component. Chemical geothermometers thus indicate that 145 ± 15 °C is the range of most probable reservoir temperature in this region.

3.4.6.2 Mixing model

The presence of measurable tritium concentrations as well as linear relationship among different conservative tracers clearly points out that the thermal waters in Tural-Rajwadi area undergo mixing with non-thermal shallow groundwater during its ascent towards the surface. In such circumstances, there are various types of mixing models such as silica-enthalpy, chloride-enthalpy and silica-carbonate mixing models that are normally used to estimate the subsurface temperature of the geothermal reservoir. In the present study area, the silica-enthalpy and chloride-enthalpy mixing models are used to calculate the reservoir temperature (Truesdell and Fournier, 1977; Fournier, 1979b). In both the above mentioned models, enthalpy is used as an axis rather than the temperature because the combined heat content (i.e. enthalpy) remain conserved even after the mixing between two water bodies having widely different temperature (Fournier, 1989b).

Table-3.4 *Estimated reservoir temperature (°C) from chemical geothermometers*

Sample ID	Chalcedony (conductive) Arnorsson (1983)	Quartz (conductive) Fournier (1977)	Quartz (Adiabatic) Fournier (1977)	Na/K Fournier (1979a)	Na/K Giggenbach (1988)	K/Mg Giggenbach (1988)	Na-K-Ca Fournier and Truesdell (1973)
THS-1	116	142	137	141	160	91	86
THS-2	107	134	130	128	148	80	77
THS-3	116	143	137	143	162	94	91
THS-4	107	135	130	139	158	85	81
RHS-1	110	137	132	135	155	99	83
RHS-2	109	136	131	133	152	96	83
RHS-3	106	133	129	127	147	91	78

3.4.6.2.1 Silica-enthalpy mixing model

In the silica-enthalpy mixing model, the analysed silica concentrations of the thermal water samples are generally plotted against their issuing enthalpies. The issuing temperatures are converted to the corresponding enthalpies using the steam tables given by Keenan et al. (1969). In this model, two end member water samples are normally considered: one is the shallow non-thermal water sample (dug well) and the other one is the thermal water sample. Afterwards the enthalpy of the geothermal reservoir is computed based on the either of the two methods. In the first method (Fig. 3.13A), it is assumed that no steam or heat loss phenomenon takes place before mixing with shallow non-thermal groundwater. A line connecting the local groundwaters (non-thermal waters) as well as the thermal water is drawn this intersects the quartz solubility curve (no steam loss curve) at point A. A vertical line is drawn from point A which intersects the enthalpy axis at point B. Point A represents the

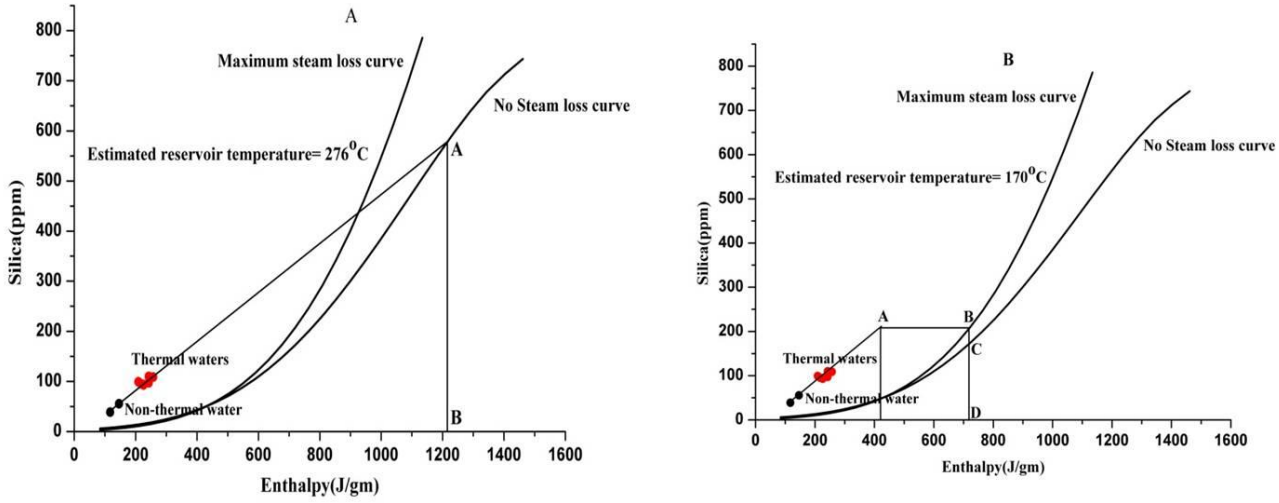

Fig. 3.13 *Silica-enthalpy mixing model*

enthalpy and the silica concentrations of the thermal water before mixing. In this method, the subsurface reservoir temperature turns out to be 276 °C which is abnormally high. This basically indicates that the thermal waters in the Tural-Rajwadi geothermal area undergo some extent of heat loss/steam loss before mixing (Fournier and Truesdell, 1974). This steam

loss/heat loss phenomenon is taken care of in the second graphical method (Fig. 3.13B). In this method a line connecting the thermal and non-thermal water is extended up to the point A which is the steam separation temperature i.e. 100 °C (corresponding enthalpy value is 419 J/g). From the point A, another line parallel to the abscissa is dawn which cuts the maximum steam loss curve at point B. The point B represents the enthalpy of the parent thermal water before boiling and mixing. The vertical line from the point B cuts the no steam loss curve at point C which gives the original silica content of the thermal water. Using this method the subsurface reservoir temperature turns out to be 170 °C which matches very well with the temperature estimation provided by Na-K geothermometer (~162 °C).

3.4.6.2.2 Chloride-enthalpy mixing model

Chloride-enthalpy mixing model or the enthalpy-chloride diagram (Fig. 3.14) is found to be very useful in defining various subsurface processes such as boiling, dilution, conductive cooling etc as well as estimate the reservoir temperature (Nicholson, 1993). In the fig. 3.14, the point A represents the enthalpy and chloride concentration of the non-thermal groundwater whereas points S_0 to S_5 represent the issuing temperature and chloride concentration of the thermal water samples. Point B denotes the steam point having constant value of 664 Cal/g. Straight lines (steam loss lines) are then drawn connecting the point B with S_0 to S_5 points. The estimated temperature of each thermal manifestation calculated from the Na-K geothermometry are then plotted on the steam loss lines (P_0-P_5). Line C and D joining the points A and P_x basically represent the dilution or mixing lines. Line C and line D intersects the line Q (upper bounding boiling curve) at points E and F respectively. The enthalpy and chloride composition of the parent thermal water is given by point E. Upon utilizing this method the estimated reservoir temperature turns out to be 160 °C which matches exactly with the results obtained from the Na/K geothermometric equation given

by Giggenbach (1988). The maximum and minimum estimate of the subsurface reservoir temperature is given by points F (180 °C) and P_0 (142 °C) respectively. The minimum value

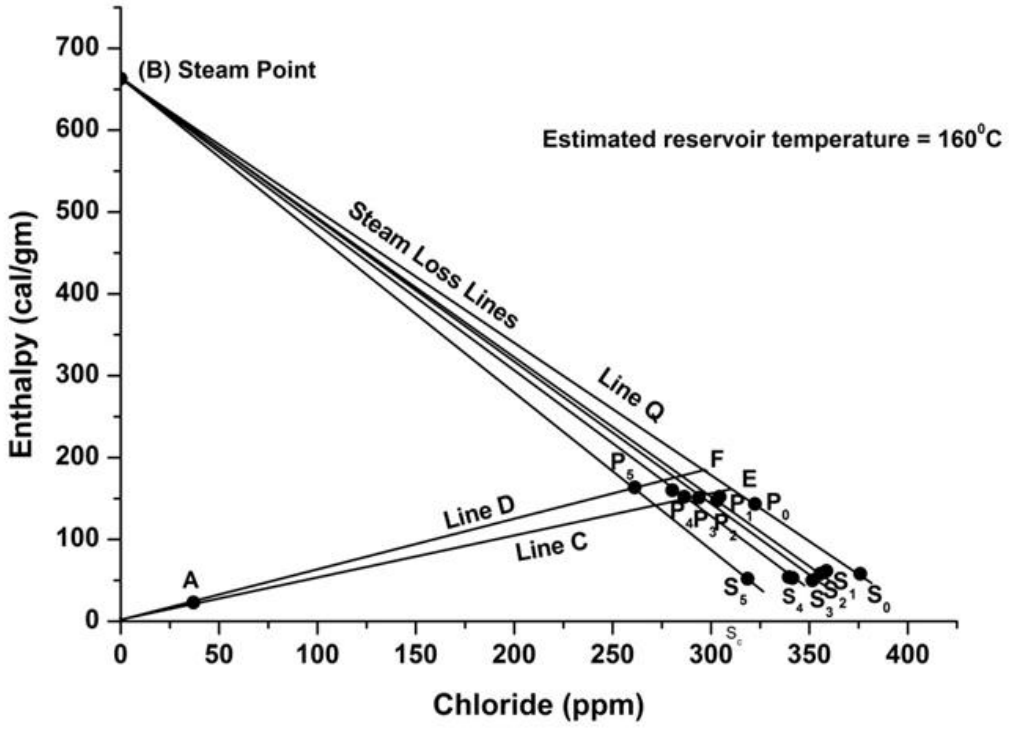

Fig. 3.14 *Chloride-enthalpy mixing diagram*

of the reservoir temperature (142 °C) matches quite well with the temperature range obtained from quartz geothermometer. Thus the two mixing models clearly suggest that the subsurface reservoir temperature of the Tural-Rajwadi geothermal area varies from 160 ± 10 °C which is also comparable with the Na-K geothermometer values.

3.5. Conclusions

The integrated multi-isotope tracing in conjunction with the geochemical analysis of the thermal waters in the Tural-Rajwadi geothermal area has opened up new vistas in characterizing thermal waters of Indian subcontinent such as the deducing the origin of the thermal waters, source of the dissolved solutes, transit time estimation and reservoir temperature estimation. All the thermal manifestations in this area are found to be Na-Cl type

i.e. old and matured water. Analysis of stable isotopes of oxygen and hydrogen (δ^2H and $\delta^{18}O$) reveals that thermal waters are not recently recharged rain water as they have depleted deuterium content compared to the modern day precipitation. In fact using tritium and carbon-14 data, the mean transit time (MTT) of the old thermal water in Tural (THS-1) and Rajwadi (RHS-1) area is found to be 13500±1500 years and 6900±900 years respectively. Significant oxygen-18 shift is observed due to extensive rock-water interaction at high temperature (~160 °C) over prolonged period of time. Silicate weathering with soil CO_2 coming from the C_3 types of plants is found to control the cabon-13 isotopic composition of DIC in the thermal waters. The application of sulphur and boron isotopes unequivocally establishes the presence of marine signature in the Tural-Rajwadi thermal waters. This marine signature probably arises due to the entrapment of paleo-seawater in the intertrappean beds between Deccan Trap layers. Boron isotopic composition of the thermal waters varies from +34 to +41‰ which show that both the sea water and rock dissolution are the main sources of dissolved boron. The strontium isotopic ratio ($^{87}Sr/^{86}Sr$) gives conclusive evidence that the thermal waters in the Tural-Rajwadi area have circulated deep down to the basement and the dissolution of the basement rocks (i.e. Achaean granite) is the predominant source of dissolved strontium. Linear relationship between several conservative tracers (δ^2H-Cl, SiO_2-Cl, ^3H-Cl) indicates the mixing phenomenon between thermal and non-thermal ground water and the extent of mixing (~30%) is quantified using tritium concentrations of the both thermal and non-thermal ground water. Thermal waters in the present study area attain surface discharge temperature largely by conductive cooling (up to ~ 67 °C) without any concomitant loss of dissolved silica. Based on the available geological, hydrological and isotopic inferences, a conceptualized hydrogeological W-E cross section map (Fig. 3.15) of the study area has been prepared. This research work also demonstrates the usefulness of long term tritium measurements in estimating the MTT of the young groundwater, old thermal water

and mixed thermal water separately using lumped parameter models. This study adopts a rigorous approach to scale the continuous tritium time series data of the Tokyo GNIP station by considering both the anthropogenic as well as the ambient levels of tritium concentration in precipitation. Two scaling factors are thus established and this scaling is absolutely essential as the present study area has no continuous record of tritium values in precipitation. This properly scaled tritium values act as input parameter in different lumped parameter models. The estimated MTT of the shallow groundwater (TDW-1 and RDW-1) in this region varies from 7 to 24 years whereas the MTT of the young water fraction present in the thermal water ranges from 16 to 42 years. The updated MTTs (derived from both tritium and carbon-14 values) of the old thermal waters of THS-1 (13500 ± 1500 years) and RHS-1 (6900 ± 900 years) reveal that these thermal waters are actually several times older than previously estimated. This updated MTT is further utilised to estimate the reservoir volume as well as the volume of thermal water discharge contributing to natural recharge. Thus the long term tritium measurements not only helps to constrain the MTT of the thermal waters very effectively but also it is found to provide a viable alternative to understand the circulation of the thermal waters compared to the usual drill hole based investigation which is not feasible due to the high subsurface temperature and difficulty in deep drilling in the geothermal areas. Furthermore the subsurface reservoir temperature in the Tural-Rajwadi geothermal area is estimated using both chemical geothermometers and mixing models. Quartz geothermometer provides lower subsurface temperature (133-143 °C) compared to the Na-K geothermometer (147-160 °C) due to the dilution phenomenon. The average reservoir temperature (160° ± 10 °C) obtained from applying both silica - enthalpy mixing model and chloride - enthalpy mixing model matches well with the Na-K geothermometer values and thus can be taken as the most probable subsurface reservoir temperature in the Tural-Rajwadi geothermal area.

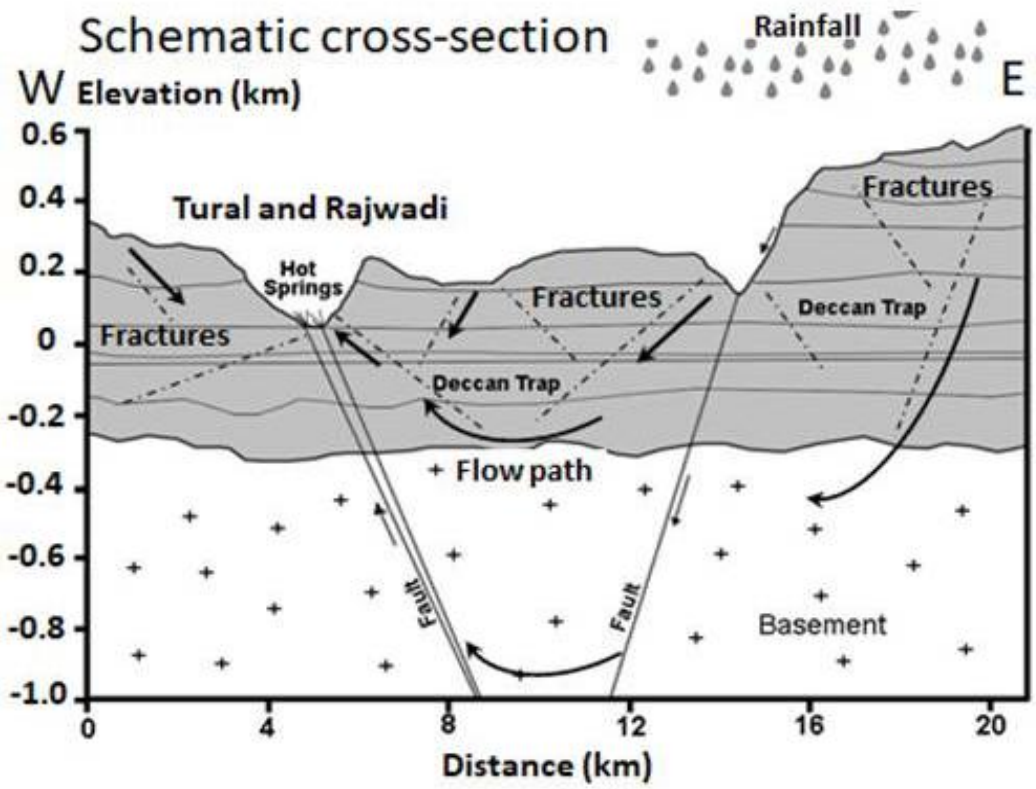

Fig. 3.15 *Conceptualized hydrogeological W-E cross section map of the study area*

CHAPTER 4

Isotope-geochemical characterization of Godavari valley geothermal field of Telangana, India

4.1 Background

Godavari valley geothermal field located in the Khammam district of Telangana state, hosts several thermal manifestations having surface discharge temperature ranging from 36 to 80 °C. The Godavari geothermal region is basically a NNW-SSE trending graben filled with the Gondwana sedimentary formation which falls within the zone II (100 - 180 mW/m^2) region in the heat flow map of India having thermal gradient as high as 60 °C/Km (Ravi Shanker, 1988). Although this region has huge potential for further development of geothermal energy (Chandrasekharam et al., 1996) yet there is no detailed study regarding the hydrogeochemical evolution and the isotopic characterization of the thermal waters. Although the chemical analysis of some of the thermal springs in this area was earlier carried out by few researchers (Saxena and Gupta, 1985, Chandrasekharam et al., 1996) but there was wide variation in the estimation of the reservoir temperature. Saxena and Gupta (1985) estimated reservoir temperature in the range of 100 to 150 °C whereas subsurface temperature calculated by Chandrasekharam et al. (1996) varied from 173 to 215 °C. Furthermore some of the thermal springs (i.e. Agnikundala spring etc.) reported earlier have now become extinct and several new thermal water manifestations have been reported from the boreholes drilled for coal exploration. Under these circumstances a comprehensive isotope hydrological investigation coupled with geochemical characterization has been carried out. Multivariate statistical methods such as HCA (Hierarchical Cluster Analysis) and PCA (Principal Component Analysis) along with the conventional graphical plots have been utilized to decipher different geochemical processes controlling the solute concentration in the thermal and non-thermal waters. Stable isotopes (δ^2H and $\delta^{18}O$) of the thermal and non-thermal waters have been analyzed to trace the origin of the thermal waters. Carbon-13 isotopic composition ($\delta^{13}C$) of the DIC is measured to find out the sources of dissolved inorganic carbon in the thermal waters. Tritium and carbon-14 dating are employed to ascertain the residence time of the

thermal waters. Subsurface reservoir temperature is estimated by using both chemical geothermometers, multicomponent fluid-mineral equilibrium method and mixing models.

4.2 Study area

Thermal manifestations in the Godavari valley geothermal field are generally observed near the Pagaderu, Shantinagar, Gollakatur, Kodichenkuntala and ST colony villages of Manuguru Tehsil of Khamman district, Telangana. Most of the thermal discharges are from the bore holes drilled for the exploration of coal reserves by the SCCL (Singareni Collieries Company Ltd.). The geological map (1:25000 scales) along with the sample location points are shown in the fig. 4.1. Four stage evolutionary sequences have been ascribed for the formation of this Godavari valley rift basin (Srinivasa Rao et al., 1979). The first two evolutionary stages happened during Eastern Ghat orogeny whereas later two stages occurred during Gondwana period (Chandrasekharam et al., 1996). This rift basin is covered with fluviatile/continental sediments of Gondwana Supergroup which are further subdivided in to Talchir formation, Barakar formation, Barren Measures formation and Kamthi formation (Krishna Murthy et al., 1985). Proterozoic Pakhal metasediments forms the basement rock of the study area. Talchir formation of Lower Gondwana subgroup rests unconformably over the Pakhal formation. Talchir formation is composed of fine sandstone, chocolate shale and pebble bed. The Barakar formation, which overlays the Talchir formation, is composed of feldspathic sandstone, carbonaceous shale and coal seams. The Barren Measure formation lies over the Barakar formation and is composed of medium to coarse grained feldspathic sandstone along with siltstone and clay. The Kamthi formation lies unconformably over the Barren Measure formation and is predominantly made up with coarse grained ferruginous sandstone, siltstone

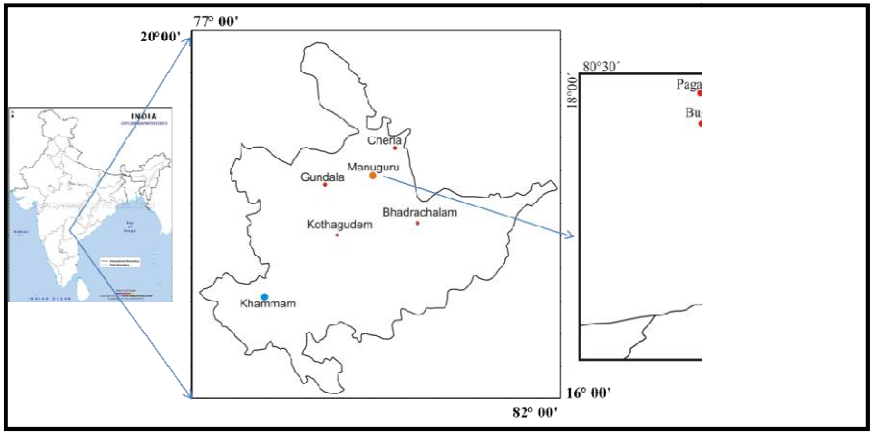

Fig. 4.1 *Sampling points along with the geological map in the Godavari valley geothermal field*

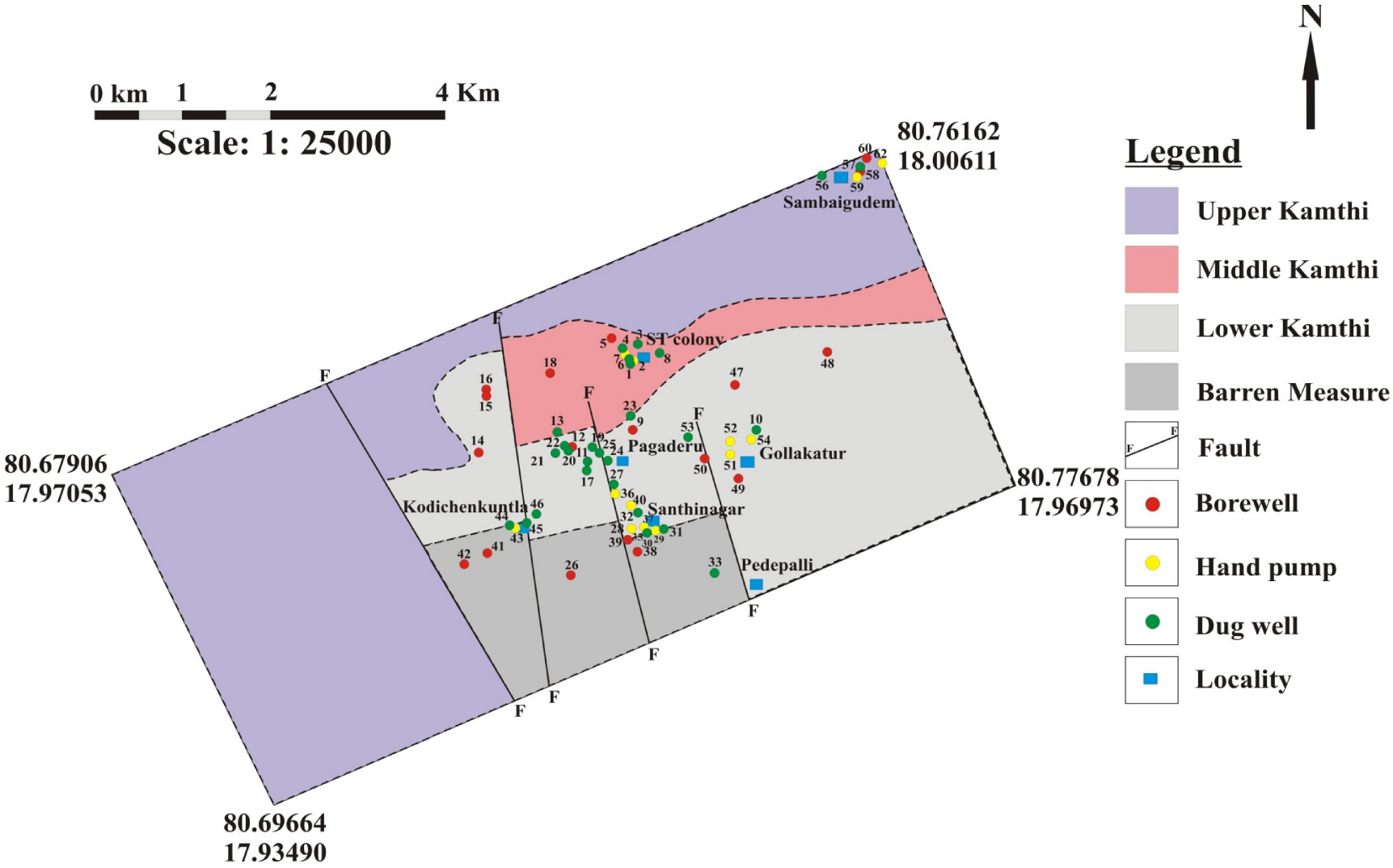

and occasional clay beds. Among the three different Kamthi formations (upper Kamthi, middle Kamthi and lower Kamthi), only the upper Kamthi formation is exposed in the study area. Prominent fault and joints along with the cross beddings are observed in the study area. Approximately thirty one faults trending in the NE-SW, NNE-SSW, NNW-SSE directions have been identified. Some of the fault systems even extend up to the basement while others are confined within the basin. NE-SW trending fault generally controls the movement of the thermal water in this basin.

The water bearing formations in this study area are categorized into consolidated, semi-consolidated and unconsolidated formation. Aquifer system in the consolidated formation is made up with the fractured granites and gneisses whereas sandstone of Lower Gondwana group forms the aquifers in semi-consolidated formation. In unconsolidated formation, the river alluvium forms the aquifer system. In confined aquifers, the water table ranges from 40 to 300 m and in unconfined aquifers the water table lies well within 15 m bgl. During pre-monsoon time the water level depth in the shallow unconfined aquifer ranges from 2 to 14 m bgl whereas in post-monsoon time it varies from 5 to 10 m bgl (CGWB, 2013).

4.3 Sampling details

Water samples (bore wells, dug wells and hand pumps) were collected from the study area during February, 2016. The water table depth in the dug well, hand pump and bore well varied from 6 to 10 m, 50 to 63 m and 450 to 470 metre respectively. Thermal water was encountered in the bore well samples. The surface discharge temperature of the thermal water ranged from 36 to 80 °C. Different physicochemical parameters such as TDS, EC, pH, temperature were measured at the field itself by using a multiparameter probe (HI 9828). Water samples were collected for analysis of major cations (Na, K, Ca and Mg), anions (Cl, SO_4 and HCO_3), dissolved silica and various isotopes (^{2}H, ^{18}O, ^{3}H, ^{13}C and ^{14}C). XLSTAT

software package and GeoT computer code were used to carry out multivariate statistical analysis (HCA and PCA) and geothermometrical modeling technique.

4.4 Results and discussion

4.4.1 Major geochemical species

The geochemical analysis results of the collected samples are given in table 4.1 and the statistical summary of different parameters is given in table 4.2. Ionic balance between cations and anions is derived using following equation:

$$CBE\ (\%) = \{(\sum \text{cations} - \sum \text{anions}) / (\sum \text{cations} + \sum \text{anions})\} \times 100 \qquad 4.1$$

The median value of pH (pH = 7.7) indicates that groundwaters in this area are almost neutral. Both dug well (EC varies from 153 to 3395 µS/cm, median=582 µS/cm) and hand pump (EC ranges from 59 to 3695 µS/cm, median=1118 µS/cm) samples show large variation in the EC compared to the bore well samples (EC= 124 to 723 µS/cm, median=421 µS/cm). Among different cations, sodium (Na^+) is found to be dominant one in all type of the groundwater samples. The maximum value of Na^+ in dug well, hand pump and bore well is found to be 425 mg/L, 325 mg/L and 159 mg/L respectively. Apart from sodium, the other dominant cations are calcium, followed by magnesium and potassium. The mean concentrations of these cations are found to be highest in hand pump samples (Ca^{2+} = 84.0, Mg^{2+} = 61 mg/L, K^+ = 33) compared to the dug well (Ca^{2+} = 60.8, Mg^{2+} = 24.2 mg/L, K^+ = 22.1) and bore well (Ca^{2+} = 14.0, Mg^{2+} = 5.6 mg/L, K^+ = 20) samples. In case of anions, bicarbonate is found to be dominant one followed by chloride and sulphate ions. The mean concentration of bicarbonate ions is found to be highest in the hand pump (HCO_3^- = 333.8 mg/L) samples followed by dug wells (HCO_3^- = 253.8 mg/L) and bore well (HCO_3^- = 234.7 mg/L). Chloride and sulphate ion concentrations also follow the similar trend i.e. highest concentration is seen in the hand pump samples followed by dug wells and deep bore well

samples. The piper diagram (Fig. 4.2) shows that the chemical facies of the groundwaters (both thermal and non-thermal) can be classified in to three main categories: (1) mixed cation (Na, Ca) - HCO_3; (2) mixed cation (Ca, Na) - HCO_3 - Cl; (3) mixed cation (Ca, Na, Mg) - Cl type. All the thermal water samples are found to be Na-HCO_3 type whereas non-thermal groundwaters are combination of both bicarbonate and chloride types.

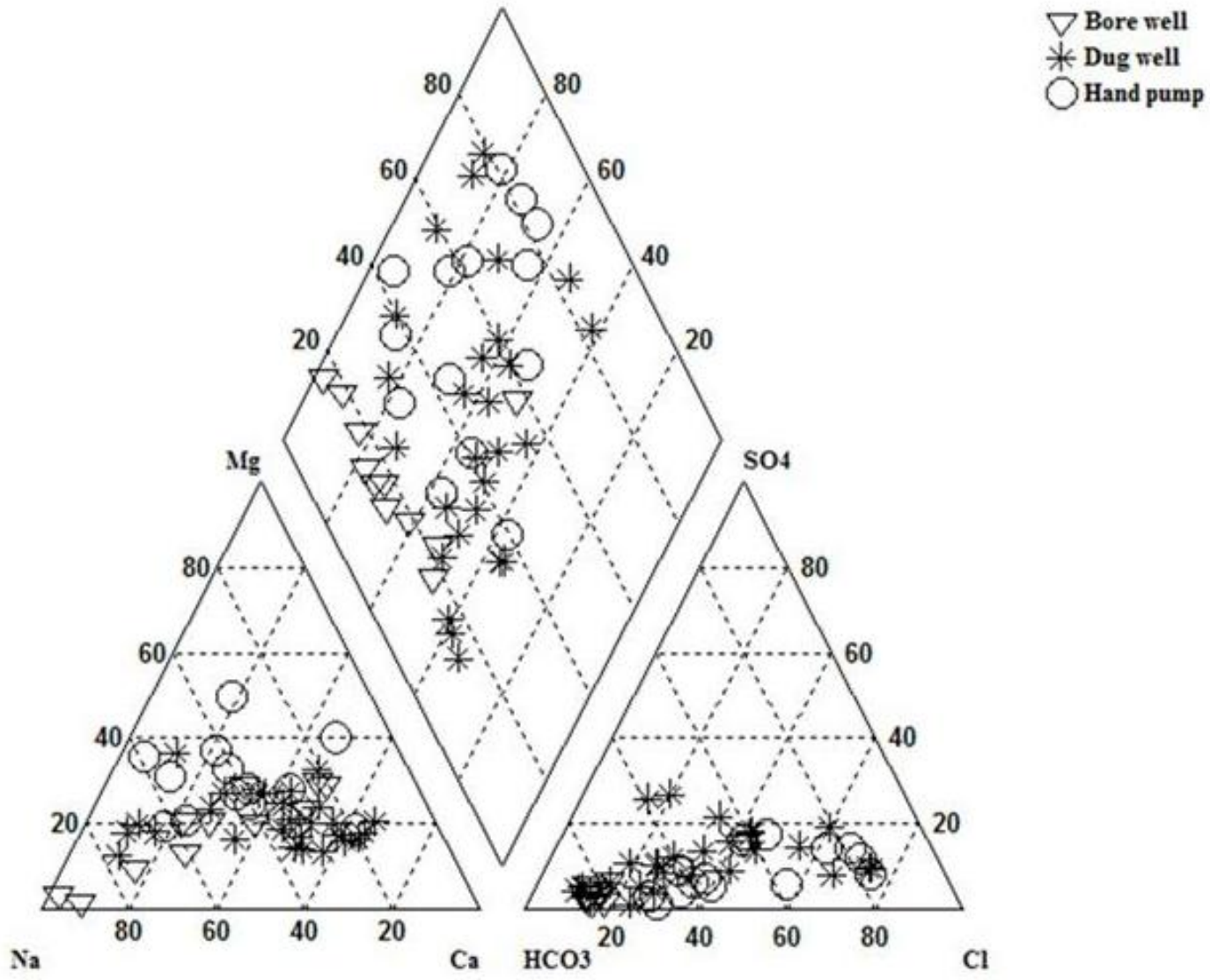

Fig. 4.2 *Piper diagram of groundwater samples*

Table 4.1 *Chemical and isotopic parameters of thermal and non-thermal samples*

Sample ID	Type	Temp (°C)	pH	EC (µs/cm)	TDS (ppm)	Ca (ppm)	Mg (ppm)	Na (ppm)	K (ppm)	SiO_2 (ppm)	HCO_3 (ppm)	Cl (ppm)	SO_4 (ppm)	NO_3 (ppm)	PO_4 (ppm)	F (ppm)	$\delta^{18}O$ (‰)	$\delta^{2}H$ (‰)	^{3}H (TU)	$\delta^{13}C$ (‰)	$a^{14}C$ pMC	Corrected age (yr)	Charge balance (%)
S-1	DW	30.3	6.6	1128	706	68	40	125	7	19	220	235	84	2	0.14	0.76	-2.55	-12.52	-	-	-	-	+1.0
S-2	HP	31.9	8.3	1361	855	18	70	220	12	31	537	225	41	2	0.07	1.4	-2.16	-10.34	-	-	-	-	-2.4
S-3	DW	31	7.5	522	329	64	14	31	16	44	123	53	46	89	1.16	0.18	-	-	-	-	-	-	+1.6
S-4	DW	30	7.4	475	299	32	14	35	26	39	89	56	32	91	0.16	0.16	-	-	-	-	-	-	-2.4
S-5	BW	54.1	8.3	522	328	3	3	159	13	49	317	32	5	1	0.1	0.89	-3.03	-14.99	-	-	-	-	+5.4
S-6	DW	29.4	7.3	981	618	88	34	70	37	60	220	137	76	113	0.25	0.37	-	-	-	-	-	-	+1.3
S-7	HP	30.2	7.2	854	539	75	39	24	21	58	164	123	63	133	0.25	0.31	-3.2	-15.25	2.81	-	-	-	-6.0
S-8	DW	24.7	8.4	1149	575	25	17	196	2	17	403	109	64	2	0	1.18	-	-	-	-	-	-	-2.1
S-9	BH	63.8	7.7	510	322	14	4	119	17	36	330	31	4	1	0.2	0.77	-2.66	-12.9	1.12	-20.2	16.5	14895	+1.6
S-10	DW	30.2	7.3	562	355	64	16	58	19	27	295	45	35	9	0.09	1.16	-	-	-	-	-	-	+3.3
S-11	DW	29.8	7.2	1022	646	118	19	87	31	28	448	102	57	47	0.85	0.41	-1.89	-8.82	-	-	-	-	-0.7
S-12	BW	51.1	7.4	357	226	14	8	42	34	26	228	20	5	1	0.19	0.46	-3.43	-16.99	0.62	-20.7	14.5	15963	-4.6
S-13	DW	29.6	7.1	237	150	34	6	16	3	13	158	15	4	3	0.12	0.27	-	-	-	-	-	-	-3.2
S-14	BW	50.6	7.3	407	258	28	9	35	43	33	242	30	4	0	0.25	0.5	-2.98	-15.63	0.84			-	-1.7
S-15	BW	65.6	7.2	340	215	18	8	38	30	37	204	19	9	1	0.2	0.45	-3.47	-18.0	1.5	-24.4	22.2	12442	-1.6
S-16	BW	80.8	7.7	485	307	9	1	116	18	72	303	33	10	0	0.09	0.91	-3.19	-15.0	1.42	-17.5	30	9952	-1.0
S-17	DW	30	7.2	484	307	58	10	47	28	20	279	34	17	15	0.09	0.34	-3.24	-16.12	-	-	-	-	+2.6
S-18	BW	34.9	7.5	439	278	14	5	73	26	31	279	29	9	4	0.34	0.66	-	-	-	-	-	-	-6.8
S-19	DW	29.5	7.7	1106	553	90	18	67	76	32	346	130	70	29	bdl	bdl	-2.3	-11.53	5.7			-	-3.0
S-20	DW	29.9	8.1	344	172	45	7	16	3	19	153	34	19	2	0.12	bdl	-	-	-	-	-	-	-4.0
S-21	DW	26.2	8	377	188	51	8	22	1	19	233	17	11	0	bdl	bdl	-	-	-	-	-	-	-3.9
S-22	DW	27	8.3	590	295	67	19	38	7	13	225	34	77	4	0.05	bdl	-	-	-	-	-	-	-0.8
S-23	DW	24.2	8.3	575	287	17	11	75	8	7	213	50	9	6	0.27	1.1	-	-	-	-	-	-	-4.2
S-24	DW	23.7	8.3	489	244	60	10	19	16	22	200	50	20	1	0.22	0.35	-	-	-	-	-	-	-4.9
S-25	DW	27.8	7.7	1133	567	62	17	95	100	24	285	143	78	67	bdl	0.35	-	-	-	-	-	-	-1.1
S-26	BW	43.5	7.6	276	174	16	5	43	12	33	180	15	6	1	0.09	0.6	-3.29	-17.45	0.93	-22.82	17.2	14552	-2.3
S-27	DW	31	7.3	1010	639	106	29	86	27	39	419	142	46	4	0.1	0.74	-	-	-	-	-	-	+0.7
S-28	HP	31.2	7.5	2755	1746	130	138	295	15	18	676	600	85	22	0.1	1.31	-	-	-	-	-	-	+1.4

Sample ID	Type	Temp (°C)	pH	EC (µs/cm)	TDS (ppm)	Ca (ppm)	Mg (ppm)	Na (ppm)	K (ppm)	SiO_2 (ppm)	HCO_3 (ppm)	Cl (ppm)	SO_4 (ppm)	NO_3 (ppm)	PO_4 (ppm)	F (ppm)	$\delta^{18}O$ (‰)	$\delta^{2}H$ (‰)	^{3}H (TU)	$\delta^{13}C$ (‰)	$a^{14}C$ pMC	Corrected age (yr)	Charge balance (%)
S-29	HP	29.9	7.4	901	569	110	20	39	31	47	357	105	42	34	0.08	0.53	-	-	-	-	-	-	-3.2
S-30	DW	30.2	7.7	3395	1698	89	158	420	25	14	561	831	135	8	<0.05	<0.10	-	-	-	-	-	-	+1.1
S-31	DW	28.2	7.9	965	483	80	28	71	18	30	301	151	43	3	<0.05	<0.10	-	-	-	-	-	-	-1.5
S-32	DW	28.5	8	2820	1421	66	65	425	50	56	350	580	250	80	0.08	1.1	-2.39	-11.93	-	-	-	-	-1.4
S-33	DW	26.1	8.1	266	133	37	7	9	4	17	150	10	6	2	<0.05	0.15	-	-	-	-	-	-	+0.2
S-35	HP	30.8	7.6	3434	1717	120	199	240	35	12	375	780	220	70	<0.05	0.75	-3.22	-17.06	-	-	-	-	-0.3
S-36	HP	31.9	8.5	850	425	18	25	85	50	14	288	90	15	3	<0.05	1.18	-	-	-	-	-	-	-1.6
S-37	HP	30.6	7.5	2345	1173	130	55	170	180	69	301	445	140	150	0.06	0.53	-	-	-	-	-	-	+0.4
S-38	BW	35.6	8.3	723	362	26	15	78	56	21	228	120	1	0	0.05	<0.10	-3.03	-15.57	-	-	-	-	-0.7
S-39	BW	33.1	8	278	139	16	9	23	15	23	164	15	3	0	0.12	<0.10	-3	-14.67	1.73				-4.1
S-40	HP	31	8.3	1117	558	74	39	118	38	29	381	149	39	0	<0.05	1.1	-	-	-	-	-	-	+2.2
S-41	BW	41.3	7.3	166	105	17	6	8	11	30	107	9	6	1	0.12	0.2	-3.27	-17.14	-	-	-	-	-4.6
S-42	BW	42.6	7	125	79	13	5	7	5	25	75	9	5	0	0.19	0.14	-3.36	-18.08	-	-	-	-	-3.3
S-43	HP	30.6	7.6	2213	1403	81	53	320	25	31	566	320	170	12	0.12	1.27	-1.35	-10.71	-	-	-	-	+1.9
S-44	DW	29.5	7.7	2343	1482	48	50	380	25	41	566	370	152	6	0.1	1.81	-	-	-	-	-	-	+1.3
S-45	DW	31.2	7.8	264	167	34	8	22	3	11	140	27	8	3	0.09	0.26	-	-	-	-	-	-	+1.6
S-46	DW	24.1	8.3	629	315	28	15	60	45	20	296	54	3	3	<0.05	1.58	-	-	-	-	-	-	-4.6
S-47	BW	54.1	8.5	648	324	7	2	130	12	34	314	35	1	2	<0.05	1.42	-3.0	-14.0	1.02	-19.8	12.5	17190	-3.5
S-48	BW	37.9	8.5	613	307	8	4	132	10	31	319	35	1	0	<0.05	1.42	-3.21	-13.29	1.45				-2.6
S-49	BW	43.2	8.4	587	294	10	1	128	16	35	314	37	1	0	0.05	0.83	-3.22	-16.05	0.68	-18.6	10.46	18663	-2.8
S-50	BW	54.6	8.4	567	284	14	5	112	21	39	306	37	1	0	<0.05	1	-3.18	-16.2	-	-	-		-0.2
S-51	HP	31	7.5	2789	1395	178	94	244	17	25	295	747	112	10	<0.05	0.26		-	-	-	-	-	-1.3
S-52	HP	30.8	8.3	1118	559	118	34	105	12	26	429	148	36	1	<0.05	1.1	-2.49	-11.44	-	-	-	-	+2.1
S-53	DW	31	7.6	1789	895	206	29	120	16	39	182	460	82	13	<0.05	0.64	-2.31	-10.59	-	-	-	-	+1.1
S-54	HP	32	7.6	3695	1846	179	137	325	25	10	370	851	192	3	0.08	<0.10	-2.32	-10.25	-	-	-	-	+1.3
S-55	DW	30.5	8.3	383	191	22	11	37	14	13	177	42	1	0	<0.05	0.19	-	-	-	-	-	-	-4.7
S-56	DW	30.5	8	153	76	11	5	13	2	7	51	11	20	11	<0.05	<0.10	-	-	-	-	-	-	-4.9
S-57	DW	30.2	7.5	430	215	33	14	17	10	16	24	64	11	45	<0.05	<0.10	-	-	-	-	-	-	+9.2
S-58	BH	31.2	8.1	124	62	14	5	9	2	28	80	9	1	0	<0.05	<0.10	-	-	-	-	-	-	-0.4
S-59	HP	31.2	7.8	109	54	10	4	8	2	27	59	13	2	0	<0.05	<0.10	-	-	-	-	-	-	-5.7
S-60	HP	32.1	8.4	464	232	16	9	47	30	9	188	47	2	0	<0.05	<0.10	-	-	-	-	-	-	-1.1
S-62	HP	32	7.6	59	30	4	3	6	1	12	21	11	1	9	<0.05	<0.10	-	-	-	-	-	-	-5.4

Note: "-'' *means not measured,* "bdl" = *below detection limit*

4.4.2 Multivariate statistical analysis

4.4.2.1 Hierarchical cluster analysis (HCA)

Hierarchical cluster analysis (HCA) basically groups the samples in to different clusters based on their similarities/dissimilarities by comparing the whole dataset. Samples falling in the same cluster have comparatively similar properties than compared to samples in the other clusters. Application of HCA on the samples of the present study area results a dendogram (Fig. 4.3) showing four clusters (C1, C2, C3 and C4). Cluster-1 (C1), cluster-2 (C2), cluster-3 (C3), cluster-4 (C4) is comprised of 34 samples, 16 samples, 7 samples and 3 samples respectively. Clusters having similar chemical properties exhibit low linkage distance amongst themselves whereas dissimilar clusters are joined at higher linkages distances. For example, C1 and C2 clusters are joined with C3 and C4 clusters having higher linkage distance implying that these two clusters (C1 and C2) are geochemically different than C3 and C4 clusters. Schoeller diagram (Fig. 4.4) represents the average value of the chemical parameters of the samples in four different clusters. Cluster-4 (C4) is found to have the highest average concentration of all the chemical parameters followed by C3, C2 and C1 respectively. Geochemically samples in C1 clusters are Na-HCO_3 type and all the thermal waters belong in this cluster. C2 cluster contains samples that are mixed cations - HCO_3 - Cl type and these samples have higher concentration of ions compared to the C1 cluster. Likewise the difference in the magnesium ion concentration is found to be the main discriminating factor between the samples of C3 and C4 clusters. Samples falling in the C4 cluster have very high Mg^{2+} concentrations than samples in C3 cluster. Thus HCA provides an easy eyeball classification by segregating the samples based on their major ion concentration.

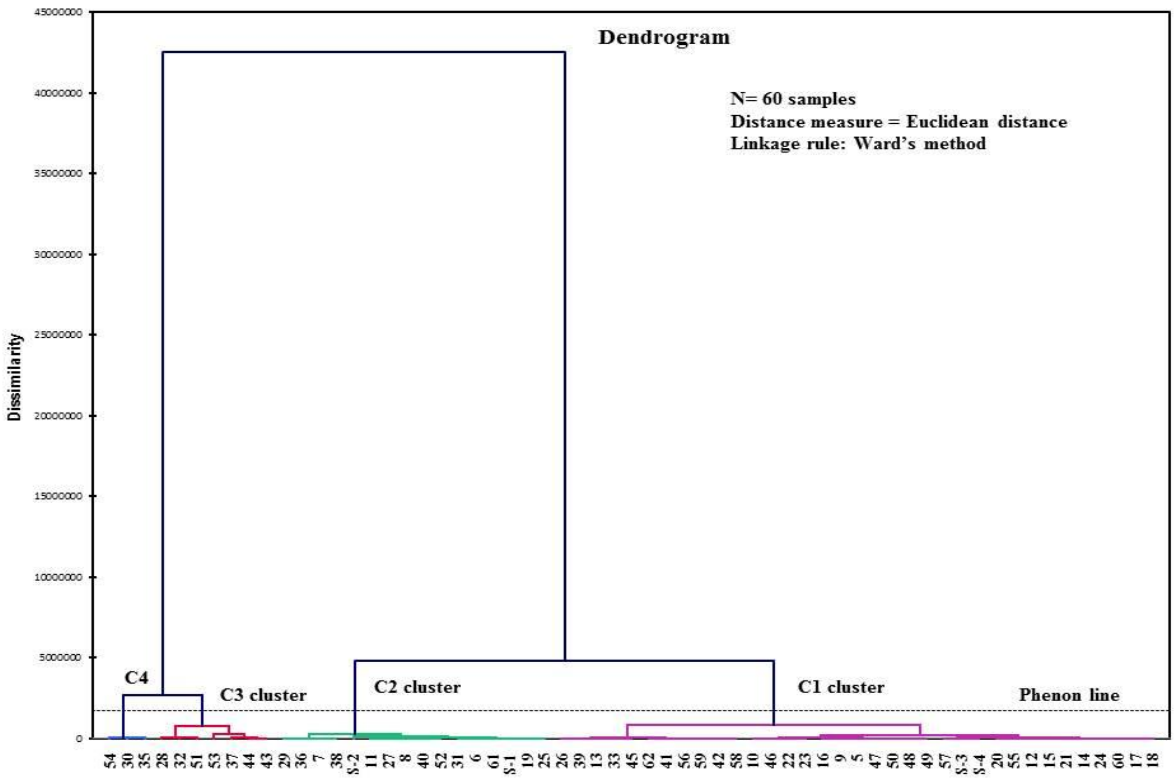

Fig. 4.3 *Dendogram of the HCA showing four different clusters*

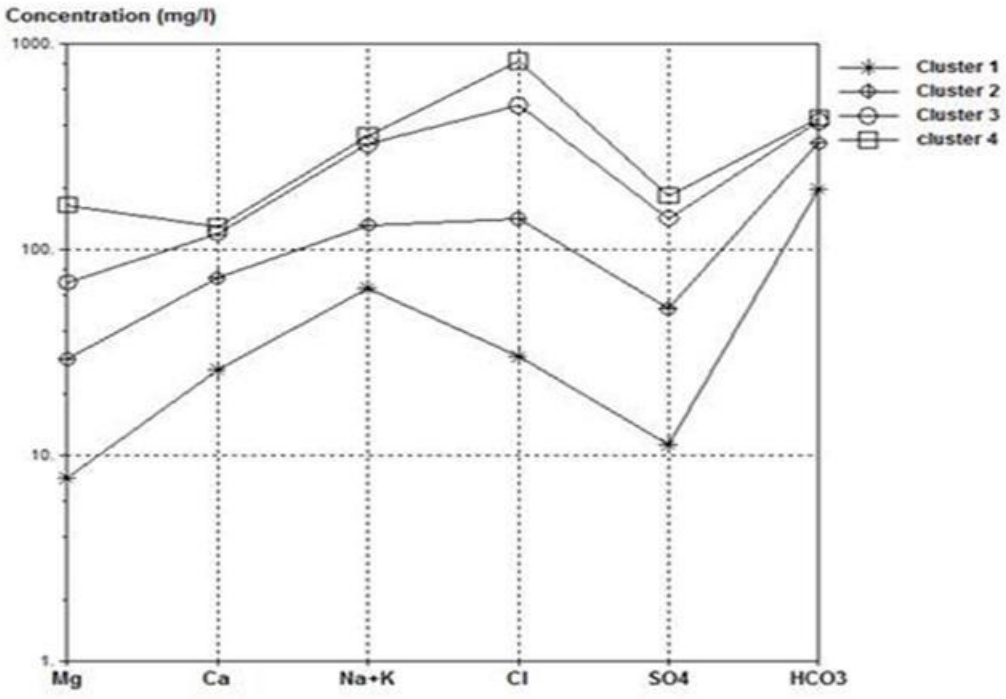

Fig. 4.4 *Schoeller diagram of the four clusters obtained from HCA*

Table 4.2 *Statistical summary of selected chemical parameters in the study area (Note: "bdl" = below detection limit)*

	Bore well (n=17)					Dug well (n=28)					Hand pump (n=15)				
Variable	Min	Max	Mean	Median	Std. deviation	Min	Max	Mean	Median	Std. deviation	Min	Max	Mean	Median	Std. deviation
pH	7	8.5	7.83	7.7	0.50	6.6	8.4	7.73	7.7	0.5	7.2	8.5	7.8	7.6	0.41
EC (µS/cm)	124	723	421	439	179	153	3395	915	582	778	59	3695	1604	1118	1138
TDS (ppm)	62	362	239	278	92	76	1698	500.0	322	412	30	1846	873.4	569	603
Ca^{2+} (ppm)	3	28	14	14	6.0	11	206	61	59	39	4.0	179	84	81.0	58.0
Mg^{2+} (ppm)	1	15	5.58	5	3.4	5	158	24	15	29	3.0	199.0	61.3	39.0	55.4
Na^{+} (ppm)	7	159	73	73	50.0	9	425	95	59	116	6.0	325	149.7	118	112
K^{+} (ppm)	2	56	20.0	16	13.5	1	100	22	16	23	1.0	180.0	33.0	25	41.0
SiO_2 (ppm)	21	72	34.3	33	11.4	7	60	25	20	14	9.0	69.0	28	26.0	17.3
HCO_3^{-} (ppm)	75	330	234.0	242	85	24	566	254	222	134	21.0	676.0	334	357.0	174
Cl^{-} (ppm)	9	120	30	30	24	10	831	142	55	190.0	11.0	851.0	310	149.0	287
SO_4^{2-} (ppm)	1	10	4.23	4	3.0	1	250	52	39	54	1.0	220.0	77	42.0	70
NO_3^{-} (ppm)	bdl	4.0	0.7	0.0	1.0	bdl	113	23	6	33.0	bdl	150.0	30	9.0	47.0
PO_4^{3-} (ppm)	0.05	0.34	0.15	0.12	0.1	0.05	1.16	0.24	0.12	0.30	0.06	0.25	0.10	0.08	0.1

4.4.2.2 Principal component analysis (PCA)

PCA is another important multivariate data analysis technique which is generally used to reduce the dimension of the larger dataset into smaller set of principal components (PCs) while retaining the original information. The largest variation of original dataset is represented by PC1 followed by PC2, PC3 and so on. Table 4.3 represents the factor loadings/component loadings of different PCs along with the eigenvalues and variance. The loading value found to be greater than 0.6 is highlighted in bold as it signifies significant correlation between variables and factors (Table 4.3). From the table 4.3, it is observed that PC1, PC2 and PC3 have eigenvalues greater than 1 and they cumulatively represent more than 79% of the total variance of original dataset. PC1 represents 51.20% of the total variance whereas PC2 and PC3 explain 18.01% and 10.49% of the total variance respectively. High loadings of Cl (0.95), SO_4 (0.92), Mg (0.89), Na (0.86), Ca (0.75) and HCO_3 (0.68) are seen in PC1 whereas in PC2 highest loadings are observed in NO_3 (0.8), SiO_2 (0.7) and K (0.6). Significant loading of K and NO_3 in PC2 clearly suggest the influence of agricultural inputs as fertilizer is one of the predominant sources of potassium. The PCA bi-plot (Fig. 4.5) comprising PC1 and PC2 reveal three different clusters of groundwaters in the present study area. Group-1 samples are mostly Na-HCO_3 type similar to the C1 cluster obtained in the HCA technique. Thermal water samples fall in this group-1. The loading vector directions indicated by the arrows show that the group-3 samples has higher loadings of Ca, SO_4, HCO_3, K, Na, Mg and Cl whereas samples (S-6, 27, 11, 19, 29, 53, 25) falling in the group-2 are governed mainly by the elevated concentrations of K, NO_3 and SiO_2. Few samples such as S-6, 7 and 37 are separated from other samples due to the abnormally high concentrations of K and NO_3. The samples showing high concentrations of K and NO_3 are clearly affected by the anthropogenic inputs mostly from agricultural activities.

Table 4.3 *Loading factor values of different PCs*

Water quality variables	PC 1	PC 2	PC 3	PC 4	PC 5
pH	-0.18	-0.47	+0.66	-0.44	-0.17
EC	**0.99**	-0.13	-0.01	-0.04	-0.03
Ca	**0.75**	+0.13	-0.32	-0.09	+0.31
Mg	**0.89**	-0.22	-0.19	-0.08	-0.10
Na	**0.86**	-0.28	+0.27	+0.20	-0.15
K	0.39	**+0.60**	+0.36	-0.40	+0.35
SiO_2	0.16	**+0.70**	+0.42	+0.47	-0.12
HCO_3	0.68	-0.29	+0.42	+0.30	+0.32
Cl	**0.95**	-0.15	-0.15	-0.06	-0.07
SO_4	**0.92**	+0.07	-0.05	-0.05	-0.19
NO_3	0.38	**+0.8**	-0.02	-0.22	-0.27
Eigenvalue	5.63	1.98	1.15	0.783	0.51
Variability (%)	51.21	18.01	10.49	7.12	4.63
Cumulative %	51.21	69.22	79.71	86.83	91.46

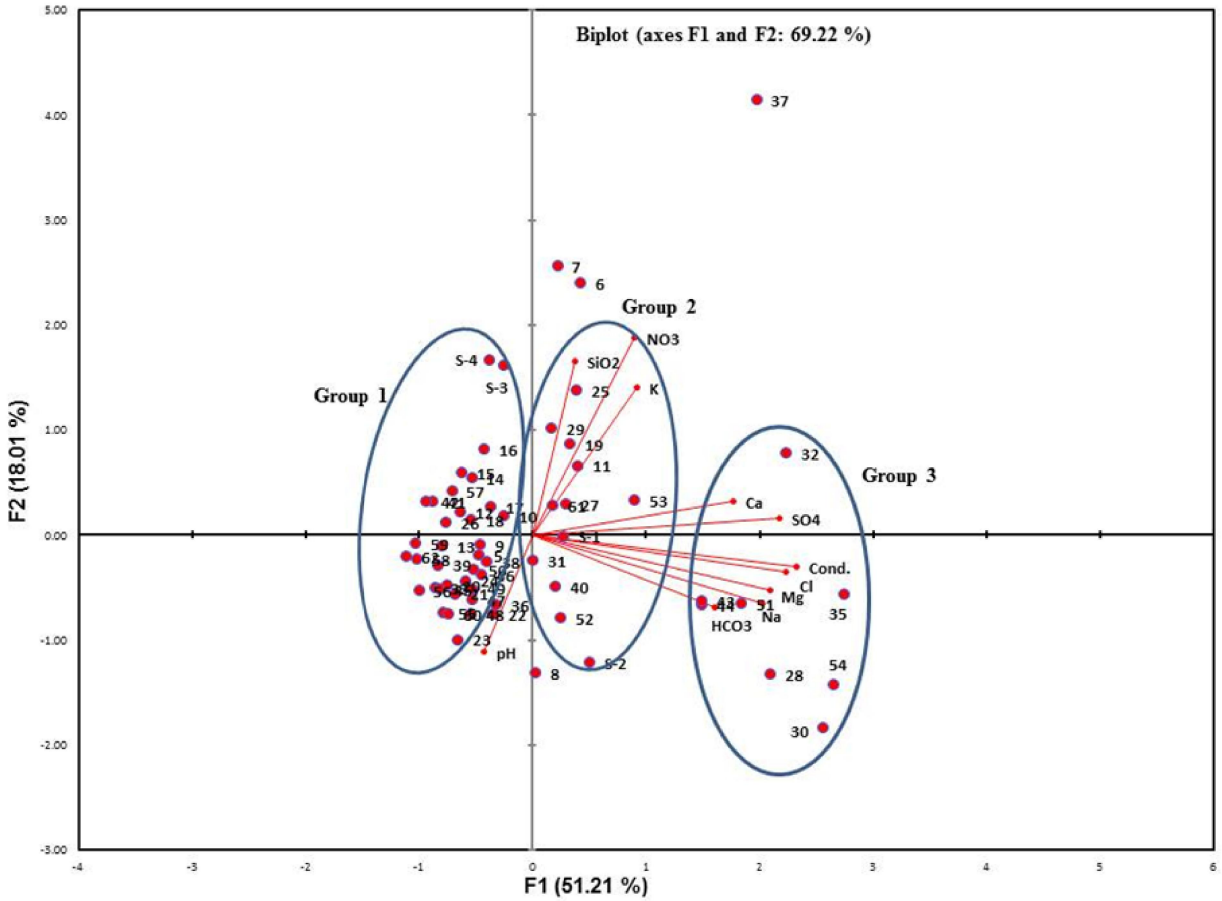

Fig. 4.5 *PCA bi-plot along with the factor loadings for PC1 and PC2*

4.4.3 Characterization of various geochemical processes

Geochemical characteristics of the groundwater depends on several factors such as magnitude of rock-water interaction, residence time, nature of the interacting rocks (carbonate or silicate etc.), chemical processes i.e. dissolution, precipitation, ion exchange etc. (Garrels and MacKenzie, 1971). Solute balance cannot solely differentiate all these various competing processes (Faure, 1998). As a result different graphical plots have been used to understand the pathways of geochemical evolution.

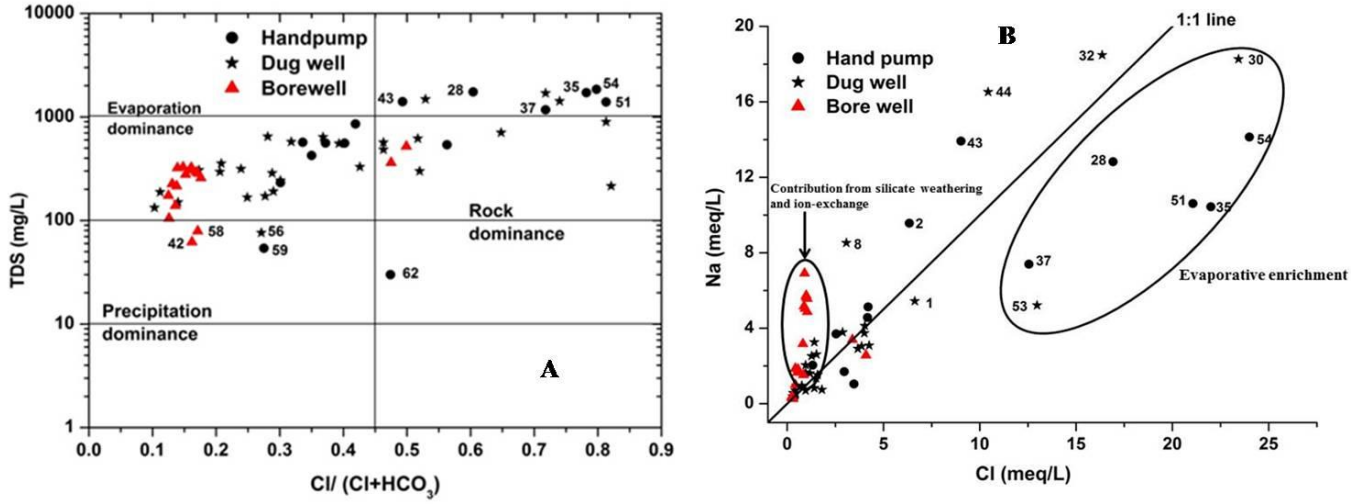

Fig. 4.6 *A) Gibbs plot showing main factors controlling geochemistry and B) scatter plot between* Na^+ *and* Cl^-

First of all, Gibbs plot (Fig. 4.6A) has been used to distinguish between the major geochemical processes (precipitation, rock-water interaction and evaporation) controlling the concentration of the dissolved ions (Gibbs, 1970). From the fig. 4.6A, it is observed that most of the thermal and non-thermal (dug well and hand pump) samples fall in the rock-dominance region implying the rock dissolution as the primary source for introduction of solutes. Few non-thermal (hand pump and dug well) water samples (S- 28, 30, 32, 35, 37, 43, 44, 51, 53, 54) are found to fall in the evaporation dominance area. This evaporation phenomenon may be the reason for enrichment in the chloride concentration of these samples which is also

exemplified in the Na vs. Cl plot (Fig. 4.6B) as the above samples (S- 28, 30, 32, 35, 37, 43, 44, 51, 53, 54) fall in the right side of the 1:1 line (Na/Cl < 1) (Fig. 4.6B). All the thermal water samples have higher Na/Cl ratio (>1) as they fall above the 1:1 line indicating other sources such as silicate weathering and ion exchange process are responsible for the excess sodium concentrations. Rock dissolution can further be classified into evaporite dissolution, carbonate dissolution and silicate weathering mechanisms. Bivariate mixing plots (Fig. 4.7) are used to differentiate among these three weathering mechanisms. From the fig. 4.7, it is

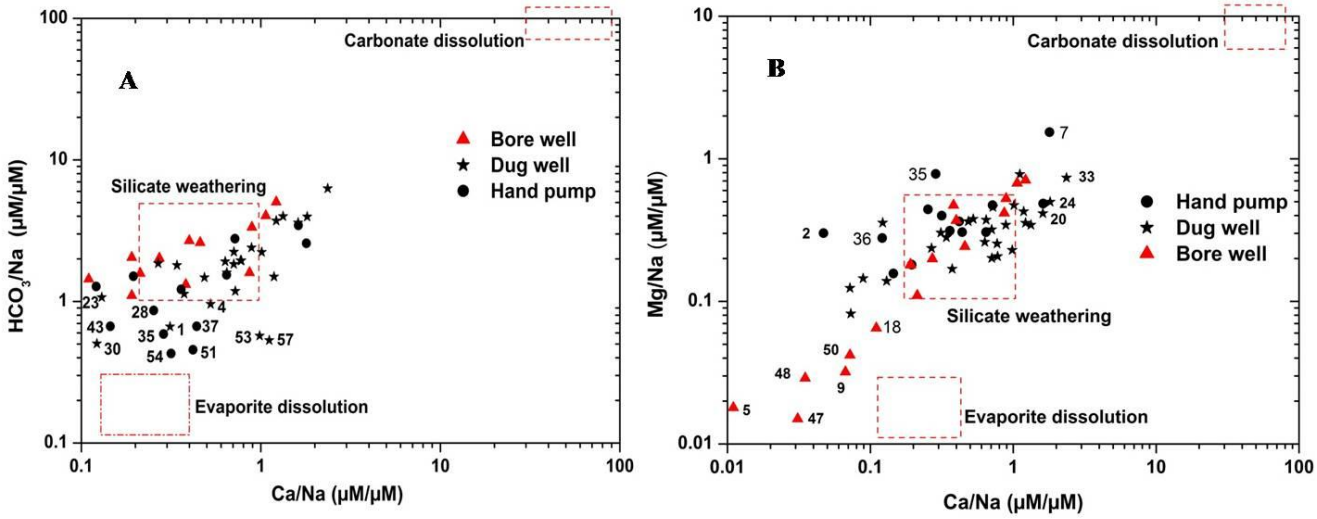

Fig. 4.7 *Bivariate plots between A) Na-normalised (µM/µM) Ca and HCO_3 B) Na-normalised (µM/µM) Ca and Mg. The dashed area denotes the global average compositions of various weathering mechanisms* (modified after Gaillardet et al. 1999)

observed that majority of the groundwater samples including all thermal water samples fall near the global average of silicate weathering region thus pointing towards the dissolution of the silicate minerals as the dominant mechanism. The weathering of silicate minerals can also be confirmed from the $\delta^{13}C$ values of the DIC. The average $\delta^{13}C$ value of the thermal water in this region is found to be ~ -20.57‰ which matches exactly with the $\delta^{13}C$ value of DIC generated from the silicate weathering with soil CO_2 coming from C_3 types of plants.

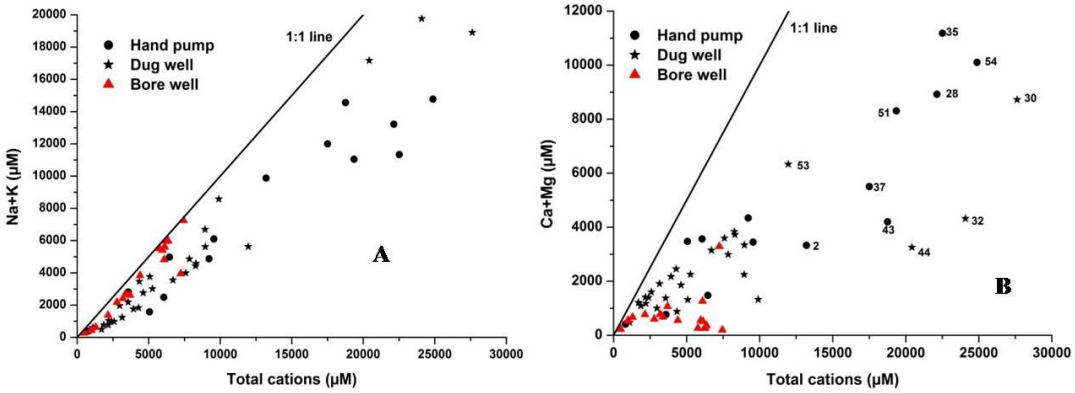

Fig. 4.8 *Graphical plots between A) Na + K and total cation concentration B) Ca + Mg and total cation concentrations* (modified after Mukherjee et al. 2009)

In weathering studies, the hydrologic system is assumed to have well-defined boundaries. Jenkins et al., (1994) has defined the following equation combining the hydrologic input and output terms:

$$R = P - ET + dS \qquad 4.2$$

where R is runoff, P is precipitation, ET is evapotranspiration, and dS is change in the storage of water in the system.

Bricker et al. (1994) has given the following equation to summarize the chemical terms to explain the weathering mechanism:

$$N_i = W_i + P_i + A_i - R_i - M_i - B_i - Si \qquad 4.3$$

where N_i is the net accumulation or depletion of component *i* in the system, W_i is the total weathering input of component *i* in the system, P_i is the atmospheric deposition input of component *i* in the system (wet precipitation, dry deposition, gaseous deposition), *Ai* is the anthropogenic input of component *i* to the system, *Ri* is the chemical erosion of component *i* in the system (dissolved components transported out of watershed), M_i is the mechanical

erosion of component *i* in the system (particulate components transported out of watershed), B_i is the biomass uptake of component *i* in the system (harvest), and *Si* is the storage of component *i* in watershed. If it is assumed that the biomass is at steady state and there is no change in storage of water or in the exchange pool in the system, then Equation (2) reduces to (Drever, 1997):

$$N_i = W_i + P_i - R_i - M_i \qquad 4.4$$

Commonly, the term M_i is not addressed or quantified, because particulates are not directly involved in chemical weathering and do not add or subtract dissolved species to or from the waters (Langmuir, 1997); then the above Equation (3) is reduced to:

$$N_i = W_i + P_i - R_i \qquad 4.5$$

which is the net mass balance equation during weathering. The graphical plots simply provide semi-qualitative approach to explain these weathering reactions. In addition to the bivariate mixing plots, graphical plots (Fig. 4.8) between Na + K and Ca + Mg versus total cation concentrations also reveal two distinct trends for thermal and non-thermal (dug well and hand pump) water samples. The Ca + Mg ratio in comparison to the total cations (Fig. 4.8B) is found to be greater in non-thermal water samples (median value = 0.44 for dug well, 0.40 for handpump and 0.21 for thermal water respectively) whereas in case of thermal waters the ratio of Na + K to the total cations (Fig. 4.8A) is found to be highest (median value = 0.79 for thermal water, 0.56 for dug well and 0.6 for hand pumps). The excess concentrations of Na and K in the thermal water samples are due to the silicate weathering (discussed earlier) and ion exchange mechanism (discussed in the subsequent portion). The preponderance of the Ca and Mg ion concentrations in the non-thermal water samples may be due to the dissolution of alkaline earth silicates present in the sediment portion (Sarin et al., 1989; Mukherjee et al., 2009). Dissolution of dolomite, calcite and gypsum may also contribute to the Ca and Mg ion

concentrations which can be confrmed from various graphical plots. The plot (Fig. 4.9A) between Ca + Mg versus HCO_3^- shows that most of the non-thermal water samples do not fall on the 1:2 trend line indicating that the calcite dissolution has negligible contribution to the Ca and Mg ion budget. This inference is further substantiated from the mineral saturation study. In the Godavari valley geothermal area most of the ground water samples (both thermal and non-thermal samples) are found to be supersaturated (saturation index > 0) with respect to calcite (Fig. 4.9B) and dolomite (Fig. 4.10A) thus clearly suggesting that these minerals have already been precipitated out from the solution and are not contributing to the Ca and Mg ion concentration. However in some of the non-thermal water samples (S- 1, 3, 4, 13, 17, 56, 59, 42, 41, 57), calcite and dolomite dissolution may contribute to the Ca and Mg ion concentration as these samples fall on the 1:2 trend line in fig. 4.9A and are also found to be undersaturated with respect to calcite and dolomite. Although all the water samples are undersaturated with respect to the gypsum (fig. 4.10B) but from fig. 4.11, it is observed that all samples are falling below 1:1 trend line ($Ca^{2+}/SO_4^{2-} > 1$) thus not contributing towards the dissolved Ca^{2+} ion concentration as in case of gypsum dissolution the molar ratio of Ca^{2+} and SO_4^{2-} should be equal to 1.

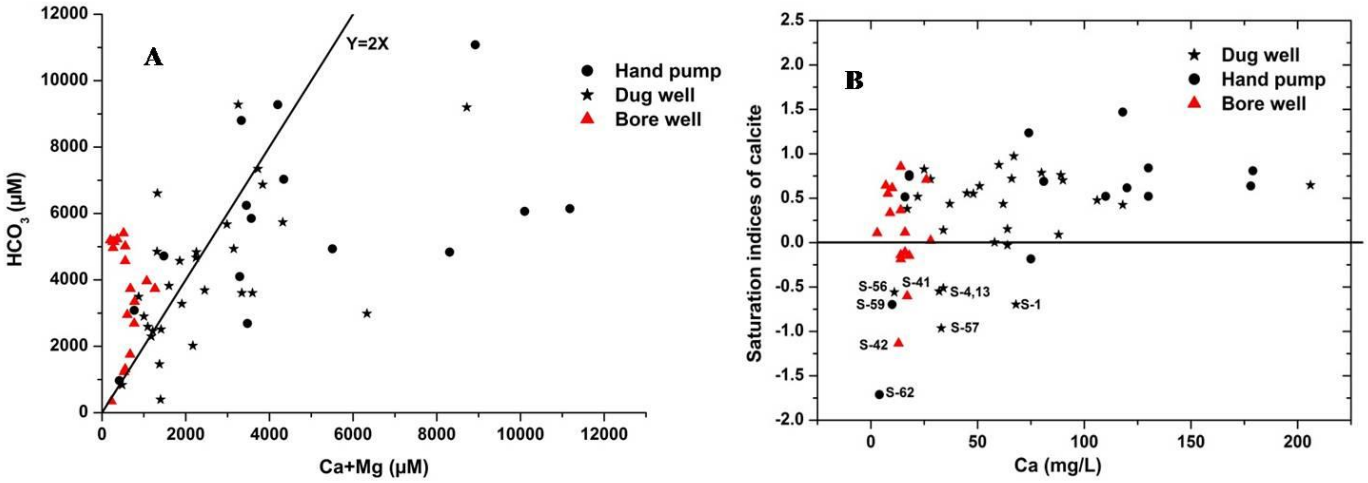

Fig 4.9 *A) Graphical plot between HCO_3 and (Ca + Mg) B) Plot of $SI_{(calcite)}$ vs. Ca concentration*

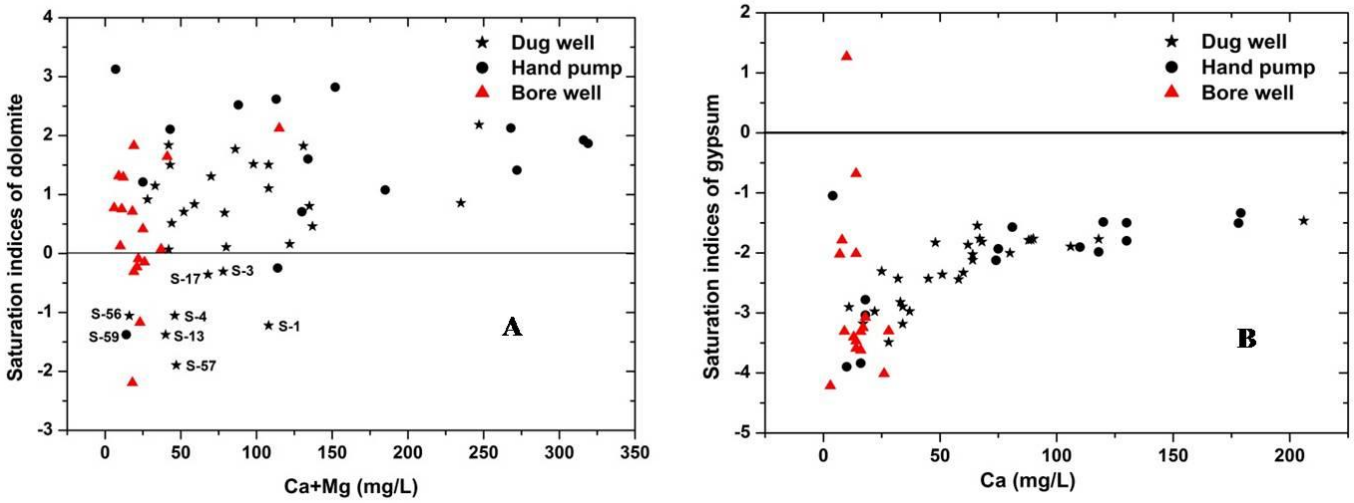

Fig 4.10 *A) Graphical plot between $SI_{(dolomite)}$ and (Ca + Mg) B) Plot of $SI_{(gypsum)}$ vs. Ca concentration*

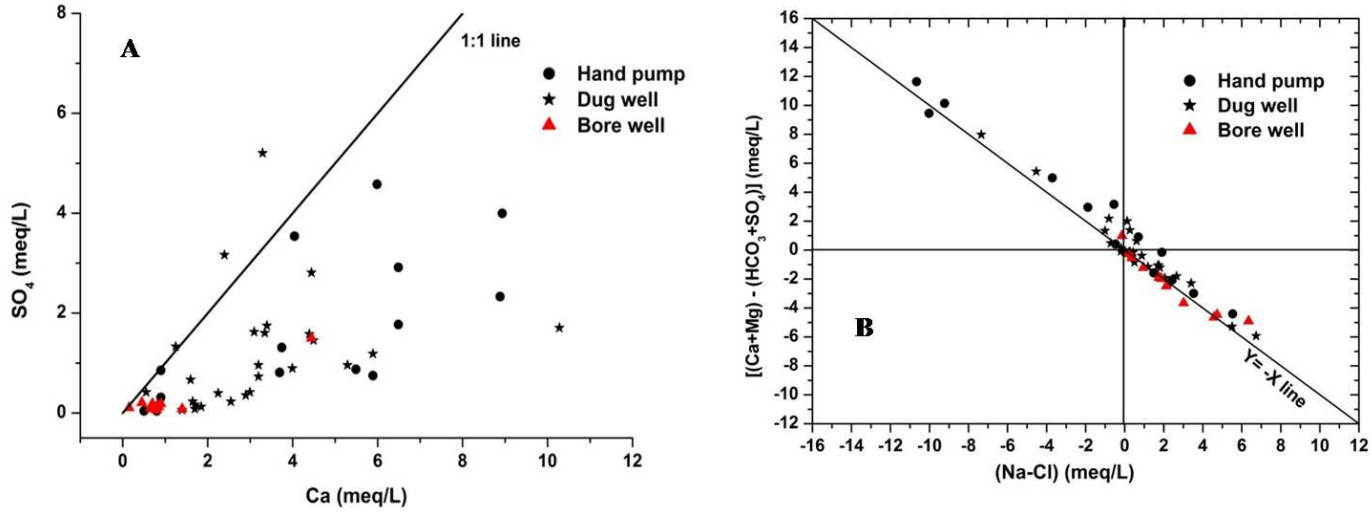

Fig 4.11 *A) Graphical plot between Ca^{2+} and SO_4^{2-} and B) $(Na^+ - Cl^-)$ vs. $\{(Ca^{2+} + Mg^{2+}) - (HCO_3^- - SO_4^{2-})\}$ to indicate cation exchange phenomenon*

Thus from the above discussions, it is evident that calcium and magnesium ion concentrations in non-thermal groundwaters are mostly governed by the dissolution of alkaline earth silicates rather than the dissolution of calcite, dolomite or gypsum. The high bicarbonate concentration in the thermal water samples (falling above the 1:2 trend line in fig. 4.9A) is mostly due to the weathering of Na-silicate minerals. The few non-thermal groundwater samples (S-7, 28, 30, 35, 37, 51, 53, 54) falling in the extreme right side in the fig. 4.8B get affected by

anthropogenic activities thereby resulting abnormally high calcium and magnesium ion concentrations.

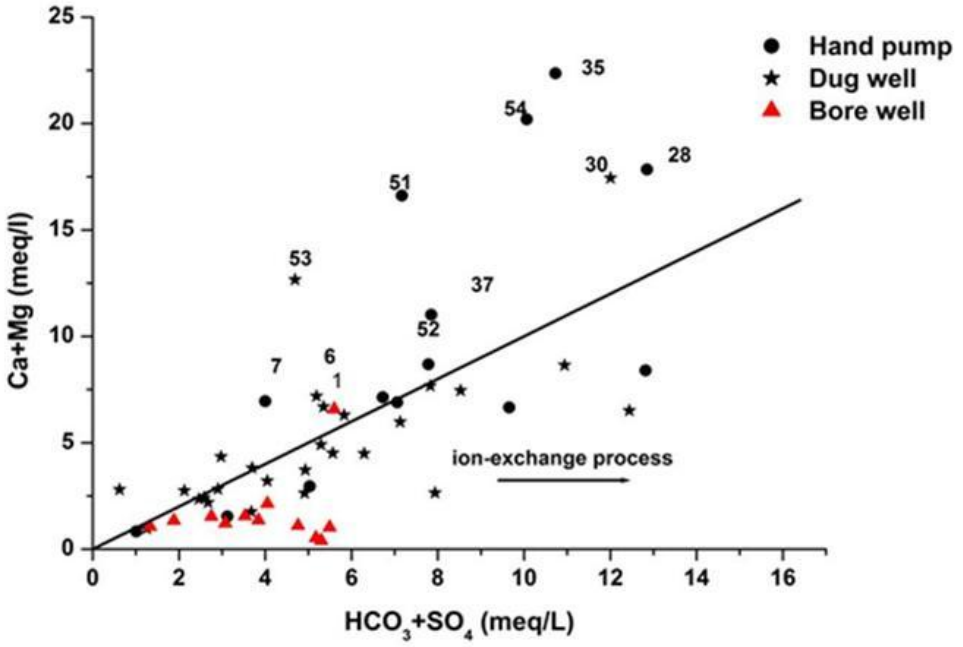

Fig 4.12 *Plot of Ca^{2+} + Mg^{2+} vs. HCO_3^- + SO_4^{2-}*

.

Ion exchange phenomenon is another important geochemical process that affects the concentrations of the dissolved ions in the groundwater. In the cation exchange process, the monovalent cations of aquifer matrix get exchanged by bivalent cations such as Ca^{2+} and Mg^{2+} according to the following equation (Karanth, 1994, Mukherjee et al. 2017):

$$0.5Ca^{2+} + \text{Na-clay} \rightarrow 0.5\text{Ca-clay} + Na^{+} \qquad 4.6$$

The occurrence of the cation exchange process can readily be identified from the bivariate plot (Fig. 4.11B) where the slope of the plot should be close to -1 (i.e. y = - x) (Jankowski et al., 1998; McLean et al., 2000, Mukherjee et al., 2009). In the fig. 4.11B, it is observed that almost all the thermal water and dug water samples fall close to the y = - x line thus implying occurrence of strong cation exchange process. Long residence time (negligible tritium value)

of the thermal waters (discussed in section 4.4.4.2) also faciliates the greater extent of cation exchange mechanism. The scatter plot between $Ca^{2+} + Mg^{2+}$ vs. $HCO_3^- + SO_4^{2-}$ (Fig. 4.12) also helps to discern this cation exchange process. The cation exchange process shifts the msjority of the samples towards the right hand side of the equiline. The groundwater samples (S- 28, 30, 35, 37, 51, 53, 54) that fall on the far left hand side of the equiline are found to be affected by anthropogenic activities (discussed in the previous sections).

Thus in the present study area, different graphical plots actually help to discern the various geochemical processes governing the concentrations of major solutes. The silicate weathering along with the cation exchange processes are found to be the dominant mechanisms in controlling the concentrations of Na^+ and K^+ ions whereas the weathering of alkaline earth sediments is the main governing factor of Ca^{2+} and Mg^{2+} ion concentrations. Among the anions, bicarbonate ion concentration is mainly controlled by the silicate weathering mechanism. Anthropogenic factors mainly agricultural inputs are found to be responsible for abnormally high concentration of calcium, magnesium, chloride and nitrate ion concentrations in some of the non-thermal ground water samples (S-7, 28, 30, 35, 37, 51, 53 and 54).

However it must be worth mentioning that the above semi-qualitative analytical approaches to explain the weathering mass balance reactions do have certain limitations.

1. It has been tacitly assumed that all the minerals have same dissolution rates which are not true. For example; weathering rates of evaporites and carbonates are up to 80 times and 12 times, respectively, faster than silicate weathering rates. Hence, even relatively minor proportions of carbonates and evaporites can significantly influence water chemistry (Meybeck, 1987).

2. The second assumption is that there is no loss or gain of the water and its solute load while entering or leaving the hydrologic system i.e. system is hydrologically 'tight' which is over simplified. The systems that do not suffer from road salt applications or where buried evaporite minerals are not present, chloride commonly is used as a conservative tracer to check for gain or loss of water by pathways other than the stream that drains the watershed. If there are other pathways, the system is not hydrologically closed.

3. Based on major ion solute chemistry alone, it is difficult to identify specific source minerals and weathering processes in silicate terrains due to the incongruent dissolution of silicate minerals (Stallard and Edmond, 1987). Cation-rich silicate minerals are generally weathered by proton-rich, cation-poor solutions (e.g. organic and carbonic acids), releasing alkali metal cations, alkaline earth cations, Si, and some Fe and Al into solution. The extent of weathering and leaching is dependent on the chemical and mineralogical composition of the minerals and clays in the source rock or soil (Mukherjee and Fryar, 2008; Mukherjee et al. 2009). Aluminum and, to some extent, Fe(III) are extremely insoluble in oxidizing conditions at near-neutral pH (which is characteristic of most surface/near-surface weathering systems). Hence, leaching tends to occur in the order Ca > Na > Mg, simultaneously depleting the source.

4. In a closed hydrologic system with distinct recharge-discharge zones and slow hydrodynamics, mineral weathering may be more obvious in the recharge zone, while cation exchange may be more active at or near the discharge zones (Guo and Wang, 2004, 2005).

4.4.4 Isotope analysis

4.4.4.1 Stable isotopes (^{18}O, ^{2}H)

The stable isotopic ratios ($^{18}O/^{16}O$ and $^{2}H/^{1}H$) of the entire thermal and some of the non-thermal water samples are analyzed to trace the origin of thermal waters and to identify the

mixing phenomenon between thermal and non-thermal waters. The analysis results are given in table 4.1. Fig. 4.13 shows the isotopic composition of both the thermal and non-thermal water samples along with the GMWL. From the fig. 4.13, it is observed that majority of the thermal water samples fall very close to the GMWL line implying their meteoric origin. The non-thermal groundwater samples (dug wells and hand pumps) fall away from the GMWL. The equation of the evaporation line (EL) of all the samples (both thermal and non-thermal waters) is given by the equation:

$$\delta^2H = (5.81 \pm 0.31) \times \delta^{18}O + 2.49 \pm 0.89 \ (r^2 = 0.97, n=26) \qquad 4.7$$

The lower slope of the EL compared to the GMWL (slope = 8) essentially indicates the evaporation effect. All most all the non-thermal water samples fall on this evaporation line thereby indicating recharge from the falling raindrops subjected to evaporative enrichment. Thermal water falling on this EL clearly point out to the mixing phenomenon with the non-

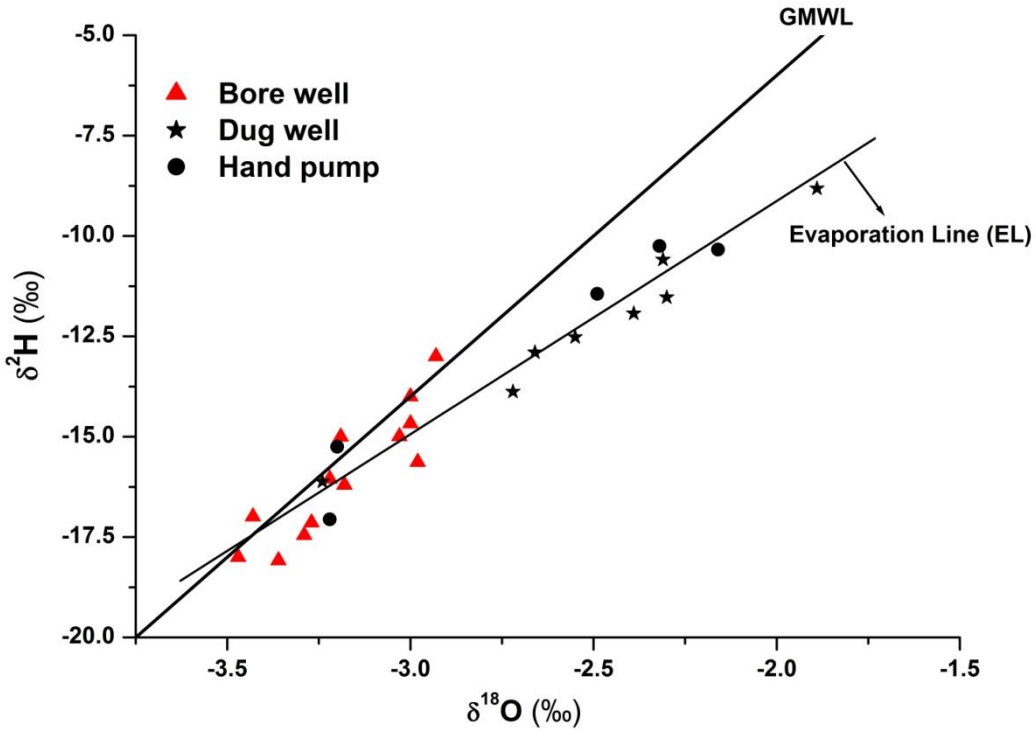

Fig 4.13 *$\delta^{18}O$-δ^2H plot of thermal and non-thermal waters in the study area*

thermal water bodies. In the Godavari valley geothermal area, the thermal water does not exhibit any oxygen-18 shift thus signifying the absence of considerable amount of rock-water interaction at elevated subsurface reservoir temperature (> 200 °C). More over the range of $\delta^{18}O$ (-3.47 to -2.66 ‰) and $\delta^{2}H$ (-18.08 to -12.9‰) values found in the thermal water clearly preclude the presence of any magmatic component ($\delta^{18}O$: +6 to +9 ‰ and $\delta^{2}H$: -40 to -80 ‰) in the present study area. Similarly the analysed stable isotopic values along with very low electrical conductivity (EC: 125 to 723 µS/cm) and the chloride concentrations (9 to 120 ppm) compared to the sea water also nullifies the admixture of any seawater component in the present thermal waters.

4.4.4.2 Tritium and ^{14}C dating

Tritium measurements of twelve water samples (nine thermal and three non-thermal samples) are carried out to approximately estimate the transit time of the thermal waters. The tritium concentrations of the thermal water range from 0.62 TU to 1.5 TU whereas in non-thermal water samples the tritium value ranges from 2.2 to 5.7 TU. Thermal water samples having tritium value less than 1 TU essentially indicate long subsurface residence time (> 50 years) and recharge of these samples might have happened before 1951 (Clark and Fritz, 1997). Few thermal water samples (S-9, 16, 47 etc.) have tritium values greater than 1 TU which can be attributed to the mixing phenomenon with the non-thermal water samples during the ascent towards the surface.

Transit time of the thermal water samples which contain negligible tritium concentration (< 1 TU) is further estimated by C-14 dating technique. C-14 dating technique is able to estimate the age of the groundwater up to 30,000 year BP (before present) (Edmunds, 2009; Cartwright, 2010). The C-14 values of the thermal waters in Godavari valley geothermal area are found to vary from 10.5 to 30 pMC. In the previous section (section 4.4.3), it is observed

that the silicate weathering majorly controls the dissolved solute concentration in the present study area. As a result correction due to the input of ^{14}C-free carbon derived from the dissolution of the carbonate rock is not required. The above inference is further supported from the $\delta^{13}C$ values of DIC of the thermal water samples which range from -17.5‰ to -24.4‰ (average $\delta^{13}C$ value = -20.57‰) with respect to VPDB, which clearly indicates silicate rather than the carbonate weathering as the predominant process. Thus in the absence of any correction factor the transit time of the thermal water is deduced directly from the decay equation:

$$\mathbf{T} = \frac{\mathbf{5730}}{\mathbf{ln2}} \mathbf{ln} \frac{\mathbf{Ao}}{\mathbf{A}} \qquad 4.8$$

where T represents the transit time, A_O and A denote the initial ^{14}C activity (100 pMC) and measured ^{14}C activity in pMC. Using the above equation the transit time of the thermal waters is found to vary from 9952 to 18663 years BP (before present). Thus ^{14}C measurement turns out to be an effective dating technique to estimate the transit time of the old thermal waters in the silicate dominated aquifer.

4.4.5 Estimation of reservoir temperature

Accurate temperature estimation in the medium enthalpy geothermal system poses unique challenge compared to the high enthalpy geothermal systems, due to lack of attainment of equilibrium between aquifer minerals and due to the presence of various processes such as mixing/ dilution (with cold waters), degassing phenomenon etc. In this current study, subsurface temperature of Godavari valley geothermal area, a medium enthalpy geothermal system, is estimated by applying chemical geothemometers, multicomponent geothermometry and mixing models.

4.4.5.1 Chemical geothermometers

Chemical geothermometers, developed since 1960s, have been widely used to estimate the subsurface reservoir temperature by correlating the fluid composition with temperature. Among chemical geothermometers, both the silica (quartz and chalcedony) and cation geothermometers (Na-K, Na-K-Ca, Mg-corrected Na-K-Ca, K-Mg) are used in the Godavari valley geothermal area. Reservoir temperatures computed from applying different geothermometers are given in the table 4.4. The conductive quartz geothermometer (Fournier, 1977) estimates the reservoir temperature varying between 72 to 120 °C whereas application of the adiabatic quartz geothermometer (maximum steam loss) also gives similar range (77 to 118 °C). On the other hand, the chalcedony geothermometer (Arnorsson, 1983) gives comparatively lower estimate of reservoir temperature (42 to 91 °C) which in some cases (S-9, 12, 15, 42 and 47) falls below the surface discharge temperature of the thermal water samples. Moreover in the Godavari valley geothermal area, dissolution of quartz rather than the chalcedony is found to control the solubility of silica in thermal waters. All these factors have rendered the chalcedony geothermometer unsuitable in the present study area. The applicability of Na-K cation geothermometer is evaluated using Giggenbach's (1988) Na-K-Mg ternary diagram (Fig. 4.14). Based on this diagram the thermal waters can be classified as fully equilibrated, partially equilibrated or immature water with respect to reservoir rocks. In the present study area, all the thermal water samples fall in the immature water region which indicates that Na-K geothermometer may not be appropriate to estimate the reservoir temperature. Exceptionally high reservoir temperature (table 4.4) obtained from applying different Na-K geothermometric equations (Fournier, 1979a; Tonani, 1980; Arnorsson, 1983; Nieva and Nieva, 1987; Giggenbach, 1988) also substantiates the lack of equilibrium between suitable Na-K mineral pairs. The subsurface temperature estimated from Na-K-Ca geothermometer (Fournier and Truesdell, 1973) and magnesium corrected Na-K-Ca

geothermometer (Fournier and Potter, 1979) ranges from 58 to 174 °C and 45 to 132 °C respectively which is often lower than the measured surface discharge temperature of the thermal waters. The reservoir temperature value (76 to 112 °C) obtained from the K-Mg geothermometer (Giggenbach, 1988) matches closely with the values calculated from the quartz geothermometer. The nearly comparable values of the K-Mg and the quartz geothermometer essentially suggest the existence of interaction of thermal waters near the surface and the possible mixing with non-thermal shallow groundwater samples.

4.4.5.2 Mixing model

The presence of measurable amount of tritium concentration in some of the thermal waters clearly points out the mixing phenomenon between the thermal and non-thermal waters. In such scenarios the silica-enthalpy mixing model is applied to estimate the subsurface reservoir temperature (Fig. 4.15). The same silica-enthalpy mixing model is also applied in the Tural-Rajwadi geothermal area to estimate the temperature of the geothermal reservoir (section 3.4.6.2.1). In this method, a line is drawn connecting the two end member fluids which intersect the quartz solubility curve (no steam loss curve) at point A. Among two end member fluids, dug well sample represents the one end member whereas the thermal water samples represent the other end member. The enthalpy and the silica concentration of the parent geothermal water before undergoing mixing phenomenon are represented by point A in fig. 4.15. Thus based on the silica-enthalpy mixing model, the subsurface reservoir temperature turns out to be ~137 °C.

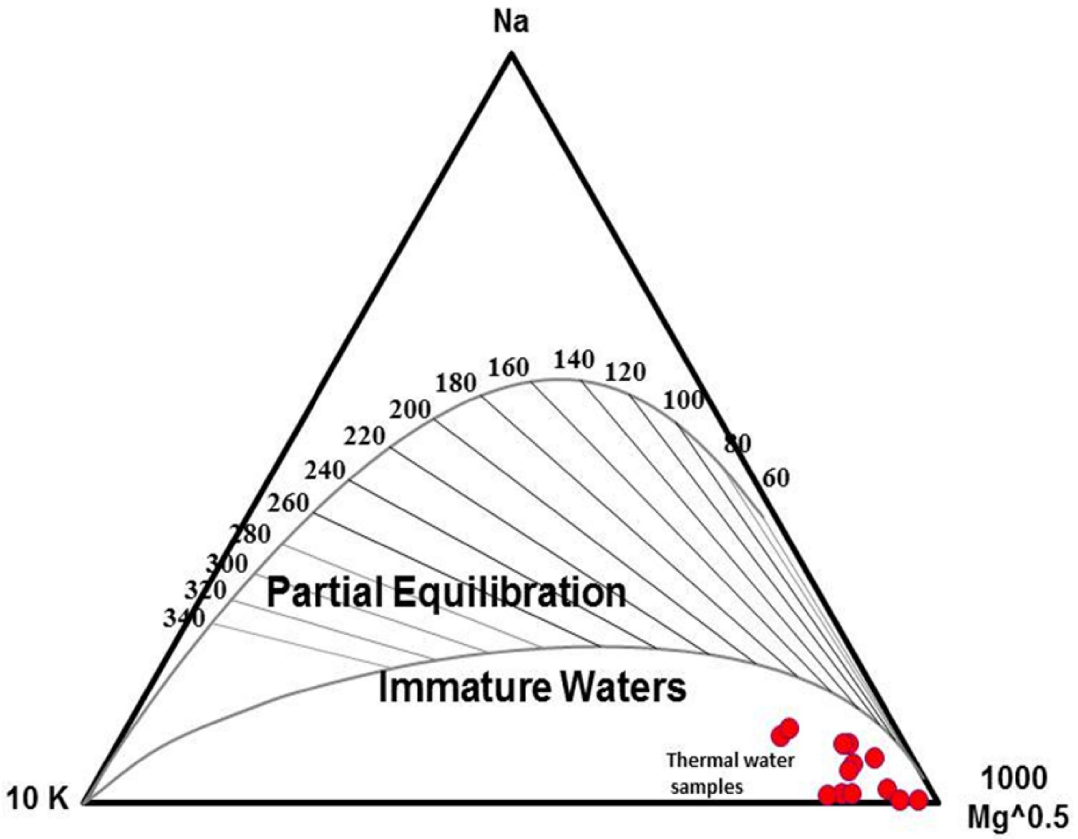

Fig. 4.14 *Na-K-Mg ternary diagram*

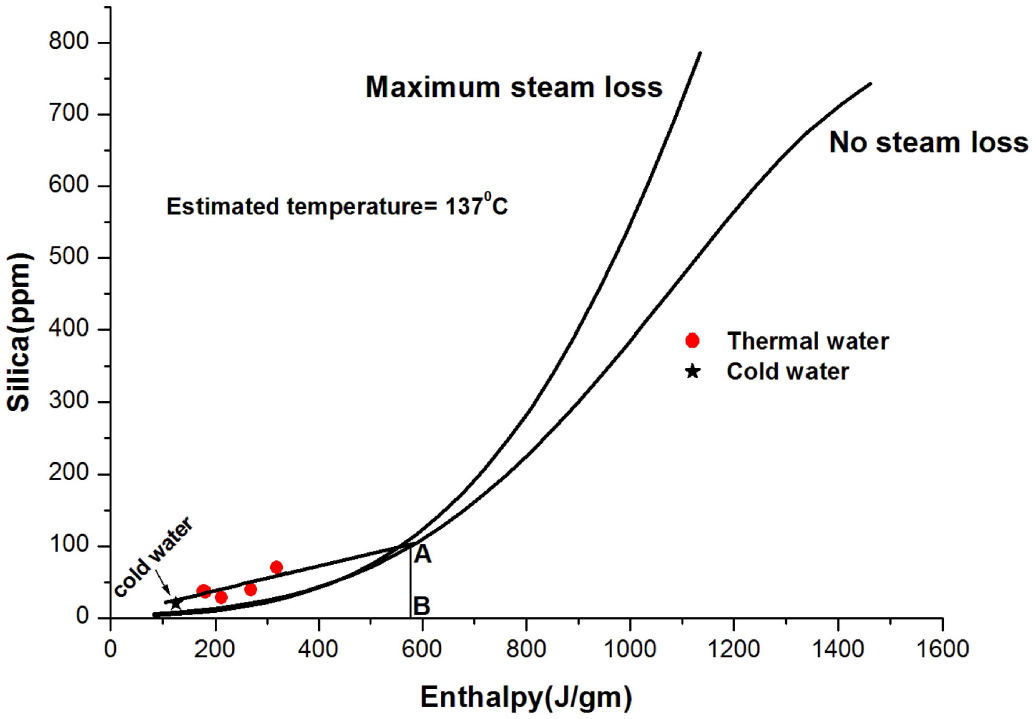

Fig. 4.15 *Silica-enthalpy mixing model*

Table 4.4 *Estimated reservoirs temperatures (°C) using classical geothermometers*

Sample ID	Chalcedony (conductive) Arnoorsson (1983)	Quartz (conductive) Fournier (1977)	Quartz (Adiabatic) Fournier (1977)	K/Mg Giggenbach (1988)	Na-K-Ca Fournier and Truesdell (1973)	Mg corr Na-K-Ca Fournier and Potter (1979)	Na/K Fournier (1979a)	Na/K Tonani (1980)	Na/K Arnorsson (1983)	Na/K Nieva and Nieva (1987)	Na/K Giggenbach (1988)
S-5	71	101	102	88	174	45	200	200	175	187	217
S-9	56	88	90	92	133	76	250	270	234	236	262
S-11	42	74	78	101	148	55	500	740	587	481	482
S-14	52	84	87	106	135	74	600	1005	759	580	564
S-15	57	89	91	97	134	59	494	727	578	476	477
S-16	91	120	118	112	148	132	258	282	245	244	270
S-26	52	84	87	80	102	67	324	389	330	309	330
S-41	48	80	83	76	78	68	632	1103	818	611	589
S-42	40	72	77	80	58	58	474	680	546	456	460
S-47	54	85	88	92	139	83	210	213	187	197	226
S-48	49	81	84	78	127	48	194	191	168	182	211
S-49	55	86	89	109	141	129	237	251	219	223	251
S-50	60	91	93	94	141	68	278	313	269	263	288
S-58	39	71	75	76	98	46	438	602	491	420	429
S-62	45	77	81	71	99	35	361	453	380	345	363

4.4.5.3 Multicomponent solute geotherometry

GeoT (version 2.1) computer program (details given in section 2.6) is used to perform the multicomponent solute geothermometry method. In this method, the saturation indices (log (Q/K)) of suitable reservoir minerals are calculated over a range of temperatures and the reservoir temperature is estimated from the clustering of saturation indices values near to zero. Moreover GeoT (version 2.1) computer program also allows in computing the effects of various secondary processes; like mixing with non-thermal water, degassing during the ascent of thermal water towards the surface; on the original composition of the thermal waters.

4.4.5.3.1 Analysis of the original fluid

Multicomponent geothermometry method is applied on the S-16 sample that has the highest surface discharge temperature as well as the high flow rate. Initially without parameter optimization, mineral saturation indices exhibit very poor clustering (Fig. 4.16A) and the reservoir temperature is estimated to be around 60 °C which is far lower than the surface discharge temperature of 80 °C. Thus in the present study area, the application of multicomponent geothermometry is found to provide poor results without fluid reconstruction technique.

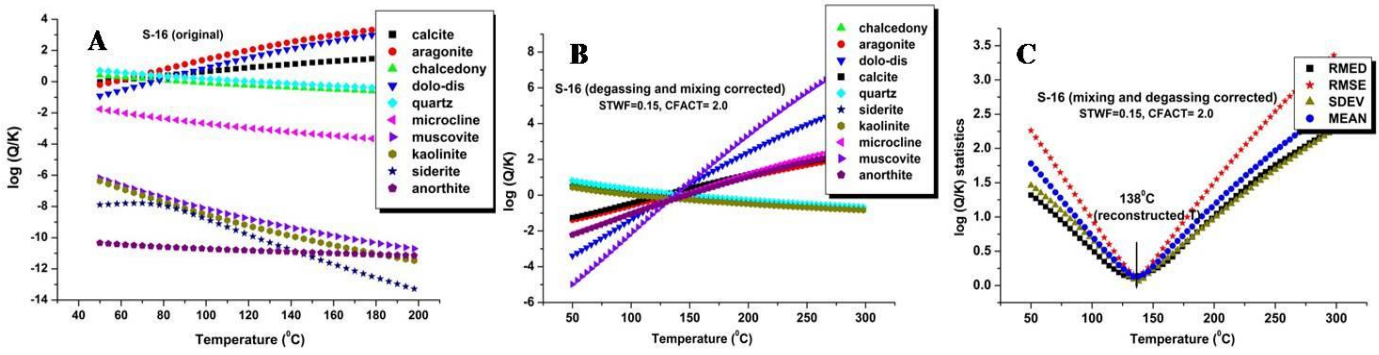

Fig. 4.16 *Computed saturation indices as a function of temperature of (A) original (B) reconstructed fluid of S-16 and (C) statistical analysis of saturation indices as a function of temperature*

4.4.5.3.2 Deep fluid reconstruction

Deep fluid reconstruction by optimizing some of the poorly constrained parameters (such as dilution and degassing) is deemed to be necessary as the sample S-16 shows very poor clustering of minerals. The tritium concentration of S-16 sample is found to be 1.42 TU which clearly points to the mixing phenomenon with non-thermal water. This effect of dilution is corrected by applying the concentration parameter ('cfact') in the GeoT program. Similarly in the GeoT program, the steam weight fraction factor ('stwf') is used to correct any amount of steam loss happened during degassing process. Very good clustering of minerals (quartz, microcline, siderite, dolomite, muscovite, aragonite, chalcedony, calcite, kaolinite and anorthite) is observed (Fig. 4.16B) when both these correction factors are incorporated in sample S-16 (cfact = 2.0 and stwf = 0.15). The log (Q/K) value of various statistical parameters such as standard deviation (SDEV), mean (MEAN), root mean square error (RMSE), median (RMED) attains almost zero value at around 138 °C (Fig. 4.16C) which can be safely taken as the probable reservoir temperature. Along with S-16 sample, integrated geothermometry method is also applied on two samples namely S-9 and S-47. The initial analysis of S-9 sample without any fluid reconstruction method, results similar poor clustering of minerals (Fig. 4.17A) and the estimated temperature turns out to be ~ 66 °C

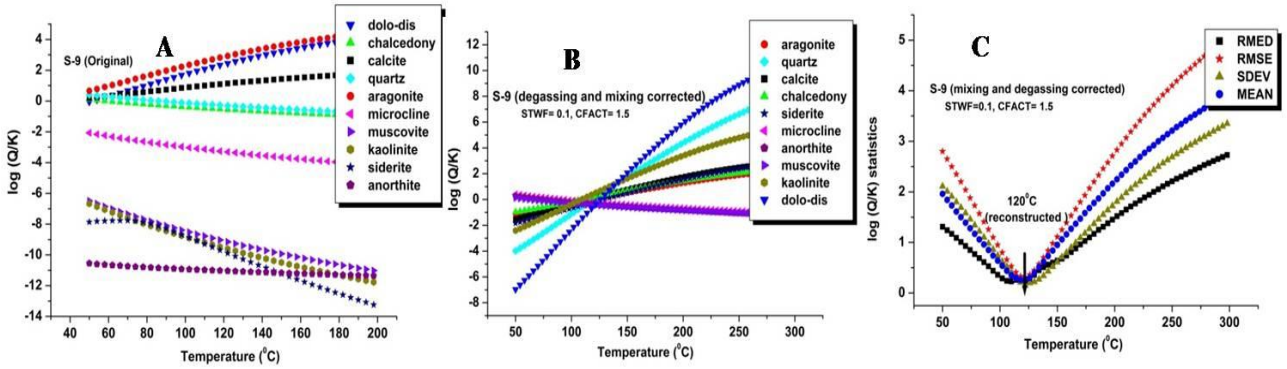

Fig. 4.17 *Computed saturation indices as a function of temperature of (A) original (B) reconstructed fluid of S-9 and (C) statistical analysis of saturation indices as a function of temperature*

which is slightly higher than the surface discharge temperature (64 °C). But after necessary correction for degassing (stwf = 0.15) and dilution (cfact = 1.5) phenomenon, excellent clustering is observed (Fig. 4.17B) and the calculated reservoir temperature becomes ~ 120 °C (Fig. 4.17C). Likewise the multicomponent geothermometry method applied on the original composition of the S-47 sample also results very poor clustering (Fig. 4.18A) of the probable reservoir minerals and after suitable correction of degassing (stwf = 0.05) and mixing phenomenon (cfact = 1.2), excellent clustering of minerals is observed (Fig. 4.18B).

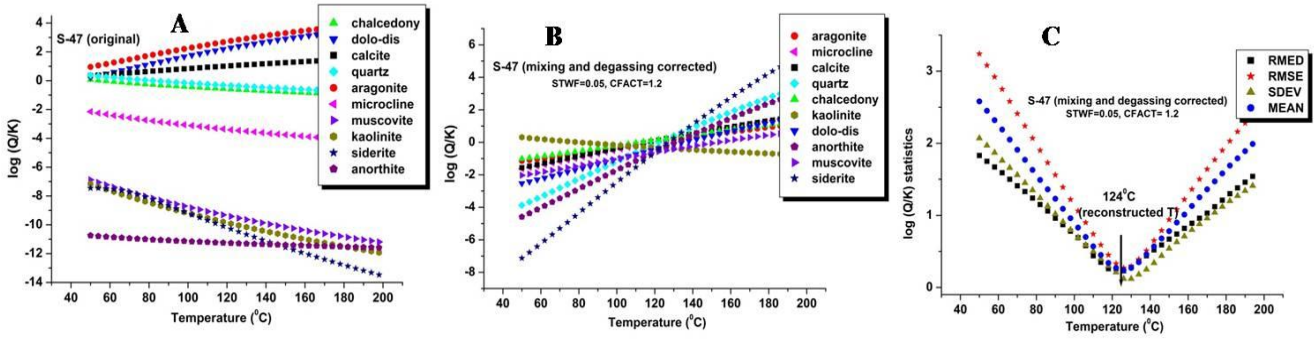

Fig. 4.18 *Computed saturation indices as a function of temperature of (A) original (B) reconstructed fluid of S-47 and (C) statistical analysis of saturation indices as a function of temperature*

In this case the subsurface reservoir temperature is estimated to be ~ 124 °C (Fig. 4.18C). The optimized parameters values of all the three samples along with the effect of fluid reconstruction on the quartz geothermometer values are given in table. 4.5. As quartz geothermometer is based on the absolute concentration of dissolved silica so fluid reconstruction has affected temperature estimate provided by quartz geothermometer. The multicomponent solute geothermometry method thus provides better constraint on the reservoir temperature estimation compared to the solute geothermometers and the average reservoir temperature is found to be 130 ± 10 °C.

Table 4.5 *Values of optimization parameters (cfact = dilution/concentration factor, sf = steam fraction) obtained from GeoT modelling and its effect on quartz geothermometer values*

Sample ID	Optimized parameters		Using original composition	Using reconstituted composition	Equilibrium temperature estimated by GeoT
	cfact (dilution)	stwf (steam fraction	(T_{quartz}) Fournier (1977)	(T_{quartz}) Fournier (1977)	
S-9	1.5	0.15	88 °C	101 °C	120 °C
S-16	2.0	0.15	120 °C	149 °C	138 °C
S-47	1.2	0.05	85 °C	91 °C	124 °C

4.5 Conclusion

The integrated isotope-geochemical characterization of the Godavari valley geothermal area has provided the holistic overview regarding the origin of the thermal waters, its geochemical evolution, source of the dissolved solutes, transit time estimation and the calculation of the subsurface reservoir temperature. The multivariate statistical techniques along with the various graphical plots are found to be effective for delineation of different geochemical processes controlling the groundwater chemistry in the study area. Thermal waters are mostly Na-HCO_3 type whereas the geochemical nature of the non-thermal water samples varies from mixed cation-HCO_3-Cl type to mixed cation-Cl type. Silicate weathering and the ion-exchange mechanisms are found to be the major factors controlling the dissolved solute concentrations in the thermal and non-thermal waters of the study area. Some non-thermal

ground water samples also show the impact of the evaporative enrichment and the effect of anthropogenic contamination (exemplified by the high nitrate and the potassium concentration). According to the Hierarchical Cluster Analysis (HCA) method, all the groundwater samples of the study area can be classified into four geochemically distinct clusters (C1, C2, C3 and C4) depending upon the gradual increase in the ion concentrations (increase in the EC value). Most of the samples falling in the C1 cluster are found to be mixed cation-bicarbonate type whereas the samples in the C2, C3 and C4 clusters are found to be mixed cation-HCO_3-Cl type and mixed cation - Cl type water, respectively. In the PCA method, three principal components (PC1, PC2 and PC3) explain ~79 % of the total variance in the dataset. PC1 is characterized by high value loadings in Cl, SO_4, Mg, Na, Ca and HCO_3, thus indicating the influence of weathering reaction. PC2 is characterized by the highest loading in NO_3 followed by the SiO_2 and K. High loading of nitrate and potassium clearly indicates impact of agricultural activities in some of the non-thermal groundwater samples. The carbon isotope composition of DIC also confirms the silicate weathering mechanism with soil CO_2 coming from C_3 type of plants. Calculations of the mineral saturation indices carried out by the PHREEQC geochemical code indicate that thermal waters are supersaturated with respect to calcite, dolomite, aragonite, chalcedony, quartz and undersaturated with respect to gypsum. The stable isotopic signature (δ^2H, $\delta^{18}O$) of the thermal springs reveals their meteoric origin. Majority of the thermal waters contain negligible (< 1 TU) tritium concentrations indicating long residence times (>50 years) of the recharging waters however few thermal water samples contain measurable tritium concentration due to the mixing with the modern non-thermal waters. Radiocarbon dating (^{14}C) quantifies the approximate residence time of the thermal waters and is estimated to vary between 9950 yr to 18660 yr BP (before present). Furthermore the subsurface temperature in the Godavari valley geothermal field is computed by using both chemical geothermometers,

mixing model and the multicomponent solute geothermometry methods. Cation geothermometer such as Na-K is found to be unsuitable in the present study area as exemplified by the abnormally high subsurface temperature (175 to 1103 °C) obtained from applying different Na-K geothermometers. The reservoir temperature estimated by the quartz geothermometer varies from 72 to 120 °C which matches with the temperature values (76 to 112 °C) obtained from applying K-Mg geothermometer. On the other hand, temperature estimate provided by the both Na-K-Ca geothermometer (58 to 174 °C) and Mg-corrected Na-K-Ca geothermometer (35 to 132 °C) is found to unreliable as often it provides base temperature lower than the surface discharge temperature. Application of the mixing model estimates the reservoir temperature close to 137 °C. To overcome this uncertainty in the estimation of reservoir temperature and to better constrain the reservoir temperature, multicomponent solute geothermometry modelling is carried out using the GeoT computer code. The GeoT modelling approach when applied to the original composition of the thermal waters results very poor clustering of the mineral assemblages and the estimated temperature becomes lower than the surface discharge temperature. However when the effects of the dilution and degassing phenomenon are taking into consideration, the GeoT modelling provides excellent clustering of the mineral assemblages (quartz, chalcedony, crystobalite, magnesite, calcite etc.) and the subsurface temperature of the geothermal reservoir turns out to be 130±10 °C. Thus this multicomponent geothermometry method is found to be very effective in constraining the reservoir temperature in medium enthalpy geothermal system.

CHAPTER 5

Isotopic and geochemical fingerprinting of thermal waters in Chamoli district of Uttarakhand, India

5.1 Background

Uttarakhand geothermal area, a part of northwest Himalayan geothermal belt, is comprised of several thermal springs having surface discharge temperature ranging from 46 to 92 °C. This geothermal area situated in the orogenic belt is characterized by the high thermal gradient (60 °C /km) and high heat flow (100-180 mW/m^2) (Ravi Shanker, 1988). The clusters of several thermal springs are mainly confined around Tapoban and Badrinath area of Chamoli district, Uttarakhand. In 1980s, GSI (Geological Survey of India) had carried out preliminary geological, geochemical mapping of the present study area and several drill holes were drilled to explore the geothermal condition (GSI, 1991). At that time five shallow drill holes (50 to 52 m) and five deep drill holes (100 to 728 m) were drilled and the maximum temperatures recorded in the shallow and deep drill holes were 57 °C and 107 °C respectively. Geophysical investigation revealed low resistivity region at a depth of 20 to 250 m at Tapoban and Badrinath area which was ascribed to the presence of thermal water in fractured gneiss or quartzite formation (Roy et al., 2005; Harinarayana et al., 2008). However there was no integrated isotope-geochemical characterisation study regarding the origin and evolution of the thermal waters in this region. In the current study, stable isotopes (δ^2H and $\delta^{18}O$) of the thermal and non-thermal waters have been measured to ascertain the origin of the thermal waters as well as to estimate the recharge altitude of the thermal springs. Tritium concentrations are measured to constrain the transit time of the thermal waters using the LPM (lumped parameter model) and historical records of tritium in precipitation. Major and trace elements are analysed to understand the geochemical processes affecting the composition of thermal and non-thermal water samples. Moreover subsurface reservoir temperature is estimated using chemical geothermometers, mixing models and multicomponent solute geothermometry method.

5.2 Study area

5.2.1 General geology

Uttarakhand geothermal area situated in the tectonically active HGB (Himalayan Geothermal Belt) is comprised of many major thrusts and faults such as ITSZ (Indus Tsangpo Suture Zone), MCT (Main Central Thrust) and MBT (Main Boundary Thrust). All the thermal manifestations of Uttarakhand geothermal area fall between the MBT and ITSZ. ITSZ basically defines the collision zone between the Asian plate and the Indian plate. The geological framework in the present study area is very complex. Central Crystalline and Garhwal are the two main group of rocks found in this area. Central Crystalline group of rocks forms the basement and is highly metamorphosed in nature. Central Crystalline group of rocks are further classified into different formations such as Yamunotri, Mana, Helang, Milam and Ralam. Lithological details of each formation are given in table 5.1 (GSI, 2012). On the other hand Garhwal group of rocks, less metamorphosed than Central Crystalline group of rocks, are classified in to Baijnath, Pithoragarh and Chamoli formations. MCT (Main Central Thrust) separates the two main groups of rocks (Central Crystalline and Garhwal) from each another. The other two prominent thrusts found in this region are Baijnath thrust and Vaikrita thrust. Baijnath thrust separates the Baijnath formation and the Chamoli formation whereas Vaikrita thrust separates the Mana formation from the Helang formation. Thermal manifestations in Chamoli district are found to be confined near the Tapoban and Badrinath area. Few thermal springs are also seen in the Langshi and Birahi areas. In Tapoban areas, rocks from the Helang formation of Central Crystalline groups are generally found whereas rocks belonging to the Mana formation of Central crystalline crystalline group are exposed the Badrinath area. Fig. 5.1 shows the sample location points along with the geological map of the study area.

Table 5.1 *Lithological details of the study area*

Age	Group	Formation	Lithology
Holocene	Channel Alluvium		Alluvium, moraine, hill wash, unconsolidated glacial and lacustrine sediments
Palaeogene	Badrinath Granite		Tourmaline granite, leucocratic granite with aplitic, pegmatitic, quartzo feldspathic and quartz veins
Mesoproter-ozoic	Garhwal	Berinag=Chamoli=Nagnithank	quartzite, slate with associated basic metavolcanics
		Pithoragarh=Pipalkothi=Shyalana= Lameri	Limestone, dolomite, phyllite, shale and cherty quartzite
		Baijnath	Biotite schist, quartz- mica schist, garnetiferous biotite schist, biotite gneiss, porphyroblastic augen gneiss, pebbly conglomerate gneiss, quartzite and amphibolite
----------Main Central thrust (MCT)----------			
Cambrian	Central Crystalline	Ralam	Basal conglomerate, grey to purple and green massive quartzite.
Neoproterozoic to Cambrian		Milam	Greenish siltstone, phyllite and quartzite with lenses of limestone
Palaeo-proterozoic		Nyu=Helang	Quartzite, quartz mica schist with sills of amphibolite, garnetiferous schist and chlorite schist
		Dar= Mana=Yamunotri	Gneiss, garnetiferous schist, kyanite-silliminite schist, quartz schist, migmatite, calc-silicate rock, granite and pegmatite

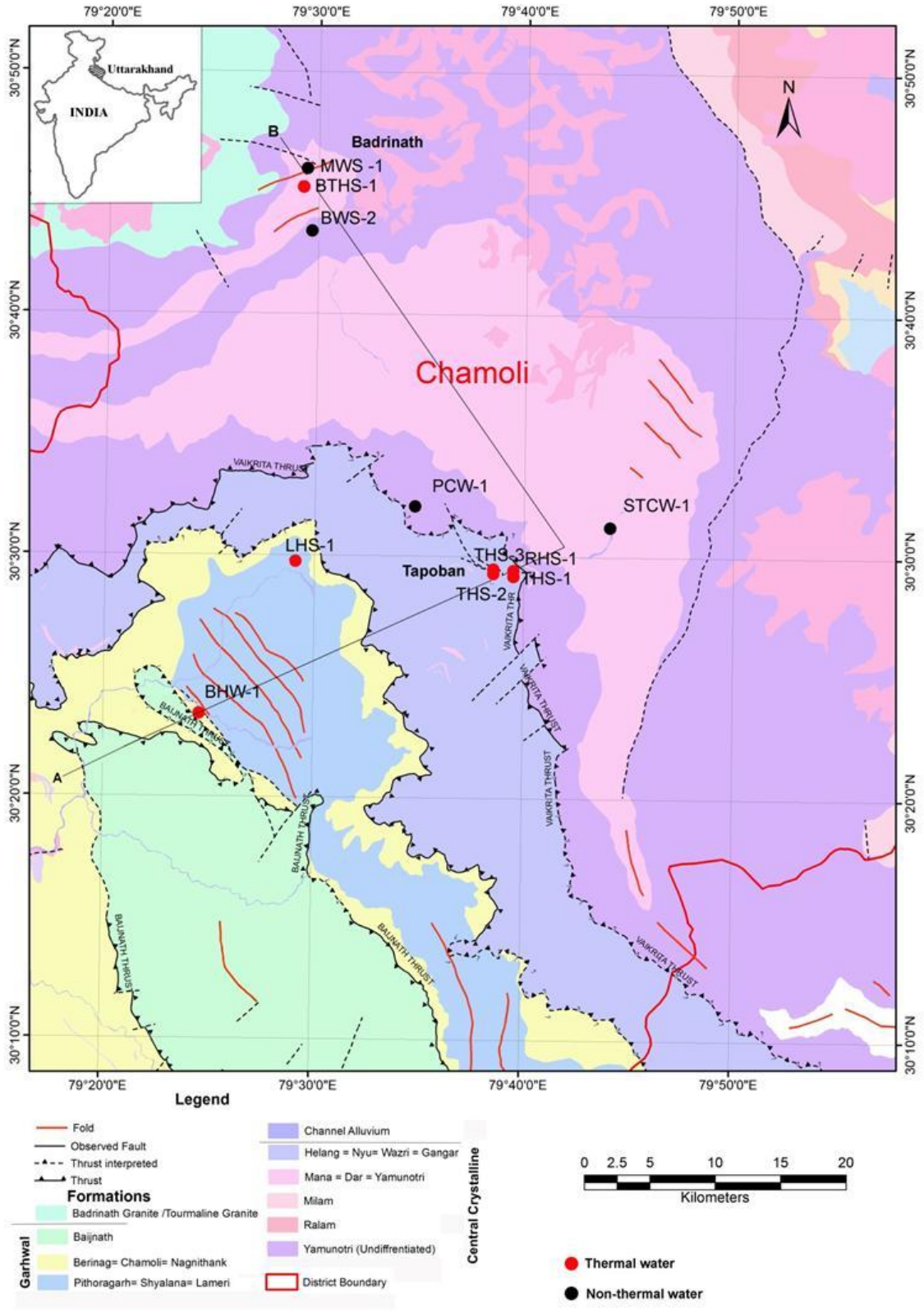

Fig. 5.1 *Geological map and sample location points*

5.2.2 Hydrogeological information

The whole study area is mainly covered by hard rock formations such as quartzite, gneisses, phyllites etc. in which primary porosity is absent mainly due to the repeated metamorphisms and recrystallization phenomenon. Only the secondary porosity due to the presence of folds, faults and fractures acts as a conduit for groundwater movement in this area. Rain water percolated through these fractures forms the local pockets of groundwater which is being extracted through the hand pumps. The depth of the hand pumps varies from 36 m to 100 metre. However local people usually use the springs as a main source for drinking and irrigation purpose. The cold springs are mostly seasonal in nature however all the thermal springs are perennial in nature with constant discharge rate.

5.3 Sampling details

Water samples from the thermal manifestations and cold springs were collected from the study area in the month of November, 2014. Measurements of several physicochemical parameters such as pH, EC (electrical conductivity), TDS (total dissolved solids), temperature were measured in the field using a multiparameter probe (HI 9828). Samples were collected for analysis of major cations (Na, K, Ca, Mg), anions (Cl, SO_4, HCO_3), trace elements (B, Li, Sr, Cs and Rb), dissolved silica and various isotopes (^{2}H, ^{18}O and ^{3}H). Tritium measurements of the Tapoban thermal spring (THS-1) and Badrinath thermal spring (BTHS-1) were carried out earlier by Sharma et al. (1996a) which were again sampled in November, 2014 to know the change in the tritium value of the thermal springs as well as to constrain the mean transit time. Ionic balance between cations and anions is derived using following equation:

$$\text{CBE (\%)} = \{(\sum \text{cations} - \sum \text{anions}) / (\sum \text{cations} + \sum \text{anions})\} \times 100 \qquad 5.1$$

5.4 Results and discussion

5.4.1 Major ion chemistry

The chemical analysis results of the thermal and non-thermal is given in the table 5.2. Thermal waters are found to be almost neutral (pH = 6.8-7.5) having moderate EC (345 to 895 µS/cm) and TDS values (235 to 582 ppm) except the samples from Gari (BHW-1) and Badrinath (BTHS-1) region which have comparatively high EC (1704 and 2420 µS/cm) and TDS concentrations (1159 and 1621ppm). In most of the thermal water samples, calcium is found to be the dominant cation (32-143 ppm) followed by magnesium (10-65 ppm) and sodium (5-47 ppm) ions. However in the thermal waters from Gari (BHW-1) and Badrinath (BTHS-1) region, sodium is found to be the dominant cation (261 to 363 ppm) followed by calcium (32 to 80 ppm) and potassium (32 to 35 ppm) ions. In case of anions, the predominant ion is found to be bicarbonate (220 to 1200 ppm) followed by the sulphate (18 to 50 ppm) and chloride (10 to 140 ppm) ions. On the other hand non-thermal groundwater samples are found to be slightly alkaline (pH = 7.9 to 8.6) having low EC (84 to 248 µS/cm) and TDS (55 to 166 ppm) concentrations. The piper plot (Fig. 5.2) shows the geochemical nature of the thermal and non-thermal water samples. Majority of the thermal water samples are Ca-Mg-HCO_3 type whereas two thermal water samples (BHW-1 and BTHS-1) are Na-HCO_3 type. Non-thermal water samples are mainly Ca-HCO_3-SO_4 type as seen from the piper plot (Fig. 5.2). Chloride ions generally act as a very good conservative tracer in the geothermal system due to the absence of any sink (Michard, 1990; Alçiçek, 2016). As a result, concentrations of various major ions are compared with the chloride concentration to examine their conservative nature in the present geothermal area (Fig. 5.3). The excellent linear correlation (Fig. 5.3A) between the electrical conductivity (EC) and chloride concentration indicates the mixing phenomenon between thermal and non-thermal waters (Alçiçek, 2016). Similar linear correlation (Fig 5.3B

Table 5.2 *Chemical parameters of thermal and non-thermal waters in Uttarakhand geothermal area*

Sample ID	Temp (°C)	pH	EC (µs/cm)	TDS (mg/L)	SiO_2 (ppm)	Na (ppm)	K (ppm)	Ca (ppm)	Mg (ppm)	Cl (ppm)	SO_4 (ppm)	HCO_3 (ppm)	F (ppm)	B (ppb)	Li (ppb)	Rb (ppb)	Cs (ppb)	Sr (ppb)	Ba (ppb)	Sb (ppb)	Charge balance
THS-1	92	7.5	520	349	97	11.0	8	64.0	27	13	25	348	0.8	279	77	78	33	33	90	77.1	-4%
THS-2	80	6.7	538	350	72	9.0	5	72.0	31	15	26	366	0.7	162	63	51	22	143	94	bdl	-2%
THS-3	52	6.1	345	235	44	5.0	4	52.0	15	10	20	220	0.6	87	39	31	14	31	32	bdl	-2%
RHS-1	68	7.8	538	366	98	12.0	10	64.0	34	13	32	348	0.7	306	66	96	34	228	329	bdl	0%
RHS-2	66	6.6	694	458	88	11.0	8	108.0	36	10	36	476	0.9	310	62	90	36	219	330	bdl	2%
LHS-1	51	7.1	895	582	47	47.0	15	40.0	65	38	49	549	2.6	1037	163	113	37	199	81	bdl	-5%
BHW-1	46	7.1	1704	1159	50	261.0	32	32.0	10	130	18	860	6.7	3408	925	164	97	25	46	bdl	7%
BTHS-1	56	6.8	2420	1621	105	363.0	35	80.0	5	140	29	1200	6.4	9076	918	404	422	513	69	bdl	-8%
STCW-1	20	8.1	84	55	4	0.7	1	12.0	3	1.5	6	55	0.2	6	10	9	10	15	7	bdl	-9%
BWS-2	21	8.2	248	166	4	3.0	1	24.0	17	5	50	104	0.4	7	8	6	12	12	10	bdl	4%
MWS-1	19	7.9	73	47	5	1.0	1	12.0	2	5	17	25	0.3	5	1	4	0.3	37	6	bdl	0%
PCW-1	22	8.4	179	120	9	3.0	2	40.0	2	8	6	122	0.2	12	7	10	14	10	12	bdl	-2%
DSCS	06	8.6	509	336	19	6.0	10	84.0	12	8	4	366	0.6	10	12	12	16	14	11	bdl	-4%

Note: "bdl" = *below detection limit*

and 5.3C) between the sodium and chloride ion as well as potassium and chloride ions clearly indicates that rock-water interaction is the dominant mechanism for controlling the concentrations of these ions (Alçiçek, 2016). Apart from these, magnesium and calcium ions also exhibit linear correlation with chloride ions (Fig 5.3D and 5.3E). However two samples such as BHW-1 and BTHS-1 do not follow the linear trends probably due to the precipitation

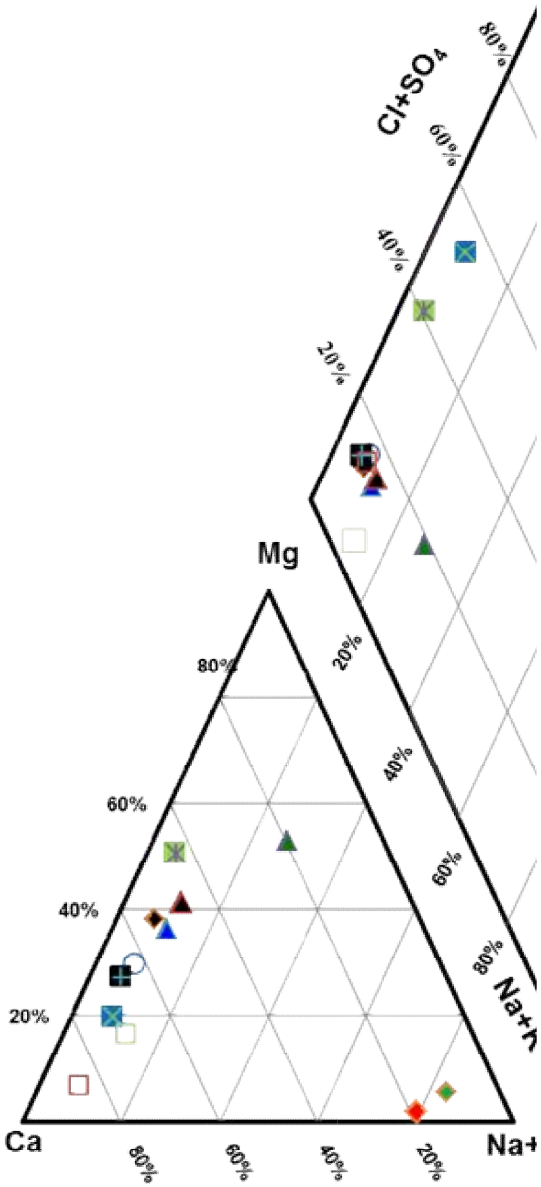

Fig. 5.2 *Piper plot showing water types of thermal and non-thermal waters*

Table 5.3 *Computed saturation indices values of selected minerals*

Sample ID	Type of water	Calcite	Dolomite	Aragonite	Gypsum	Anhydrite	SiO_2 (a)	Chalcedony	Quartz	Fluorite
THS-1	Thermal	1.13	2.16	1.03	-2.22	-1.85	-0.54	0.12	0.37	-1.85
THS-2	Thermal	0.30	0.63	0.19	-2.2	-1.97	-0.59	0.09	0.38	-1.85
THS-3	Thermal	-0.93	-1.89	-1.06	-2.37	-2.46	-0.63	0.13	0.48	-1.84
RHS-1	Thermal	1.14	2.5	1.02	-2.19	-2.1	-0.4	0.32	0.63	-1.85
RHS-2	Thermal	0.29	0.60	0.17	-1.97	-1.89	-0.42	0.3	0.62	-1.41
LHS-1	Thermal	0.23	1.18	0.10	-2.32	-2.38	-0.59	0.17	0.52	-0.89
BHW-1	Thermal	0.28	0.48	0.11	-2.80	-2.9	-0.53	0.25	0.61	-0.9
BTHS-1	Thermal	0.54	0.4	0.42	-2.28	-2.29	-0.27	0.47	0.81	0.14
STCW-1	cold	-0.72	-1.99	-0.87	-3.3	-3.55	-1.30	-0.39	0.10	-2.77
MWS-1	cold	-1.26	-3.25	-1.42	-2.85	-3.1	-1.20	-0.29	0.19	-2.41

of calcite and dolomite from the solution. Mineral saturation study of the thermal water samples shows that the most of the thermal water samples (except THS-3) are supersaturated with respect to quartz, chalcedony, calcite, dolomite and aragonite whereas they are found to be udersaturated with respect to gypsum, anhydrite and amorphous silica (Table 5.3). Badrinath thermal water (BTHS-1) is also found to be supersaturated with fluorite mineral. Thermal waters are found to be undersaturated with respect to amorphous silica due to the higher solubility of amorphous silica compared to quartz and chalcedony (Rimstidt and Barnes, 1980).

5.4.2 Trace element geochemistry

Thermal waters from the Uttarakhand geothermal area are also analysed for trace elements like boron (B), strontium (Sr), Rubidium (Rb), Caesium (Cs), lithium (Li) and barium (Ba). Concetrations of these trace elements are generally found to be higher in thermal waters compared to the non-thermal waters due to the greater extent of rock-water interaction at the high temperature prevalent in the geothermal reservoir (Stüben et al., 2003; Das et al., 2005, Tarcan and Gemici, 2003). The conservative nature of these trace elements is examined by comparing with the chloride ion concentrations (Fig. 5.4). From the various scatter plots, it is

observed than except lithium, boron and caesium, the concentrations of other trace elements (i.e. Sr, B and Rb) get affected by a number of various secondary processes (such as precipitation, uptake in secondary minerals etc.) resulting non-linear correlation with the chloride concentrations. The existence of these various secondary processes is also exemplified when the relative concentrations of lithium, caesium and rubidium are plotted in a ternary diagram (Fig. 5.5) (Giggenbach and Goguel, 1989). Scaling factors have been used in the ternary diagram to evenly spread out the data points. Data points of the thermal waters are found to be away from the compositional area of the crustal rocks thereby indicating the presence of various secondary processes as discussed earlier. From the fig. 5.5, it is also seen that except BHW-1, all other thermal springs (THS-1, 2, 3; LHS, RHS-1 and BTHS-1) fall in a same cluster indicating that these thermal water samples undergo same mineralogical interaction while coming to the surface. In fact geological mapping shows that the thermal water from the Birahi region (BHW-1) is associated with the Garhwal group of rocks whereas other thermal water samples are issuing through the Central Crystalline group of rocks as a result BHW-1 sample undergo different mineralogical interaction. Moreover in geothermal areas, the chloride and boron concentrations generally show good correlation and all the thermal springs belonging to the same geothermal area exhibit linear correlation thereby indicating common source of boron and chloride (Arnorsson and Andresdottir, 1995). In the present study area, except BTHS-1, all other thermal springs show linear correlation thereby implying that the same reservoir is feeding all the thermal springs (except BTHS-1). The Cl/B ratio thus shows that probably completely different reservoir system is feeding the Badrinath thermal water (BTHS-1). Thermal waters in the Uttarakhand region also contain variable amount (0.6 to 6.7 ppm) of fluoride concentrations. Badrinath thermal water (BTHS-1) is found to contain highest concentration of dissolved fluoride and is also found to be supersaturated with fluorite mineral (Table 5.3). Linear correlation between chloride and

fluoride ions (Fig. 5.4D) further supports the mixing phenomenon between thermal waters containing high fluoride concentrations with non-thermal waters having low fluoride contents. This mixing phenomenon is also confirmed from the scatter plot between tritium and electrical conductivity (section 5.4.3.2.1). Although thermal waters in the present study area show evidence of mixing with non-thermal groundwater yet the trace element concentrations in the surrounding potable water bodies are well below the guideline values prescribed by WHO (WHO, 2008). Moreover water samples from the existing hand pumps are found to be safe both for irrigation and drinking purposes (CGWB, 2016). So the mixing between the thermal and non-thermal water bodies does not have posses any immediate threat for consumption of water from potable water bodies in the study area.

5.4.3 Isotope analysis

5.4.3.1 ^{18}O and ^{2}H

The $\delta^{18}O$ and $\delta^{2}H$ values of the thermal and non-thermal water samples collected from the study area are shown in table 5.4. Fig. 5.6A shows the stable isotope composition of the collected samples along with the GMWL (Global Meteoric Water Line) and LMWL (Local Meteroic Water Line). The LMWL line of nearby Uttarkashi district (situated ~50 km away from the study area) of Uttarakhand state is used as a reference in this study (Kumar et al. 2010). The equation of the Uttarkashi LMWL is given below:

$$\delta^{2}H = 8.07\ (\pm 0.23) \times \delta^{18}O + 13.89\ (\pm 1.68)\ (r^{2} = 0.98, n=23)\ \text{(Kumar et al. 2010)} \quad 5.2$$

In the present study, the equation of the best fit line (BFL) based on the non-thermal water sample is:

$$\delta^{2}H = 7.73\ (\pm 0.18) \times \delta^{18}O + 12.79\ (\pm 1.5)\ (r^{2} = 0.98, n=10) \quad 5.3$$

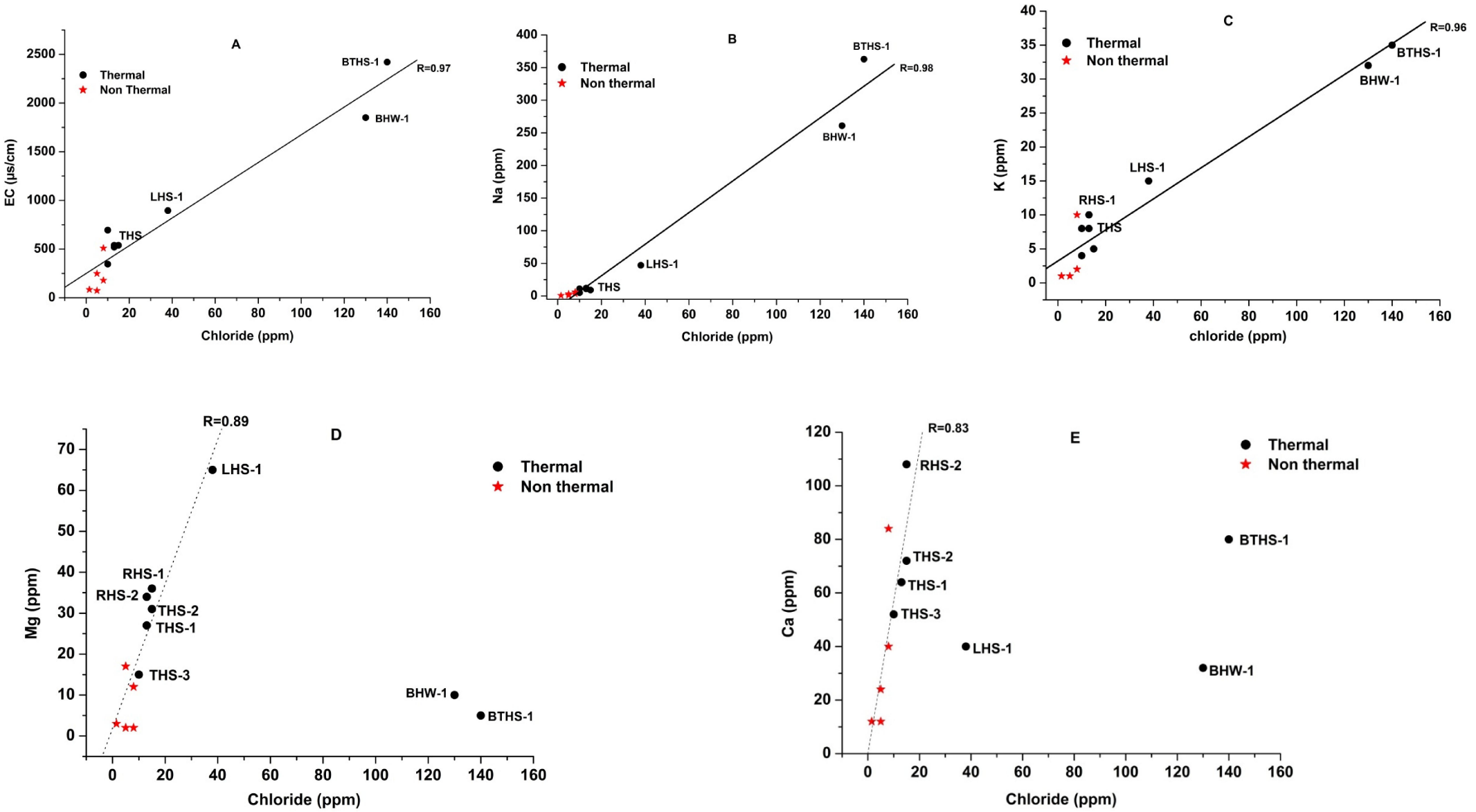

Fig. 5.3 *Scatter plots between various major ions versus chloride ion (A) EC vs. Cl (B) Na vs. Cl (C) K vs. Cl (D) Mg vs. Cl (E) Ca vs. Cl*

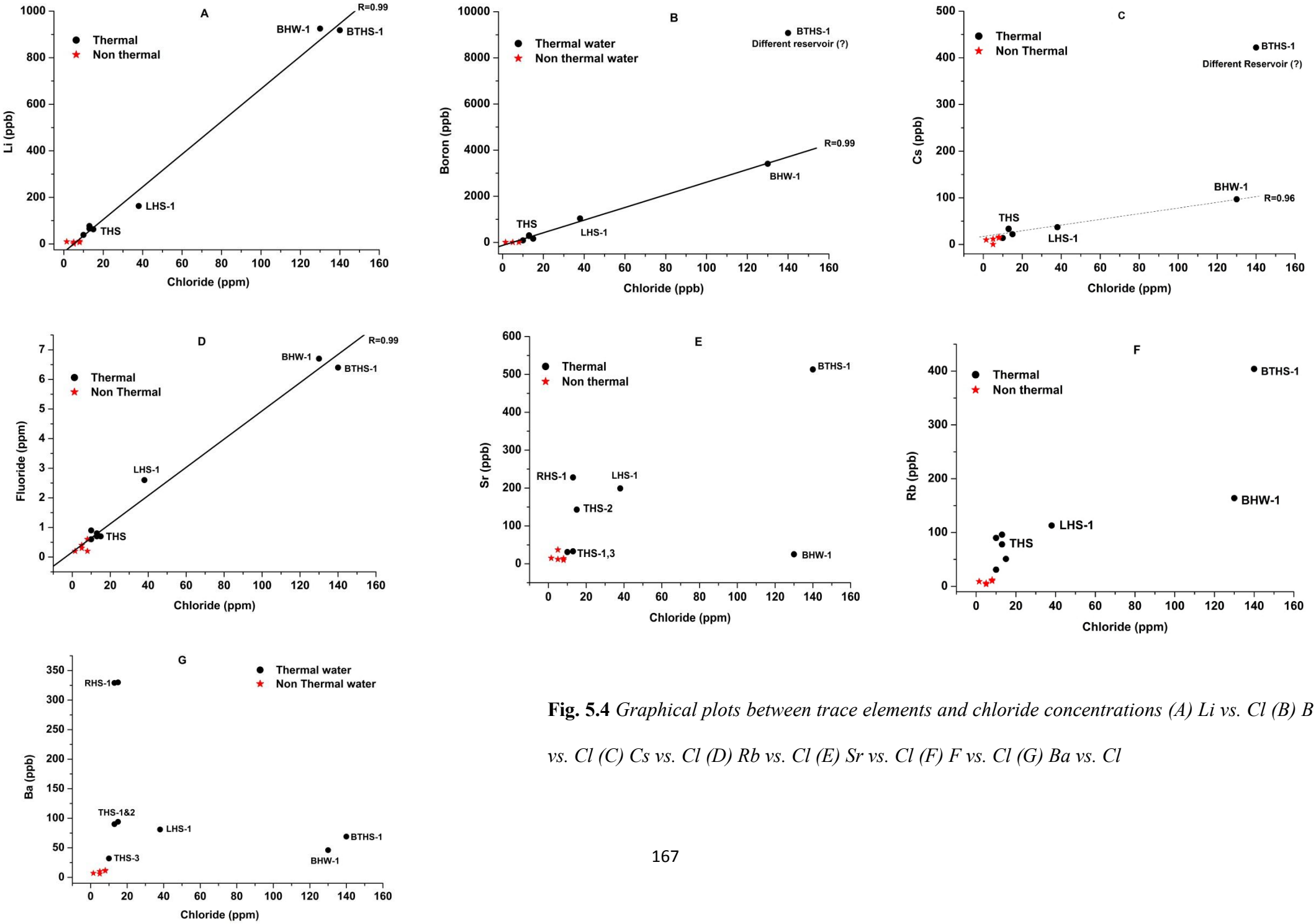

Fig. 5.4 *Graphical plots between trace elements and chloride concentrations (A) Li vs. Cl (B) B vs. Cl (C) Cs vs. Cl (D) Rb vs. Cl (E) Sr vs. Cl (F) F vs. Cl (G) Ba vs. Cl*

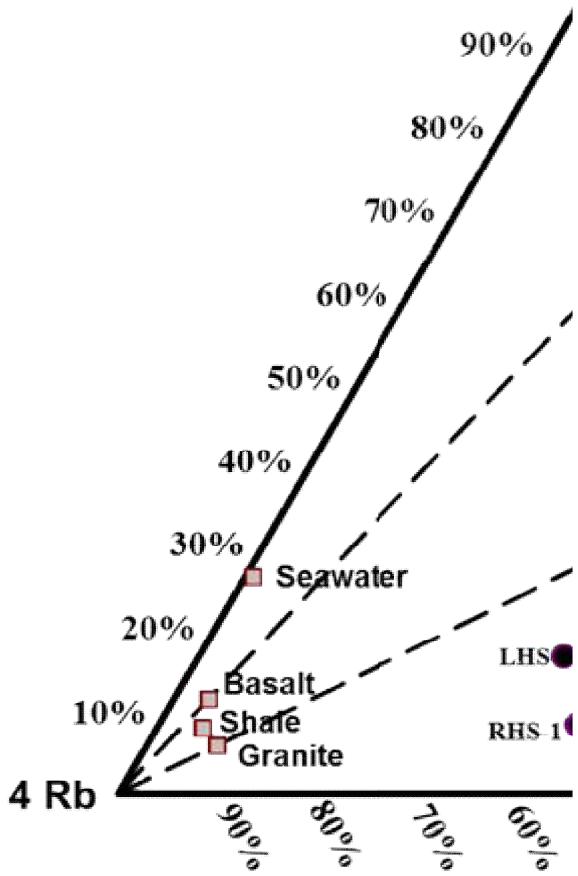

Fig. 5.5 *Li-Rb-Cs ternary diagram*

which closely resembles to the LMWL of the Uttarkashi district. Thermal waters in the study area have $\delta^{18}O$ and $\delta^{2}H$ values ranging from -9.43 to -13.56 ‰ and -61.58 to -95.1 ‰ respectively which clearly nullifies the presence of any magmatic component ($\delta^{18}O$: +6 to +9 ‰, $\delta^{2}H$: -40 to -80 ‰) in the thermal water. Similarly the absence of enriched $\delta^{18}O$ and $\delta^{2}H$ values along with the low EC (345 to 2420 µS/cm) and chloride concentrations (5 to 140 ppm) also rules out the possibility of sea water component in the thermal waters. So the thermal waters are basically meteoric water which has gained heat due to the deep subsurface circulation before emerging as thermal springs. Fig. 5.6A also shows that the thermal waters fall close to the BFL thereby confirming their meteoric origin. Badrinath thermal water shows

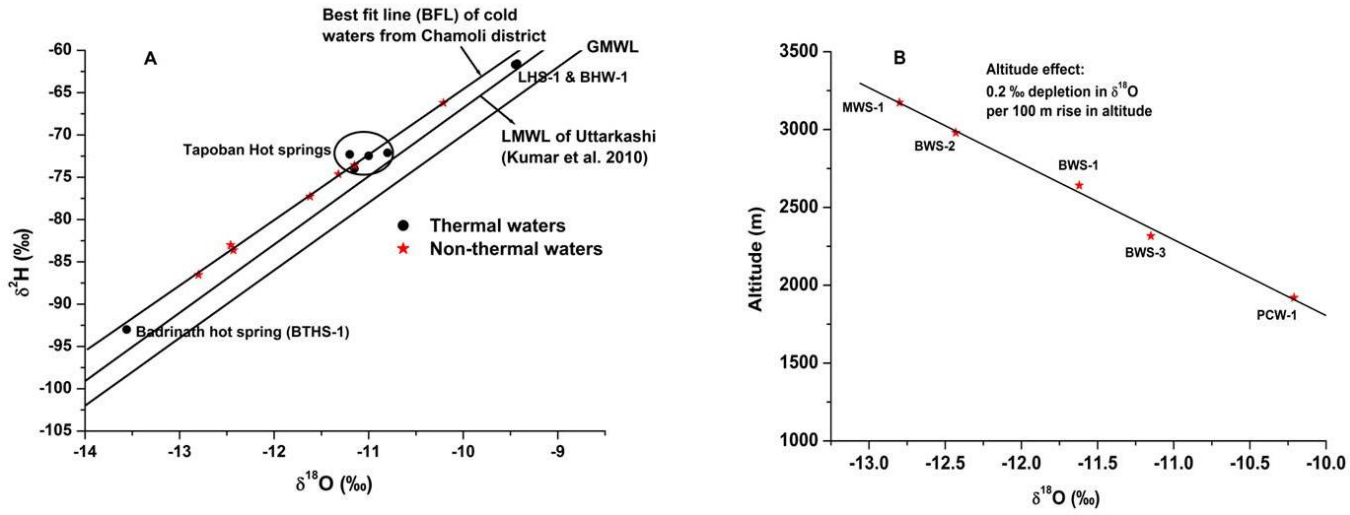

Fig. 5.6 *A) $\delta^{18}O$-$\delta^{2}H$ plot of thermal and non-thermal waters and B) altitude vs. $\delta^{18}O$ plot*

most depleted isotopic values compared to the surrounding non-thermal water samples which points out to the possibility of the higher altitude recharge of these thermal springs. The recharge altitude can be measured using the $\delta^{18}O$-altitude plot in which the $\delta^{18}O$ contents of the non-thermal waters (i.e. cold springs) are plotted against their discharge altitude (Fig. 5.6B). The inverse of the slope of the best fit line basically gives the estimation of the altitude effect. The altitude effect is found to be -0.2‰ per 100 metre rise in altitude for $\delta^{18}O$ i.e. ^{18}O value decreases 0.2‰ (permil) per 100 metre rise in altitude. Incorporating this value of altitude effect, the recharge altitude of the Tapoban thermal water is estimated to be around 2712 metre whereas for Badrinath thermal water the recharge altitude is found to be about 3542 metre. Similarly the recharge altitude for Langshi (LHS) and Birahi (BHW-1) thermal water is around 1543 metre. So from the above discussion, it is evident that the isotopic variation of the thermal waters in this region occurs mainly due to difference in the recharge altitudes. Thermal waters show progressively decreasing isotopic values with concomitant increase in the recharge altitude. For example, Badrinath thermal water (BTHS-1) having highest recharge altitude (3542 metre) shows most depleted isotopic values ($\delta^{18}O$ = -13.56‰ & $\delta^{2}H$ = -95.1‰) among all the samples.

Table 5.4 *Environmental isotope values and extent of mixing*

Sample ID	Type of water	Discharge altitude (m)	$\delta^{18}O$ (‰)	$\delta^{2}H$ (‰)	^{3}H (TU)	Fraction of cold water component (x) (%)
THS-1	Thermal water	1856	-11.20	-72.3	7.5	75
THS-2	Thermal water	1843	-11.0	-72.47	7.2	72
THS-3	Thermal water	1853	-10.8	-72.11	-	
RHS-1	Thermal water	1790	-11.15	-74	-	-
LHS-1	Thermal water	1240	-9.43	-61.58	6.9	69
BHW-1	Thermal water	1255	-9.45	-61.69	3.6	36
BTHS-1	Thermal water	3203	-13.56	-95.1	3.0	30
STCW-1	Non-themal	1206	-12.46	-83.02	10.5	-
MWS-1	Non-thermal	3173	-12.8	-86.53	9.5	-
DSCS	Non-thermal	2190	-11.32	-74.64	-	-
BWS-1	Non-thermal	2641	-11.62	-77.28	-	-
BWS-2	Non-thermal	2980	-12.43	-83.63	-	-
BWS-3	Non-thermal	2316	-11.15	-73.59	-	-
PCW-1	Non-thermal	1920	-10.21	-66.22	-	-

Note: "-'' *means not measured*

5.4.3.2 Tritium (^{3}H) analysis

Tritium, the radioactive isotope of hydrogen and a constituent of water molecule (in HTO form), is widely used to estimate the approximate mean transit time of both surface and groundwater systems. Apart from that, tritium is also used to identify and quantify the mixing phenomenon between the thermal and non-thermal waters (Panichi and Gonfiantini, 1977). In this study, seven samples comprising both thermal and no-thermal waters are collected for tritium analysis and the values are given in table 5.4. The tritium value of the thermal water samples in this region ranges from 3 to 7.5 TU whereas in non-thermal water samples the tritium value varies from 9.5 to 10.5 TU. Thermal water in Tapoban (THS-1) and Badrinath region has tritium values 7.1 TU and 3.0 TU respectively whereas the tritium measurements carried out in 1995 by Sharma et al. (1996a) showed that the tritium values in Tapoban and Badrinath thermal waters were 25 TU and 7.0 TU. The availability of previous tritium data in the Tapoban and Badrinath thermal water actually helps in estimating the mean transit time using lumped parameter models (Section 5.4.2.2.2).

5.4.3.2.1 Mixing phenomenon

The mixing phenomenon between thermal and non-thermal water can also be identified using tritium values. In earlier sections (Section 5.4.1 and 5.4.2) the linear relationships between the conservative tracers (sech as Na vs. Cl, B vs. Cl etc) indicate the mixing process. Tritium also shows negative correlation with both chloride (Fig. 5.7A) and EC values (Fig. 5.7B). This type of situation arises when thermal water containing low tritium concentrations (high mean transit time) and high EC values gets mixed with non-thermal water having low EC and high tritium values. Similar phenomenon is also observed in the Tural-Rajwadi geothermal field (section 3.4.2.2). The extent of mixing can be quantified using the following formula (Sammel and Craig 1981; Giggenbach et al. 1983):

$$x = (T_{sp}/T_{gw}) \quad 5.4$$

Where T_{sp} denotes the tritium value of the mixed thermal spring, T_{gw} represents the tritium value of non-thermal water and 'x' is the cold water fraction present in the thermal water. In this study average tritium concentration of 10 TU is taken as T_{gw}. Thus using the above

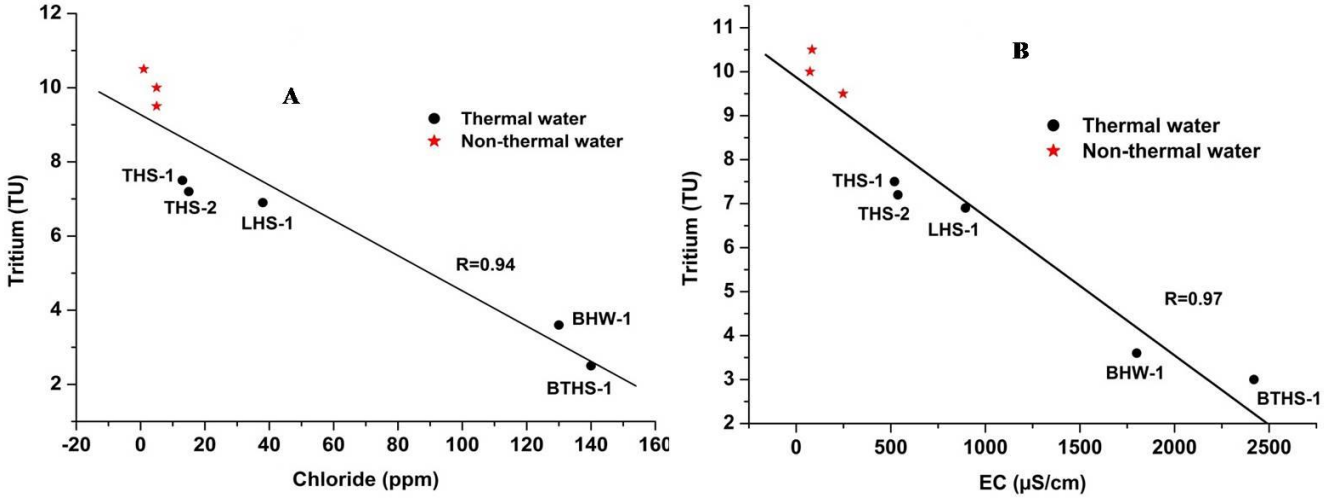

Fig. 5.7 *A) Plot between tritium and chloride B) Plot of tritium vs. EC*

equation, the cold water fractions present in the THS-1, THS-2, LHS-1, BHW-1 and BTHS-1 are estimated to be 0.75, 0.75, 0.69, 0.36 and 0.30 respectively. The Badrinath thermal water (BTHS-1) is found to be least diluted compared to the other thermal waters.

5.4.3 Transit time estimation

Mean transit time of Tapoban thermal water (THS-1) and Badrinath thermal water (BTHS-1) is calculated using both the historical and modern day tritium concentrations along with suitable lumped parameter models (LPMs). Tritium concentrations of these two thermal waters are available for the year 1995 and 2014 respectively.

Table 5.5 *Yearly weighted mean ^{3}H values in precipitation from 1961 to 1995*

Time (year)	Ottawa ^{3}H (TU)	New Delhi ^{3}H (TU)	Time (year)	Ottawa ^{3}H (TU)	New Delhi ^{3}H (TU)
1961	227.3	73.1	1978	73.6	24.7
1962	992.4	410.8[a]	1979	49.6	17.4[a]
1963	2900.1	1207.0[a]	1980	49.5	17.3[a]
1964	1532.8	636.3[a]	1981	55.1	19.6[a]
1965	778.2	321.4[a]	1982	47.3	16.4[a]
1966	560.8	268.6	1984	36.5	11.9[a]
1967	324.2	91.9	1985	35.3	11.4[a]
1968	216.9	62.9	1986	42.5	14.4[a]
1969	253.7	102.5[a]	1987	37.4	12.3[a]
1970	190.8	76.3[a]	1988	36.7	9.4
1971	206.1	82.7[a]	1989	40.3	13.5
1972	92.3	35.2[a]	1990	39.1	13.0[*]
1973	90.4	33.5	1991	34.7	15.4
1974	98.1	36.1	1992	21.0	15.2
1975	75.9	28.3[a]	1993	18.5	10.8
1976	58.9	21.2[a]	1994	20.3	12.3
1977	73.9	28.7	1995	16.1	17.7

Note: "a" superscript denotes the calculated values of New Delhi GNIP station using the known ^{3}H concentration in Ottawa

5.4.3.1 Construction of the tritium input data

Estimation of mean transit time (MTT) by using the lumped parameter models essentially requires the continuous tritium series data of the local precipitation as an input function. As the present study area does not have tritium records of precipitation so the data from the nearest GNIP (Global Network of Isotopes in Precipitation) station i.e. New Delhi is taken as representative values. In New Delhi station, the discontinuous tritium concentration of the precipitation is available from the year 1961 to 1995. The missing tritium data of the New Delhi GNIP station is estimated by comparing the weighted mean tritium concentration of New Delhi station with that of the Ottawa GNIP station which has continuous tritium records from the year 1953. This type of correlation method has been widely applied to estimate the missing tritium concentration in other GNIP stations (Rabinowitz et al., 1977; Pearson and Truesdell, 1978; Campana and Mahin, 1985). The equation of the linear correlation between New Delhi and Ottawa GNIP station is found to be (Fig. 5.8):

$$^{3}H_{\text{New Delhi}} = 0.41734 \times (^{3}H_{\text{Ottawa}}) - 3.345 \ (R^2 = 0.926) \qquad 5.5$$

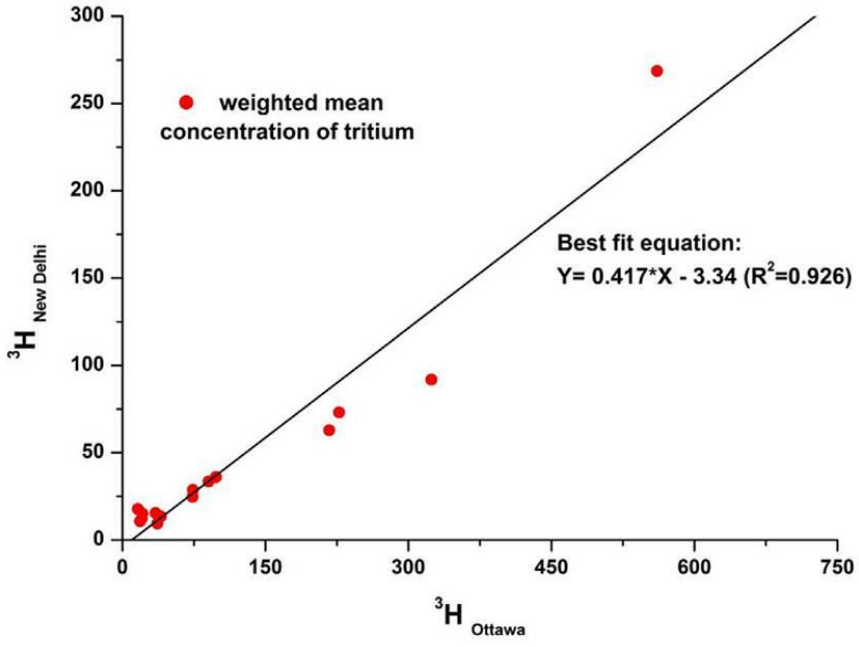

Fig. 5.8 *Correlation between tritium values of New Delhi and Ottawa GNIP station*

Thus the tritium concentrations in the Ottawa GNIP station are scaled by the factor of 0.41 to estimate the missing tritium values of the New Delhi GNIP station. Table 5.5 shows the estimated (correlation with the Ottawa station) and measured tritium values of New Delhi GNIP station which acts as the input parameters in TracerLPM worksheet.

5.4.3.2 Transit time estimation of THS-1

The Tapoban thermal water (THS-1) shows tritium concentration of 25 TU and 7.1 TU in the year 1995 and 2014 respectively. To estimate the MTT of the THS-1 sample, four LPMs such as PFM (Piston Flow Model), EMM (Exponential Mixing Model), EPM (Exponential Piston Flow Model) and DM (Dispersion Model) are used in this study and later the best fit models based on the relative difference between the modelled output and the measured tritium values are chosen for the MTT estimation. PFM gives the most simplistic scenario where it is tacitly assumed that from the recharge to the discharge point, the tracer molecule does not undergo any mixing and/or dispersion. Fig. 5.9A shows the model output concentration of tritium with the measured tritium value. The relative squared error becomes lowest (~ 19.2%) when MTT of the THS-1 becomes ~36 years. However the large error in the MTT estimation clearly shows the possibility of applying other suitable LPMs.

Exponential mixing model (EMM) on the other hand takes in to account of the homogenous mixing thereby providing the other extreme of an idealistic situation. The best fit MTT from the application of EMM is found to be ~ 22 years and the corresponding relative squared error turns out to be ~ 33% which also renders this model ineffective in calculating the actual MTT. Fig. 5.9B shows the graphical plot of the model output concentrations obtained from various EMMs having different transit times.

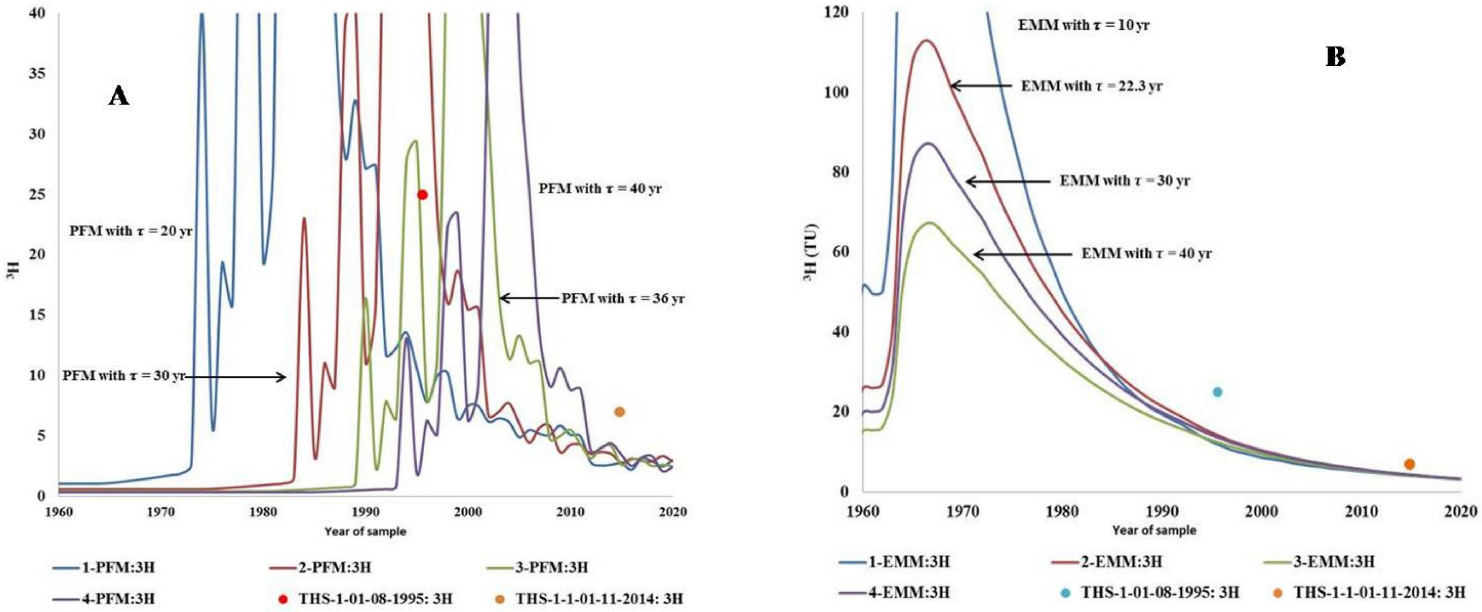

Fig. 5.9 *Simulated tritium concentration with varying transit times along with the measured tritium value of THS-1 by applying A) Piston flow model (PFM) and B) Exponential mixing model (EMM)*

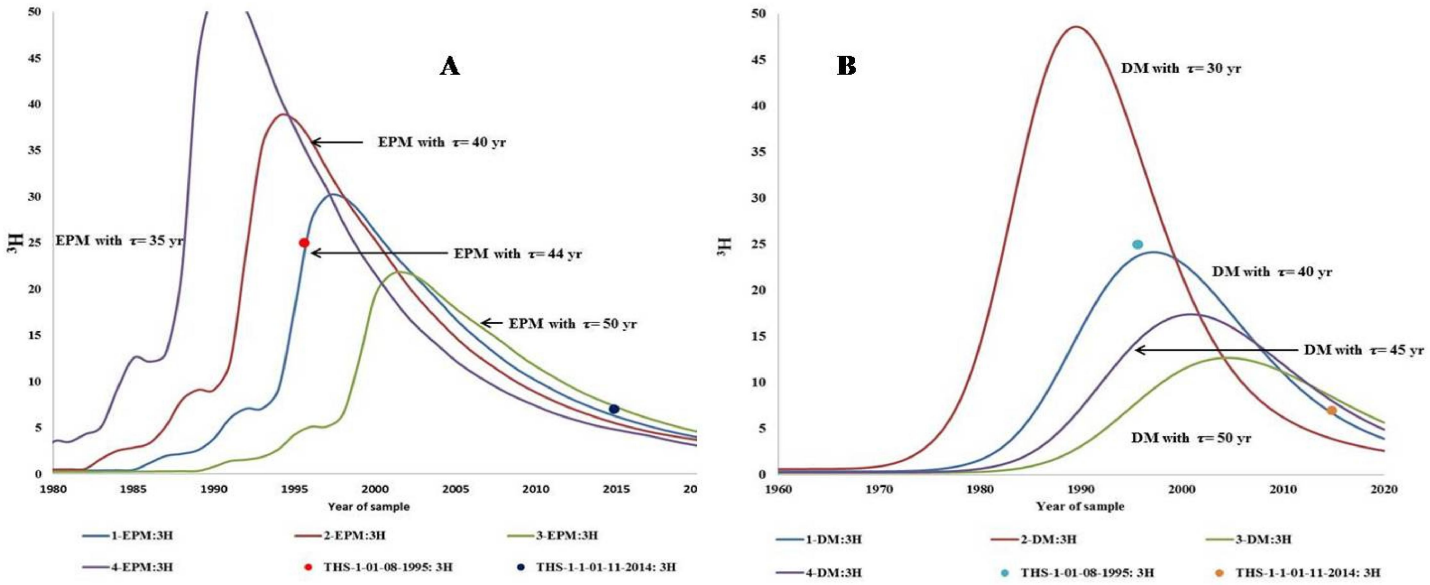

Fig. 5.10 *Simulated tritium concentration with varying transit times along with the measured tritium value of THS-1 by applying A) Exponential piston flow model (EPM) and B) Dispersion model (DM)*

EPM (Exponential Piston Flow Model) is far more realistic than PFM or EMM models as it is a combination of both models. In the EPM, there are two unknown parameters such as mean age and EPM ratio. EPM ratio basically denotes the fraction of piston flow part compared to that of the exponential flow part. EPM model converts to EMM model when the EPM ratio equals to zero and similarly EPM model becomes converts to PFM model when the value of EPM ratio becomes greater than 5 (Jurgens et al., 2012). In the present study, using the EPM model the best fit MTT turns out to be ~ 44 years (EPM ratio: 2.45) and the relative squared error becomes ~ 0.95% implying excellent matching between the modelled and observed tritium values. Fig. 5.10A shows the graphical representation of the simulated tritium time series along with measured values.

Dispersion model (DM) is generally used to calculate the MTT of the fluid that comes out from the aquifer having various configurations. Dispersion model also contains two unknown parameters such as dispersion parameter and the mean age. Dispersion parameter is basically the ratio between dispersion to advection (Zuber and Maloszewski, 2001). Low dispersion ratio narrows down the age distribution peak and the centre of that peak lies close to the mean age whereas the higher dispersion ratio shifts the age distribution peak towards the younger fraction of water. The use of dispersion model in this study shows that the best fit MTT of THS-1 is around 40 years and the relative squared error further narrows down to ~ 0.3%. The pictorial presentation of simulated tritium time series data resulting from dispersion model is shown in fig.5.10B.

So from the above discussions it is observed that among various LPMs, the simulated tritium concentration obtained from the EPM and DM models matches closely with the measured tritium concentrations of the Tapoban thermal water (THS-1) and the estimated MTT varies from 40 to 44 years.

5.4.3.3 Transit time of BTHS-1

Badrinath thermal water (BTHS-1) also has two tritium measurements, first one in the year of 1995 (7.7 TU) and second one in 2014 (3.0 TU). In both the field seasons, the tritium concentration of the BTHS-1 is found to be less than the THS-1 sample indicating higher residence time of the BTHS-1. MTT estimation of the BTHS-1 sample is carried out using the same procedure as that of THS-1 sample. Fours LPMs namely PFM, EMM, EPM and DM are applied and their suitability in deducing the MTT are assessed.

In case of BTHS-1, the best fit piston flow model estimates MTT in the range of 17 years having ~ 3.1% relative squared error value. Fig. 5.11A shows the simulated tritium time series data of PFM model concentration of the BTHS-1 is found to be less than the THS-1 sample indicating higher residence time of the BTHS-1. MTT estimation of the BTHS-1 sample is carried out using the same procedure as that of THS-1 sample. Fours LPMs namely

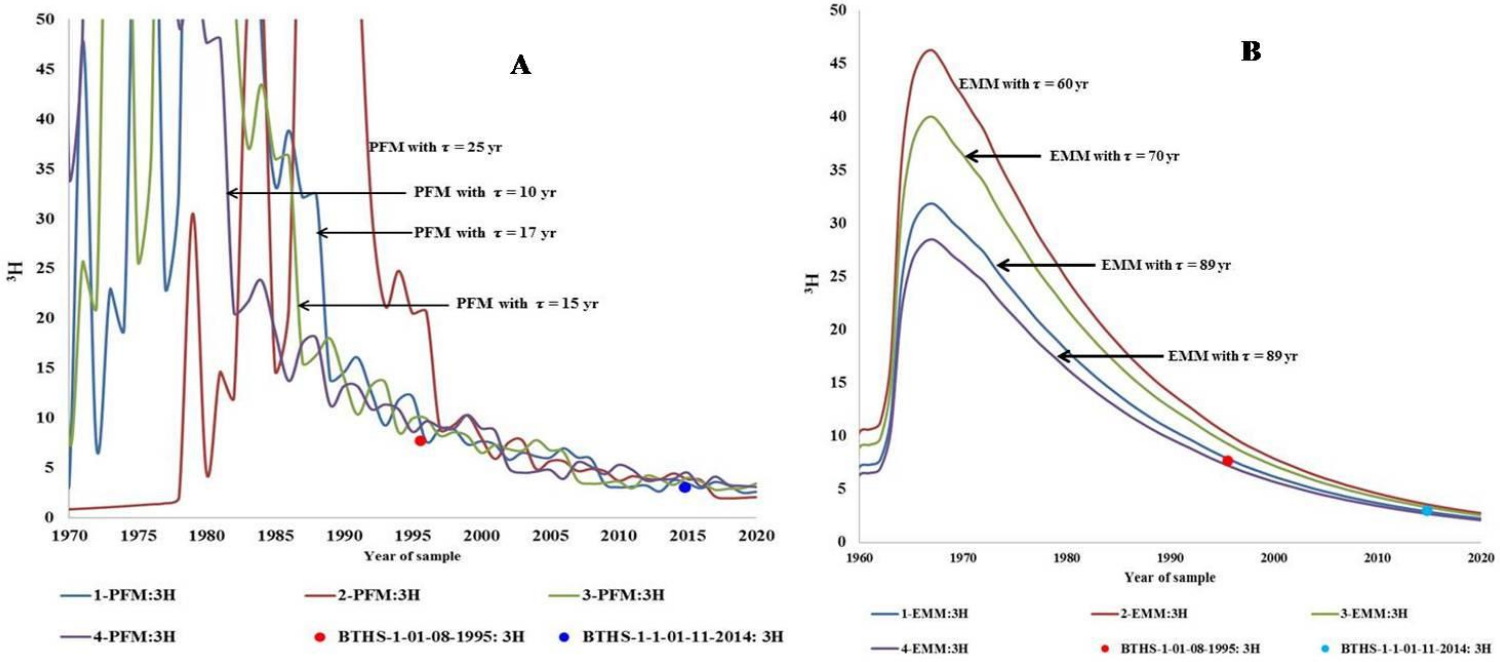

Fig. 5.11 *Graphical plot of simulated ^{3}H time series along with the measured ^{3}H values of BTHS-1 sample by applying A) PFM model and B) EMM model*

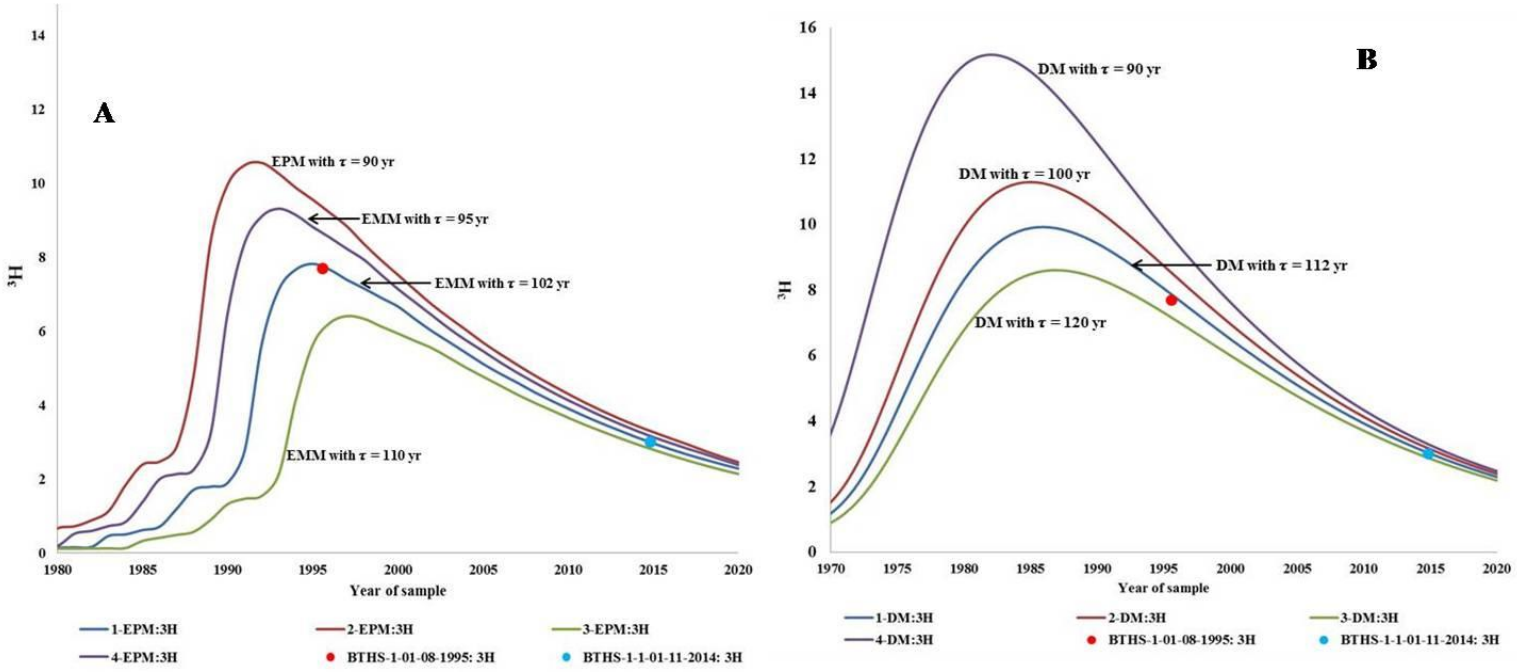

Fig. 5.12 *Graphical plot of simulated ^{3}H time series along with the measured ^{3}H values of BTHS-1 sample by applying A) EPM model and B) DM model*

EMM model gives MTT in the range of 89 years and the error associated with it narrows down to ~0.13%. The simulated time series plot derived from the EMM model having different transit time along with the measured values is shown in fig. 5.11B. The application of the EPM model shows that the best fit MTT for BTHS-1 sample lies in the range of ~102 years having EPM ratio of 0.38 (fig. 5.12A). Similarly the application of the dispersion model indicates that the best fit MTT of the BTHS-1 turns out to be ~112 years having dispersion parameter of 0.52 (Fig. 5.12B). The relative squared error in both the EPM and the DM model lies close to zero thereby implying close matching between the simulated and measured tritium concentration. Thus the MTT of the Badrinath thermal water (BTHS-1) is found to vary between 102 to 112 years.

The MTT estimation of both the THS-1 and BTHS-1 also throws light on the flow characteristics of the feeding aquifers. The EPM ratio of the THS-1 is found to be 2.45

indicating that the aquifer has the contribution of both exponential and piston flow segments. On the other hand, the EPM ratio of the BTHS-1 sample is found to be lower (0.38) compared to the THS-1 which points out that the aquifer feeding the BTHS-1 sample mostly contain exponential mixing segment. The above inference is further validated from the value of the dispersion parameter. BTHS-1 sample containing mostly exponential mixing part shows higher dispersion parameter (0.52) compared to the THS-1 sample (dispersion parameter: 0.03) which contains greater amount of piston flow segment. The MTT estimation of the thermal waters utilising the measurements of tracer concentration over a period of time provides a valuable alternative as the conventional borehole based investigation is not possible in geothermal area due to high temperature as well as difficulty in deep drilling.

5.4.4 Reservoir temperature estimation

5.4.4.1 Chemical geothermometry

The subsurface reservoir temperature estimation of the Uttarakhand geothermal area is carried out by using both silica (quartz and chalcedony) and cation geothermometers (Na-K, Na-K-Mg, Na-K-Mg corrected and K-Mg). The estimated reservoir temperatures from different chemical geothermometers are given in the Table 5.6. Conductive quartz geothermometer (no steam loss) (Fournier, 1977) estimates the reservoir temperature in the range of 96 to 140 °C whereas adiabatic quartz geothermometer (maximum steam loss) (Fournier, 1977) estimates temperature range from 97 to 135 °C. The similar range of temperature obtained from both the adiabatic and conductive quartz geothermometer indicates that the no appreciable extent of steam loss happens during the ascent of the thermal waters. Lower temperature range (72 to 109 °C) is observed when the chalcedony geothermometer (Arnoorsson, 1983) is employed. The Na-K-Mg ternary diagram (Giggenbach, 1988) is applied to check the applicability of the Na-K geothermometer in the present study area. From the Na-K-Mg ternary diagram (Fig. 5.13), it is seen that all the

thermal water samples fall in the 'immature' region rendering the samples unsuitable for applying Na-K geothermometer. The above inference is further substantiated from the abnormally high subsurface temperature (Table. 5.6) obtained from applying different Na-K geothermometric equations (Fournier, 1979a; Tonani, 1980; Arnorsson, 1983; Nieva and Nieva, 1987; Giggenbach, 1988). Similarly other cation geothermometers such as Na-K-Ca geothermometer (Fournier and Truesdell, 1973), magnesium corrected Na-K-Ca geothermometer (Fournier and Potter, 1979) and K-Mg geothermometer (Giggenbach, 1988) are also found to be unsuitable in the present study area as the estimated reservoir temperature obtained from applying these geothermometers often falls below the surface discharge temperature of the thermal waters. So among all the chemical geothermometers, quartz geothermometer provides somewhat reliable subsurface reservoir temperature (96 to 140 °C).

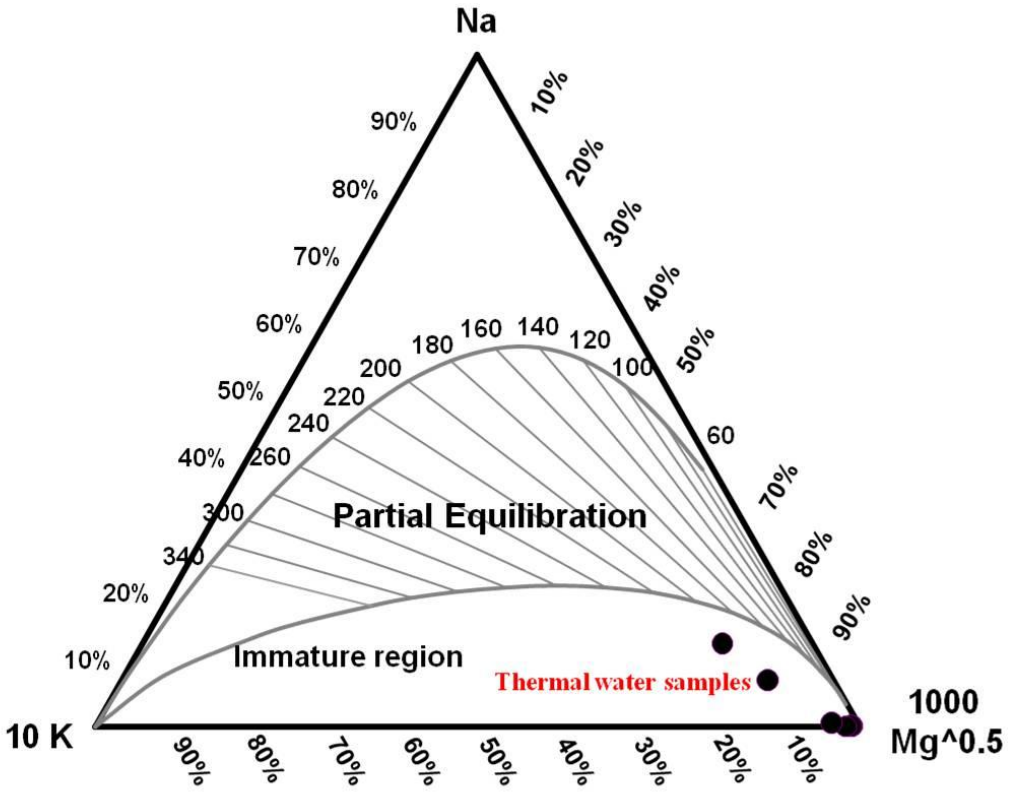

Fig. 5.13 *Na-K-Mg ternary diagram of the thermal water samples*

Table 5.6 *Estimated reservoirs temperatures (°C) using classical geothermometers*

Sample ID	Chalcedony (conductive) Arnoorsson (1983)	Quartz (conductive) Fournier (1977)	Quartz (Adiabatic) Fournier (1977)	K/Mg Giggenbach (1988)	Na-K-Ca Fournier and Truesdell (1973)	Na-K-Ca Mg correction Fournier and Potter (1979)	Na/K Fournier (1979a)	Na/K Tonani (1980)	Na/K Arnorsson (1983)	Na/K Nieva and Nieva (1987)	Na/K Giggenbach (1988)
THS-1	109	136	131	52	45	45	477	688	552	459	463
THS-2	91	120	118	41	30	30	427	580	474	410	420
THS-3	66	96	97	44	25	25	497	734	583	479	479
RHS-1	109	136	132	54	52	52	506	755	597	487	487
RHS-2	103	130	127	49	36	36	477	688	552	459	463
LHS-1	69	99	100	70	260	13	439	606	493	422	431
BHW-1	72	102	103	96	196	71	235	249	217	221	249
BTHS-1	114	140	135	108	180	149	214	219	191	201	229

5.4.4.2 Mixing model

In previous sections (section 5.4.3.2.1) the linear correlation between various conservative tracers has already confirmed the mixing phenomenon between the thermal and non-thermal waters. In this scenario various types of mixing models such as silica-enthalpy, chloride-enthalpy and silica-carbonate mixing models are generally used to estimate the subsurface temperature of the deep geothermal reservoir. Among all these mixing models, the silica-enthalpy mixing model has been applied in the Uttarakhand geothermal area (Fig. 5.14). The silica-enthalpy mixing model is also applied in the Tural-Rajwadi geothermal area, Maharashtra (section 3.4.6.2.1). In the silica-enthalpy mixing model (Fig. 5.14), the enthalpy is chosen as abscissa and the silica concentrations of thermal and non-thermal water samples are plotted in the vertical axis.

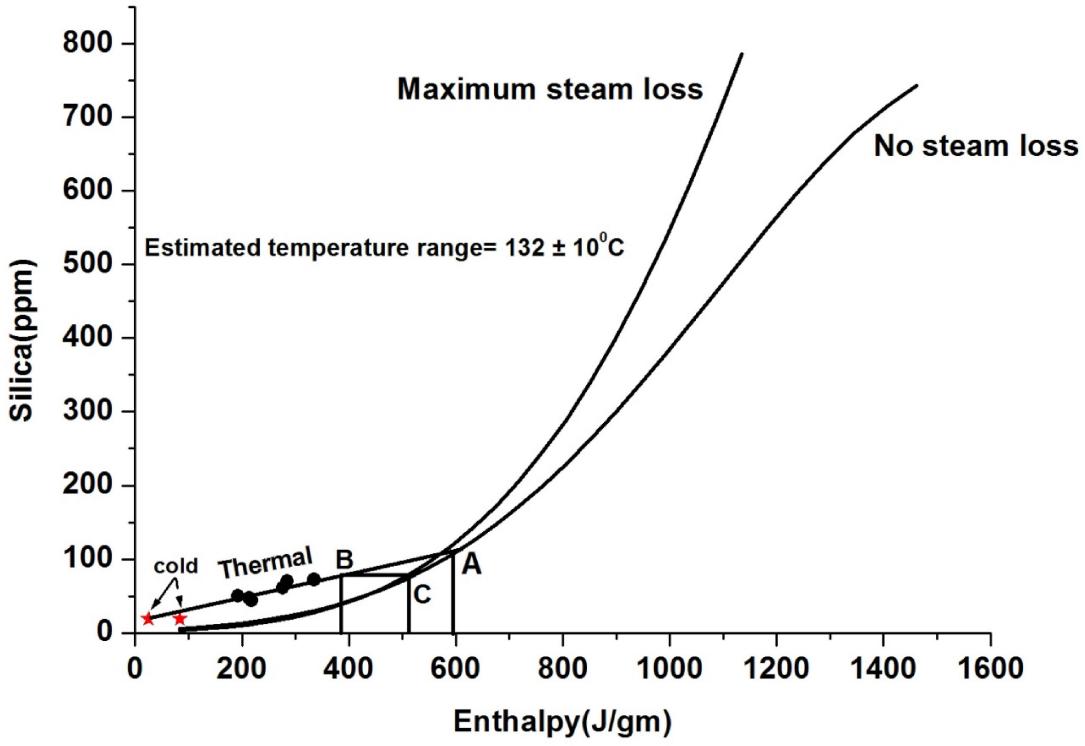

Fig. 5.14 *Silica-enthalpy mixing model*

After that the reservoir temperature is estimated using any of the two different methodologies. In the first methodology, it is tacitly assumed that no steam loss phenomenon has taken place during the ascent of the thermal waters towards the surface. In this methos, the line joining the thermal and non-thermal water samples cuts the no steam loss curve of quartz at the point A which basically gives the enthalpy of the geothermal reservoir. Using this method, the subsurface temperature (after converting enthalpy to temperature) is estimated to be ~ 141 °C. In the second method, to account the steam loss phenomenon, a vertical line is drawn corresponding to the enthalpy value of 385.4 J/g (boiling point of the water in the study area i.e. 92 °C) which cuts the mixing line joining the thermal and no-thermal water samples at point B. From point B, a horizontal line parallel to the enthalpy axis is dawn that intersects the maximum steam loss curve at point C. Enthalpy value at point C gives the estimation of reservoir temperature i.e. ~ 124 °C. Thus using the mixing model, the average subsurface temperature turns out to be 132 ± 10 °C.

5.4.4.3 Multicomponent solute geothermometry

In this study, integrated multicomponent solute geothermometry method has been applied to better constrain the reservoir temperature as the temperature estimation by applying different chemical geothermometers show wide variation (96 to 140 °C). GeoT (version 2.1), the standalone computer program is used to calculate the solute geothermometry method (details of this method is already discussed in section 2.6). This multicomponent solute geothermometry method is performed on the four thermal water samples (THS-1, THS-3, RHS-1 and BTHS-1) to access the range of variation of reservoir temperature. In Tapoban thermal water (THS-1), the multicomponent geothermometry method shows that the quartz, tridymite, chalcedony, cristobalite, brucite, phlogopite etc. are in simultaneous equilibrium with each other (Fig. 5.15A) and the equilibrium temperature is found to be ~ 134 °C (fig. 5.15B) which is in very good

agreement with quartz geothermometer value (136 °C). Similarly for THS-3 sample various minerals such as calcite, tremolite, talc, dolo-dis, magnesite etc. are found to be in simultaneous equilibrium (Fig. 5.16A) and the estimated reservoir temperature turns out to be ~128 °C (Fig. 5.16B). In the case of the RHS-1 sample, the multicomponent geothermometry method yields the reservoir temperature at ~ 124 °C and the same suite of minerals are found to be in equilibrium (Fig. 5.17A and 5.17 B).

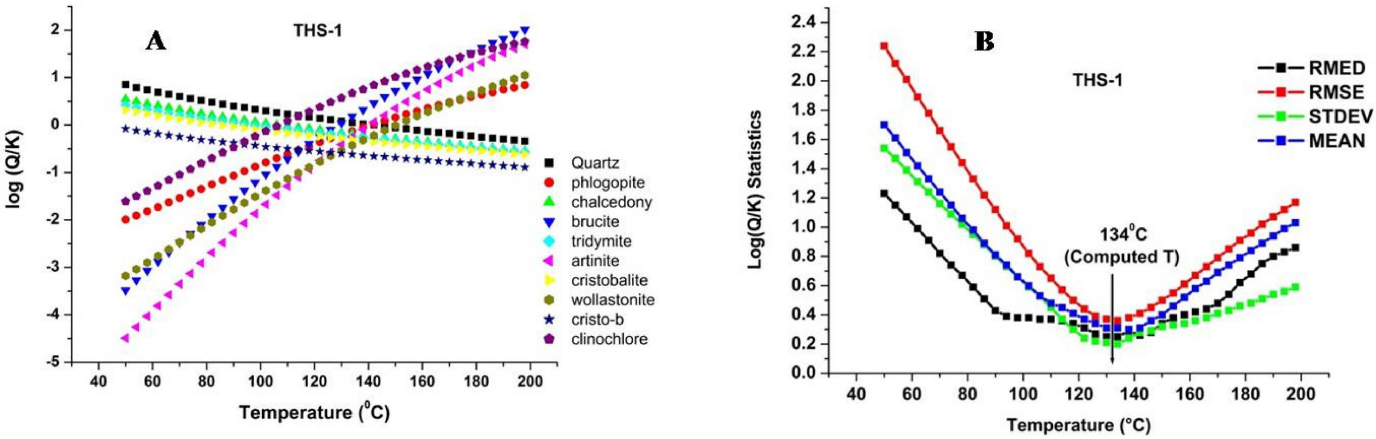

Fig. 5.15 *A) Computed saturation indices of minerals as a function of temperature for THS-1 and B) statistical parameters as a function of temperature*

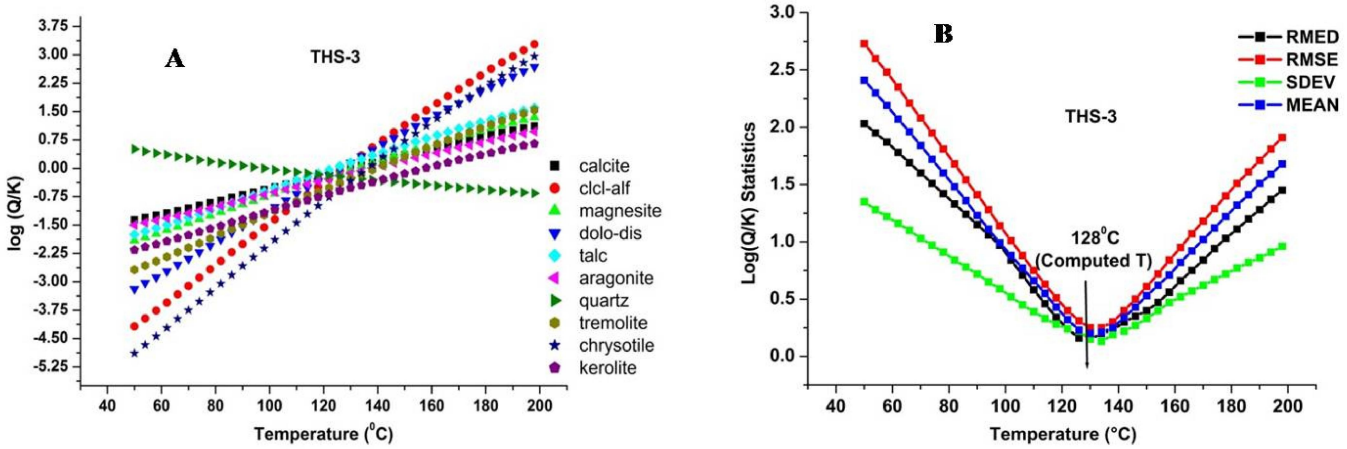

Fig. 5.16 *A) Estimated saturation indices of different minerals as a function of temperature for THS-3 and B) variation of different statistical parameters with temperature*

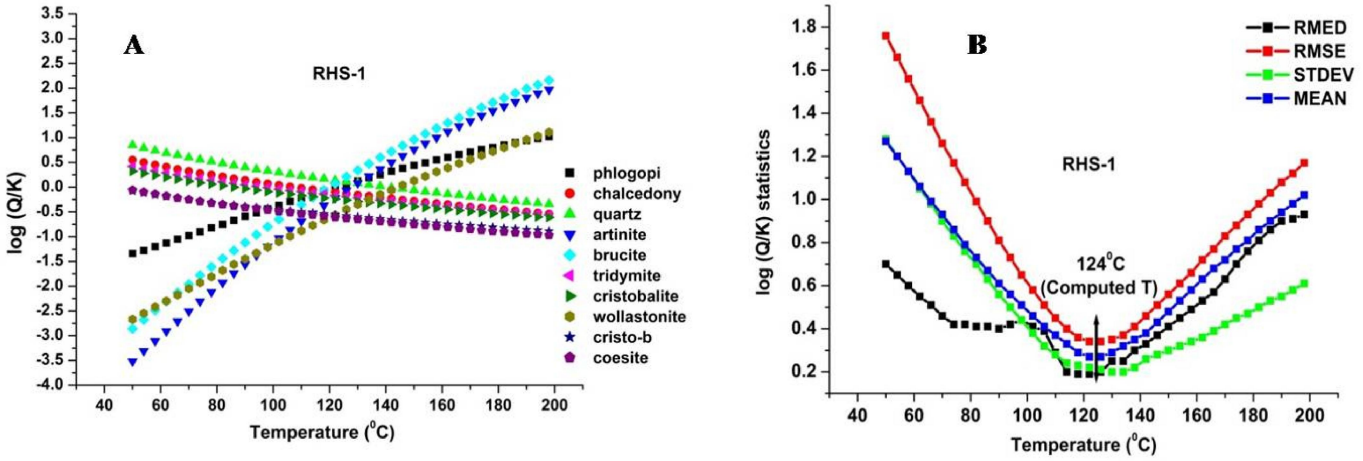

Fig. 5.17 *A) Computed saturation indices of minerals as a function of temperature for RHS-1 and B) various statistical parameters as a function of temperature and equilibrium temperature*

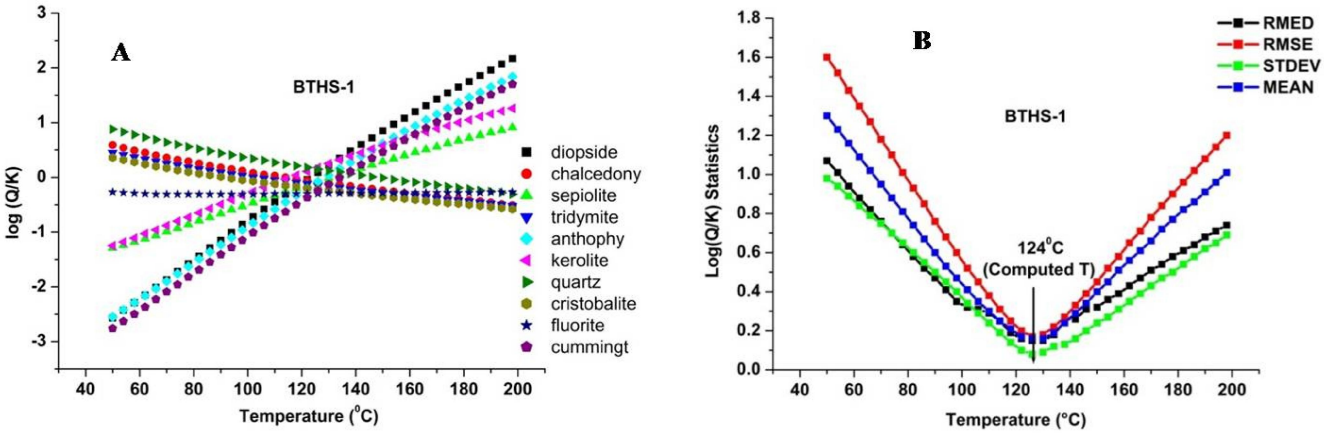

Fig. 5.18 *A) Computed saturation indices of minerals as a function of temperature for BTHS-1 and B) various statistical parameters as a function of temperature and the estimated equilibrium temperature*

Likewise in Badrinath thermal water (BTHS-1), the estimated reservoir temperature is found to be exactly same (~ 124 °C) as that of the RHS-1 sample and the minerals such as sepiolite, fluorite, cristobalite, chalcedony, quartz, tridymite etc. are found to be in equilibrium (Fig. 5.18A and 5.18B). Thus the multicomponent solute geothermometry method provides better

constrained reservoir temperature (130 ± 5 °C) which matches closely with the average temperature (132 ± 10 °C) obtained from applying the mixing model.

5.5 Conclusion

The integrated isotope-geochemical assessment of thermal waters from Chamoli district of Uttarakhand geothermal area provides very pertinent information regarding the origin of the thermal waters, their recharge altitude, characteristics of major and trace elements, mean transit time estimation and calculation of reservoir temperature. Most of the thermal waters in this region are Ca-Mg-HCO_3 type having low TDS and moderate silica concentrations. Saturation indices study shows that the thermal waters are supersaturated in calcite, quartz, dolomite, chalcedony etc. and undersaturated with respect to amorphous silica, gypsum and anhydrite. Among different trace elements, only lithium, boron and caesium act as conservative tracers whereas concentration of other elements gets affected by number of other secondary processes. The meteoric origin of the thermal waters is conclusively established from the δ2H - δ18O plot as the thermal water samples fall near the best fit line of the cold water samples. No oxygen-18 shift in the thermal water samples is observed indicating the comparative lower reservoir temperature (< 200 °C) and /or the very fast circulation of the thermal water through faults and fractures resulting less interaction time. In this region, altitude effect has been observed and is also quantified based on the isotopic composition of the non-thermal waters and discharge altitude. Due to this altitude effect the 18O value is found to decrease 0.2‰ (permil) per 100 metre rise in altitude. It is also established that the thermal waters in this region show variation in the isotopic concentration due to the difference in recharge altitude. Badrinath thermal water (BTHS-1) is found to have the most depleted isotopic signature due to its highest recharge altitude (~3542 metre) followed by Tapoban thermal water (THS-1) (~ 2712 metre) and Langshi

(LHS-1) and Birahi (BHW-1) (~1543 metre). Tritium value of the thermal waters indicates the presence of modern day recharge component which is further substantiated from the linear correlation between various conservative tracers. Tapoban thermal water is found to have highest amount (~ 75%) of mixing with the non-thermal water whereas the Badrinath thermal water (BTHS-1) is found to be least diluted (~ 25%). Combining the geological, hydrological and isotopic information, a conceptualized hydrogeological cross section map of the study area has been prepared (Fig. 5.19). The transit time of the Tapoban thermal water (THS-1) and Badrinath thermal water (BTHS-1) is estimated using the present day tritium concentrations along with the historical tritium measurements and lumped parameter models. In the absence of any long term tritium measurements of the precipitation in the study area, the tritium values of the nearby New Delhi GNIP station is scaled with the continuous tritium record of the Ottawa GNIP station. This properly scaled tritium vales act as an input concentration in the lumped parameter model. In case of the Tapoban thermal water (THS-1) thermal water sample, the simulated tritium concentration obtained from the EPM and DM model matches closely with the measured tritium values and the estimated MTT turns out to vary between 40 to 44 years whereas for Badrinath thermal water (BTHS-1) the MTT is estimated to be 102 to 112 years. This constrained MTT estimation can further be used to quantify the volume of the thermal water discharge contributing to the natural recharge as well as it helps to estimate the reservoir volume. This study also explores the subsurface reservoir temperature estimation by using both the chemical geothermometers, mixing models as well as multicomponent solute geothermometry. Among different chemical geothermometers, only the quartz geothermometer is found to be suitable whereas cation geothermometers (Na-K, Na-K-Ca, K-Mg etc.) are found to be unsuitable in this

region. But the quartz geothermometer is found to provide wide variation (96-140 °C) in the reservoir temperature estimation. On the other hand the applied mixing model estimates reservoir

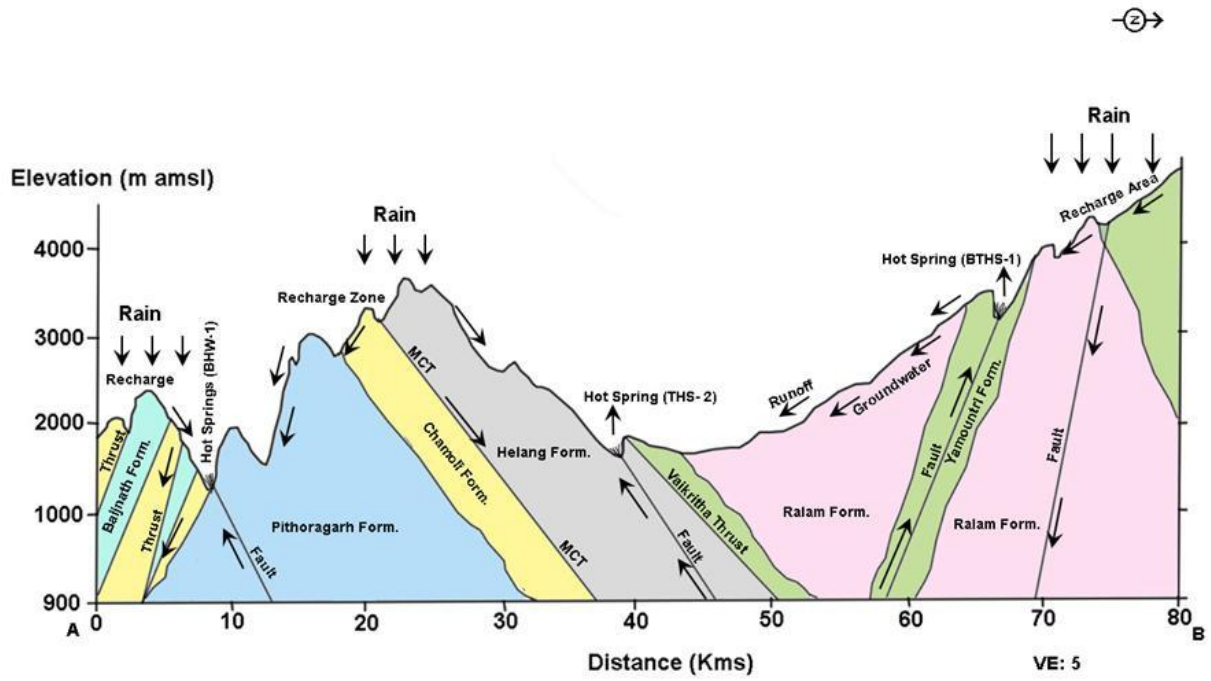

Fig. 5.19 *Hydrogeological cross section of the study area along with major thrusts, faults and circulation pattern*

in the range of ~ 132±10 °C. The integrated solute geothermometer is employed to further constrain the reservoir temperature. Multicomponent modeling using the GeoT code demonstrates that the thermal waters in the Uttarakhand area have attained simultaneous equilibrium with several minerals such as quartz, calcite, crystobalite, tridymite etc. and the corresponding average equilibrium temperature is ~ 130 ± 5 °C which may well be taken as the reservoir temperature.

CHAPTER 6

Summary and scope of the future study

6.1 Summary

The integrated isotope geochemical assessment of the three geothermal areas in India having entirely different geological settings provides very unique information regarding their origin, geochemical evolution, source of the solutes, mixing phenomenon, residence time and subsurface reservoir temperature. The comparative analysis of all the three geothermal areas has been given in table 6.1. The major salient features of this study are:

(1) All the thermal springs found in the Tural-Rajwadi (Deccan Trap region), Godavari Valley (Sedimentary formation) and Uttarakhand region (Himalayan belt) are meteoric in origin. Based on the isotopic evidence the probability of magmatic water is found to be negligible even in the Uttarakhand geothermal region which is a part of tectonically active Himalayan geothermal system.

(2) Tural-Rajwadi geothermal area located near the sea shows comparatively enriched stable isotopic value than the Godavari valley geothermal area which is situated deep inside the island (continental effect).

(3) Among all the three geothermal areas, Uttarakhand geothermal area shows most depleted stable isotopic values due to its high altitude. Stable isotopic variation among the various thermal springs in the Uttarakhand region is ascribed due to their different recharge altitude. Badrinath thermal water (BTHS-1) has the most depleted isotopic signature due to its highest altitude of recharge.

(4) Oxygen-18 isotopic shift is observed only in the Tural-Rajwadi geothermal area probably due to the significant rock-water interaction at elevated temperature over longer duration. (5) Geochemically thermal waters in the Tural-Rajwadi region are more mature (Na-Cl type) compared to the thermal waters in Godvari valley and Uttarkkand region (bicarbonate type).

(6) Geochemical evolution of the thermal waters in these three areas is identified using various graphical plots and statistical techniques.

(7) Application of the lumped parameter models (LPM) along with the tritium time series data in precipitation are found to be very useful in constraining the mean transit time (MTT) of the thermal water. In Tural-Rajwadi geothermal area, this method especially helps to estimate the MTT of the younger fraction present in the mixed thermal water.

(8) Tritium dating also allows in quantifying the extent of mixing of the thermal water with the non-thermal water. The highest extent of mixing is observed in the Tapoban thermal spring (THS-1) of Uttarakhand geothermal area.

(9) Carbon-14 dating technique helps to estimate the transit time of the very old thermal water present in the Tural-Rajwadi and the Godavari valley geothermal area.

(10) Among the three geothermal areas investigated in this study, the thermal waters from the Uttarakhand geothermal area have the least transit time (range varies from 40 to 112 years) i.e. they represent the most younger geothermal system. On the other hand, the geothermal systems from the peninsular India i.e. Tural-Rajwadi (rang varies from 6000 to 15000 years) and Godavari valley (range varies from 9900 to 18600 years) contains much more old thermal waters.

(11) Chemical geothermometers, mixing models as well as multicomponent geothermometry technique have been simultaneously applied to better constrain the reservoir temperature. Among the various chemical geothermometers, only the quartz geothermometer provides somewhat reliable estimation of reservoir temperature in all the three geothermal areas. Cation geothermometer, namely Na-K geothermometer is applicable only in the Tural-Rajwadi geothermal area due to the probable attainment of the respective mineral equilibrium. However

integrated multicomponent solute geothermometry technique carried out by the GeoT computer code is found to be most effective technique in estimating the reservoir temperature of these medium enthalpy geothermal fields. The subsurface reservoir temperature is found to be highest in the Tural-Rajwadi geothermal area (160° ± 10 °C) whereas the estimated reservoir temperature in Uttarakhand and Godavari valley geothermal area is found to be similar (~130 ± 10 °C).

Table 6.1 *Comparative analysis of three geothermal areas*

	Tural - Rajwadi, Maharashtra	**Godavari valley, Telengana**	**Chamoli, Uttarakhand**
Formation	**Granitic**	**Sedimentary**	**Quartzite**
Surface Temperature	**54-61 °C**	**50-75 °C**	**56-92 °C**
Reservoir Temperature	**~160 °C**	**~ 130 ± 10 °C**	**~130 ± 5 °C**
Geochemical nature	**Na-Cl type**	**Na-HCO_3 type**	**Ca–Mg-HCO_3 type**
Origin	**Meteoric**	**Meteoric**	**Meteoric**
Stable isotope	**$\delta^{18}O$: -1 to -2‰ $\delta^{2}H$: -7to -10 ‰**	**$\delta^{18}O$: -2 to -3‰ $\delta^{2}H$: -13 to -18 ‰**	**$\delta^{18}O$: -9 to -11 ‰ $\delta^{2}H$: -61 to -86 ‰**
Tritium	**0.8 to 1.2 TU**	**0.6 to 1.4 TU**	**3.6 to 7.5 TU**
Transit time	**~ 13500 years BP**	**~ 11400 year to 18600 year BP**	**40-110 year BP**

(12) Although the estimated reservoir temperature of the Uttarakhand and Godavari valley geothermal area is found to be similar, the surface discharge temperatures of the thermal springs are found to be highest in the Uttarakhand region which can be ascribed to the rapid circulation (less transit time) of the thermal waters through faults and fractures resulting less amount of conductive heat loss. On the other hand the conductive heat loss is found to be highest in the Tural-Rajwadi geothermal area.

6.2 Future scope of the study

The future scope of this work involves the periodic analysis of the both stable and radioactive isotopes which is very essential to know the long term variation in their concentrations. The quantification of the rock-water interaction needs to be carried out in the Tural-Rajwadi geothermal area to find out the possible correlation with the oxygen-18 shift observed in the thermal waters. In future, efforts would be made to explore the application of various isotope geothermometers (like sulphate-water geothermometer) which will further narrow down the uncertainties in the temperature estimation of the geothermal reservoir. Apart from these, the geophysical studies as well as shallow and deep drilling need to be performed to further explore the geothermal resources in these areas.

References

1. Abidin Z, Alip D, Nenneng L, Ristin PI, Fauzi A (2005). Environmental isotopes of geothermal fluids in Sibayak geothermal field. In: Use of isotope techniques to trace the origin of acidic fluids in geothermal systems, IAEA-TECDOC-1448, 37-61.
2. Absar A, Shanker R, Jangi BL, Srivastava GC, Kapoor A (1996). Recharge areas and water-rock isotope exchange trends for some Indian geothermal systems. Geol. Surv. Ind. Spl. Pub., 45, 311-317.
3. Ahmad M, Akram W, Ahmad N, Tasneem MA, Rafiq M, Latif Z (2002). Assessment of reservoir temperatures of thermal springs of the northern areas of Pakistan by chemical and isotope geothermometry. Geothermics, 31, 613-631.
4. Alçiçek H, Bülbül A, Alçiçek MC (2016). Hydrogeochemistry of the thermal waters from the Yenice Geothermal Field (Denizli Basin, Southwestern Anatolia, Turkey). J. Volcanol. Geotherm. Res., 309, 118-138.
5. Apollaro C, Vespasiano G, Muto F, Rosa RD, Barca D, Marini L (2016). Use of mean residence time of water, flowrate, and equilibrium temperature indicated by water geothermometers to rank geothermal resources. Application to the thermal water circuits of Northern Calabria. J. Volcanol. Geotherm. Res., 328, 147–158.
6. Apollaro C, Vespasiano G, Rosa RD, Marini L (2015). Use of mean residence time and flowrate of thermal waters to evaluate the volume of reservoir water contributing to the naturaldischarge and the related geothermal reservoir volume. Application to Northern Thailand hot springs. Geothermics, 58, 62–74.
7. Appelo CAJ, Postma D (1996). Geochemistry, groundwater and pollution (rev. ed.): Rotterdam, Netherlands, CRC Press / Balkema, pp. 536.

8. Ármannsson H, Fridriksson T (2009). Application of geochemical methods in geothermal exploration, presented at "Short Course on Surface Exploration for Geothermal Resources", organized by UNU-GTP and LaGeo in Ahuachapan and Santa Tecla, El Salvador.

9. Armannsson H, Gíslason G, Hauksson T (1982). Magmatic gases in well fluids aid the mapping of the flow pattern in a geothermal system. Geochimica et Cosmochimica Acta., 46 (2), 167-177. https://doi.org/10.1016/0016-7037(82)90244-7

10. Arnason B (1977a). Hydrothermal systems in Iceland traced by deuterium, Geothermics, 5, 125-151.

11. Arnason B (1977b). The hydrogen and water isotope thermometer applies to geothermal areas in Iceland, Geothermics, 5, 75-80.

12. Arnorsson S (1975). Application of the silica geothermometer in low temperature hydrothermal areas in Iceland. Amer. J. Sci, 275, 763-784. doi: 10.2475/ajs.275.7.763

13. Arnorsson S (1983). Chemical equilibria in Icelandic geothermal systems - implications for chemical geothermometry investigations. Geothermics, 12, 119-128.

14. Arnorsson S (1985). The use of mixing models and chemical geothermometers for estimating underground temperatures in geothermal system. J. Volcanol. Geotherm. Res., 23, 299-335.

15. Arnorsson S (2000). Isotopic and chemical techniques in geothermal exploration, development and use. International Atomic Energy Agency, Vienna, 1-362.

16. Arnorsson S, Andresdottir A (1995). Processes controlling the distribution of boron and chlorine in natural waters in Iceland. Geochim. Cosmochim. Acta., 59, 4125–4146.

17. Arnorsson S, Gunnlaugsson E (1985) New gas geothermometers for geothermal exploration – calibration and application. Geochim. Cosmochim. Acta., 49, 1307-1325.

18. Arnorsson S, Gunnlaugsson E, Svavarsson H (1983). The chemistry of geothermal waters in Iceland. III. Chemical geothermometry in geothermal investigations. Geochim. Cosmochim. Acta., 47 (3), 567-577.

19. Arnorsson S, Sigurðsson S, Svavarsson H (1982). The chemistry of geothermal waters in Iceland. I. Calculation of aqueous speciation from 0° to 370 °C. Geochim. Cosmochim. Acta., 46, 1513-1532.

20. Arnorsson S, Stefansson A (1999). Assessment of feldspar solubility constants in water in the range of 0 degrees to 350 degrees C at vapor saturation pressures. Amer. J. Sci., 299 (3), 173-209. https://doi.org/10.2475/ajs.299.3.173

21. Arnorsson, S., Sveinbjornsdottir A. E., Andresdottir, A. (1995). Processes influencing δ^2H, $\delta^{18}O$, B and Cl distribution in cold and thermal waters in the NW-Peninsula and in the Southern lowlands, Iceland, IAEA. In: Isotope and Geochemical Techniques Applied to Geothermal Investigations, IAEA-TECDOC-788, pp 45–62.

22. Azeez KKA, Harinarayana T (2007). Magnetotelluric evidence of potential geothermal resource in Puga, Ladakh, NW Himalaya. Current Geoscience, 93, 323-329.

23. Ballentine CJ, Onions RK, Oxburgh ER, Horvath F, Deak J (1991). Rare-gas constraints on hydrocarbon accumulation, crustal degassing and groundwater-flow in the Pannonian Basin. Earth Planet. Sci. Lett., 105 (1–3), 229–246.

24. Bayon FEB, Ferrer H (2005). Sulphur isotope ratios in Philippine geothermal systems. In: Use of isotope techniques to trace the origin of acidic fluids in geothermal systems, IAEA-TECDOC-1448, 111-133.

25. Benderitter Y, Cormy G (1990). Possible approach to geothermal research and relative cost estimate. In: Dickson, M.H., Fanelli, M. (Eds.), Small Geothermal Resources. UNITAR/UNDP Centre for Small Energy Resources, Rome, Italy, pp. 61-71.

26. Benjamin T, Charles R, Vidale R (1983). Thermodynamic parameters and experimental data for the Na-K-Ca geothermometer. J. Volcanol. Geotherm. Res., 15 (1–3), 167-186.

27. Bertani R (2016). Geothermal power generation in the world 2010–2014 update report. Geothermics, 60**,** 31-43.

28. Birkle P, Marín EP, Pinti DL, Castro MC (2016) Origin and evolution of geothermal fluids from Las Tres Vírgenes and Cerro Prieto fields, Mexico-Co-genetic volcanic activity and paleoclimatic constraints. Appl. Geochem., 65, 36-53.

29. Bischoff JL, Radtke AS, Rosenbauer RJ (1981). Hydrothermalalteration ofgreywacke by brine and seawater: roles of alteration and chlorite complexing on metal solubilities at 200 ^{O}C and 350 ^{O}C. Econ. Geol., 76 (3), 659-676.

30. Bottinga Y (1969). Calculated fractionation factors for carbon and hydrogen isotope exchange in the system calcite-carbon dioxide-graphite-methane-hydrogen-water vapour. Geochim. Cosmochim. Acta., 33 (1), 49-64.

31. Bottrell SH, Newton RJ (2006). Reconstruction of changes in global sulphur cycling from marine sulphate isotopes. Earth-Sci. Rev., 75, 59–83.

32. Bricker OP, Paces T, Johnson CE, Sverdrup H (1994). Weathering and erosion aspects of small catchment research. In Biogeochemistry of Small Catchments: A Tool for Environmental Research (eds. B. Moldan and J. Cerny). Wiley, Chichester, England, 85 – 105.

33. Campana ME, Mahin DA (1985). Model-derived estimates of groundwater mean ages, recharge rates, effective porosities and storage in a limestone aquifer. J. Hydrol., 76, 247–264.

34. Cartwright I (2010). Using groundwater geochemistry and environmental isotopes to assess the correction of ^{14}C ages in a silicate-dominated aquifer system. J. Hydrol., 382, 174–187.

35. Cartwright I, Morgenstern U (2016). Using tritium to document the mean transit time and sources of water distributing to a chain-of-ponds river system: Implications for resource protection. Appl. Geochem., 75, 9-19.

36. Cartwright I, Morgenstern U (2018). Using tritium and other geochemical tracers to address the "old water paradox" in headwater catchments. J. Hydrol., 563, 13-21. https://doi.org/10.1016/j.jhydrol.2018.05.060.

37. CGWB (Central Ground Water Board of India) (2013). Ground water brochure, Khammam District, Andhra Pradesh, 1-22.

38. CGWB (Central Ground Water Board of India) (2016). Ground water year book 2014-2015, Uttarakhand, 1–99.

39. Chandrasekhar T, Minissale A, Vaselli O, Chandrasekharam D, Singh SK (2018) Understanding the evolution of thermal fluids along the western continental margin of India using geochemical and boron isotope signatures. Geothermics, 74, 197-209.

40. Chandrasekharam D (2001). Use of geothermal energy for food processing-Indian status. Geo-heat Centre. Quarterly Bulletin, 22 (4), 8-11.

41. Chandrasekharam D, Alam MA, Minissale A (2005). Thermal discharges at Manikaran, Himachal Pradesh, India. In Proc. World Geothermal Congress, 24-29 April, Antalya, Turkey.

42. Chandrasekharam D, Antu MC (1995). Geochemistry of Tattapani thermal springs, Madhya Pradesh, India—field and experimental investigations. Geothermics, 24(4), 553–559.

43. Chandrasekharam D, Chandrasekhar V (2010). Geochemistry of thermal springs of Orissa, India. GRC Trans., 34, 665–667.

44. Chandrasekharam D, Ramesh R, Balasubramanian J (1989). Geochemistry, oxygen and hydrogen isotope ratio of thermal springs, western continental margin of India-field and experimental results. In: Douglas L, Miles AA (Eds.), Proc. 6th Water-Rock Interaction Congress, Balkema, The Netherlands, 149-154.

45. Chandrasekharam D, Rao VG, Jayaprakash SJ (1996). Geothermal energy potential and direct use of geothermal springs, Godavari valley, Andhra Pradesh. Geol. Surv. Ind. Spl. Pub., 45, 151-161.

46. Chatterjee S, Ansari MA, Deodhar AS, Sinha UK, Dash A (2017a). A multi-isotope approach (O, H, C, S, B and Sr) to understand the source of water and solutes in some the thermal springs from West Coast geothermal area, India. Arab J. Geosci., 10, 242. DOI 10.1007/s12517-017-3022-0.

47. Chatterjee S, Gusyev MA, Sinha UK, Mohokar HV, Dash A (2019b). Understanding water circulation with tritium tracer in the Tural-Rajwadi geothermal area, India. Appl. Geochem., 109: 104373. https://doi.org/10.1016/j.apgeochem.2019.104373.

48. Chatterjee S, Sinha UK, Biswal BP, Jaryal A., Jain PK, Patbhaje S, Dash A (2019a). An Integrated Isotope-Geochemical Approach to Characterize a Medium Enthalpy Geothermal System in India. Aquatic Geochemistry, 25, 63–89. DOI: 10.1007/s10498-019-09352-z.

49. Chatterjee S, Sinha UK, Ansari MA, Mohokar HV, Dash A. (2018). Application of lumped parameter model to estimate mean transit time (MTT) of the thermal water using environmental tracer (3H): Insight from Uttarakhand geothermal area (India). Appl. Geochem., 94, 1-10. https://doi.org/10.1016/j.apgeochem.2018.04.013

50. Chatterjee S, Sinha UK, Deodhar AS, Arzoo MA, Singh N, Srivastava AK, Aggarwal RK, Dash A (2017b). Isotope–geochemical characterization and geothermometrical modeling of Uttarakhand geothermal field, India. Environ Earth Sci 76: 638. https://doi.org/10.1007/s12665-017-6973-2.

51. Chesson LA, Tipple BJ, Mackey GN, Hynek SA, Fernandez DP, Ehleringer JR (2012). Strontium isotopes in tap water from the coterminous USA. Ecosphere, 3(7), 67. https://dx.doi.org/10.1890/ES12-00122.1.

52. Chiodini G, Cioni R (1989). Gas geobarometry for hydrothermal systems and its application to some Italian geothermal areas. Appl. Geochem., 4, 465-472.

53. Chowdhury AN, Bose BB, Banerjee G (1964). Studies on Geochemistry of Thermal Springs at Bakreswar. Proc. 22nd Int. Geol. Cong., 12, 143–160.

54. Cinti D, Pizzino L, Voltattorni N, Quattrocchi F, Walia V (2009). Geochemistry of thermal waters along fault segments in the Beas and Parvati Valleys (north-west Himalaya, Himachal Pradesh) and in the Sohna town (Haryana), India. Geochemical Journal, 43, 65-76.

55. Clark I, Fritz P (1997). Environmental Isotope in Hydrogeology. Lewis Publishers, New York, 328-350.

56. Claypool GE, Holser WT, Kaplan IR, Sakai H, Zak I (1980). The age curve of sulphur and oxygen isotopes in marine sulphate and their mutual interpretation. Chem. Geol, 28, 199–260. doi:10.1016/0009-2541(80)90047-9.

57. Courtillot V, Jaupart C, Manegheeti I, Tapponnier P, Besse J (1999). On casual links between flood basalts and continental breakup. Earth Planet. Sci. Lett., 166, 177–195.

58. Craig H (1953). The geochemistry of the stable carbon isotopes. Geochim. Cosmochim. Acta, 3 (2-3), 53-92.

59. Craig H (1961). Isotopic Variations in Meteoric Waters. Science, 133 (3465), 1702-1703. DOI: 10.1126/science.133.3465.1702

60. Craig H (1963). The isotopic geochemistry of water and carbon in geothermal areas, in: Nuclear Geology on Geothermal Areas, CNR, Pisa, 17-53.

61. Craig H, Boato G, White DE (1956). Isotope geochemistry of thermal waters. National Research Council Publication, 400, 29-38.

62. Craig J, Absar A, Bhat G, Cadel G, Hafiz M, Hakhoo N, Kashkari R, Moore J, Ricchiuto TE, Thurow J, Thusu B (2013). Hot springs and the geothermal energy potential of Jammu & Kashmir State, N.W. Himalaya,India. Earth-Science Reviews, 126, 156-177.

63. Craig H, Lupton JE (1976). Primordial neon, helium, and hydrogen in oceanic basalts. Earth Planet. Sci. Lett., 31, 369-385.

64. D'Amore F (1992). Gas geochemistry as a link between geothermal exploration and exploitation. Application of Geochemistry in Geothermal Reservoirs Development (F. D'Amore, Coordinator). UNITAR/UNDP, 93-118.

65. D'Amore F, Fancelli R, Saracco L, Truesdell AH (1987) Gas geothermometry based on CO content – application in Italian geothermal fields; Proc. 12th Workshop Geothermal Reservoir Eng., Jan. 1987, Sanford Univ., Stanford, California.

66. D'Amore F, Panichi C (1980). Evaluation of deep temperatures of hydrothermal systems by a new gas geothermometer. Geochim. Cosmochim. Acta., 44, 549-556.

67. Das A, Krishnaswami S, Bhattacharya SK (2005). Carbon isotope ratio of dissolved inorganic carbon (DIC) in rivers draining the Deccan Traps, India: Sources of DIC and their magnitudes. Earth Planet. Sci. Lett., 236, 419-429.

68. Dasgupta S, Bose S, Das K (2013). Tectonic evolution of the Eastern Ghats belt, India. Precambrian Research, 227, 247-258.

69. Dasgupta S, Sengupta, P (2003). Indo-Antarctic correlation: a perspective from the Eastern Ghats granulite belt, India. Geological Society, London, Special Publications, 206(1), 131-143.

70. Deb S, Mukherjee AL (1969) On the genesis of few groups of thermal springs in Chhotnagpur gneissic complex, India. J. Geochem. Soc. India, 4, 1–9.

71. Deshpande RD, Bhattacharya SK, Jani RA, Gupta SK (2003). Distribution of oxygen and hydrogen isotopes in shallow groundwaters from southern India: Influence of a dual monsoon system. J. Hydrol., 271, 226–239. DOI: 10.1016/S0022-1694(02)00354-2.

72. Dotsika E, Poutoukis D, Kloppmann W, Guerrot C, Voutsa D, Kouimtzis TH (2010). The use of O, H, B, Sr and S isotopes for tracing the origin of dissolved boron in groundwater in Central Macedonia, Greece. Appl. Geochem., 25, 1783-1796.

73. Dowgiallo J (1977). Hot springs of the West Coast (Konkan) Region, Maharashtra. Unpublished UNDP report. IND/73/008 UN Project.

74. Drever JI (1997). The Geochemistry of Natural Waters. Prentice Hall, Englewood Cliffs, NJ, pp. 436.

75. Edmunds WM (2009). Geochemistry's vital contribution to solving water resource problems. Appl. Geochem., 24, 1058–1073.

76. Elderfield H, Greaves MJ (1981). Strontium isotope geochemistry of Icelandic geothermal systems and implications for sea water chemistry. Geochim. Cosmochim. Acta., 45 (11), 2201-2212.

77. Ellis AJ (1979). Chemical geothermometry in geothermal systems. Geothermics, 25, 219-226.

78. Ellis AJ, Mahon WAJ (1964). Natural hydrothermal systems and experimental hot-water/rock interaction. Geochim. Cosmochim. Acta, 28, 1323-1357.

79. Ellis AJ, Mahon WAJ (1967). Natural hydrothermal systems and experimental hot-water/rock interactions (Part II). Geochim. Cosmochim. Acta, 31, 519-538.

80. Ellis AJ, Wilson SH (1960). The geochemistry of alkali metal ions in the Wairakei hydrothermal systems. N. Z. J. Geol. Geophys., 3, 593-617.

81. Faure G (1998). Principles and Applications of Geochemistry, second ed. Prentice Hall, Upper Saddle River, New Jersey

82. Fiebig J, Hofmann S, Tassi F, Alessandro WD, Vaselli O, Woodland AB (2015). Isotopic patterns of hydrothermal hydrocarbons emitted from Mediterranean volcanoes. Chemical Geology, 396, 152–163.

83. Fouillac C, Michard G (1981). Sodium/Lithium ratios in water applied to geothermometry of geothermal reservoirs. Geothermics, 10, 55–70.

84. Fournier RO (1977). Chemical geothermometers and mixing models for geothermal systems. Geothermics, 5, 40-41.

85. Fournier RO (1979a). A revised equation for Na/K geothermometer. Geotherm. Resources Council Trans. 3, 221-224.

86. Fournier RO (1979b). Geochemical and hydrologic considerations and the use of enthalpy-chloride diagrams in the prediction of underground conditions in hot-spring systems. J. Volcanol. Geotherm. Res. 5, 1-16.

87. Fournier RO (1989a). Geochemistry and dynamics of the Yellowstone National Park hydrothermal system. Ann. Rev. Earth Planet. Sci. Lett., 17, 13-53.

88. Fournier RO (1989b). Lectures on geochemical interpretation of hydrothermal waters. UNU Geothermal Training Programme. Reykjavik, Iceland, 1989. Report 10, pp.73.

89. Fournier RO, Potter RW (1979). Magnesium correction to the Na-K-Ca chemical geothermometer. Geochim. Cosmochim. Acta., 43, 1543-1550.

90. Fournier RO, Potter RW II (1982a). An equation correlating the solubility of quartz in water from 25 °C to 900 °C at pressures up to 10000 bars. Geochim. Cosmochim. Acta., 46, 1969-1974.

91. Fournier RO, Potter RW II (1982b). A revised and expanded silica (quartz) geothermometer. Geoth. Res. Council Bull., 11-10, 3-12.

92. Fournier RO, Truesdell AH (1973). An empirical Na-K-Ca geothermometer from natural waters. Geochim. Cosmochim. Acta., 37, 1255-1275.

93. Fournier RO, Truesdell AH (1974). Geochemical indicators of subsurface temperature-Part 2, Estimation of temperature and fraction of hot water mixed with cold water. Jour. Research U.S. Geol. Survey, 2(3), 263-270.

94. Gardner WP, Susong DD, Solomon DK, Heasler HP (2011). A multitracer approach for characterizing interactions between shallow groundwater and the hydrothermal system in the Norris Geyser Basin area, Yellowstone National Park. Geochem. Geophys. Geosyst., 12(8), Q08005, 1-17. https://doi.org/10.1029/2010GC003353

95. Garrels RM, MacKenzie FT (1971). Evolution of Sedimentary Rocks. Norton, New York.

96. Gherardi F, Panichi C, Gonfiantini R, Magro G, Scandiffio G (2005). Isotope systematics of C-bearing gas compounds in the geothermal fluids of Larderello, Italy. Geothermics, 34, 442–470.

97. Ghosh PK (1954). Mineral springs of India. Rec. Geol. Surv. India, 80, 541–558.

98. Gibbs RJ (1970). Mechanisms controlling world water chemistry. Science, 170 (3962), 1088–1090.

99. Gibson JAB (1980). Modern Techniques for measuring correction in Liquid Scintillation counter: a critical review, In Liquid Scintillation Counting: Recent Applications and development, eds C.T. Peng, D.L. Horrocks and E.L. Alpen, Academic Press New York, 153-172.

100. Giggenbach WF (1977). Chemistry of Indian geothermal discharge. UNDP Project, IND/73/008, February.

101. Giggenbach WF (1978). The isotopic composition of waters from the El Tatio geothermal field, Northern Chile. Geochim. Cosmochim. Acta., 42 (7), 979-988.

102. Giggenbach WF (1980). Geothermal gas equilibria. Geochim. Cosmochim. Acta., 44, 2021-2032.

103. Giggenbach WF (1987). Redox processes governing the chemistry of fumarolic gas discharges from White Island, New Zealand. Appl. Geochem., 2, 143-161.

104. Giggenbach WF (1988). Geothermal solute equillibria. Derivation of Na-K-Mg-K geoindicators. Geochim. Cosmochim. Acta., 52, 2749-2765.

105. Giggenbach WF (1991). Chemical techniques in geothermal exploration. In Applications of geochemistry in geothermal reservoir development (F. D'Amore, Coordinator), UNITAR/UNDP publication, Rome, 119-142.

106. Giggenbach WF (1992). Isotopic shift in waters from geothermal and volcanic systems along convergent plate boundaries and their origin. Earth Planet. Sci. Lett., 113, 495–510.

107. Giggenbach WF (1993) Redox control of gas compositions in Philippine volcanic-hydrothermal systems. Geothermics, 22 (5-6), 575-587.

108. Giggenbach WF, Glover RB (1992). Tectonic regime and major processes governing the chemistry of water and gas discharges from the Rotorua geothermal field, New Zealand. Geothermics, 21 (1-2), 121-140.

109. Giggenbach WF, Goguel RL (1989). Collection and analysis of geothermal and volcanic water and gas discharges; DSIR report CD 2401, 4th ed., Pentone, NZ.

110. Giggenbach WF, Gonfiantini R, Jangi BL, Truesdell AH (1983). Isotopic and chemical composition of Parbati valley geothermal discharges, north-west Himalaya, India. Geothermics, 12 (2-3), 199-222.

111. Gaillardet J, Dupre B, Louvat P, Allegre CJ (1999). Global silicate weathering and CO_2 consumption rates deduced from the chemistry of large rivers. Chem. Geol. 159, 3–30.

112. Goguel RL (1983). The rare alkalies in hydrothermal alteration at Wairakei and Broadlands geothermal fields, N.Z. Geochim. Cosmochim. Acta., 47, 429-437.

113. Gonfiantini R (1977). Report on Mission to India. UNDP Project, IND/73/008, June

114. GSI (Geological Survey of India) (1987). A collection of geothermal papers. Geol. Surv. Ind. Rec., 115(6), 1-206.

115. GSI (Geological Survey of India) (1991). Geothermal Atlas of India. Geol. Surv. Ind. Spl. Pub., 19, pp. 144.

116. GSI (Geological Survey of India) (2002). Geothermal Energy Resources of India. Geol. Surv. Ind. Spl. Pub., 70-72.

117. GSI (Geological Survey of India) (2012). Miscellaneous Publication No. 30, Part-XII: Uttar Pradesh and Uttarakhand.

118. Gunter BD, Musgrave BC (1971). New evidence on the origin of methane in hydrothermal gases. Geochim. Cosmochim. Acta., 35 (1), 113-118.

119. Gupta GK (1996). Hydrogeology and hydrogeochemistry of Beas valley geothermal system, Kulu District, Himachal Pradesh. GSI Spl. Publ. No. 45, 249–256.

120. Gupta ML, Sharma SR, Drolia RK, Singh SB (1983). Subsurface thermal conditions of Puga valley hydrothermal field, Himalaya, India. Journal of Geophysical Research, 54, 51-59.

121. Guo HM, Wang YX (2004). Hydrogeochemical processes in shallow quaternary aquifers from the northern part of Datong Basin, China. Appl. Geochem., 19, 19-27.

122. Guo HM, Wang YX (2005). Geochemical characteristics of shallow groundwater in Datong Basin, northwestern China. J. Geochem. Explor, 87, 109-120.

123. Gurav T, Chandrasekharam D, Singh HK (2015) Trace Element and REE Concentrations in the Thermal Waters, West Coast Geothermal Province, India. Proceedings World Geothermal Congress, Melbourne, Australia, 19-25 April 2015, 1-9.

124. Gusyev MA, Morgenstern U, Nishihara T, Hayashi T, Akata N, Ichiyanagi K, Sugimoto A, Hasegawa A, Stewart MK (2019). Evaluating anthropogenic and environmental tritium effect using precipitation and Hokkaido snowpack at selected coastal locations in Asia. Science of Total Environment, 659, 1307-1321.

125. Gusyev MA, Morgenstern U, Stewart MK, Yamazaki Y, Kashiwaya K, Nishihara T, Kuribayashi D, Sawano H, Iwami Y (2016). Application of tritium in precipitation and baseflow in Japan: a case study of groundwater transit times and storage in Hokkaido watersheds. Hydrol. Earth Syst. Sci., 20, 3043–3058. https://doi.org/10.5194/hess-20-3043-2016.

126. Harada Y, Kamahori H, Kobayashi C, Endo H, Kobayashi S, Ota Y, Onoda H, Onogi K, Miyaoka K, Takahashi K (2016). The JRA-55 Reanalysis: Representation of atmospheric circulation and climate variability. J. Meteor. Soc. Japan, 94, 269-302. DOI:10.2151/jmsj.2016-015.

127. Harinarayana T, Azzez KKA, Murthy DN, Veeraswamy K, Rao SPE, Manoj C, Naganjaneyulu C (2006). Exploration of geothermal structure in Puga geothermal field, Ladakh Himalayas, India by magnetotelluric studies. Journal of Applied Geophysics, 58, 280-295.

128. Harinarayana T, Azzez KKA, Naganjaneyulu C, Manoj C, Veeraswamy K, Murthy DN, Rao SPE (2004) Magnetotelluric studies in Puga geothermal field, NW Himalaya, India. J. Volcanol. Geotherm. Res., 138, 405-424.

129. Harinarayana T, Virupakshi G, Murthy DN, Veeraswamy K, Rao PE, Azeez KKA, Basava S, Naidu GD, Ravi Shankar, Sreedhar SV, Rani KS, Gupta AK, Sreenivasulu T, Sreenivas M (2008). Magnetotelluric investigations in the Geothermal fields of Satluj-Spiti, Beas-

Parbati valleys in Himachal Pradesh, Badrinath-Tapovan in Uttarakhand and Surajkund in Jharkhand areas, India. Tech. No. NGRI-2008-EXP-637.

130. Hochstein, MP (1990). Classification and assessment of geothermal rresources. In: Dickson, M.H., Fanelli, M. (Eds.), Small geothermal resources. UNITAR/UNDP centre for small energy resources, Rome, Italy, 31-59.

131. Horita J (2001). Carbon isotope exchange in the system CO_2-CH_4 at elevated temperatures. Geochim. Cosmochim. Acta, 65 (12), 1907-1919.

132. Horrocks DL (1974). Application of Liquid Scintillation Counting, Academic Press, New York, pp. 346.

133. Hulston JR (1983). Environmental isotope investigations of New Zealand geothermal systems—A review. Geothermics, 12 (2-3), 223-232.

134. Hulston JR (2004). Factors controlling the carbon isotopic composition of methane and carbon dioxide in New Zealand geothermal and natural gases. Geochem Soc. Spec. Pub., 9, 67–83.

135. Hulston JR, McCabe WJ (1962). Mass spectrometer measurements in the thermal areas of New Zealand: Part 2. Carbon isotopic ratios. Geochim. Cosmochim. Acta., 26 (3), 399-410.

136. Husain MS, Umar R, Ahmad S (2020). A Comparative study of springs and groundwater chemistry of Beas and Parbati valley, Kullu District, Himachal Pradesh, India. HydroResearch, 3, 32-47.

137. Jankowski J, Acworth RI, Shekarforoush S (1998). Reverse ion-exchange in a deeply weathered porphyritic dacite fractured aquifer system, Yass, New South Wales, Australia.

In: Arehart, G.B., Hulston, J.R. (Eds.), Ninth Internat. Symp., Water– Rock Interaction. A.A. Balkema, Rotterdam, 243–246.

138. Jenkins A, Peters NE, Rodhe A (1994). Hydrology. In Biogeochemistry of Small Catchments: A Tool for Environmental Research (eds. B. Moldan and J. Cerny). Wiley, Chichester, England, pp. 31 – 54.
139. Jha SK, Puppala H (2018). Conceptual modeling and characterization of Puga geothermal reservoir, Ladakh, India. Geothermics, 72, 326-337.
140. Jurgens BC, Böhlke JK, Eberts SM (2012). TracerLPM (Version 1): An Excel® workbook for interpreting groundwater age distributions from environmental tracer data. U.S. Geological Survey Techniques and Methods Report 4-F3, pp. 60.
141. Kanzaki T, Yoshida M, Nomura M, Kakihana H, Ozawa T (1979). Boron isotopic composition of fumarolic condensates and sassolites from Satsuma Iwo-Jima, Japan. Geochim Cosmochim Acta 51, 1939–1950.
142. Karanth KR (1994). Groundwater Assessment Development and Management. Tata McGraw-Hill Publishing Company Ltd., New Delhi.
143. Karim A, Veizer J (2000). Weathering processes in the Indus River Basin: implications from riverine carbon, sulfur, oxygen, and strontium isotopes. Chem Geol, 170, 153–177. doi:10.1016/S0009-2541(99)00246-6.
144. Karingithi CW (2009). Chemical geothermometers for geothermal exploration. Short Course IV on Exploration for Geothermal Resources, organized by UNU-GTP, KenGen and GDC, at Lake Naivasha, Kenya, November 1-22, 2009.
145. Kazemi GA, Lehr JH, Perrochet P (2006). Groundwater Age. Wiley, New Jersey, pp. 325.

146. Keenan JH, Keyes FG, Hill PG, Moore JG (1969). Steam Tables - Thermodynamic Properties of Water Including Vapour, Liquid and Solid Phases (International Edition – metric units). Wiley, New York, pp. 162.

147. Keesari T, Chatterjee S, Pant D, Kumar M, Sakhare V, Sinha UK, Mohokar H, Jaryal A, Roy AS, Maitra A (2020). Dating of hot springs at Attri, Tarabalo and Athmalik sites in Odisha, India using radiocarbon technique. Journal of Radioanalytical and Nuclear Chemistry, 323, 1227–1235.

148. Kharaka YK, Lico MS, Law LM (1982). Chemical geothermometers applied to formation waters, Gulf of Mexico and California basins. American Association of Petroleum Geologists Bulletin, 66, pp. 588.

149. Kharaka YK, Mariner RH (1989). Chemical geothermometers and their application to formation waters from sedimentary basins. Thermal History of Sedimentary Basins (N.D Naeser, T.H. McCulloh, Eds) Springer-Verlag, Berlin; 99-117. https://doi.org/10.1007/978-1-4612-3492-0_6

150. Kharaka YK, Mariner RH (2005). Geothermal systems. In: Gat JR, Froehlich FO, Aggarwal PK (eds), Isotopes in the water cycle, Springer, Netherlands, 243–270.

151. Kharaka YK, Thordsen JJ (1992.) Stable isotope geochemistry and origin of water in sedimentary basins. Isotope Signatures and Sedimentary Records (N. Clauer, S.Chaudhuri, Eds), Springer-Verlag, Berlin, 411-466.

152. Kharaka YK, Thordsen JJ, White LD (2002). Isotope and Chemical Compositions of Meteoric and Thermal Waters and Snow from the Greater Yellowstone National Park Region. U.S. Geological Survey Open-File Report 02-194, 57.

153. Kreft A, Zuber A (1978). On the physical meaning if the dispersion equation and its solutions for different initial and boundary conditions. Chemical Engineering Science, 33, 1471–1480.

154. Krishna Murthy K, Mattaiah G, Venkatappaiah A (1985). Hot water seepage in to shallow coal mines of Manuguru coalbelt, Godavari valley coalfield Andhra Pradesh, India. IMWA proceedings, 979-989.

155. Krishnaswamy VS (1965). On the utilization of geothermal stream and the prospects of developing the hot springs in the North-western Himalayas. Indian Geohydrology, 1(1), 27–45.

156. Krishnaswamy VS, Shanker R (1982). Scope of development, exploration and preliminary assessment of the geothermal resource potentials of India. Rec. Geol. Surv. India III, pt 2, 18–38.

157. Krouse HR (1989). Sulfur Isotope Studies of the Pedosphere and Biosphere. In: Rundel PW, Ehleringer JR, Nagy KA (eds) Stable Isotopes in Ecological Research. Ecological Studies (Analysis and Synthesis), Springer, New York, 68, 424-444. https://doi.org/10.1007/978-1-4612-3498-2_24

158. Kumar B, Rai SP, Saravanakumar U, Verma SK, Garg P, Vijaya Kumar SV, Jaiswal R, Purendra BK, Kumar SR, Pande NG (2010). Isotopic characteristics of Indian precipitation. Water Resour. Res., 46, W12548, DOI: 10.1029/2009WR008532.

159. Kumar R, Singh SB, Gupta ML, Rao GV (1982). Geophysical surveys in Parvati valley geothermal field, Kullu, India. J. Volcanol. Geotherm. Res., 13(3-4), 213-222.

160. Kushnir AR, Heap MJ, Baud P, Gilg HA, Reuschle T, Lerouge C, Dezayes C, Duringer P (2018). Characterizing the physical properties of rocks from the Paleozoic to Permo-Triassic transition in the Upper Rhine Graben. Geothermal Energy 6, 16.

161. Kyser TK, O'Neil JR (1984). Hydrogen isotope systematics of submarine basalts. Geochim. Cosmochim. Acta 48, 2123-2133.

162. Langmuir D (1997). Aqueous Environmental Geochemistry. Prentice Hall, Upper Saddle River, NJ.

163. Levet S, Berger G, Munoz M, Toutain JP (2006). A new and fast method to determine mixing and conductive cooling of thermal waters in carbonate-evaporite environments. Geothermics, 35, 285-301.

164. Lloyd RM (1968). Oxygen isotope behavior in the sulfate–water system. J. Geophys. Res, 73, 6099–6110.

165. Lollar BS, Ballentine CJ (2009). Insights into deep carbon derived from noble gases. Nature Geoscience, 2 (8), 543–547.

166. Longinelli A, Craig H (1967). Oxygen-18 variations in sulfate ions in sea-water and saline lakes. Science, 146, 56–59.

167. Lund JW, Freeston DH, Boyd TL (2011). Direct utilization of geothermal energy 2010 worldwide review. Geothermics, 40, 159–180.

168. Lyon GL (1974) Geothermal gases. In: Kaplan, I.R. (ed.) Natural gases in marine sediments. Plenum Press, Nwe York, 141-150.

169. Lyon GL, Hulston JR (1984). Carbon and hydrogen isotopic compositions of New Zealand geothermal gases. Geochim. Cosmochim. Acta 48, 1161–1171.

170. Mahala SC, Singh P, Das M, Acharya S (2012). Genesis of thermal springs of Odisha, India. Int. J. Earth Sci. Eng., 5(6), 1572–1577.

171. Mahon WAJ (1967). Natural hydrothermal systems and the reaction of hot water with sedimentary rocks. N. Z. J. Sci., 10, 206-221.

172. Mahoney JJ (1988). Deccan traps. In: Macdougall JD (eds) Continental Flood Basalts. Springer Science & Business Media, Dordrecht, 151-194.

173. Majumdar N, Majumdar RK, Mukherjee AL, Bhattacharya SK, Jani RA (2005). Seasonal variations in the isotopes of oxygen and hydrogen in geothermal waters from Bakreswar and Tantloi, Eastern India: implications for groundwater characterization. J. Asian Earth Sci., 25, 269–278.

174. Majumdar N, Mukherjee AL, Majumdar RK (2009). Mixing hydrology and chemical equilibria in Bakreswar geothermal area, Eastern India. J. Volcanol. Geotherm. Res., 183, 201-212.

175. Maloszewski P, Zuber A (1982). Determining the turnover time of groundwater systems with the aid of environmental tracers: 1. Models and their applicability. J. Hydrol., 57, 207–231.

176. Mariner RH, Wiley LM (1976). Geochemisty of thermal waters in Long Valley, Mono County, California. Journal of Geophysical Research, 81, 792-800.

177. Marschall HR, Jiang SY (2011). Tourmaline isotopes: no element left behind. Elements, 7, 313–319.

178. Mazor E, Truesdell AH (1984). Dynamics of a geothermal field traced by noble gases: Cerro Prieto, Mexico. Geothermics, 13, 91-102.

179. McKenzie WF, Truesdell AH (1977). Geothermal reservoir temperatures estimated from the oxygen isotope compositions of dissolved sulfate and water from hot springs and shallow drillholes. Geothermics, 5, 51-61.

180. McKibben MA, Williams AE, Okubo S (1988). Metamorphosed Plio-Pleistocene evaporites and the origins of hypersaline brines in the Salton Sea geothermal system, California: fluid inclusion evidence. Geochim. Cosmochim. Acta, 52, 1047-1056.

181. McLean W, Jankowski J, Lavitt N (2000). Groundwater quality and sustainability in an alluvial aquifer, Australia. In: Sililo O et al. (Eds.), XXX IAH Congress on Groundwater: Past Achievements and Future Challenges. A.A. Balkema, Rotterdam, 567-573.

182. Meybeck M (1987). Global chemical weathering from surficial rocks estimated from river dissolved loads. Am. J. Sci. 287, 401–428.

183. Michard G (1990) Behaviour of major elements and some trace elements (Li, Rb, Cs, Sr, Fe, Mn, W, F) in deep hot waters from granitic areas. Chem. Geol., 89, 117–134.

184. Minissale A, Chandrasekharam D, Vaselli O, Magro G, Tassi F, Pansini GL, Bhramhabut A (2003). Geochemistry, geothermics and relationship to active tectonics of Gujarat and Rajasthan thermal discharges, India. J. Volcanol. Geotherm. Res., 127, 19-32.

185. Minissale A, Vaselli O, Chandrasekharam D, Magro G, Tassi F, Casiglia A (2000). Origin and evolution of'intracratonic' thermalfluids from central-western peninsular India. Earth Planet. Sci. Lett., 181 (3), 377–394.

186. Mizutani Y, Rafter TA (1969). Oxygen isotopic composition of sulphates—Part 3. Oxygen isotopic fractionation in the bisulphate ion–water system. N.Z. J. Sci., 12, 54–59.

187. Mook WG, Van der Plicht J (1999). Reporting ^{14}C activities and concentrations. Radiocarbon, 41(3), 227-239.

188. Morgenstern U, Stewart MK, Stenger R (2010). Dating of streamwater using tritium in a post nuclear bomb pulse world: continuous variation of mean transit time with streamflow. Hydrol. Earth Syst. Sci., 14, 2289–2301. https://doi.org/10.5194/hess-14-2289-2010.

189. Mukherjee A, Bhattacharya P, Shi F, Fryar AE, Mukherjee AB, Xie ZM, Jacks G, Bundschuh J (2009). Chemical evolution in the high arsenic groundwater of the Huhhot basin (Inner Mongolia, PR China) and its difference from the western Bengal basin (India). Appl. Geochem., 24, 1835–1851.

190. Mukherjee A, Fryar AE (2008). Deeper groundwater chemistry and geochemical modeling of the arsenic affected western Bengal basin, West Bengal, India. Appl. Geochem. 23, 863–892.

191. Mukherjee A, Fryar AE, Rowe HD (2007). Regional-scale stable isotopic signatures of recharge and deep groundwater in the arsenic affected areas of West Bengal, India. J. Hydrol. 334, 151–161.

192. Mukhopadhyay DK (1996). Geothermal parameters and thermal energy potential of Bakreswar, Tantloi group of hot springs in Birbhum district, West Bengal and Dumka district, Bihar. Geol. Surv. Ind. Spl. Pub., 45, 87–98.

193. Muthuraman K (1987). Geochemistry of thermal waters of west coast, Maharashtra, based on sea water-basalt experimental interaction studies. Geol. Surv. India Rec., 115, 137-149.

194. Muthuraman K, Mathur PK (1981). Experimental water/rock interaction studies and the thermal waters of the West Coast of Maharashtra, India. J Geol Soc Ind 2:69-77.

195. Naqvi SM, Divakara Rao V, Narain H (1978). The primitive crust: evidence from the Indian shield. Precambrian Res., 6(3), 323–45. DOI: 10.1016/0301-9268(78)90021-9.

196. Navada SV, Nair AR, Sharma S, Kulkarni UP (1995). Geochemical and isotope studies of the geothermal areas of central and northern India. In: Isotope and geochemical techniques applied to geothermal investigations. IAEA-TECDOC-788, 63-83.

197. Negrel Ph, Casanova J, Aranyossy JF (2001) Strontium isotope systematic used to decipher the origin of groundwater sampled from granitoids: the Vienne case (France). Chem. Geol., 177, 287–308.

198. Negrel Ph, Dupre B, Seimbille F, Allegre CJ (1988). Quantitative modelisation of differential erosion between crystalline and sedimentary area of a French basin by isotopic analysis of strontium in river waters. Chem. Geol., 70, 13. https://doi.org/10.1016/0009-2541(88)90212-4

199. Nehring NL, D'Amore F (1984). Gas chemistry and thermometry of the Cerro Prieto, Mexico, geothermal field. Geothermics, 13, 75-89.

200. Nicholson K (1993) In: Geothermal Fluids Chemistry and Exploration Techniques, Springer-Verlag, 1-215.

201. Nieva D, Nieva R (1987). Developments in geothermal energy in Mexico, Part 12. A cationic geothermometer for prospecting of geothermal resources. Heat recovery systems and CHP, 7, 243-258.

202. Norman DI, Moore JN (1999). Methane and excess N_2 and Ar in geothermal fluid inclusions. Proc. 24th Workshop Geothermal Reservoir Eng., Stanford Univ., Stanford, Calif., 196-202.

203. Oldham T, Oldham RD (1882). The thermal springs of India. GSI Mem. No. 19, 99–161.

204. Palmer, M. R., Sturchio, N. C. (1990). The boron isotope systematic of the Yellowstone National Park (Wyoming) hydrothermal system: a reconnaissance. Geochim Cosmochim Acta 54:2811–2815.

205. Pandey OP, Negi JR (1995). Geothermal fields of India: a latest update. Proc. World Geothermal Congress, Florence, Italy, 163-171.

206. Pang ZH, Reed MH (1998). Theoretical chemical thermometry on geothermal waters: problems and methods. Geochim. Cosmochim. Acta., 62, 1083–1091.

207. Panichi C, Gonfiantini R (1977) Environmental isotopes in geothermal studies. Geothermics, 6 (3–4), 143-161. https://doi.org/10.1016/0375-6505(77)90024-4.

208. Pearson FJ, Truesdell AH (1978). Tritium in the waters of Yellowstone National Park. U.S. Geol. Surv. Open-File Rep., 78-701, pp. 3.

209. Pennisi M, Gonfiantini R, Grassi S, Squarci P (2006). The utilization of boron and strontium isotopes for the assessment of boron contamination of the Cecina River alluvial aquifer (central-western Tuscany, Italy). Appl. Geochem. 21, 643–655.

210. Pin C, Bassin C (1992). Evaluation of a strontium-specific extraction chromatographic method for isotopic analysis in geological materials. Analytica Chimica Acta 269, 249-255.

211. Pitale UL, Dubey R, Saxena RK, Prasad JM, Muthuraman K, Thussu JL, Sharma SC (1987). Review of geothermal studies of west coast hot spring belt, Maharashtra. Geol. Surv. India Rec., 115: 97-136.

212. Powell T (2000). A review of exploration gas geothermometry. In: proceedings, Twenty-Fifth Workshop on Geothermal Reservoir Engineering, Stanford University, Stanford, California, January 24-26, SGP-TR-165.

213. Rabinowitz, D., Gross, G.W., Holmes, C.R., 1977. Environmental tritium as a hydro meteorological tool in the Roswell Basin, New Mexico, II. Tritium patterns in ground water. J. Hydrol. 32, 19–32.

214. Ravi Shanker (1988). Heat flow map of India and discussion on the geophysical and economc significance. Indian Min., 42, 89-110.

215. Ray R, Shukla AD, Sheth HC, Ray JS, Duraiswami AR, Vanderkluysen L, Rautela CS, Mallik J (2008). Highly heterogeneous Precambrian basement under the central Deccan Traps, India: Direct evidence from xenoliths in dykes. Gondwana Research, 13, 375-385.

216. Reddy DV, Nagabhushanam P, Ramesh G (2013). Turnover time of Tural and Rajwadi hot spring waters, Maharashtra, India. Current Science, 104, 1419-1424.

217. Reed MH, Spycher NF (1984). Calculation of pH and mineral equilibria in hydrothermal waters with application to geothermometry and studies of boiling and dilution. Geochim. Cosmochim. Acta., 48, 1479–1492.

218. Richet P, Bottinga Y, Javoy M (1977). A Review of Hydrogen, Carbon, Nitrogen, Oxygen, Sulphur, and Chlorine Stable Isotope Fractionation Among Gaseous Molecules. Ann. Rev. Earth Planet. Sci. Lett., 5, 65-110. https://doi.org/10.1146/annurev.ea.05.050177.000433

219. Rimstidt JD, Barnes HL (1980). The kinetics of silica-water reactions. Geochim. Cosmochim. Acta., 44, 1683–1699.

220. Robinson BW (1973). Sulphur isotope equilibrium during sulphur hydrolysis at high temperatures. Earth. Planet. Sci. Lett., 18 (3), 443-450.

221. Roy S, Labani, Bhattacharya A (2005). Examination of subsurface temperature regime along proposed tunnel section in the Loharinag-Palahydro power project, Uttaranchal. In: Magnetotelluric and Geothermal Investigations in Loharinag-Pala Hydro power project,

Uttaranchal. Report submitted to Water and Power Consultancy Services (India) Limited, Technical Report No. NGRI- 2006-EXP-525.

222. Sack AL, Sharma S (2014). A multi-isotope approach for understanding sources of water, carbon and sulfur in natural springs of the Central Appalachian region. Environ Earth Sci., 71, 4715–4724.

223. Saha A, Shah D, Deb SB, Saxena MK, Mishra VG, Nagar BK, Tomar BS (2015) Simultaneous quantification and isotope ratio measurement of boron in uranium-silicon-aluminium compounds by inductively coupled plasma orthogonal acceleration time of flight mass spectrometry (ICP-oa-TOFMS) after its separation by pyrohydrolysis. Microchemical Journal, 121, 56-64.

224. Sakai H (1977). Sulfate-water isotope thermometry applied to geothermal systems. Geothermics, 5 (1–4), 67-74. https://doi.org/10.1016/0375-6505(77)90010-4

225. Sammel EA, Craig RW (1981). The geothermal hydrology of Warner valley, Oregon: a reconnaissance study. US Geological Survey Professional Paper 1044-1, pp. 47.

226. Sanjuan B, Millot R, Innocent Ch, Dezayes Ch, Scheiber J, Brach M (2016). Major geochemical characteristics of geothermal brines from the Upper Rhine Graben granitic basement with constraints on temperatureand circulation. Chemical Geology, 428, 27–47. http://dx.doi.org/10.1016/j.chemgeo.2016.02.021

227. Sano Y, Urabe A, Wakita H, Chiba H, Sakai H (1985). Chemical and isotopic compositions of gases in geothermal fluids in Iceland. Geochemical Journal, 19, 135-148.

228. Sarin MM, Krishnaswami S, Dilli K, Somayajulu BLK, Moore WS (1989). Major ion chemistry of the Ganga Brahmaputra river system: weathering processes and fluxes to the Bay of Bengal. Geochim. Cosmochim. Acta, 53(5), 997–1009.

229. Sarolkar PB (2005). Geochemical characters of Hot Springs of West Coast, Maharashtra State, India. Proceedings World Geothermal Congress, Antalya, Turkey.

230. Saxena MK, Gupta ML (1985). Aquifer chemistry of thermal waters of the Godavari valley, India. J. Volcanol. Geotherm. Res., 25, 181-191.

231. Saxena VK, D'Amore F (1984) Aquifer chemistry of the Puga and Chumathang high temperature geothermal systems in India. J. Volcanol. Geotherm. Res., 21, 333-346.

232. Saxena VK, Gupta ML (1987). Evaluation of reservoir temperature and local utilization of geothermal waters of the Konkan coast, India. J. Volcanol. Geotherm. Res., 33, 337-342.

233. Schiagintweit R De (1862). Enumeration of the hot springs in India and high Asia. JASB, XXXIII, 49–58.

234. Sen G (1986) Mineralogy and petrogenesis of the Deccan Trap lava flows around Mahabaleshwar. India J Petrol 27:627–663

235. Sharma S, Nair AR, Kulkarni UP, Navada SV, Pitale UL (1996b). Isotope and geochemical studies in Tattapani geothermal area, Sarguja District, Madhya Pradesh. Geol.Surv.Ind. Spl. Pub., 45, 233-242.

236. Sharma S, Nair AR, Kulkarni UP, Navada SV, Sharma SC (1996a). Environmental isotope studies in Badrinath and Tapoban geothermal areas, Chamoli district, Uttar Pradesh. Geol. Surv. Ind. Spl. Pub., 45, 223-231.

237. Shevenell L, Goff F (1995). The use of tritium in groundwater to determine fluid mean residence times of Valles caldera hydrothermal fluids, New Mexico, USA. J. Volcanol. Geotherm. Res., 67(1–3), 187–205. https://doi.org/10.1016/0377-0273(94)00102-M

238. Singh HK, Chandrasekharam D, Trupti G, Mohite P, Singh B, Varun C, Sinha SK (2016). Potential Geothermal Energy Resources of India: A Review. Curr. Sustain. Energy. Rep., 3, 80–91. DOI: 10.1007/s40518-016-0054-0.

239. Singh HK, Sinha SK, Alam MA, Chandrasekharam D (2020). Tracing the evolution of thermal springs in the Hazaribagh area of Eastern Peninsular India through hydrogeochemical and isotopic analyses. Geothermics, 85, 101817. DOI: 10.1016/j.geothermics.2020.101817.

240. Singh SB, Drolia RK, Sharma SR, Gupta ML (1983). Application of resistivity surveying to geothermal exploration in the Puga valley, India. Geoexploration, 21 (1), 1-11.

241. Spivack AJ, Edmond JM (1987). Boron isotope exchange between seawater and oceanic crust. Geochim. Cosmochim. Acta., 51, 1033–1042.

242. Spivack AJ, Palmer MR, Edmond JM (1987). The sedimentary cycle of the boron isotopes. Geochim. Cosmochim. Acta., 51, 1939–1950.

243. Spycher N, Peiffer L, Saldi G, Sonnenthal E, Reed MH, Kennedy BM (2014). Integrated multicomponent solute geothermometry. Geothermics, 51, 113–123.

244. Srinivasa Rao, Subbaraju K, Srinivas T, Khan IA, Silekar VS (1979). Tectonic evolution of Godavari graben. IV Inter. Gondwana Sym., Calcutta, Hindustan Pub. Corp., Delhi, 54-67.

245. Stallard RF, Edmond JM (1987). Geochemistry of the Amazon. 3. Weathering chemistry and limits to dissolved inputs. J. Geophys. Res. – Oceans, 92, 8293– 8302.

246. Stüben D, Berner Z, Chandrasekharam D (2003). Arsenic enrichment in groundwater of West Bengal, India: geochemical evidence for mobilization of As under reducing conditions. Appl. Geochem., 18, 1417–1434.

247. Stuiver M, Polach HA (1977). Reporting of ^{14}C data. Radiocarbon, 19(3), 355-363.

248. Tarcan G, Gemici Ü (2003). Water geochemistry of the Seferihisar geothermal area, İzmir, Turkey. J. Volcanol. Geotherm. Res., 126, 225–242.

249. Thussu JL (2002). Geothermal energy resources of India. Geol. Surv. Ind. Spl. Pub., 69, pp. 210.

250. Tiwari SK, Gupta AK, Asthana AKL (2020). Evaluating CO_2 flux and recharge source in geothermal springs, Garhwal Himalaya, India: stable isotope systematics and geochemical proxies. Environ. Sci. Pollut. Res., 27, 14818–14835. https://doi.org/10.1007/s11356-020-07922-1.

251. Tiwari SK, Rai SK, Bartarya SK, Gupta AK, Negi M (2016). Stable isotopes ($\delta^{13}C_{DIC}$, δD, $\delta^{18}O$) and geochemical characteristics of geothermal springs of Ladakh and Himachal (India): evidence for CO2 discharge in northwest Himalaya. Geothermics, 64, 314–330.

252. Tonani F (1980). Some remarks on the application of geochemical techniques in geothermal exploration. Proceedings Adv. Eur. Geoth. Res., Second symp., Strasbourg, pp. 428-443.

253. Truesdell AH, Fournier RO (1977). Procedure for estimating the temperature of a hot water component in mixed water using a plot of dissolved silica vs. enthalpy. Jour. Research U.S. Geol. Survey, 5(1), 49-52.

254. Truesdell AH, Hulston JR (1980). Isotopic evidence on environments of geothermal systems. In: P. Fritz and J.C. Fontes (eds) Handbook of Environmental Isotope Geochemistry, vol. 1, Elsevier, Amsterdam, 179-226.

255. Truesdell AH, Nathenson M, Rye RO (1977). The effects of subsurface boiling and dilution on the isotopic compositions of Yellowstone thermal waters. Journal of Geophysical Research, 82, 3964-3704.

256. Urey HC (1947). The thermodynamic properties of isotopic substances. J. Chem. Soc., 562-581.

257. Vengosh A, Helvaci C, Karamanderesi IH (2002). Geochemical constraints for the origin of thermal waters from western Turkey. Appl Geochem, 17, 163–183.

258. Vengosh A, Heumann KG, Juraske S, Kasher R (1994). Boron isotope application for tracing sources of contamination in groundwater. Environ. Sci. Technol., 28, 1968–1974.

259. Vogel JC (1967). Investigation of groundwater flow with radiocarbon: Isotopes in hydrology, proceedings from Conference on Isotopes in Hydrology, Vienna, International Atomic Energy Agency, 355–368.

260. White DE (1957). Thermal waters of volcanic origin. Geological Society of America Bulletin, 68, 1637-1657.

261. White DE (1970). Geochemistry applied to the discovery, evaluation, and exploitation of geothermal energy resources. Geothermics, 2 (1), 58-80.

262. White D (1986). Subsurface waters of different origins. In: Ólafsson J and Ólafsson, M. (editors) Fifth International Symposium on Water-Rock Interaction. Extended abstracts. Inernational Association of Geochemistry and Cosmochemistry, Orkustofnun, Reykjavík, 629-632.

263. WHO (World Health Organisation) (2008). Guidelines for drinking-water quality. Third edition incorporating the first and second agenda, Vol 1, 1–668.

264. Xiao J, Xiao YK, Jin ZD, He MY, Liu CQ (2013). Boron isotope variations and its geochemical application in nature. Australian Journal of Earth Sciences, 60, 431–447. http://dx.doi.org/10.1080/08120099.2013.813585

265. Xu T, Hou Z, Jia X, Spycher N, Jiang Z, Feng B, Na J, Yuan Y (2016). Classical and integrated multicomponent geothermometry at the Tengchonggeothermal field, Southwestern China. Environ. Earth Sci. 75, 1502. DOI 10.1007/s12665-016-6298-6

266. Zimik HV, Farooq SH, Prusty P (2017). Geochemical evaluation of thermal springs in Odisha, India. Environ. Earth Sci., 76, 593.

267. Zuber A, Maloszewski P (2001). Lumped parameter models (Mook, WG and Yurtsever, Y. eds.) In: Modelling in Environmental isotopes in the hydrological cycle: Principles and applications: Paris, France, UNESCO, Technical Documents in Hydrology, 39 (1), 5–35.

Thesis highlights

1. Name of the Student: SITANGSHU CHATTERJEE

2. Enrolment No. : CHEM01201504010

4. Title of the Thesis: Integrated isotope-geochemical investigation in the selected geothermal areas of India

The thesis enumerates the in-depth isotope-geochemical assessment of three promising geothermal areas (Tural-Rajwadi geothermal area of West coast geothermal province, Godavari valley geothermal area and Tapoban-Badrinath geothermal area) situated in the three distinct geological settings. The major highlights of the present work are:

- All the thermal springs found in the Tural-Rajwadi (Deccan Trap region), Godavari Valley (Sedimentary formation) and Uttarakhand region (Himalayan belt) are meteoric in origin.
- Tural-Rajwadi geothermal area located near the sea shows enriched stable isotopic values whereas Uttarakhand geothermal area shows most depleted stable isotopic values due to its high altitude.
- Geochemically thermal waters in the Tural-Rajwadi region are more mature (Na-Cl type) compared to the thermal waters in Godvari valley and Uttarkkand region (bicarbonate type).
- The thermal waters from the Uttarakhand geothermal area are found to be younger (40 to 112 years) compared to the geothermal systems from the peninsular India i.e. Tural-Rajwadi (6000 to 15000 years) and Godavari valley (9900 to 18600 years) which contains much more old thermal waters.